



Mathematical optimization methods for aircraft conflict resolution in air traffic control

Author:

Cunha Dias, Fernando

Publication Date:

2021

DOI:

<https://doi.org/10.26190/unsworks/22643>

License:

<https://creativecommons.org/licenses/by-nc-nd/3.0/au/>

Link to license to see what you are allowed to do with this resource.

Downloaded from <http://hdl.handle.net/1959.4/71000> in <https://unsworks.unsw.edu.au> on 2024-04-28

Mathematical optimization methods for aircraft conflict resolution in air traffic control



UNSW
SYDNEY

Fernando H. C. Dias
School of Civil and Environmental Engineering
University of New South Wales

A thesis submitted for the degree of
Doctor of Philosophy



UNSW
SYDNEY

Australia's
Global
University

Thesis/Dissertation Sheet

Surname/Family Name	: Cunha Dias
Given Name/s	: Fernando Hugo
Abbreviation for degree as give in the University calendar	: PhD
Faculty	: Engineering
School	: School of Civil and Environmental Engineering
Thesis Title	: Mathematical optimization methods for aircraft conflict resolution in air traffic control

Abstract 350 words maximum: (PLEASE TYPE)

Air traffic control is a very dynamic and heavy constrained environment where many decisions need to be taken over short periods of time and in the context of uncertainty. Adopting automation under such circumstances can be a crucial initiative to reduce controller workload and improve airspace usage and capacity. Traditional methods for air traffic control have been exhaustively used in the last decades and are reaching their limits, therefore automated approaches are receiving a significant and growing attention. In this thesis, the focus is to obtain optimal aircraft trajectories to ensure flight safety in the short-term by solving optimization problems.

During cruise stage, separation conditions require a minimum of 5 Nautical Miles (NM) horizontally or 1000 feet (ft) vertically between any pair of aircraft. A conflict between two or more aircraft is a loss of separation among these aircraft. Air traffic networks are organized in flights levels which are separated by at least 1000 ft, hence during cruise stage, most conflicts occur among aircraft flying at the same flight level. This thesis presents several mathematical formulations to address the aircraft conflict resolution problem and its variants.

The core contribution of this research is the development of novel mixed integer programming models for the aircraft conflict resolution problem. New mathematical optimization formulations for the deterministic aircraft conflict resolution problem are analyzed and exact methods are developed. Building on this framework, richer formulations capable of accounting for aircraft trajectory prediction uncertainty and trajectory recovery are proposed.

Results suggest that the formulations presented in thesis are efficient and competitive enough with the state-of-art models and they can provide an alternative solution to possibly fill some of the gaps currently present in the literature. Furthermore, the results obtained demonstrates the impact of these models in solving very denser air space scenarios and its competitive with state-of-the-art formulations without regarding variable discretization or non-linear components.

Declaration relating to disposition of project thesis/dissertation

I hereby grant to the University of New South Wales or its agents a non-exclusive licence to archive and to make available (including to members of the public) my thesis or dissertation in whole or in part in the University libraries in all forms of media, now or here after known. I acknowledge that I retain all intellectual property rights which subsist in my thesis or dissertation, such as copyright and patent rights, subject to applicable law. I also retain the right to use all or part of my thesis or dissertation in future works (such as articles or books).

Signature

13/04/2021
Date

Statement of Originality

"I hereby declare that this submission is my own work and to the best of my knowledge it contains no materials previously published or written by another person, or substantial proportions of material which have been accepted for the award of any other degree or diploma at UNSW or any other educational institution, except where due acknowledgement is made in the thesis. Any contribution made to the research by others, with whom I have worked at UNSW or elsewhere, is explicitly acknowledged in the thesis. I also declare that the intellectual content of this thesis is the product of my own work, except to the extent that assistance from others in the project's design and conception or in style, presentation and linguistic expression is acknowledged."

Signed

Date

COPYRIGHT STATEMENT

'I hereby grant the University of New South Wales or its agents a non-exclusive licence to archive and to make available (including to members of the public) my thesis or dissertation in whole or part in the University libraries in all forms of media, now or here after known. I acknowledge that I retain all intellectual property rights which subsist in my thesis or dissertation, such as copyright and patent rights, subject to applicable law. I also retain the right to use all or part of my thesis or dissertation in future works (such as articles or books).'

'For any substantial portions of copyright material used in this thesis, written permission for use has been obtained, or the copyright material is removed from the final public version of the thesis.'

Signed

Date

AUTHENTICITY STATEMENT

'I certify that the Library deposit digital copy is a direct equivalent of the final officially approved version of my thesis.'

Signed

Date



Australia's
Global
University

INCLUSION OF PUBLICATIONS STATEMENT

UNSW is supportive of candidates publishing their research results during their candidature as detailed in the UNSW Thesis Examination Procedure.

Publications can be used in their thesis in lieu of a Chapter if:

- The candidate contributed greater than 50% of the content in the publication and is the “primary author”, ie. the candidate was responsible primarily for the planning, execution and preparation of the work for publication
- The candidate has approval to include the publication in their thesis in lieu of a Chapter from their supervisor and Postgraduate Coordinator.
- The publication is not subject to any obligations or contractual agreements with a third party that would constrain its inclusion in the thesis

Please indicate whether this thesis contains published material or not:

This thesis contains no publications, either published or submitted for publication
(if this box is checked, you may delete all the material on page 2)

Some of the work described in this thesis has been published and it has been documented in the relevant Chapters with acknowledgement
(if this box is checked, you may delete all the material on page 2)

This thesis has publications (either published or submitted for publication) incorporated into it in lieu of a chapter and the details are presented below

CANDIDATE'S DECLARATION

I declare that:

- I have complied with the UNSW Thesis Examination Procedure
- where I have used a publication in lieu of a Chapter, the listed publication(s) below meet(s) the requirements to be included in the thesis.

Candidate's Name
Fernando Hugo Cunha
Dias

Signature

Date (dd/mm/yy)

13/04/2021

This thesis is dedicated to my parents Marta and Pedro for being the best parents that they possibly could. They came from nothing and gave me everything I could ask for and I am eternally grateful.

”Thought I’d end up with Dani,
But she wasn’t a match,
Wrote some code with David,
Now I cite and sketch,
Even almost got buried,
And for Felipe, I’m so thankful,
As nothing happens as random,
Cause they’re all my angels”
- *Thank U, Next* - 2019

Acknowledgements

In this thesis, I would like to thank everyone that directly or indirectly help me to achieve this milestone that means the world to me. First and foremost, I would like to thank my parents Marta and Pedro. The person that I am and everything I got is because of them. They always give me the support that I needed, once financial but always emotional. Since the beginning, they taught me that education and knowledge are the base of everything in life, that does not matter what happens to a person in life, those two things cannot be taken away from you. Even though we are separated from miles away, we never stopped being a family. My father has always been a headstrong and determined man that raised me with strong and decisive hands and show me the importance of discipline, duty and organization. My mother is a very caring woman and taught me about empathy, respect and self-respect. All those traits together helped me to shape myself into somewhat of an adult. I do not have enough words to thank them for everything in my life.

To Prof. Antonio Alonso-Ayuso and Prof. Marcel Mongeau, the reviewers of this thesis that devoted their time, effort and knowledge to thoroughly and extensively read and mark my work, my sincere "Thank You". Both of your works and careers are inspiration and example of excellence to me. I am truly privileged to have my work assessed by giants in this field that I have hoped to contribute with my best efforts.

To my supervisor, David Rey (aka *TeamDavid*), thank you for accepting to supervise me back in 2017, I hope I made you proud of what I have achieved so far. It is not much, but it is the beginning and it means the world to me. You also showed me how to be a dignified, honest and ethical researcher and how to channel my best effort in order to produce competitive and cutting-edge research outputs. To my second supervisor, Prof. S. Travis Waller, thank you for your support and leadership. You are

an example of excellence and high achievement done throughout extensive and dedicated work. Your career is something to admire and to aim for.

To my previous supervisors, Dani, Felipe and Chico, thank you for my start and my introduction into the world of research. All of you are incredible role models to me and showed that even if the conditions are not ideal, world-class level research can be conceived given the right amount of care, dedication and sacrifices.

To friends all over the world.: thank you for all the support on so many different levels. Some of you are still close, others life drove us apart, but I know that you are always hoping for my best and my success. To Daniel, thank you for dealing with my desperation and exasperation for many years already. I really do not know how you do this. By thank you for the immense support all the way from across the Pacific. To Guilherme (aka Guilermo), thank you for being so chilled and cool under any circumstances. You have always been an unexpected friendship that proved more and more that I cannot judge a book by its cover. One of the best people I met throughout the last days of undergrad. To Gabi, the best thing that happened to me during UFMG years. Thank you for being my partner in crime in some years of tiring assignment and sleepless night working on some projects, we created a beautiful friendship that I cherish the most. To Thais, we started in the van and then took over the world. Thank you for your friendship and support, you know exactly how intense that undergrad course was and gave me the partnership I need through and through. To Stephani and Joseane, the longest of them all, we know each other since we were literally children and until this day, the friendship never fades and it will never. Thank you for being part of my life after almost 20 years. To Patrick, the only Brazilian friend here in Sydney, thank you for the hilarious moments and the delightful encounters. You are a ray of sunshine in this city and I cannot wish nothing but the best for you at all times. To Flaviane, my "older sister from another mother", thank you for helping me from all this distance and for the advice and wisdom. To the LIGP family, Michelle, Joao, Laila, Ana, Mari, Carol and many others thank you for my first experience in a research group, you are the absolute best. To the rCITI group, thank you all.

Abstract

Air traffic control is a very dynamic and heavy constrained environment where many decisions need to be taken over short periods of time and in the context of uncertainty. Adopting automation under such circumstances can be a crucial initiative to reduce controller workload and improve airspace usage and capacity. Traditional methods for air traffic control have been exhaustively used in the last decades and are reaching their limits, therefore automated approaches are receiving a significant and growing attention. In this thesis, the focus is to obtain optimal aircraft trajectories to ensure flight safety in the short-term by solving optimization problems.

During cruise stage, separation conditions require a minimum of 5 Nautical Miles (NM) horizontally or 1000 feet (ft) vertically between any pair of aircraft. A conflict between two or more aircraft is a loss of separation among these aircraft. Air traffic networks are organized in flight levels which are separated by at least 1000 ft, hence during cruise stage, most conflicts occur among aircraft flying at the same flight level. This thesis presents several mathematical formulations to address the aircraft conflict resolution problem and its variants.

The core contribution of this research is the development of novel mixed integer programming models for the aircraft conflict resolution problem. New mathematical optimization formulations for the deterministic aircraft conflict resolution problem are analyzed and exact methods are developed. Building on this framework, richer formulations capable of accounting for aircraft trajectory prediction uncertainty and trajectory recovery are proposed.

Results suggest that the formulations presented in thesis are efficient and competitive enough with the state-of-art models and they can provide an alternative solution to possibly fill some of the gaps currently present in the literature. Furthermore, the results obtained demonstrates the

impact of these models in solving very denser air space scenarios and its competitive with state-of-the-art formulations without regarding variable discretization or non-linear components.

Abstrato

O controle de tráfego aéreo é um ambiente muito dinâmico e fortemente restrito, onde muitas decisões precisam ser tomadas em curtos períodos de tempo e no contexto de incerteza. A adoção da automação nessas circunstâncias pode ser uma iniciativa crucial para reduzir a carga de trabalho do controlador e melhorar o uso e a capacidade do espaço aéreo. Os métodos tradicionais de controle de tráfego aéreo têm sido exaustivamente utilizados nas últimas décadas e estão atingindo seus limites, por isso as abordagens automatizadas vêm recebendo uma atenção significativa e crescente. Nesta tese, o foco é obter trajetórias de aeronaves ideais para garantir a segurança de vôo no curto prazo, resolvendo problemas de otimização.

Durante a fase de cruzeiro, as condições de separação exigem um mínimo de 5 milhas náuticas (NM) horizontalmente ou 1000 pés (ft) verticalmente entre qualquer par de aeronaves. Um conflito entre duas ou mais aeronaves é uma perda de separação entre essas aeronaves. As redes de tráfego aéreo são organizadas em níveis de voo separados por pelo menos 1000 pés, portanto, durante o estágio de cruzeiro, a maioria dos conflitos ocorre entre aeronaves voando no mesmo nível de voo. Esta tese apresenta diversas formulações matemáticas para abordar o problema de resolução de conflitos de aeronaves e suas variantes.

A principal contribuição desta pesquisa é o desenvolvimento de novos modelos de programação inteira mista para o problema de resolução de conflitos de aeronaves. Novas formulações de otimização matemática para o problema de resolução determinística de conflitos de aeronaves são analisadas e métodos exatos são desenvolvidos. Com base nesta estrutura, são propostas formulações mais ricas capazes de contabilizar a incerteza de previsão da trajetória da aeronave e a recuperação da trajetória.

Os resultados sugerem que as formulações apresentadas na tese são eficientes e competitivas o suficiente com os modelos do estado da arte e podem fornecer uma solução alternativa para possivelmente preencher algumas das lacunas atualmente presentes na literatura. Além disso, os resultados obtidos demonstram o impacto desses modelos na resolução de cenários de espaço aéreo muito mais denso e sua competitividade com formulações de última geração, sem considerar discretização variável ou componentes não lineares.

List of Publications

- Journal articles (accepted)
 - **Dias, F.H.C.**, Hijazi H, Rey D, Disjunctive separation constraints and formulation for aircraft resolution by speed and altitude control. *European Journal of Operational Research*. Accepted for publication in 2021. <https://www.sciencedirect.com/science/article/abs/pii/S0377221721002897>
- Journal articles (under review)
 - **Dias, F.H.C.**, Rey D, Robust aircraft conflict resolution under trajectory prediction uncertainty. *Annals of Operations Research*. Submitted in 2021 <https://arxiv.org/abs/2012.08230>
- Journal articles (current in development)
 - **Dias, F.H.C.**, Rey D, A two-stage algorithm for aircraft conflict resolution with trajectory recovery. *Journal of Global Optimization*. Submission in 2021.
 - **Dias, F.H.C.**, Hijazi H, Rey D, Analytical solution for 2D aircraft conflict resolution problem. *Operations Research Letter*. Submission in 2021.
- Peer-reviewed conference proceedings
 - **Dias, F.H.C.**, Rahme S, Rey D, A two-stage algorithm for aircraft conflict resolution with trajectory recovery., 2020 *9th International Conference on Research in Air Transportation (ICRAT)* http://www.icrat.org/ICRAT/seminarContent/2020/papers/ICRAT2020_paper_75.pdf
- Conference presentations
 - **Dias, F.H.C.**, Rey D, Aircraft conflict resolution and heading recovery with mixed-integer programming. *23rd International Symposium on Mathematical Programming*, Bordeaux, France, 2018

- **Dias, F.H.C.**, Rey D, Conflict Avoidance and Recovery using mixed-integer formulation. *Inaugural Transport Research Association for NSW Symposium*, Sydney, Australia, 2018
- **Dias, F.H.C.**, Rey D, Scalable global optimization approach for aircraft conflict resolution by speed control and altitude. *2nd Transport Research Association for NSW Symposium*, Sydney Australia, 2019
- **Dias, F.H.C.**, Rey D, Robust aircraft conflict resolution under trajectory prediction uncertainty. *3rd Transport Research Association for NSW Symposium*, Sydney, Australia, 2020
- **Dias, F.H.C.**, Hijazi H, Rey D, Analytical Solution for the Two-Aircraft Conflict Resolution Problem. *31st European Conference on Operational Research*, Athens, Greece, 2021

Contents

1	Introduction	1
1.1	History of Aviation and Air Traffic Control	1
1.2	Airspace Structure	3
1.3	Air Traffic Management	7
1.4	Air Traffic Control	9
1.5	Aircraft Conflict Resolution	12
1.6	Mathematical Programming Methods for Aircraft Conflict Resolution	14
2	Literature Review	17
2.1	Introduction	17
2.2	Air Traffic Management	19
2.3	Air Traffic Control	23
2.4	Aircraft Conflict Resolution	25
2.4.1	Early Studies on Conflict Detection and Resolution	26
2.4.2	Mathematical programming approaches for the deterministic aircraft conflict resolution problem	30
2.4.3	Advanced formulations for aircraft conflict resolution problems	32
3	Formulations for the Aircraft Conflict Resolution Problem	37
3.1	Characterisation of 2D Separation Conditions	37
3.2	Non-convex Quadratic Formulation	43
3.3	Non-convex Disjunctive Formulation	43
3.4	Non-convex Shadow Formulation	49
3.5	Equivalence Between Formulations	52
3.6	Data For Numerical Experiments	54
3.7	Numerical Results	55
3.8	Summary of Findings	60
3.9	Conclusion	61

4	Exact Solution Methods for the Deterministic Aircraft Conflict Resolution Problem	63
4.1	Pre-processing	64
4.2	Complex Number Formulation for the 2D Aircraft Conflict Resolution Problem	66
4.3	Complex Number Formulation for the 2D+FL Aircraft Conflict Resolution Problem	69
4.4	Mixed-Integer Quadratic Relaxation for the 2D Aircraft Conflict Resolution Problem	72
4.5	Mixed-Integer Quadratically Constrained Relaxation and Constraint Generation Algorithm	73
4.6	Decomposition Algorithm for the 2D+FL Aircraft Conflict Resolution Problem	77
4.7	Numerical Results	80
4.7.1	Experiments Design	81
4.7.2	Sensitivity Analysis on the Preference Weight w	82
4.7.3	Results on 2D instances	83
4.7.4	Results on 2D+FL instances	96
4.8	Analytical Solution for the Two-Aircraft Conflict Resolution Problem	102
4.8.1	Analytical Problem Definition	102
4.8.2	Solution of Sub-Problems \mathcal{SP}_0 and \mathcal{SP}_1	103
4.8.3	Discussion	108
4.9	Conclusion	109
4.9.1	Summary of Findings	109
4.9.2	Future Research and Perspectives	111
5	Robust aircraft conflict resolution under trajectory prediction uncertainty	112
5.1	Robust Aircraft Conflict Resolution Problem	112
5.1.1	Uncertainty Model	113
5.1.2	Robust Counterpart Formulation	115
5.1.3	Solution Method for the Robust ACRP	117
5.2	Numerical Experiments	118
5.2.1	Experiments Design	118
5.2.2	Analysis of the robust ACRP	119
5.2.3	Sensitivity analysis on the level of robustness	123

5.2.4	Sensitivity analysis on the size of the uncertainty set	127
5.2.5	Feasibility analysis	130
5.3	Conclusion	136
5.3.1	Summary of Findings	136
6	Aircraft Conflict Resolution Problem with Trajectory Recovery	138
6.1	Conflict Resolution with Trajectory Recovery with Discretised Heading Change Angles	139
6.1.1	Collision Avoidance	139
6.1.1.1	Separation Conditions	139
6.1.1.2	Speed Control, Heading Changes and Objective Function	140
6.1.1.3	Disjunctive formulation	141
6.1.2	Trajectory Recovery	142
6.1.2.1	Exact-Recovery	144
6.1.2.2	Greedy-Recovery	145
6.2	Numerical Experiments	147
6.2.1	Experimental Framework	147
6.2.2	Illustration	147
6.2.3	Performance of the Two-stage Algorithm	149
6.3	Conflict Resolution with Trajectory Recovery with Continuous Heading Change Angle	154
6.3.1	Collision Avoidance	154
6.3.2	Trajectory Recovery	156
6.3.2.1	Two-Stage Iterative Algorithm	157
6.4	Numerical Results	158
6.4.1	Experimental Framework	158
6.4.2	Illustration	160
6.4.3	Performance of the Two-Stage Iterative Algorithm	161
6.5	Conclusion	166
6.5.1	Summary of Findings	166
6.5.2	Future Research and Perspectives	167
7	Conclusion	169
7.1	Summary and Contributions	169
7.2	Limitations and Future Research	173
7.3	Final Remarks	175

Bibliography	176
------------------------	-----

List of Abbreviations

2D	two-dimensional	64
AAR	Airport Acceptance Rate	21
ACRP	Aircraft Conflict Resolution Problem	13
AEA	Association of European Airlines	17
ANSP	Air Navigation Service Provider System	8
ASBU	Aviation System Block Upgrades	8
ASM	Available Seat Miles	7
ATC	Air Traffic Control	2
ATFM	Air Traffic Flow Management	7
ATM	Air Traffic Management	7
ATS	Air Traffic System	7
CDR	Conflict Avoidance and Recovery	25
CMATS	Civil-Military ATM System, Australia	11
EATCHIP	European Air Traffic Control Harmonization and Integration Programme	22
FAA	Federal Aviation Administration	2
FIS	Flight Information Service	7
FREER	Free-Route Experimental Encounter Resolution	27
ICAO	International Civil Aviation Organization	vi
IFR	Instrumental Flight Rules	4
KKT	Karush-Kuhn-Tucker	104
NextGen	Next Generation Air Transportation System	11
NM	Nautical Miles	5
ONESky	ONESky	11
PAR	Precision Approach Radar	11
RVT	Remote Virtual Tower	9
RAS	Radar Advisory Service	11
SAAM	System for Traffic Assignment and Analysis at a Macroscopic Level	22
SAR	Search And Rescue	7
SESAR	Single European Sky ATM Research	11
TCAS	Traffic Collision Avoidance System	25
TRACON	Terminal Radar Approach CONTROL	10
VFR	Visual Flight Rules	3

List of Figures

1.1	Impact of Covid-19 in international flights. In this picture, the "aircraft" symbol represents total number of trips, the "individual" symbol represents traveller and the dollar sign represents revenue. All three metrics are calculated over an year estimate. The upside triangle in red and orange represent decline of those metrics. All data presented in this chart is from domestic flights. (Bureau, 2020)	3
1.2	Impact of Covid-19 in domestic flights. In this picture, the "aircraft" symbol represents total number of trips, the "individual" symbol represents traveller and the dollar sign represents revenue. All three metrics are calculated over an year estimate. The upside triangle in red and orange represent decline of those metrics. All data presented in this chart is from domestic flights. (Bureau, 2020)	4
1.3	Evolution of airspace demand throughout the decades	5
1.4	Communication between different units of airspace	6
1.5	Different stages in ATC	7
1.6	ATM Structure and its subdivisions	8
1.7	Aircraft separation standards. The aircraft is represented by the red dot. By International Civil Aviation Organization (ICAO) standards, the horizontal separation required is at least 5 NM of horizontal separation and 1000 ft. of vertical separation.	13
1.8	Airspace Structure. The airspace is structured in layers that are multiple of 1000 ft. In each layer, there are referential points used to assist in navigation, referred as waypoints.	14
2.1	Airspace and Air Traffic Research Hierarchy	18
2.2	Airport System Hierarchy	19
3.1	Pre-Processing Configurations	41
3.2	Plane $\{(v_{ij,x}, v_{ij,y}) \in \mathbb{R}^2\} - g_{ij}(v_{ij,x}, v_{ij,y}) \leq 0$	45
3.3	Plane $\{(v_{ij,x}, v_{ij,y}) \in \mathbb{R}^2\} - \text{Disjunction}$	46

3.4	Geometrical analysis of conflict between two aircraft based on relative velocity	50
3.5	Benchmarking instances	56
4.1	Mixed-Integer Approximation	74
4.2	Sensitivity Analysis	83
4.3	Four candidate solution obtained via the analytical solutions. The point in orange represents Case I, in blue Case II, in green Case III and in black Case IV.	107
4.4	Benchmarking instances	108
5.1	Random relative velocity box	114
5.2	Illustration of aircraft optimal trajectories using the robust complex number formulation with a maximum uncertainty of $\bar{\epsilon} = 5\%$	120
5.3	Distribution of aircraft pairwise minimal separation distances after optimisation for varying level of robustness Γ	121
5.4	Distribution of aircraft pairwise minimal separation distances after optimisation for varying maximum uncertainty $\bar{\epsilon}$	122
5.5	Histogram and density plot for instances RCP-10-1, RCP-20-1 and RCP-30-1. The red dashed line represents the minimum separation distance of 5 NM.	123
5.6	Feasibility of 100 RCP-10 instances based on the number of conflict n_c and the total pairwise minimal distance between all pairs of aircraft D^{\min} using $\bar{\epsilon} = 5\%$	132
5.7	Feasibility of 100 RCP-20 instances based on the number of conflict n_c and the total pairwise minimal distance between all pairs of aircraft D^{\min} using $\bar{\epsilon} = 5\%$	133
5.8	Feasibility of 100 RCP-10 instances based on the number of conflict n_c and the total pairwise minimal distance between all pairs of aircraft D^{\min} using $\Gamma = 4$	134
5.9	Feasibility of 100 RCP-20 instances based on the number of conflict n_c and the total pairwise minimal distance between all pairs of aircraft D^{\min} using $\Gamma = 4$	135
6.1	Illustration of $f_{ij}(t)$ for a configuration with $g_{ij} < 0$ and $t_{ij}^{\min} > 0$. τ_{ij} represents the start time of the conflict.	142

6.2	Illustration of the two-stage algorithm with Exact-Recovery. Dashed grey lines represent aircraft initial trajectories. Red lines represent aircraft collision avoidance trajectories obtained via Model 10. Blue lines represent recovery trajectories obtained via Model 11.	148
6.3	Stage 1: collision avoidance. Distribution of objective function values for Model 10. Each boxplot represent 100 instances of each instance size (10, 20 and 30 aircraft).	152
6.4	Stage 1: Collision avoidance. Distribution of runtimes for Model 10. Each boxplot represent 100 instances of each instance size (10, 20 and 30 aircraft).	152
6.5	Stage 2: Trajectory recovery. Distribution of objective function values for ER (Model 11) and GR (Algorithm 4). Each boxplot represent 100 instances of each instance size (10, 20 and 30 aircraft).	153
6.6	Stage 2: Trajectory recovery. Distribution of runtimes for ER (Model 11) and GR (Algorithm 4). Each boxplot represent 100 instances of each instance size (10, 20 and 30 aircraft).	153
6.7	Comparison in the profile of solutions using discrete angle (first column) and using continuous angle (second column). In the first row, the avoidance stage is in red while the recovery stage is in blue. In the second row, the avoidance stage is in green while the recovery stage is in green.	163

List of Tables

3.1	Summary of Results for 2D CP instances with a speed control range of $[-6\%, +3\%]$ and a heading control range of $[-30^\circ, +30^\circ]$. All runtimes (Time) are reported in seconds. The optimality gaps (Gap) are the proportion of time-outs (n_t) are reported in percentage.	57
3.2	Summary of Results for 2D FP instances with a speed control range of $[-6\%, +3\%]$ and a heading control range of $[-30^\circ, +30^\circ]$. All runtimes (Time) are reported in seconds. The optimality gaps (Gap) are the proportion of time-outs (n_t) are reported in percentage.	58
3.3	Summary of Results for 2D GP instances with a speed control range of $[-6\%, +3\%]$ and a heading control range of $[-30^\circ, +30^\circ]$. All runtimes (Time) are reported in seconds. The optimality gaps (Gap) are the proportion of time-outs (n_t) are reported in percentage.	58
3.4	Summary of Results for 2D RCP-10 instances with a speed control range of $[-6\%, +3\%]$ and a heading control range of $[-30^\circ, +30^\circ]$. All runtimes (Time) are reported in seconds. The optimality gaps (Gap) are the proportion of time-outs (n_t) are reported in percentage. . . .	59
3.5	Summary of Results for 2D RCP-20 instances with a speed control range of $[-6\%, +3\%]$ and a heading control range of $[-30^\circ, +30^\circ]$. All runtimes (Time) are reported in seconds. The optimality gaps (Gap) are the proportion of time-outs (n_t) are reported in percentage. . . .	60
4.1	Results for 2D CP instances with subliminal speed and standard heading control.	88
4.2	Results for 2D CP instances with subliminal speed and reduced heading control	89
4.3	Results for 2D FP instances with subliminal speed and standard heading control.	90
4.4	Results for 2D FP instances with a subliminal speed and reduced heading control.	91

4.5	Results for 2D GP instances with subliminal speed and standard heading control.	92
4.6	Results for 2D GP instances with subliminal speed and reduced heading control	93
4.7	Results for 2D RCP instances with subliminal speed and standard heading control.	94
4.8	Results for 2D RCP instances with subliminal control and reduced heading control	95
4.9	Results for 2D+FL RCP instances with subliminal speed and standard heading control	100
4.10	Results for 2D+FL RCP instances with subliminal speed and reduced heading control	101
5.1	Summary of results for CP instances with a speed control range of $[-6\%, +3\%]$ and a heading control range of $[-30^\circ, +30^\circ]$ using a maximal uncertainty of $\bar{\epsilon} = 5\%$	124
5.2	Summary of results for RCP instances with a speed control range of $[-6\%, +3\%]$ and a heading control range of $[-30^\circ, +30^\circ]$ using a maximal uncertainty of $\bar{\epsilon} = 5\%$	126
5.3	Summary of results for CP instances with a speed control range of $[-6\%, +3\%]$ and a heading control range of $[-30^\circ, +30^\circ]$ using a level of robustness of $\Gamma = 4$	128
5.4	Summary of results for RCP instances with a speed control range of $[-6\%, +3\%]$ and a heading control range of $[-30^\circ, +30^\circ]$ using a level of robustness of $\Gamma = 4$	129
6.1	Results on the Circle Problem with 4 to 15 aircraft.	150
6.2	Summary of results for 2D CP instances with a speed control range of $[-6\%, +3\%]$ and a heading control range of $[-30^\circ, +30^\circ]$. All runtimes (Time) are reported in seconds while $\frac{1}{ A } \sum_{i \in A} t_i, \max_{i \in A} t_i$ and $\min_{i \in A} t_i$ are in hours. The optimality gap (Gap) is reported in percentage.	164
6.3	Summary of results for 2D RCP instances with a speed control range of $[-6\%, +3\%]$ and a heading control range of $[-30^\circ, +30^\circ]$. All runtimes (Time) are reported in seconds while $\frac{1}{ A } \sum_{i \in A} t_i, \max_{i \in A} t_i$ and $\min_{i \in A} t_i$ are in hours. The optimality gap (Gap) is reported in percentage.	165

List of Algorithms

1	Pre-processing of aircraft pairs	66
2	Solution algorithm for the 2D ACRP	78
3	Solution algorithm for the lexicographic 2D+FL conflict resolution problem	80
4	Greedy-Recovery Algorithm	146
5	Solution algorithm for the 2D ACRP with Trajectory Recovery	159

List of Models

3.17	Non-convex 2D Formulation using Non-Linear Separation Conditions . . .	43
3.22	Non-convex 2D Formulation using Disjunctive Separation Conditions . . .	49
3.28	Non-convex 2D Formulation using Shadow Separation Conditions	52
4.10	Non-convex Complex Number Formulation	69
4.17	Non-convex Lexicographic 2D+FL Complex Number Formulation	71
4.18	MIQP 2D Formulation	73
4.25	MIQCP 2D Formulation	76
4.29	FL Assignment Formulation	79
5.10	Robust Counterpart Formulation of the ACRP	117
6.6	Heading-Discretised Disjunctive Formulation	142
6.15	Exact-Recovery	145
6.19	Non-convex 2D Formulation using Manoeuvre Control Variable	156

Chapter 1

Introduction

In this chapter, the main definitions and concepts that are necessary and used throughout the thesis are introduced. It starts with a brief history of aviation and air traffic control in Section 1.1 followed by the structure and the organisation of airspace in Section 1.2. The components of air traffic management are discussed in Section 1.3 while the details related to air traffic control are reviewed in Section 1.4. In Section 1.5, the role of aircraft conflict resolution is addressed in details. Finally, the air traffic control applications created via mathematical programming are highlighted in Section 1.6.

1.1 History of Aviation and Air Traffic Control

Since the creation of the first aircraft by Santos Dumont in 1908 (Mattos, 2004), the usage of aircraft as a way of transport increased rapidly. With the popularisation of air travel after World War I, the necessity of air traffic control becomes inherent. The first airport to hire air traffic controllers was the St. Louis Airport in Missouri in 1929 (Erotokritou, 2012). Modern systems of communication for air traffic control were first spotted at the Cleveland Airport where a control tower was placed on top of an old hangar. This facility was equipped with radio transmitting and receiving simple and rudimentary instruments were used. With those tools in their availability, air traffic controllers could communicate directly with the pilots of properly equipped aircraft. Four airliners were encouraged to start using the newly implemented systems in the USA.

The first setback in the structure of air traffic control started with World War II (Harrison, 1998). The impact was visible in the structure of airspace control and the aviation industry as a whole. Because of the overwhelming usage in the war to support and military advances, by 1943, the aviation industry becomes the largest

in the world and its importance could not be overstated. All resources and effort of the industry were put solely in the custody of the military reaching staggering 85% of the total budget. Most Air Traffic Control (ATC) technology dates back to WWII technology such as radar localisation, two-way radio communication and in specific regions, paper flight progress strips are still in use.

A series of unfortunate and tragic accidents in the airspace, including the Grand Canyon that killed 128 people, mid-air collision (Conway, 2004) prompted the funding and subsidy of air traffic control. The collision showed that many uncontrolled airspace areas represent a danger to the air service system and more effective surveillance should be implemented (Machol, 1995). After the multiple unfortunate mid-air collision, the responsibility for the American airspace was commissioned to a specific organisation, the Federal Aviation Administration (FAA) (Preston, 2005). Following that, some countries in Western Europe created the Eurocontrol organisation, merging the airspace in those regions hoping to increase its efficiency in the next decades.

The ATC system and aviation industry began to show the first glimpses of the issues related to overload in the early 1990s and then a series of unfortunate events brought a massive reduction and put the whole system in check. The 9/11 terrorist attack in the USA in 2001 (Lee, 2006) caused major concerns related to security and safety. Another event at the end of the second decade of the 21st century, the COVID-19 pandemic (Abu-Rayash and Dincer, 2020), reshaped the industry in terms of globalisation and how to improve safety for passengers in order to avoid contamination and spread over air travel. Figures 1.1 and 1.2 reveal how much the aviation industry was affected by the ongoing pandemic and how this compared to other life-changing events in history in Figure 1.3. Figure 1.2 shows that in all six regions highlighted there were setbacks caused by the pandemic. In North America, where the damage was the most drastic, there was a reduction of 41% of flights, 523 fewer passengers and revenue lost over 61 billion dollars. In the other regions, these proportions repeat, especially in Asia and the Pacific, where a major loss of revenue (over 39 billion dollars) and reduction of 35% of flights. International flights were more severed by the pandemic, given that many countries or regions have chosen to close their borders in order to protect their own citizens. In this scenario, Europe had a major setback with 65% fewer flights and a loss of 92 billion in revenue and 663 million fewer passengers. North America and Asia/Pacific also reported a major loss in revenue (89 and 32 billions, respectively). Asia and Pacific had the largest loss in flights: 74%. All those losses are summarised in Figure 1.3 where the steady growth

of the airspace industry had a drastic drop that has never been witnessed before surpassing major crisis such as the oil crisis, Iran-Iraq war and the SARS pandemic.

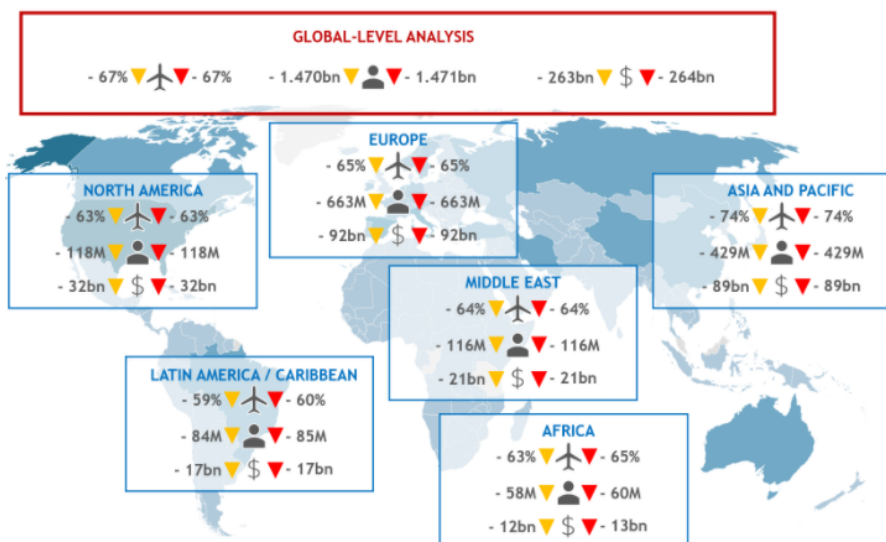


Figure 1.1: Impact of Covid-19 in international flights. In this picture, the "aircraft" symbol represents total number of trips, the "individual" symbol represents traveller and the dollar sign represents revenue. All three metrics are calculated over an year estimate. The upside triangle in red and orange represent decline of those metrics. All data presented in this chart is from domestic flights. (Bureau, 2020)

The structure of the airspace has changed over the years to accommodate the growing demand and capacity. In the next section, the details and components of the airspace structure are described.

1.2 Airspace Structure

Airspace is the part of the atmosphere under the control of a country or region that is directly above its territory, including maritime and inland. It differs from aerospace because the latter corresponds to the general term for Earth's atmosphere and outer space proximity. It is composed of two main parts: controlled airspace and uncontrolled airspace. The first corresponds to areas that are necessary for transportation, air traffic control and other air traffic services while it also has control over all aircraft decision involving their usage of air space. The second corresponds to an area out of the scope of air traffic controller, and aircraft flying in those regions rely on Visual Flight Rules (VFR) to guarantee flight safety.

By international laws, a country, state or region has complete and exclusive sovereignty over the airspace above its territory. This territory, for this matter, in-

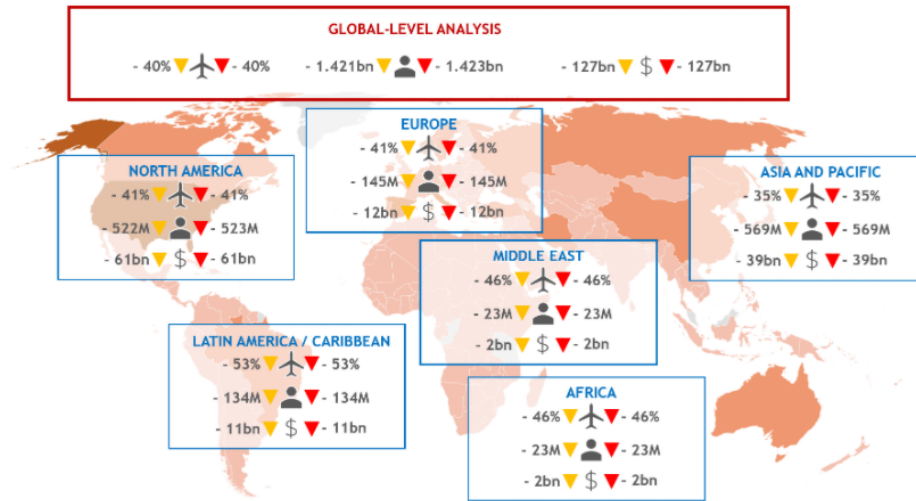


Figure 1.2: Impact of Covid-19 in domestic flights. In this picture, the "aircraft" symbol represents total number of trips, the "individual" symbol represents traveller and the dollar sign represents revenue. All three metrics are calculated over an year estimate. The upside triangle in red and orange represent decline of those metrics. All data presented in this chart is from domestic flights. (Bureau, 2020)

cludes the territorial waters surrounding it, which is around 12 nautical miles out of its cost area. Similar to the definition of "high sea", where the oceanic area outside the control of some countries is called "international water", the airspace that is not related to a country or region is called international airspace. This can be, however, disputed. By international agreement, a section of the international airspace can be claimed and controlled by specific countries and region. This is the case with most oceans. In those circumstances, regions such that are called flight information region. For example, the United States provides air traffic control over most of the Pacific Ocean, even though the airspace is international. In terms of vertical boundaries, there is not clear con-sense about the vertical limit of the airspace. The International Federation of Aeronautics created the Karman Line McDowell (2018) which defines that any airspace above 100 km is considered outer spaced. However, such a definition is disputable. For example, in the USA, any flight above 80 km is considered airspace.

The controlled airspace is any region of airspace where ATC service is provided. The airspace are separated into different levels of control which also define the classes of airspace. The main reasons behind this stratification of airspace are the higher traffic volume such as around airports, for instances, security and Instrumental Flight Rules (IFR). The ICAO divides the airspace into seven different classes where dif-

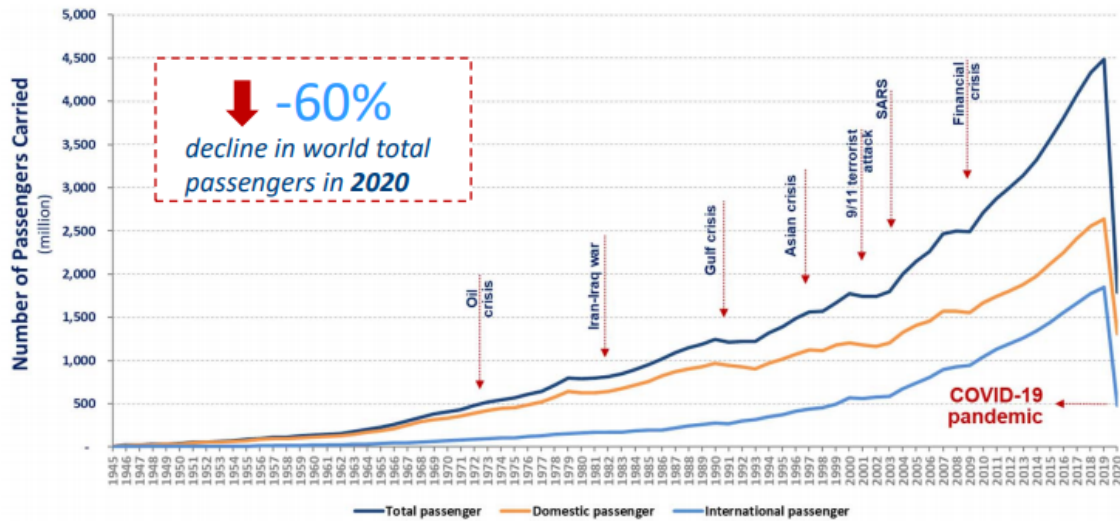


Figure 1.3: Evolution of airspace demand throughout the decades

ferent levels of control are established. The first six classes (A, B, C, D and E) are organised in decreasing the level of ATC regulation of flights. In those different classes, VFR and IFR are allowed to be used except for VFR in class A.

Class A is generally between 18,000 to 60,000 feet tall. It covers all areas overlying land and 12 nautical miles away from shorelines. It corresponds to less specific areas worldwide. Unless, given special authorisation, all operations in this class need to be processed under IFR. In Class B, it surrounds areas with busier airports. Each region re-organises and tailors according to its particular necessity. Once an aircraft enters the airspace, all published instrument procedures should be followed and respected. For Class C, the airspace is composed by the space above the airport elevation and surrounding areas such as operational control tower, radar approach control and a certain number of IFR operations. The space can also be individually tailored, the airspace consists of a surface that is usually 5 Nautical Miles (NM) radius and at most 10,000 feet above the airport. Upon entering this airspace, aircraft are required to establish two-way communication with ATC facilities and to maintain it throughout. In Class D, the proprieties of such airspace are similar to class D, with the sole difference regarding the arrival extensions for instrument approach procedures. For Class E, the remaining controlled airspace that does not belong to previous sectors is gathered into this Class. In these categories, if VFR aircraft are present, they are not required to establish continuous contact with ATC units. Class F does not exist in this context and the uncontrolled airspace is called Class G. Even though this is considered an uncontrolled region, it is expected that pilots operate under the same VFR conditions. Special use airspace of a special area of operation is used to name a

particular region of airspace that is used for special activities and therefore needs to be confined or limited from other activities. The most common cases are related to military and training purposes. The communication between aircraft, control towers and ground-based infrastructure are summarised in Figure 1.4.

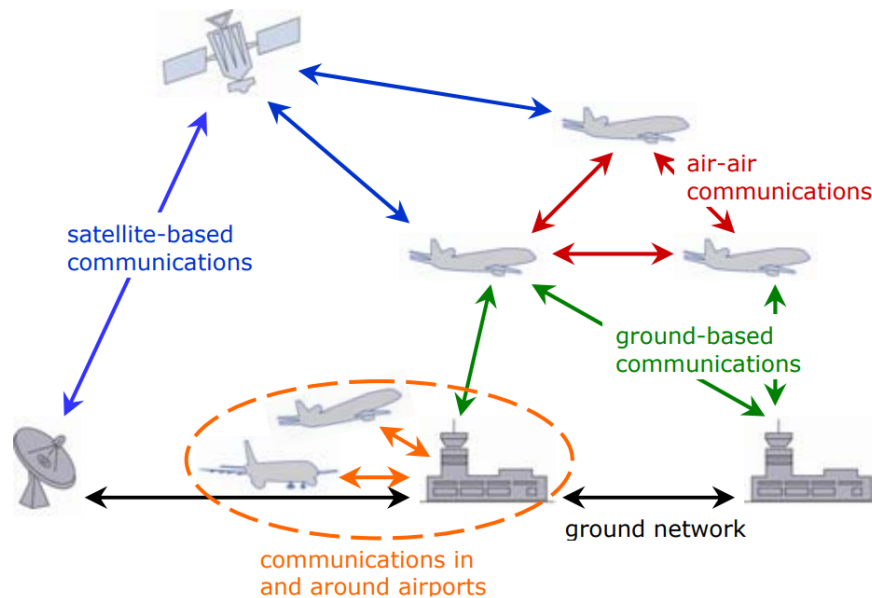


Figure 1.4: Communication between different units of airspace

One more aspect that also needs to be taken into account in air conflict resolution is how the aviation sector is impacting the environment and the weather. Aircraft has an emission range of greenhouse gases throughout the different stages of flight and most of those emissions are directly into the higher levels of the atmosphere. Such gases can have different effects (Schäfer et al., 2003), especially at this altitude when compared to the effect when emitted from ground level. At the same time, the noise pollution affects residents that are located in areas around the airport and surrounding areas, where the level of such noise has been considered to cause community annoyance. Furthermore, such noises can harm wildlife and biodiversity in areas surrounding airports.

Besides the structure of airspace, the management component has been through massive changes throughout the decades. In most cases, it is related to the imposition of regulations and rules to guarantee that all components are safe and protected. In the next section, details related to air traffic management are neglected.

1.3 Air Traffic Management

Air traffic management is the integrated management of air traffic and airspace through services in collaboration with all stakeholders involved and it compasses airborne and ground-based capacities. The combination of air traffic services and ground-based components are very complex. Their safety and efficiency throughout the whole operation and stages of aircraft flight can also be challenging. Air Traffic Management (ATM) encompasses all systems that assist aircraft to depart from an aerodrome, transit airspace, and land at a destination aerodrome, including ATC, Air Traffic System (ATS), Available Seat Miles (ASM), and Air Traffic Flow Management (ATFM). Figure 1.5 provides an overview of an aircraft move between different layers.

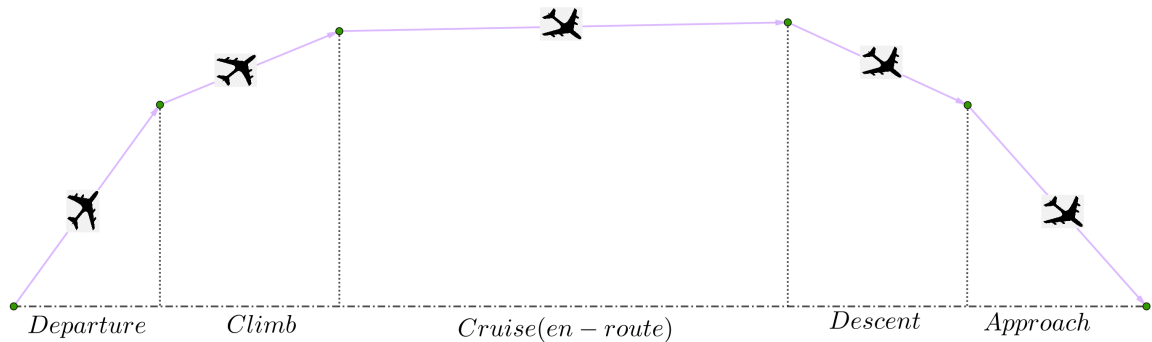


Figure 1.5: Different stages in ATC

ATS has the purpose of overseeing the safety in traffic flow (facilitated by the ATC). It also provides the information required for pilots and crew (via Flight Information Service (FIS)). In the case of emergencies, alerting service (such as Search And Rescue (SAR)) can also be provided. Activities in ATC are mostly performed by air traffic controllers and their function is to prevent loss of separation between aircraft and prevent eventual mid-air collisions. This is achieved by applying the appropriate separation standards and issuing clearances and instructions to supervise the traffic flow. ATS is based on tactical interventions by the controllers and direct communication with the flight crews throughout the flights.

ATFM has as its primary objective to regulate the flow of aircraft as efficiently as possible, by avoiding congestion in most controlled sectors. Moreover, it needs to guarantee smooth functioning of ATS. One of the alternative approaches to this is by controlling the demand and planning the control capacities to be applied correctly to

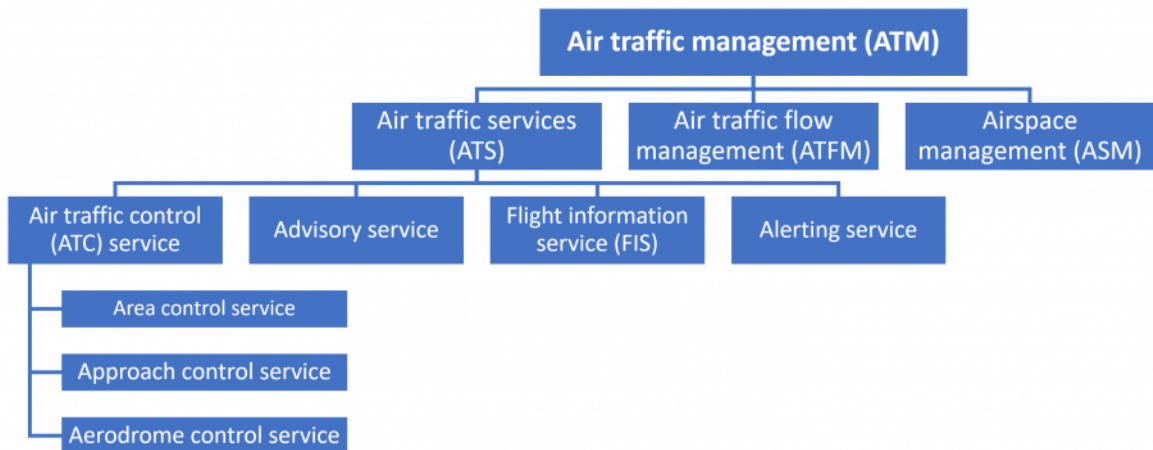


Figure 1.6: ATM Structure and its subdivisions

meet such demand. As a vital component in the flight plan management, ATFM behaves as a pre-tactical strategy. Even though it does not affect the current situation, by setting up the path for aircraft, its operation can influence future airspace configurations. ASM is in charge to manage the airspace itself as efficiently as possible to satisfy all the stakeholders, both civil and military. This service concerns both the way airspace is allocated and how it is organised to provide and guarantee continuity of air traffic services. The diagram (see Figure 1.6) shows the structure of ATM and explains the relations between ATM, ATS and ATC.

The increasing emphasis of modern ATM is on assistance and supporting systems that allow an aircraft to operate without interference by air traffic controller or without any impact in the trajectory of neighbouring aircraft. ATC systems have traditionally been developed by individual groups that concentrated on their requirements, creating different levels of service and capability around the world and limiting a unified service. Most Air Navigation Service Provider System (ANSP) do not provide a ATC service that matches the capabilities of modern aircraft, therefore ICAO has unified them and developed the Aviation System Block Upgrades (ASBU), for example, in the Pacific region, the ICAO Regional Office in Bangkok, Thailand is responsible to provide this type of service for all countries in the region. It is developing a Seamless ATM Plan by 2020, which is intended to change the paradigm for ATM upgrades in the world's busiest aviation region by incorporating revenue passenger Kilometres as a new metric of performance.

Among the main challenges ATM faces in day-to-day operations, the most common is traffic and congestion. The volume of air traffic demand placed on the airspace system can change very drastically based on several factors such as weather condi-

tions. For instance, each aircraft must touch down safely, exit the runway so that another aircraft can use it safely. This whole process can last up to four minutes. In this scenario, each runway can take up to 30 arrivals per hours in good weather. However, a significant problem starts when airlines schedule more flights surpassing the airport capacity. When this happens, aircraft must be delayed in the air until clearance to the runway is given. Despite environmental concerns and cost implications, aircraft waiting for landing would circumnavigate around the airport as common manoeuvres. However, like aviation and air traffic control progress over the years, such circumstances can be carefully predicted and countermeasure can be applied in order to avoid these problems. In some circumstances, planes can be delayed before they even take off or reduced their speed mid-flight to reduce the number of holding aircraft drastically. All those phenomena are related to congestion and hence, flight cancellation and delays. With growing traffic, delays increased by 70% between 2012 and 2017 in the USA only. In China, the average delays in domestic flight saw a significant increase of more than half of its usual amount in 2017 and most delays are around 15 minutes per flight. Finally, Eurocontrol reported an increase of 17.6 billion euros due to delays applied to flights in cruise stage and most of those cases were related to breaches of capacity in many airports.

ATC is a major part of air traffic management and it comprehends all the effort in order to avoid loss of separation and eventual collisions. In the next section, details related to this field are discussed in depth.

1.4 Air Traffic Control

The primary technique to control an airport and its surrounding is via visual observation from airport towers. From those posts, air traffic controllers are responsible to provide efficient instructions for aircraft on the taxiways and runways or airborne within 5 to 10 nautical miles depending on its specificity. The responsibilities of control towers are subdivided into three categories: air control, ground control and flight data. Most major complex airports have all different targets delegated within the tower environment, while smaller airport might have only one or two of those goals addressed locally. In this case, Remote Virtual Tower (RVT) is used instead.

Ground control is responsible for taxiways, runways, holding areas and some transitional intersections where aircraft arrives, vacate a runway or departure gate. Tower control (or air control) is in charge of occupied and active runways, by providing clearance for runways for take-off and landing. Besides ground and tower control, clearance

is also an important step in air traffic control. Clearance data are typically contain details relating to route clearance, therefore aircraft can start taxiing. The primary responsibility is to ensure that the aircraft has information related to weather conditions, airport conditions, route conditions after departure and time restriction for the flight.

En-route control is the control performed when aircraft are on the cruise or en-route stage (between the areas of jurisdiction of two or more airports). En-route air traffic controllers are responsible to provide clearances and instructions for airborne and ultimately transfer the control to another sector. According to the ICAO, they are also a set of separation standards to define the minimum distance between aircraft. Each ANSP is responsible for thousands of square miles of airspace and the airports within such region. Between these activities, they assign all manoeuvres necessary while guaranteeing that minimum separation is always ensured. At the same time, they are in charge to fully maximise the usage of the air routes. However, this task can be quite challenging under higher demand, such as crossing traffic, severe weather, special missions that might utilise airspace allocation of significant large areas and dense traffic. Upon arrival at its destination, the pilot and crew are informed regarding altitude requirements and instructions regarding their landing. At the same time, when an aircraft is reaching the "boundaries" of a centre's control area, the process of "handing over" involves the transfer of identification and details between them, which can be seamless as "silent handovers" or in a more dynamic approach involving direct communication between controllers and crew.

In ATC, radar coverage is a vital part of the system. Considering that centres control large areas at the time, radars provide the ability to identify any aircraft around 200 nautical miles around the radar antenna. Besides that, Terminal Radar Approach CONtrol (TRACON) can also be used to obtain a better profile of traffic and even fill the gap in areas that are not fully covered by conventional radars. In the USA, for instance, most aircraft are covered by radar at higher altitudes (even multiple radar systems). However, at a lower altitude, coverage is not always imposed or present, especially in unpressurised aircraft. An air traffic controller has access to data from different radar systems and many reports coming from direct aircraft. This leads to an excessive amount of data, that being fully processed, requires assistance from automated systems that polish and filter the data received and displays it in an effective and simple format. Because of the lack of radar systems for oceanic areas, most of the control is done by procedural control. In these cases, aircraft position, time, altitude, distance and speed are reported to ensure separation. This process

ends up in a larger separation distance between aircraft over oceanic routes which consequently reduces the overall capacity potential. Some nations have developed automatic dependent surveillance that works in the opposite way of radar. Aircraft with those systems sends their position as reports to air traffic controllers. The frequency of such reports can be requested to be changed by air traffic controllers, even though it is not a standard operation, unless in emergencies. This system is quite efficient because it hinders the necessity of radar systems around it. This technology is already in use in the portion of North Atlantic and the Pacific Ocean by many countries sharing the responsibility for that area. A special type of radar system is the Precision Approach Radar (PAR) that military controllers used to assist pilot before landing instead of relying on airborne equipment that might not be available because of visibility conditions. In case of search and rescue, the radar archive system Radar Advisory Service (RAS) can be used to record all information exchanged over communication, that can also be recorded and saved in case of accidents and crash as well as radar maintenance.

The future of ATM is filled with promises with more assistance and privatisation of the sectors. In the United States, the Next Generation Air Transportation System (NextGen) is expected to assume overhaul in the national airspace system and the free flight is a trend that has more and more acceptance in many industry sectors, hence, more sectors are inclined to a slow transition to such forms of air traffic control. In Europe, a similar approach is also expected via the Single European Sky ATM Research (SESAR) which is expected to develop technologies, methods and procedures to improve overall control of the airspace and reduce congestion over such a dynamic and dense region. A similar project is the ONESky (ONESky) which is an attempt at a unified air traffic control system covering the whole continent of Australia, a vast part of the western Indian Ocean and New Zealand. It is a partnership between Airservices Australia and the Department of Defence, replacing existing air traffic management systems with an advanced integrated system known as the Civil-Military ATM System, Australia (CMATS). It is expected to deliver more efficient air services, support future air traffic growth and enhance national security. The program is expected to deliver more than AUD 1.2 billion of economic benefits to Australian airspace users over 20 years.

All those previous improvements might require the participation of private sectors to partially support them financially. In the USA, for instance, ATC is already partially funded by private companies. However, there is a risk with the inconsistency which can demise the implementation of new developments. In those cases, the

government corporation is a viable solution. In Germany, for example, this model has been implemented and funding is guaranteed via public fundings. In the United Kingdom, another system is applied, based on a for-profit corporation, but many issues have caused the system to have a major failure in 2014 (Adler et al., 2014). In Canada, most of the system is already controlled by a private organisation, with the creation of Nav Canada. This organisation is a private, non-profit organisation that has reduced costs and implemented new technologies by simplifying the bureaucratic process inside ATC.

A major part of the job of an air traffic controller is to solve any given conflict. This makes their jobs highly intense and stressful. Following up, the different components of air traffic control are addressed and discussed thoroughly.

1.5 Aircraft Conflict Resolution

ATC is an extremely dynamic and constrained environment where many decisions need to be taken in a short amount of time. Adopting automation within such an environment can be vital to reduce controller workload and improve airspace capacity (Durand et al., 1997; Barnier and Allignol, 2009; Rey et al., 2016). With the expansion of air travel, it is expected that higher demand will lead to more crowded airspace. This is expected to a higher workload for air traffic controllers. With a higher level of automation, it is expected that this workload is diminished. Automated systems are designed to provide aid and support in difficult configurations. In order to have such systems operating in perfect conditions, it is necessary to infuse these systems with optimisation. Therefore, it can be guaranteed that the solutions provided will be free-of-errors and precise.

Traditional methods for air traffic control have been exhaustively used and are reaching their limits, hence automated approaches are receiving significant and growing attention in the field (Vela et al., 2009b). The International Civil Aviation Organisation (ICAO) determines all regulations related to civil aviation (ICAO, 2010). One of its main roles is to set separation standards for commercial aviation. We focus on aircraft separation for en-route traffic. During the cruise stage, separation conditions require a minimum of 5 Nautical Miles (NM) horizontally or 1000 feet (ft.) vertically between any pair of aircraft. A conflict between two or more aircraft is a loss of separation between these aircraft (see Figure 1.7). Air traffic networks are organised in flights levels, which are separated by at least 1000 ft. (see Figure 1.8),

hence during the cruise stage, most conflicts occur among aircraft flying at the same flight level.

Congested air traffic networks can lead to the loss of separation between aircraft which impairs flight safety and may result in collisions. The Aircraft Conflict Resolution Problem (ACRP) can be formulated as an optimisation problem in which the objective is to find least-deviating conflict-free trajectories for a set of aircraft. Different strategies have been used to address this problem based on the type of deconfliction manoeuvres available, namely: speed control (acceleration or deceleration), heading control, vertical control (flight level reassignment) or a combination of these manoeuvres.

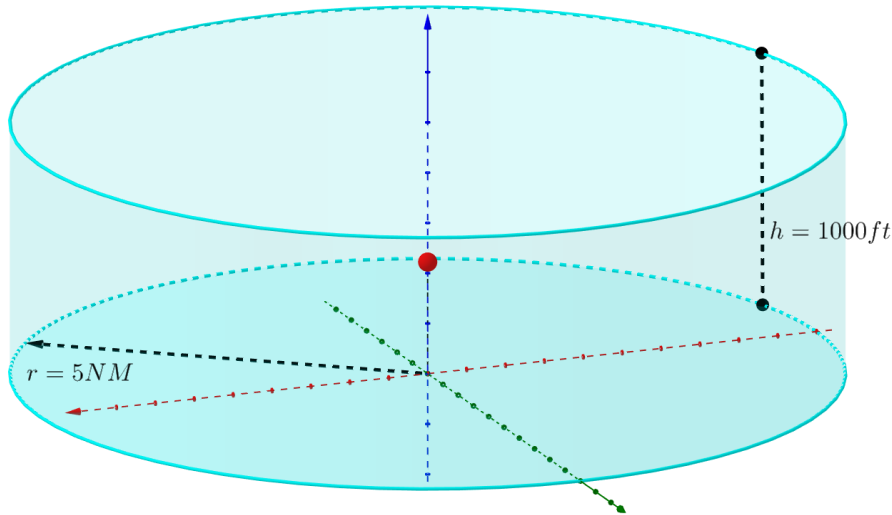


Figure 1.7: Aircraft separation standards. The aircraft is represented by the red dot. By ICAO standards, the horizontal separation required is at least 5 NM of horizontal separation and 1000 ft. of vertical separation.

One more aspect that also needs to be taken into account in air conflict resolution is how the aviation sector is impacting the environment, and the weather. Aircraft has an emission range of greenhouse gases throughout the different stages of flight and most of those emissions are directly into the higher levels of the atmosphere. Such gases can have different effects (Schäfer et al., 2003), especially at this altitude when compared to the effect when emitted from ground level. At the same time, the noise pollution affects residents that are located in areas around the airport and surrounding areas, where the noise level has been considered to cause community annoyance. Furthermore, such noises can harm wildlife and biodiversity in areas surrounding airports.

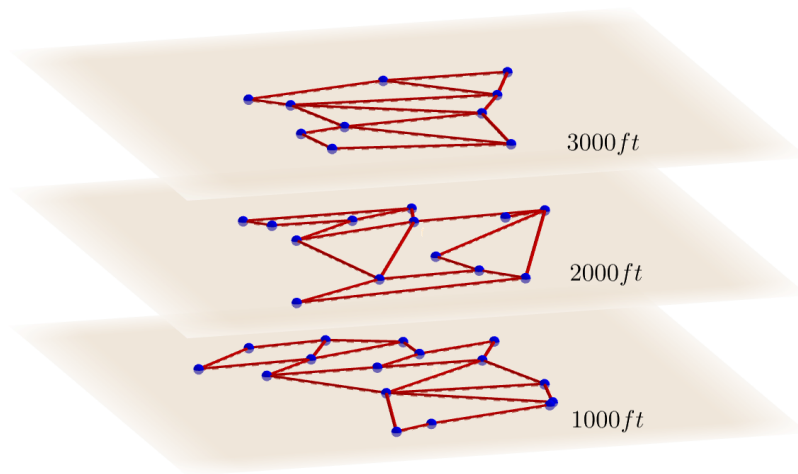


Figure 1.8: Airspace Structure. The airspace is structured in layers that are multiple of 1000 ft. In each layer, there are referential points used to assist in navigation, referred as waypoints.

1.6 Mathematical Programming Methods for Aircraft Conflict Resolution

There are many different approaches to solve the aircraft conflict resolution problem. In the literature, examples are using diverse types of heuristics, meta-heuristics, genetic algorithms, graph theory, etc.. The main challenge is to obtain a method that supports all the components and at the same time is capable of providing feasible solutions in a matter of seconds. The ACRP is typically formulated as a non-convex, non-linear optimisation problem which is challenging to solve for instances with a large number of aircraft (which is common in denser areas). Most of the mathematical programming approaches for the ACRP require some form of linearisation, variable or space discretisation. Although they can provide high-quality solutions, they might not represent a complete representation of what is indeed necessary to solve such instances. In this thesis, mathematical programming methods for the ACRP are explored and it is applied throughout all the formulations created.

For that, many of the intrinsic characteristics of the problem will be maintained and novel reformulations that avoid trigonometric components and that provide more compact formulations for separation constraints are explored. Based on that, the

aircraft trajectory will be studied and discussed as extensions such as trajectory recovery and trajectory prediction under uncertainty.

Even though this is a simplistic approach and it differs from the continuous smooth trajectories used in different techniques, the goal in this thesis is global optimisation without any major simplifications and focusing on mathematical approaches. Therefore, the avoidance corresponds to the set of manoeuvres necessary to be taken in order for avoiding loss of separation conditions. This means, speed changes, heading angle and altitude (which are the set of manoeuvres available) to guarantee that the safety and security of all aircraft are ensured. The trajectory recovery requires a set of manoeuvres that restore the initial conditions of the aircraft to guarantee that the nominal trajectory is maintained. It is important to highlight that such division is common in mathematical programming approaches, but they are not the only alternative to model aircraft trajectory. In addition, stochastic elements have to be taken into account. Most formulations consider all variable as deterministic as there is no source of uncertainty. Given the impact of the weather on airspace activities and the inevitable existence of measurement errors, such issues can cause a disturbance in the aircraft trajectory and it requires to be handled properly.

This thesis has four main aims: i) scalable global optimisation methods based on mathematical programming; ii) formal analysis of the aircraft separation conditions and conflict-free trajectories characterisations for the deterministic version of the ACRP, iii) incorporating uncertainty on trajectory prediction within mathematical programming based approaches for the ACRP and iv) identifying to what extent richer mathematical programming formulations can be developed to accommodate realist ATC operations.

In order to achieve those aims, in this thesis, a series of novel models are proposed to help bridge some of the gaps presented in the literature. First, an extensive literature review of major contributions in air traffic management and air traffic control is presented in Chapter 2. Following that, the classical state-of-art formulations for ACRP using mathematical programming are presented in Chapter 3 where numerical results highlight their advantages and limitations. Then, an exact constraint generation algorithm is presented to solve the deterministic ACRP using the complex number formulation in Chapter 4. An analytical solution for the special two aircraft conflict is also provided. In Chapter 5, randomness is incorporate into ACRP using different levels of robustness and a different size of uncertainty sets. The performances of the proposed model are explored as well as the analysis of the feasibility of the instances based on a different level of robustness and dimension of uncertainty sets. In

Chapter 6, two different alternatives to address trajectory recovery are featured. The first is composed of a two-stage algorithm with continuous speed and discretised angle adapted and the recovery stage where time is discretised. It is also shown how this can be improved by incorporating continuous heading angle and manoeuvre variable into the avoidance stage and incorporate into an iterative model revealing a trade-off between deviation in the avoidance stage and recovery time in the recovery stage. The thesis is concluded by summarising the main contributions, the main results and the prospective research targets in Chapter 7.

Chapter 2

Literature Review

In this chapter, optimisations methods for conflict resolution are reviewed. It starts off with research dedicated to air traffic management, followed by its direct application and impact on optimisation in air traffic control. In this case, the focus is on conflict resolution and earlier research that solidified and paved the way for recent trends in the field is emphasized. Finally, specific sub-fields as explored such as trajectory recovery and conflict resolution under uncertainty. The main objective is to highlight the state-of-the-art research currently present in the literature and outline research gaps, which will be the focus of this thesis.

2.1 Introduction

As many factors contributed to its increase in popularity and accessibility, higher demand in air transport ultimately results in higher demands in aerospace systems. Except for situations like the recent COVID-19 pandemic or terrorism attacks as September 11th in New York City, USA, the demand for air travel has been steadily increasing. With those components, airport operation and air traffic management became a vital point to guarantee high levels of safety and efficiency for millions of passengers worldwide. Among factors that impact passengers, delays are the most common consequence of overload in such systems and as reported by the Association of European Airlines (AEA) more than 45% of those delays are caused by airport operations and ATC (Wu and Caves, 2002). European company Lufthansa reported that the amount of fuel consumed by airborne holding surpassed 26 thousand tons and United Airlines claimed that 20 million dollars were consumed by inefficient air traffic services.

These numbers highlight that ATM and ATC services are intrinsic for the optimal operation of the airspace system and therefore vital for the financial success of this

industry. A report from EuroControl reveals that around 80% of the delays are caused by insufficient operational capabilities in ATC and statistical studies showed that an accumulated total of 7.5 million flights per year were delayed by more than 15 minutes. It is clear that the operation and efficiency of ATS are a direct consequence of how the utilisation of those system resources are applied. In order to improve capacity, those systems need to be upgraded and this process requires massive investments in research. Earlier results have already shown positive outcomes. A summary of how the literature review in airspace is defined can be seen in Figure 2.1.

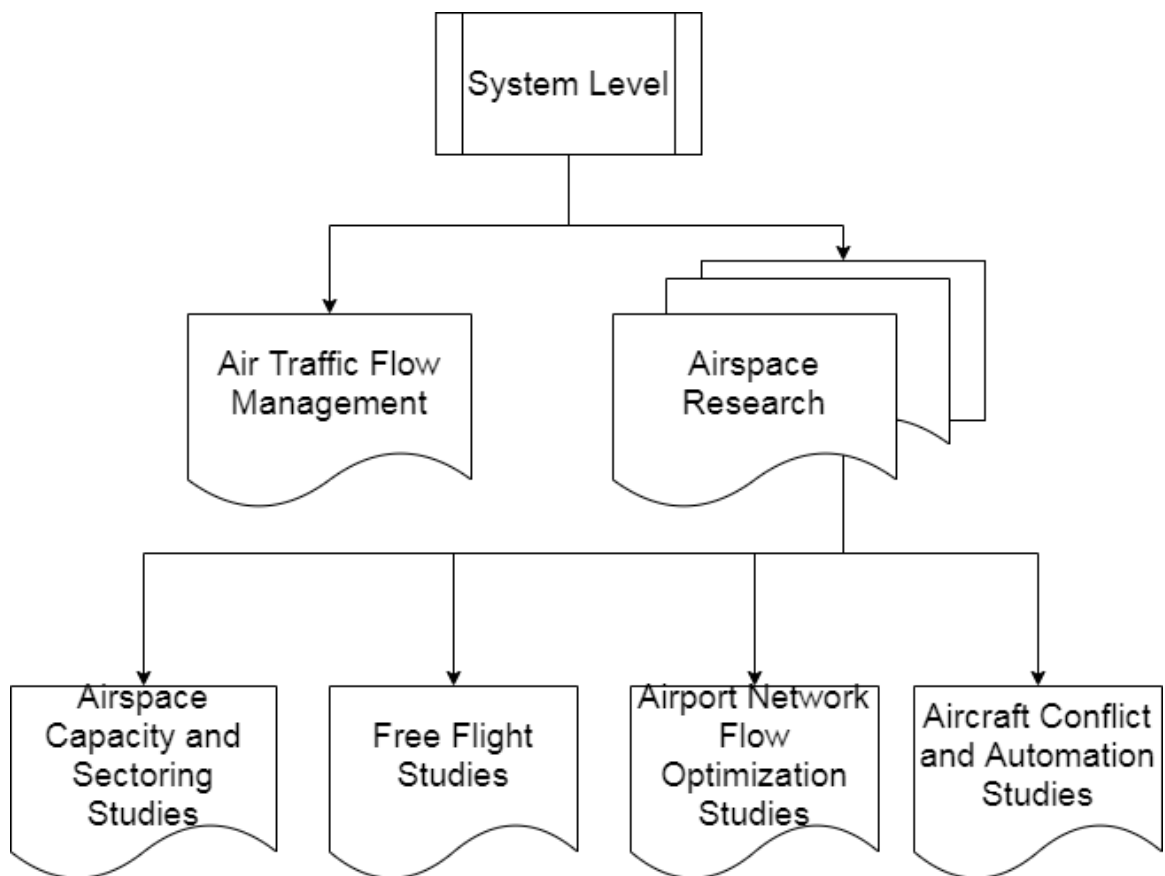


Figure 2.1: Airspace and Air Traffic Research Hierarchy

The structure of air transport can be synthesised in Figure 2.2. It is composed of airspace, which is systematically layered and separated, airports and aircraft operating between airports. While airport management handles the airport section, ATFM handle the airspace and all aircraft in movement and their manoeuvres as they are effectively controlled by the ATC. The jurisdiction of ATC is divided into section such as inert stage, which handles operations in the airspace and aircraft movements and terminal which control the area of roughly 50 miles around airports (Horonjeff et al.,

2010). In the former, there are four sub-areas such as airspace capacity, conflict, free flight and airport network flow. In this thesis, the focus is mostly on the efforts on ATC aspects of ATM.

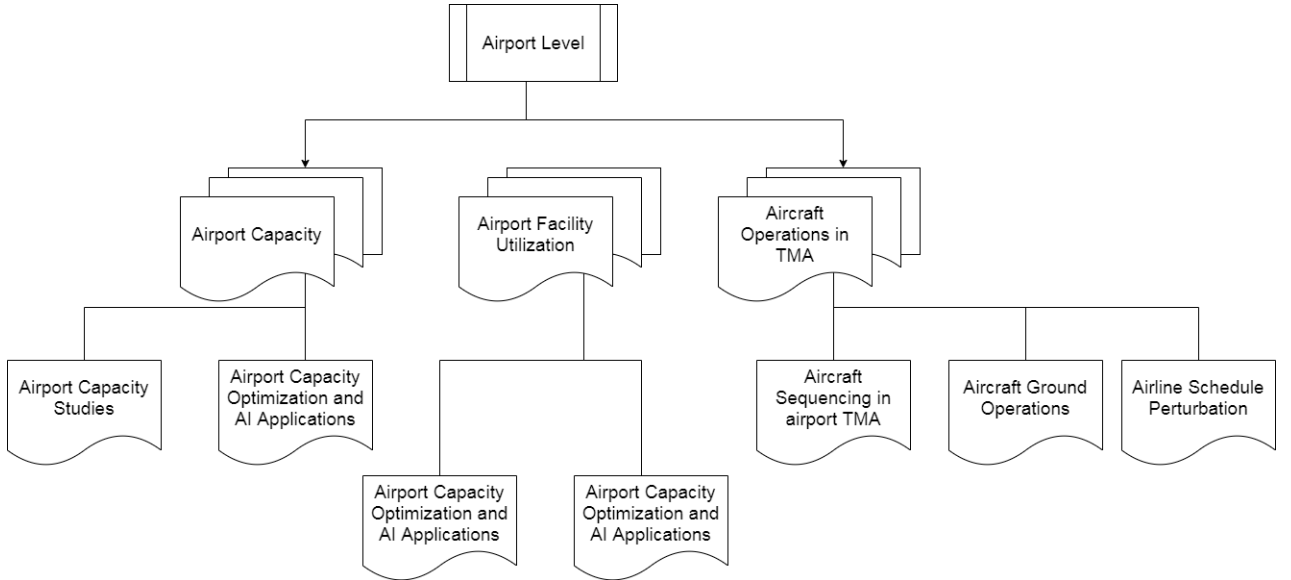


Figure 2.2: Airport System Hierarchy

This chapter is organised as follows: in Section 2.2, the air traffic management is discussed; further investigation in air traffic control by reviewing the state-of-the-art literature is presented in Section 2.3. Further, the focus is on conflict resolution in Section 2.4. At last, in Subsection 2.4.1, early studies on conflict detection are reviewed from traditional research approaches where heuristics were initially proposed to handle such problem followed by recent trends using mathematical programming. Specific topics such as models based on mathematical programming for deterministic optimisation are addressed in Subsection 2.4.2 and advanced formulations such as stochastic and robust optimisation applied to ACRP and trajectory recovery in Subsection 2.4.3.

2.2 Air Traffic Management

In this section, the definitions and concepts utilised in air traffic management are described and contextualised to how this is relevant to the research of this thesis.

Air traffic management ATM, which is the sub-field in aviation, encompasses all the systems that are used in assistance for aircraft operation. They range from depart from aerodrome (such as runways or heliports) to transit and to land at a

destination. It is composed of a series of different elements such as air traffic services, air traffic control, airspace management, etc. This thesis focuses exclusively on air traffic control performance during the cruise stage. For that reason, two subsystems deserve some emphasises: ATFM and ATC. Therefore, all components related to take-off, ascending, descending, and landing will not be mentioned unless they are relevant to cruise stage. ATFM is the focus of this section while ATC will be discussed next.

The ATFM is defined as the sector of air system responsible to control the traffic that is established between aircraft. This is directly influenced by the airports and the airspace capacity. Considering the operation of airports, their performance is heavily influenced by operations in other airports in its vicinity and through the circulation of people and goods. This leads to a continuous flux of aircraft between airports in a certain amount of time and this is influenced by weather conditions and other causes, and it might result in delays and flight cancellations. The airspace capacity is controlled by the ATFM itself. Its purpose is to allocate airspace capacity to all users to guarantee that any negative impact related to delay and airport capacity is mitigated.

ATFM problems have been studied using different models in the literature and they were initially proposed as deterministic models. In models such as proposed by Andreatta and Romanin-Jacur (1987), Richetta and Odoni (1993), Bianco and Bielli (1992) and Terrab and Odoni (1993), the authors proposed a series of model where the decision was defined by deterministic events only. The results obtained revealed that even though significant and applicable, such methodologies could not encapsulate the core parts of the problem and such solutions were not fully capable of replicating the real situation. As stated by Odoni (1987), ATFM should take into account stochastic and deterministic features and strategies by means of simulations as a way to incorporate unexpected and random behaviour. Later, dynamic ground-holding assignment and stochastic models were proposed by Terrab and Odoni (1993), Richetta (1995), Richetta and Odoni (1993), Vranas et al. (1994b), Vranas et al. (1994a), Tomic and Babic (1995) and Richetta and Odoni (1994). In Terrab and Odoni (1993), the authors addressed the case where a single airport is responsible to schedule aircraft arriving from different sources by comparison of deterministic and stochastic version. In the former, a minimum cost flow algorithm was used while the stochastic version was reduced to heuristics. Richetta (1995) proposed heuristics by stochastic linear programming by using the probabilistic forecast of the airport landing. Richetta

and Odoni (1993) and Richetta and Odoni (1994) proposed a stochastic model using a single airport initially using heuristics to handle larger instances and providing near-optimal solutions. Further, it improved the formulation by incorporating the ground-control and by handling the aircraft into two groups instead of single flights. In papers by Vranas et al. (1994a) and Vranas et al. (1994b), generic integer programming models were proposed by addressing a static version of this problem, but subject dynamic behaviour in time horizon aspect such as by changing weather and modifying the runway use. Lastly, in Tomic and Babić (1995), many other efforts and projects to solve such problems were revised and summarised. The common trend of those papers is a single airport usage, where multiple sources would send many aircraft towards a unique target. The main challenge was the management required to supervise the waiting time and runway usage of such airspace around that specific airport. Therefore, the solutions were decentralised for each aircraft. More recently, the effort has shifted towards optimisation of air traffic control using a network of airports inside a planning framework horizon. In Teodorović and Babić (1993), the authors applied a fuzzy interference technique to consider landing operations over a time period framework in a model, where the delay costs were minimised. Navazio and Romanin-Jacur (1998) proposed an integer linear programming model to handle this problem and incorporating preceding flights and multiple connections. Overall, this study has observed that a crucial point in the efficiency of ATFM is to acknowledge the short-term airport capacity referred to as Airport Acceptance Rate (AAR). However, this has been a hurdle and in order to predict and correct address it in flow management problems, deterministic approaches such as Vranas et al. (1994a) and Andreatta and Romanin-Jacur (1987) have been attempted. As discussed by Vranas et al. (1994b), the flow management problem is similar to any general flow problem, with the extra component that the capacity of the destination is fundamental to obtain a feasible solution. Therefore, the correct simulation of AAR is vital to its efficiency. More importantly, according to Vranas et al. (1994b), such simulation is extremely imperative to ATFM, especially how precise it can forecast such conditions. There are many factors that will corroborate to reliable simulations, *i.e.* measurements and weather conditions, which leads to stochastic models that are more effective in encapsulating those particularities as expressed by Peterson et al. (1995). In Shumsky (1998), however, the time of those AAR estimates is also very important. Because it is a forecast, imprecision increases as time passes by and therefore it can cause an increase in delay costs. Therefore, the authors proposed that AAR could be

provided at optimised time intervals to account for future events. Nevertheless, this problem still needs extra investigation and future research.

Another relevant discussion in ATFM strategies are the equity across users. For each aircraft, the delays are calculated by unit delay costs, delays probabilities and flight priorities, and all those factors can vary simultaneously and independently. In the literature, a common process to prioritise airport usages is via a first-in-first-out rule, which is not optimal but a fair choice. Similarly, methods to control en-route flight time can be used to improve ATFM performance, given that prior to that, as explained by Vranas et al. (1994b), Zenios (1991) and Janić (1997), simple assumptions were adopted such as constant en-route flight time approaches. Models involving airspace and air traffic control can be used as a tool to calculate an estimate of free flight. Nevertheless, those models, especially ATC can compensate or hinder even further possible delays caused by ground controls, which make those options less reliable as tools to balance the delay costs for all users and further research is still necessary.

While the effort into ATFM involving airport connection has been extensive, research into the increasing airspace capacity is still a growing sector that has received more attention in recent years. In a report by EuroControl, it is suggested that safety, capacity and assisting technologies are necessary. Some examples can be seen in the EC plan for the twenty-first century, such as dynamic sectoring of airspace in Europe and air traffic service route network to improve airspace capacity. In Zenios (1991), an airport network was proposed to monitor airspace congestion and optimise air traffic flow. Despite the inherent complexity, his model was a prototype to simulate route assignment in congested airspace. In the late 90s, EuroControl developed a program aiming to model the structure and air traffic flow in the region called European Air Traffic Control Harmonization and Integration Programme (EATCHIP). Another system is the System for Traffic Assignment and Analysis at a Macroscopic Level (SAAM) provided an integrated visual for macroscopic design, evaluation and presentation in airspace and airport level.

The general objective in airspace network modelling is minimisation of congestion costs. Due to its random nature, a stochastic and dynamic behaviour is observed, such as in costs, that are highly unstable and therefore, this condition makes it a hurdle to quantify such differences. Alternative formats of cost minimisation can be seen as fuel consumption such as in the model proposed by Janic (1994), whose approach served as a base to airspace congestion model from an econometric perspective. In Janić and Tošić (1991), the author proposed a model for airspace capacity based on

mathematical programming while Tofukuji (1996) and Tofukuji (1997) proposed a similar model, but using human factors, such as air traffic controller efficiency and workload, as components. Those efforts highlighted how airspace capacity is crucial to optimise the efficiency of ATFM and ATC.

In a scenario where air travel increases drastically, the airspace capacity will reach a point where the current measure will ultimately become obsolete and new techniques like the concept of free flight might emerge. The objective for this is to make the most of airspace capacity in order to improve overall efficiency by removing the necessity of a centralised control system that can eventually hinder its successful operation. In this system, flight operators and pilots are given more independence to choose optimal manoeuvres based on the set of aircraft that is surrounded by, instead of a global solution involving the whole airspace. Therefore, the solution is more localised and improvements can be achieved easier. The success of free flight relies heavily on the performance of many advisory systems such as trajectory and conflict resolution. Currently, some systems (EATCHIP by EuroControl, for instance) have shown promising attempts of usage of those systems and with the perspective of advance in avionics and communications systems, air traffic control and air traffic management can change quite drastically.

Assisted systems as guidance for aircraft have been researched by Niedringhaus (1995), whose model is an advisory system that established the foundation for management and control for an aircraft. An alternative approach by Ratcliffe (1995) was proposed by accounting clearance in aircraft routes by also considering conflict probabilities and resolutions, and even further, with the advance of avionics those technologies can become even safer.

2.3 Air Traffic Control

ATC is the part of the air service system that is operated by a ground-based operator called air traffic controllers. Their main function is to provide a set of manoeuvres and information to aircraft on the ground and in controlled areas. The main goal is to prevent collisions, therefore, increase the safety and security in air traffic (Nolan, 2010), especially in civil aviation. The ICAO provides a set of rules and metrics that should be followed worldwide while each country or region decides on how to impose them.

Air traffic controllers observe the location and position of each aircraft in their specific airspace region via radar measurements and communication with the crew.

Based on these data, they enforce a set of rules to guarantee enough separation between aircraft at all times. Most countries provide air traffic control services to private, military and commercial aircraft within their airspace. Although they have a great authority to suggest manoeuvres and changes in each aircraft's path, pilots have the final decision and in an emergency can override the ATC instructions to maintain the safe operation of their respective aircraft. Therefore, air traffic controllers have an immensely important job, but mainly as a consulting role. In this thesis, the focus is exclusively on civil aviation.

Air traffic control was introduced in the earlier 1920s at the Croydon Airport in London operating in rudimentary conditions and providing only simple information to aircraft in its vicinity. A few years later, in the USA, airmail radio stations were established after WWI as a tool to direct and track the position of the aircraft and it was later incorporated into flight service stations. This was used as the base configuration for airport control towers, controlling arrivals and departures at Cleveland in 1930, the first of its kind. With the advance of radar to monitor and control denser regions, airport tower becomes a popular presence in airports, especially in North America. In 1935, the first route completely assisted by the air traffic control centre was inaugurated in Newark, New Jersey, followed by Cleveland and Chicago in 1936 (Preston, 2005).

In the earlier stages, most of the air traffic control was established by basic visual rules and done only during daytime using clear flight conditions. A common practice was "see and be seen" and it was used as the main method of imposing separation. According to this method, pilots were required to fly only under conditions such as clear of any clouds and only in areas where the visibility was at least 3 miles. Nowadays there are two forms of control available as described by Gaertner and Lutz (2016): IFR, as the rules under conditions in which flight by outside visual are not considered feasible or safe; and VFR which encompasses regulations based on the capacity of pilots and crew to directly visualise outside the aircraft and use such input as the main source of their decisions. VFR was based on those initial conditions and it is still in use favourably over IFR. Since the aircraft used by the airlines at the early stages were relatively slow and VFR was enough, the establishment of an organised air traffic control system was not necessary. Therefore, it did not exist until late 1930, where the capability of aircraft to fly at night and in marginal weather conditions had improved tremendously. Hence, overall organisation and systematisation were deemed important. Instrumentation that would permit pilots to control the aircraft without visual reference (early stages of IFR) were developed and in addition, a system of

ground-based radio navigation was being constructed to permit pilots to navigate without ground reference.

Future prospective in air traffic control is to develop and merge into the NextGen NextGen (Darr et al., 2008). It has been developed by the FAA in the USA as a strategy to overhaul the national airspace system. In its full operation, it will have the capability to integrate satellite-based navigation and communication technologies. It is an attempt to improve capacity and transform it into a satellite-based system. The idea is to convert such system into a fully automated and assistance-oriented system to work with air traffic controllers in order to reduce their workload.

2.4 Aircraft Conflict Resolution

In airspace where the amount of aircraft is considerably large and congestion is observed, loss of separation between aircraft becomes a dangerous problem, impairing flights' safety. In order to ensure separation, ATC performs its major task known as conflict detection and resolution, Conflict Avoidance and Recovery (CDR) or aircraft deconfliction. This is divided into three main stages: strategic deconfliction, which occurs prior to flight departure and it is based on beforehand manoeuvres based only on priority information and that can be subject to changes throughout long distance flights; tactical deconfliction, which happens during the flight, at least 5 minutes ahead of the actual conflict; and finally the collision avoidance systems such as Traffic Collision Avoidance System (TCAS), which is the final avoidance to avoid mid-air collisions.

Methods based on separation conditions are the the foundation of air routes and they have evolved over the years. Humans are vital components in conflict resolution due to their abilities to analyse different sources of information and being capable of making judgements calls on them. However, they are still prone to make mistakes. Because of eventual failures and operational errors, assisting systems have started to be available in the cockpit and on the ground control to provide support and serve as alerting systems. Such technology is composed of sensors to predict eventual conflict and suggest a set of manoeuvres to solve it. Simpler cases can already be solved by existing systems such as TCAS (implemented since the 1990s) (Kuchar and Yang, 2000).

CDR has been most commonly addressed as an optimisation problem. The basis of these systems is to identify manoeuvres to ensure that minimum separation is maintained throughout the whole flight, especially in the en-route stage. Due to

the nature of such problems, which involves quadratic equations involving Euclidean distance and trigonometric functions, those problems are non-convex. Solutions are required to be obtained free of errors and to be precise and quick. Under those circumstances, the first initial attempt to solve this problem is a series of specific formulations based on heuristic and meta-heuristics as reviewed by Kuchar and Yang (2000). With the advances in computational power in the late 1990s and at the beginning of the 21st century, the ground layers to attempt exact solutions were established and therefore, many exact solutions were proposed utilising mathematical programming as reviewed by Pelegrín and d’Ambrosio (2020).

Nevertheless, given that this particular problem continues to evolve and to incorporate new elements such as the probability of conflict and trajectory prediction, new heuristics have been proposed. In this section, the state-of-the-art research is reviewed. First, the earlier research studies on conflict detection and resolution, followed by mathematical programming approaches for conflicting resolution and finishing with advanced formulations for aircraft conflict resolution problem.

2.4.1 Early Studies on Conflict Detection and Resolution

As described in Kuchar and Yang (2000), initial efforts to solve CDR problems can be classified into three main categories based on their state propagation, which is the ability they have to predict the future. Those three categories are: the first is the nominal approach, in which trajectories are projected in a single profile, without any regards towards uncertainties or inconsistency in the data that might culminate in a prediction error (for example, assuming that the position of the aircraft are solely predictable via its current velocity vector). The second case is based on worst-case projection, where there is a range of manoeuvres that each aircraft can perform and if any circumstances result in a conflict, it will be predicted. It is a more conservative approach and it is limited by the length and dimension of the range of manoeuvres available. Finally, the third approach is the probabilistic method, which is attempting to model the uncertainties via variables into the model. Uncertainties are modelled as potential variations in trajectories via a position error, from which conflict probabilities can be calculated and it provides a balance and compromise between the two previous methods.

In terms of models exploring the nominal trajectory, there has been a great effort into this area. Andrews (1977) proposed a model based on relative motion to detect horizontal collisions in which the author projects the positions in which each aircraft will be and it is based on the time horizon. Chakravarthy and Ghose (1998), proposed

a similar formulation using a collision cone as an alternative route projector, but instead of only aircraft, it also incorporates airborne obstacles as part of the pathway. In earlier works, Frazzoli et al. (2001) proposed a model based on convex programming and randomised search that recasts the formulation into a quadratically constrained quadratic program using speed and heading control as the only available manoeuvres. In Zeghal (1998), the author proposed a model called the symmetrical force field which is a fully distributed and reactive coordination algorithm which relies on each aircraft taking action independently. Another autonomous approach was defined by Duong and Hoffman (1997), where the authors worked in an initiative called Free-Route Experimental Encounter Resolution (FREER) introduced by EuroControl and it was initially tested in low-density airspace.

Tomlin et al. (1998) address the possibilities for free flight and calculates the maximal set of safe initial conditions for each aircraft so that separation is assured in the presence of uncertainties in the actions of the other aircraft. Kelly (1999), a model based on instantaneous state vectors is proposed and in Irvine (1998), this approach is expanded by incorporating different type of airborne objects and using different models inside of a manoeuvre generator. Another model that generates the possible manoeuvres was presented by Ota et al. (1998) where the authors create a set of geometric solutions called "threat map" to identify possible conflicts and determine a series of horizontal and vertical manoeuvres. Durand et al. (1997) proposes an automatic conflict solver which was validated using the flight data over France in a similar manner. Krozel and Peters (1997) utilise the free-flight control framework to create an optimisation model to minimise costs via a cost-benefit analysis, explore how it impacts on different levels of separation (from 5NM to 1NM in free flight conditions). Another system based on free flight is the Manoeuvres Option Manager (MOM) which decompose complex air traffic control situations, where manoeuvres are tested for different time instants and decided which one is the optimal as stated at Niedringhaus (1992).

Human factors in free-flight have also being incorporated. Hoekstra et al. (1998) treated as a non-linear problem with rules design based on cockpit displays, system description and operation implications. Zhao et al. (1997) and Menon et al. (1999) proposed a point-mass level flight aircraft model (which is heavily based on simulation of particles physics) formulated as a non-linear problem, using terminal constraints to force to recover initial trajectories. Instead of individual elements, Burdun and Parfentyev (1999) observed collective behaviour in nature, such as bird flocking, fish schooling and insect swarming were extensively used in their analysis. In an upgraded

system, Harper et al. (1999) simulated the ATC and pilot behaviour, divided into three models containing a simple representation of information processing, situation assessment and collaborative decision-making via inter-agent negotiation. Another upgraded model is the Stream Option Manager described by Niedringhaus (1995), especially in a stream based on linear programming techniques.

Self-organising strategies in free-flight scenarios were also proposed by Eby and Kelly (1999) and Eby (1994) based on potential fields and show that such algorithms are extremely robust in solving CDR without a centralised authority. The greatest challenge in ATM is the computational resource and load necessary to handle scenarios with higher density. Occasionally, some simplifications are necessary. As presented by Sridhar and Chatterji (1997), some simplifications can be done via spatial and temporal discretisation, which can also be applied individually or in combination. The ground system can also be of assistance in conflict resolution as explored by Havel and Husarčík (1989), where the authors can detect conflicts in a given time interval frequency. GPS systems can also be used as a source for aircraft position and speed as described by Gazit (1997). For details relating the papers reviewed in this section and more intensive literature, Kosecka et al. (1997) and Bilimoria et al. (2000) provide a complete review. Some systems used in ATC are also explained in details in Burgess et al. (1994), Ford (1987), Williamson and Spencer (1989), LOVE (1988) and Zeghal (1998).

For the worst-case projection, some models have been released over the years. Starting with the proposal by Lachner (1997), where an approach initially designed for an autonomous and semi-autonomous car based on pursuit-evasion differential games. In that case, the representation of an optimal collision avoidance strategy was created using Taylor series expansions of the value function's gradient. Similarly, a new threat detection criterion in order to reduce miscalling and undesirable alerts was proposed by Ford and Powell (1990). In Shepard et al. (1991), a prediction algorithm using intent information was designed based on worst-case scenario analysis. Under free-flight, the worst-case scenario presents greater flexibility. Using linear matrix inequalities and positive semi-definitive programming, the separation in complex examples can be investigated using polynomial-time algorithm as described by Shewchun et al. (1997). One of the sources used for the worst-case scenario is weather conditions, and in the NASA report by Waller and Scanlon (1996) where flight conditions in instrument meteorological conditions were used. Another model was proposed by Vink et al. (1997) created by the EuroControl called European ATC

Harmonisation and Integration Program, which establishes separation under uncertainty conditions.

The probabilistic models have been addressed in the literature in the past decades. In the works of Paielli and Erzberger (1997) and Prandini et al. (1999), the authors address the probability of conflict in free-flight circumstances and Taylor (1990) used a similar approach by using probability theory, that is fitted into the trajectory course by a fitness model. As in Bakker and Blom (1993), the risk of collision was also calculated using similar formulation and the Reich model and Markov process. In Wangermann and Stengel (1998) and Wangermann and Stengel (1999), Intelligent Aircraft/Airspace System (IAAS) is described as a rule-based expert system agents and principled negotiation, allowing distributed optimisation. This allows the agents to search for solutions that would not be available otherwise, while the principled negotiation moderate consensus between those elements. In Rome and Kalafus (1988), the authors describe systems that track intersection capacities based on geometry, flow rates and distribution of the errors and measures the effectiveness and error in the performance of collision risk.

Warren (1997) focuses on a conflict probe system based on free-routing and by applying Monte-Carlo and co-variance analysis to explore different behaviour in terms of path prediction uncertainty. Another metric described by the author uses statics decision theory to control aircraft under uncertainty region in Williams (1992). By calculating position and velocity confidence ellipsoid associated with aircraft radar track, that allows for the definition of the optimal collision avoidance decision rule and this model is solely based on statistical properties. Another probabilistic model was suggested by Carpenter et al. (1997) where it determines the collision probabilities based on hazard levels corresponding to the current precision runway monitor system of one accident in every thousand cases and probability contour were designed using Monte Carlo simulations.

Optimal stopping policy as variational inequality was also used to compute worst-case scenario solutions used in low-density ATC scenarios by Heuvelink and Blom (1988). In a model to encapsulate all sorts of hazards into a single system, von Viebahn and Schiefele (1997) divide the airspace into discrete volume elements. Then, it calculates the threat levels associated with each one individually based on sensor output, databases or information provided via data link. Centre/TRACON Automation System (CTAS) has also been tested in conflict prediction and trial planning capability by McNally et al. (1998) and Isaacson and Erzberger (1997). In those, operational conditions in the Denver Air Route Traffic Control Centre in September

1997 were used as test subjects. It showed that the direct route resolved a conflict in the tactical stage as shortcuts.

Another system that was attempted and tested is the Advanced En Route ATC by Brudnicki et al. (1997) and Brudnicki and McFarland (1997), which is composed of a continuous conflict probe checkout. It also encapsulates an evaluation mechanism to address possible alternative before clearances are given. Using data link between the aircraft and conflict solved initially at the flight deck, the prototype developed by YangL (1997) and Yang and Kuchar (1998) creates a series of alerting signals depending on the likelihood and gravity of future conflicts. Those probabilities are determined via Monte Carlo simulation and tested in different configurations.

2.4.2 Mathematical programming approaches for the deterministic aircraft conflict resolution problem

The first exact global optimisation approach to conflict resolution problems was proposed by Pallottino et al. (2002) which introduced two MIP formulations: a first model was based on speed control only, and a second model was based on heading control only and assumed that all aircraft fly at the same speed. In the proposed MIP formulation for conflict resolution with speed control, the authors derived linear pairwise aircraft separation constraints based on the geometric construction introduced by Bilimoria (2000). These separation conditions are obtained by projecting the shadow of an intruder aircraft onto the trajectory of a reference aircraft. Frazzoli et al. (2001) was the first to observe that this geometric construction provided a basis to characterise the set of aircraft pairwise conflict-free trajectories via linear half-planes in the relative velocity (speed and heading) plane. The authors introduced a non-convex formulation for the conflict resolution problem with speed and heading control, and proposed a convex relaxation based on semi-definite programming as well as a heuristic algorithm to find feasible solutions on problems with up to 10 aircraft.

The shadow separation conditions were subsequently used in several formulations. Alonso-Ayuso et al. (2011) proposed a mixed-integer linear programming (MILP) formulation for conflict resolution by speed and altitude control and reported solving instances with up to 50 aircraft in competitive time. Alonso-Ayuso et al. (2014) proposed a two-step formulation in which only heading control is available for deconfliction and the available angle changes are discretised. The same group of authors also proposed a non-convex formulation involving trigonometric functions based on the shadow separation conditions that enable speed, heading and altitude control

(Alonso-Ayuso et al., 2016). The authors used mixed-integer non-linear programming (MINLP) solver to solve the resulting non-convex formulations and reported results for the 2D ACRP with up to 7 aircraft on structured instances and up to 20 aircraft on un-structured instances. An alternative representation of pairwise aircraft separation based on conflict points has been proposed by several authors. In Vela et al. (2009c,b,a), the authors proposed several MILP formulations which aim to minimise fuel consumption, incorporate air traffic controller workload in the objective function, and account the impact of uncertainty in trajectory prediction due to wind effects. Omer (2015) proposed a space-discretised MILP formulation involving a finite set of turning angles. In contrast to most other approaches, the heading control manoeuvres consist of two actions: a first heading change for collision avoidance and a subsequent turn to recover the initial heading. Rey et al. (2012, 2016) proposed linear upper bounds for the ACRP with speed control only and the resulting MILP formulations are able to solve realistic large-scale instances to optimality within a few seconds.

More recently, non-linear global optimisation approaches received increasing attention in the literature. Omer and Farges (2013) proposed a hybrid algorithm which uses the optimal solution of a MILP as the starting point for solving a non-linear formulation of the same problem. Cafieri and Rey (2017) proposed an MINLP approach for conflict resolution with speed control only which highlights that subliminal speed control alone may not be sufficient to resolve all conflicts in dense traffic scenarios. Using a similar framework, Cafieri and Omheni (2017) presented a two-step approach where a maximum number of conflicts are first solved using speed control only and outstanding conflicts are solved by heading control. Cerulli et al. (2020) proposed a formulation based on bi-level optimisation with multiple follower problems, each of which representing a two-aircraft separation problem. The authors presented two formulations, one using speed control only and another using heading control only. A cut generation algorithm is proposed to solve the corresponding bi-level optimisation problems. Recently, Pelegrín and d’Ambrosio (2020) conducted a review of the literature on exact conflict resolution approaches, and have shown that the disjunctive linear separation conditions introduced by Rey and Hijazi (2017) and the shadow separation conditions are equivalent.

Several rich heuristic approaches for conflict resolution have also been proposed in an attempt to model conflict-free trajectories for aircraft more completely and accurately. In particular, meta-heuristics such as genetic algorithms (Durand et al., 1997)

and ant colony algorithms (Durand and Alliot, 2009) have proposed to find conflict-free solutions that ensure aircraft to safely recover their initial trajectories. Other approaches proposed light propagation algorithms (Dougui et al., 2013, 2011), which use the light refraction index to determine conflict-free trajectories; and B-splines (Peyronne et al., 2015) to design smooth navigable paths for aircraft. In Lehouillier et al. (2017), the authors propose a graph formulation for conflict resolution wherein each node of the graph represents a possible manoeuvre. This manoeuvre-discretised model is able to scale well, but its solutions may be characterised as suboptimal if compared to a non-discretised formulation.

2.4.3 Advanced formulations for aircraft conflict resolution problems

In mathematical programming approaches, the trajectory of aircraft is usually divided into stages. These stages are traditionally called avoidance (or action) which encapsulates the manoeuvres necessary to avoid any conflict while the trajectory recovery corresponds to the manoeuvres necessary to restore the aircraft to its original trajectory. Different approaches (such as genetic programming and heuristics) might consider trajectory recovery as part of the conflict resolution, but in mathematical programming, this is normally separated due to its non-trivial aspects, which brings many non-convexity and non-linearity to their formulations.

Despite their potential effectiveness, most efforts in conflict resolution have focused on ensuring collision avoidance, but have overlooked the costs and mechanisms for modelling aircraft’s recovery to their original trajectory. This may be critical when conflict resolution is performed using heading control which may significantly cause deviation in the aircraft from their initial trajectory, thus possibly increasing flight operating costs. Trajectory recovery has received very little attention in the literature due to the challenging nature of the problem. Meta-heuristics such as genetic algorithms (Durand et al., 1997) and ant colony algorithms (Durand and Alliot, 2009) have been proposed to find conflict-free solutions that ensure aircraft to avoidance and recovery safely. (Dougui et al., 2013) proposed a model which uses an analogy with light propagation theory to create conflict-free aircraft trajectories with recovery. (Peyronne et al., 2015) proposed a B-splines model which uses way-points of a given trajectory to design conflict-free trajectories with recovery. In Omer (2015), the authors proposed a formulation providing parallel trajectory recovery while minimising fuel consumption and delays. In this model, aircraft are assumed to perform a

preventive manoeuvre before the intersection and the formulation is focused on separating aircraft on their parallel trajectories. Heading angles are discretised and the optimisation controls both aircraft heading and recovery time. Recently, (Lehouillier et al., 2017) proposed a manoeuvre-discretised model in which pre-defined sets of manoeuvres are available for aircraft and a clique-based formulation is proposed to find the optimal combination of conflict-free manoeuvres. This review of the literature highlights that despite recent improvements in computational optimisation, there remain significant open challenges in the design of scalable and exact global optimisation approaches for conflict resolution in air traffic control, especially on how to incorporate recovery in a scalable and effective way.

The aircraft conflict avoidance and resolution problem can be expressed in the form of an optimisation problem, which has the objective to find conflict-free trajectories for all aircraft in delimited airspace. Many strategies have been proposed to address this problem based on the type of manoeuvres (applied separately or in combination) that can be issued to aircraft: speed, heading and/or altitude control. Recently, conflict resolution using global optimisation has received growing attention due to its ability to provide optimal solutions that take into account all traffic within an airspace region and are able to consider the overall state. One of the first global optimisation approaches for air conflict resolution was introduced by Pallottino et al. (2002) which proposed two formulations: one focusing on speed control and another focusing on heading control and both minimise the overall flight time. Subsequent approaches proposed speed control and altitude level-assignment to minimise fuel consumption by metering aircraft at conflict points (Vela et al., 2010). In Vela et al. (2009b), the authors proposed a two-stage stochastic optimisation model accounting for wind uncertainty and using speed control. Multi-objective optimisation formulations attempting to balance flight deviation with the total number of manoeuvres (velocity, heading and/or altitude change), building on the work of Pallottino et al. (2002) were proposed by (Alonso-Ayuso et al., 2011, 2014). Subliminal speed control methods, which focus on speed control only for conflict resolution, have also proven to be a powerful tool. Although it may fail to resolve all conflicts (Rey et al., 2016; Cafieri and Rey, 2017), it has a low impact in terms of deviation and fuel consumption. More recently, Rey and Hijazi (2017) proposed a complex number formulation for speed and heading control without any form of discretisation.

As highlighted in this review of the literature, most efforts are either focused on probabilistic models to calculate conflict rates and to improve the accuracy of decision-support systems for ATC by providing a more comprehensive model of reality; or on

(meta-)heuristic approaches that aim to solve the ACRP under uncertainty. To the best of our knowledge, no attempts have been made to solve the ACRP to optimality without any form of discretisation while accounting for uncertainty in a robust optimisation framework. To this end, Irvine (2002), Regnier (2008) and Jacquemart and Morio (2016) used information and data observed from weather forecast or observed weather data collected over the years to estimate the probability of a loss of separation between aircraft under uncertainty. Different approaches to solve the ACRP under uncertainty have not been widely attempted throughout literature and the most widely used approach consists of calculating probabilistic distributions of possible conflict and delays. At the same time, some studies such as Morgan et al. (1990) and Murça (2017) also incorporate the random effects that can happen from measurements in faulty sensors or loss of data throughout communications. In those cases, their models are related to system reliability and performance.

To guarantee and improve safety, ACRP plays a critical role. Based on the current situation of the many systems in operation, this challenge is divided into two different stages: detection and resolution. The state-of-the-art methods to address the resolution part are mainly based on the prediction of the aircraft velocity and position. This alternative cannot be always applied given that, in ATC, many variables cannot be previously assessed and their distributions are not known beforehand. Even though data collected about weather conditions can be used as source material, they are suitable for real-time solutions with random variables. Therefore, the robust formulation is crucial when it is difficult to assess how uncertainty elements will cause trajectory prediction instability and imprecision. Among the different sources of random effects, weather uncertainty is one the most predominant (Morgan et al., 1990) and can be induced by limited knowledge about present conditions and, especially, future meteorological conditions, such as wind speed and direction, snowfall, fog and storms. All those circumstances may cause many negative effects in the ATM performance, such as delays and flight cancellation, which translate into extra costs for all parts involved.

In Atamtürk and Zhang (2007), the authors proposed a network design problem where the uncertainty sets are used to define the demand. Similarly, Lee et al. (2013) used Benders decomposition in robust network design with flow bifurcations and demand under uncertainty and Chiou (2016) used uncertain travel demands for signal-controlled robust stochastic design. In another network flow problem, Ordóñez and Zhao (2007) proposed a robust model by expanding the arc capacity using uncertainty sets. Other problems in the transport field were addressed using this formula-

tion such as facility location problem and Snyder (2006) presents a review of different studies under uncertainty and different techniques to approach randomness. Another review work was addressed by Verderame et al. (2010) for planning and scheduling using multiple factors as sources of uncertainty and how all of them can be handled using the same technique. In power flow, Bienstock et al. (2014) proposed a chance-constrained problem and used uncertainties to account to risk-awareness; Ding et al. (2016) analysed the consequences of adjustable robust power flow in large-scale systems and how the price of robustness can provide the trade-off between deterministic and robust models and in Bienstock et al. (2013), the authors model uncertainty in smart grids due to data ambiguity.

Most of the effort for trajectory prediction under uncertainty assumes that weather is the primary source of randomness, considering that wind, rain and fog may affect the aircraft trajectory prediction. More generally, adverse weather conditions can cause delays due to low visibility, loss of friction in take-off and arrivals, etc., and has been the focus of several works in ATM. In Nilim et al. (2001), a dynamic routing mechanism was proposed to account for expected delays if the nominal trajectory is inaccessible due to weather conditions. By modelling the uncertainty using a statistical analysis of forecast data, Hentzen et al. (2018) calculated the probability of an aircraft reaching its destination given that some action is taken to avoid the area affected by adverse weather. Similarly, Clarke et al. (2009) used available stochastic weather information into a dynamic model to determine the route capacity for each aircraft. Pepper et al. (2003) presented a Bayesian model to incorporate uncertainty from weather into air traffic flow to understand capacity behaviour under weather conditions. A sequential optimisation approach was developed by Grabbe et al. (2009) to adapt route capacity to account for varying weather conditions. Zheng and Zhao (2011) developed a statistical model of wind uncertainty and trajectory prediction using constant speed. The authors used curated data from previous years, to estimate and calibrate the parameters in their statistical model and used that knowledge to determine optimal manoeuvres. In a more generic uncertainty context, Murça (2017) presented a robust approach for optimising runway usage and taxi-out time, and Radmanesh et al. (2018) solved the problem of path planning for unmanned air vehicles under random circumstances. Different sources of uncertainty were explored by Kim et al. (2009) who discretised flight speed, and model uncertainty using a white Gaussian function and removing the crosswind effect to assess the efficiency of traffic flow. González Arribas et al. (2016) analysed flight paths determined via pseudo-spectral methods of assessing wind-optimal trajectories. In Franco et al. (2017), the

authors created a structured space and applied the Dijkstra algorithm to obtain optimal paths. Rivas et al. (2017) and Valenzuela et al. (2017) analysed the effects of wind uncertainty in fuel consumption and demand.

Chapter 3

Formulations for the Aircraft Conflict Resolution Problem

In this section, mixed-integer formulations for aircraft conflict resolution are presented. The focus is on the 2D problem under velocity, i.e. speed and heading, control which aims to represent a single flight level during cruise stage air traffic conditions. Then, it is presented the characterisation of three different classic formulations for 2D separation conditions for a pair of aircraft that are state-of-the-art in the literature. First, the characterisation of 2D separation conditions is presented in Section 3.1 followed by the non-convex quadratic formulation proposed by Cafieri and Omheni (2017), then non-convex non-linear formulation using the disjunctive formulation by Rey and Hijazi (2017) in Section 3.2 and last the non-convex shadow formulation, initially proposed by Bilimoria et al. (2000) and expanded by Pallottino et al. (2002) and Alonso-Ayuso et al. (2014). The proof presented by Pelegrín and d'Ambrosio (2020) which shows that the formulation by Frazzoli et al. (2001) and Rey and Hijazi (2017) are equivalent is also replicated. Finally, some numerical experiments and the limitations of each formulation are presented in Section 3.7.

3.1 Characterisation of 2D Separation Conditions

In this section, the separation conditions for a pair of aircraft are derived and then a compact characterisation of the conflict-free region based on aircraft available deconfliction resources is presented. The goal is to find least-deviating conflict-free trajectories for a set of aircraft in cruise stage, i.e. flying at a fixed altitude and at a constant speed. Let $t = 0$ be the time instant representing aircraft current positions at the time of decision, also referred to as aircraft initial positions. It is also assumed

that all aircraft are separated at $t = 0$ and seek to derive separation conditions to ensure that aircraft trajectories are separated for any time $t \geq 0$.

Let \mathcal{A} be the set of aircraft. For each $i \in \mathcal{A}$, $[\hat{x}_i, \hat{y}_i]$ is the aircraft initial position in the 2D plane, \hat{v}_i is its nominal speed (in NM/h) and $\hat{\theta}_i$ is its heading angle. Assuming uniform motion laws, aircraft motion can be described as: $p_i(t) = [x_i(t), y_i(t)]^\top$, where $x_i(t) = \hat{x}_i + q_i \hat{v}_i \cos(\hat{\theta}_i + \theta_i)t$ and $y_i(t) = \hat{y}_i + q_i \hat{v}_i \sin(\hat{\theta}_i + \theta_i)t$. In this model, the decision variables are q_i , which is the speed control variable that determines the acceleration or deceleration with regards to the nominal speed \hat{v}_i (q_i equals to 1 means no speed variation) and θ_i , which is the heading control variable that determines the deviation with regards to the nominal trajectory (θ_i equal to 0 means no deviation in heading angle).

Let $\mathcal{P} = \{i, j \in \mathcal{A} : i < j\}$ be the set of aircraft pairs, the relative motion of $(i, j) \in \mathcal{P}$ is denoted $p_{ij}(t) = p_i(t) - p_j(t)$. Let d be the minimum separation distance (e.g. 5 NM). Next, the motion of 2D separation for a pair of aircraft is defined.

Definition 1 (2D separated trajectories). *The trajectories of a pair of aircraft $(i, j) \in \mathcal{P}$ is said to be 2D separated, i.e. conflict-free, if and only if:*

$$\|p_{ij}(t)\| \geq d, \quad \forall t \geq 0. \quad (3.1)$$

Let $v_{ij} = v_i - v_j$ be the 2D relative velocity vector of $(i, j) \in \mathcal{P}$, i.e. $v_{ij} = [v_{ij,x}, v_{ij,y}]^\top$ with:

$$v_{ij,x} = q_i \hat{v}_i \cos(\hat{\theta}_i + \theta_i) - q_j \hat{v}_j \cos(\hat{\theta}_j + \theta_j), \quad (3.2a)$$

$$v_{ij,y} = q_i \hat{v}_i \sin(\hat{\theta}_i + \theta_i) - q_j \hat{v}_j \sin(\hat{\theta}_j + \theta_j). \quad (3.2b)$$

Aircraft relative velocity equations are linear with regards to speed control variables q_i and q_j , but non-linear with regards to heading control variables θ_i and θ_j . Expanding the expression in Eq. (3.1) (as suggested by Cafieri and Durand (2014)) and denoting \hat{p}_{ij} the relative initial position of aircraft pair $(i, j) \in \mathcal{P}$, a second-order polynomial function is obtained:

$$f_{ij}(t) \equiv \|v_{ij}\|^2 t^2 + 2\hat{p}_{ij} \cdot v_{ij} t + \|\hat{p}_{ij}\|^2 - d^2 \geq 0. \quad (3.3)$$

Since the coefficient of the second-order term is positive, $f_{ij}(t)$ admits a minimum which corresponds to the time instant of minimum separation between aircraft i and j . Let $t_{ij}^{\min}(v_{ij})$ be the function corresponding to this time instant parameterised by aircraft relative velocity vector, then:

$$t_{ij}^{\min}(v_{ij}) = \frac{-\hat{p}_{ij} \cdot v_{ij}}{\|v_{ij}\|^2}. \quad (3.4)$$

Evaluating Eq. (3.3) at $t_{ij}^{\min}(v_{ij})$ yields a time-independent separation condition (Rey and Hijazi, 2017; Cafieri and Rey, 2017; Cafieri and Omhenni, 2017):

$$f_{ij}(t_{ij}^{\min}(v_{ij})) = \frac{-(\hat{p}_{ij} \cdot v_{ij})^2}{\|v_{ij}\|^2} + \|\hat{p}_{ij}\|^2 - d^2 \geq 0. \quad (3.5)$$

Let $g_{ij}(v_{ij}) \equiv \|v_{ij}\|^2 f_{ij}(t_{ij}^{\min}(v_{ij}))$. By abusing the notation, $g_{ij}(\cdot)$ and $t_{ij}^{\min}(\cdot)$ can be rewritten as functions of aircraft velocity components $v_{ij,x}$ and $v_{ij,y}$. After expanding and factorising, the following expression is obtained:

$$g_{ij}(v_{ij,x}, v_{ij,y}) = v_{ij,x}^2 (\hat{y}_{ij}^2 - d^2) + v_{ij,y}^2 (\hat{x}_{ij}^2 - d^2) - v_{ij,x} v_{ij,y} (2\hat{x}_{ij} \hat{y}_{ij}) \geq 0. \quad (3.6)$$

Assuming aircraft are initially separated, if $t_{ij}^{\min}(v_{ij,x}, v_{ij,y}) \leq 0$, then they are diverging and do not incur any risk of future conflict. If $t_{ij}^{\min}(v_{ij,x}, v_{ij,y}) \geq 0$ and $g_{ij}(v_{ij,x}, v_{ij,y}) \geq 0$, aircraft are converging but separation is ensured. Otherwise, if $t_{ij}^{\min}(v_{ij,x}, v_{ij,y}) \geq 0$ and $g_{ij}(v_{ij,x}, v_{ij,y}) \leq 0$, there is a loss of separation and aircraft trajectories should be adjusted to avoid it. Hence, pairwise aircraft separation conditions for $(i, j) \in \mathcal{P}$ can be written as:

$$g_{ij}(v_{ij,x}, v_{ij,y}) \geq 0 \vee t_{ij}^{\min}(v_{ij,x}, v_{ij,y}) \leq 0. \quad (3.7)$$

To characterise the set of 2D conflict-free trajectories, it is necessary to examine the relative velocity vector v_{ij} as a function of trajectory control bounds. For each aircraft $i \in \mathcal{A}$, it is assumed that the speed rate variable is lower bounded by \underline{q}_i and upper bounded by \bar{q}_i , i.e.:

$$\underline{q}_i \leq q_i \leq \bar{q}_i, \quad \forall i \in \mathcal{A}. \quad (3.8)$$

Assuming that the heading deviation is lower bounded by $\underline{\theta}_i$ and upper bounded by $\bar{\theta}_i$, the heading deviation bounds can be expressed as:

$$\underline{\theta}_i \leq \theta_i \leq \bar{\theta}_i, \quad \forall i \in \mathcal{A}. \quad (3.9)$$

To derive lower and upper bounds on relative velocity components $v_{ij,x}$ and $v_{ij,y}$, the Eq. (3.2) can be rearranged as trigonometric identities:

$$v_{ij,x} = q_i \hat{v}_i \cos(\hat{\theta}_i) \cos(\theta_i) - q_i \hat{v}_i \sin(\hat{\theta}_i) \sin(\theta_i) - q_j \hat{v}_j \cos(\hat{\theta}_j) \cos(\theta_j) + q_j \hat{v}_j \sin(\hat{\theta}_j) \sin(\theta_j), \quad (3.10a)$$

$$v_{ij,y} = q_i \hat{v}_i \sin(\hat{\theta}_i) \cos(\theta_i) + q_i \hat{v}_i \cos(\hat{\theta}_i) \sin(\theta_i) - q_j \hat{v}_j \sin(\hat{\theta}_j) \cos(\theta_j) - q_j \hat{v}_j \cos(\hat{\theta}_j) \sin(\theta_j). \quad (3.10b)$$

Let $\underline{v}_{ij,x}, \bar{v}_{ij,x}$ and $\underline{v}_{ij,y}, \bar{v}_{ij,y}$ be the lower and upper bounds for $v_{ij,x}$ and $v_{ij,y}$, respectively. These bounds can be determined using Eq. (3.10) and the bounds on speed and heading control provided in Ineqs. (3.8) and (3.9). The derived bounds on the relative velocity components can be used to define a box in the plane $\{(v_{ij,x}, v_{ij,y}) \in \mathbb{R}^2\}$.

Definition 2 (Relative velocity box). *Consider a pair of aircraft $(i, j) \in \mathcal{P}$. Let \mathcal{B}_{ij} be the subset of \mathbb{R}^2 defined as*

$$\mathcal{B}_{ij} = \{(v_{ij,x}, v_{ij,y}) \in \mathbb{R}^2 : \underline{v}_{ij,x} \leq v_{ij,x} \leq \bar{v}_{ij,x}, \underline{v}_{ij,y} \leq v_{ij,y} \leq \bar{v}_{ij,y}\}. \quad (3.11)$$

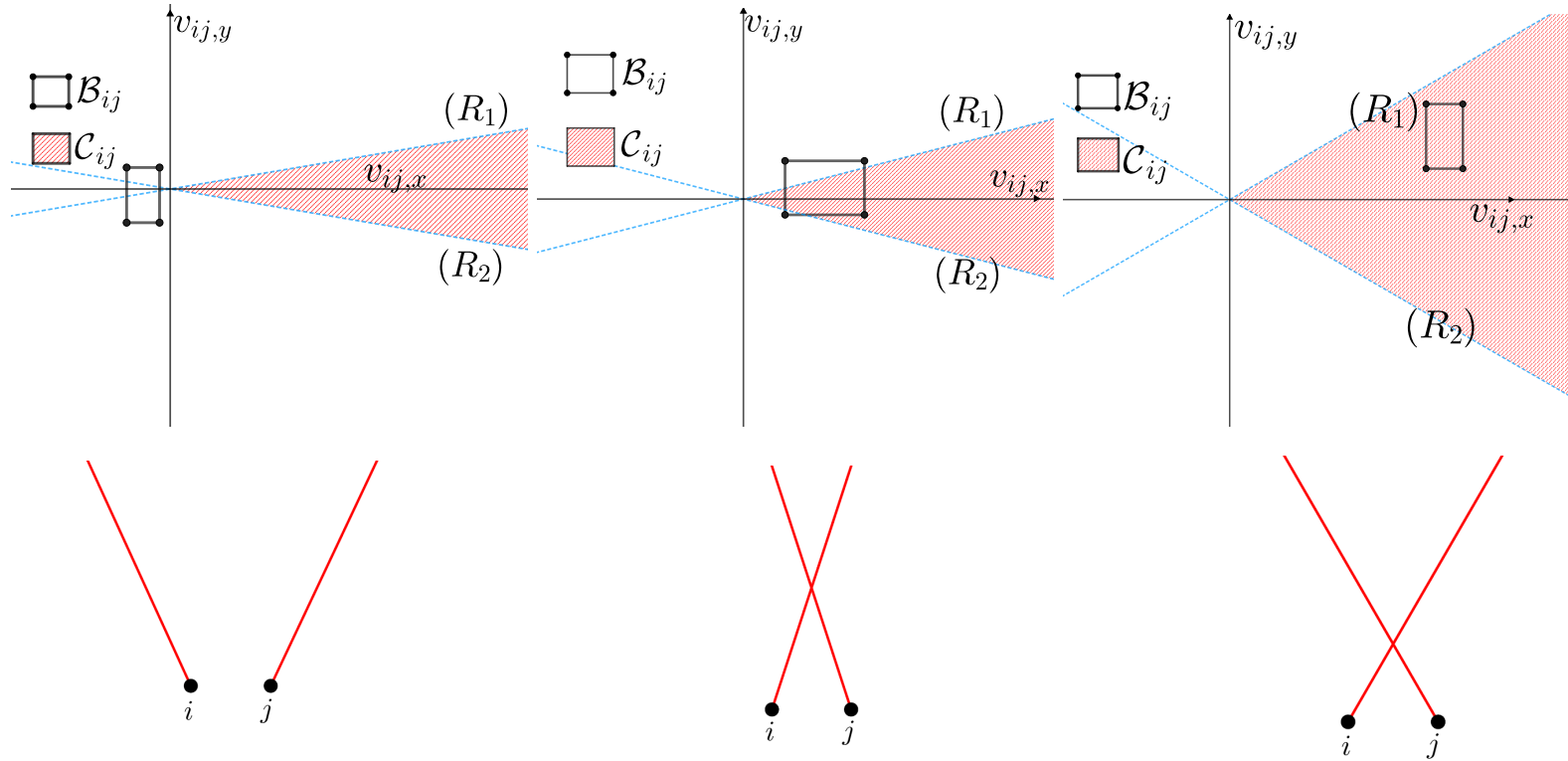
\mathcal{B}_{ij} is the relative velocity box of $(i, j) \in \mathcal{P}$.

The relative velocity box \mathcal{B}_{ij} characterises all possible trajectories for the pair $(i, j) \in \mathcal{P}$ based on the available 2D deconfliction resources, i.e. speed and heading controls. To characterise the set of conflict-free trajectories of a pair of aircraft $(i, j) \in \mathcal{P}$, it is required to compare the relative position of the relative velocity box \mathcal{B}_{ij} with the conflict region of this pair of aircraft. Observe that the conflict region is convex and can be defined based on reversing the inequalities (3.6).

Definition 3 (Conflict region). *Consider a pair of aircraft $(i, j) \in \mathcal{P}$. Let \mathcal{C}_{ij} be the subset of \mathbb{R}^2 defined as*

$$\mathcal{C}_{ij} = \{(v_{ij,x}, v_{ij,y}) \in \mathbb{R}^2 : v_{ij,x}\gamma_{ij}^l - v_{ij,y}\phi_{ij}^l \geq 0 \wedge v_{ij,x}\gamma_{ij}^u - v_{ij,y}\phi_{ij}^u \leq 0\}. \quad (3.12)$$

\mathcal{C}_{ij} is the conflict region of $(i, j) \in \mathcal{P}$.



(a) Conflict-free aircraft pair, i.e. $\mathcal{B}_{ij} \cap \mathcal{C}_{ij} = \emptyset$. Nominal headings are $\hat{\theta}_i = 2.01$ and $\hat{\theta}_j = 1.30$.

(b) Separable aircraft pair, i.e. $\mathcal{B}_{ij} \cap \mathcal{C}_{ij} \neq \emptyset$ and $\mathcal{B}_{ij} \not\subset \mathcal{C}_{ij}$. Nominal headings are $\hat{\theta}_i = 1.25$ and $\hat{\theta}_j = 1.88$.

(c) Non-separable aircraft pair, i.e. $\mathcal{B}_{ij} \subset \mathcal{C}_{ij}$. Nominal headings are $\hat{\theta}_i = 1.04$ and $\hat{\theta}_j = 2.09$.

Figure 3.1: Three aircraft configurations illustrating conflict-free (3.1a), separable (3.1b) and non-separable (3.1c) pairs. Aircraft initial positions and trajectories are depicted at the bottom part of each sub-figure, where black dots correspond to initial positions and red lines represent initial trajectories. The top part of each sub-figure shows a graph of the relative velocity box \mathcal{B}_{ij} represented by a black rectangle, and the conflict region \mathcal{C}_{ij} represented by a red hashed area. Dashed blue lines represent the solutions of $g_{ij}(v_{ij,x}, v_{ij,y}) = 0$ (R_1 and R_2). In all cases, aircraft i and j have nominal speeds $\hat{v}_i = \hat{v}_j = 500$ NM/h and are initially separated by 30 NM in the x-axis direction.

To design the objective function, a preference weight $w \in]0, 1[$ to balance the trade-offs among velocity controls, i.e. speed and heading is introduced. This is a standard objective function used by researchers and it represents the minimisation of combined deviation in all aircraft.

$$\text{minimise } \sum_{i \in \mathcal{A}} w\theta_i^2 + (1-w)(1-q_i)^2. \quad (3.13)$$

Next, it is shown that the objective function (3.13) attains its minimum value when aircraft have deviation-free trajectories, i.e. $q_i = 1$ and $\theta_i = 0$ for all $i \in \mathcal{A}$ and it is a convex.

Proposition 1. *The 2D objective function (3.13) is convex with regards to decision variables θ_i and q_i for any value $w \in]0, 1[$, and is minimal for $q_i = 1$ and $\theta_i = 0$ for all aircraft $i \in \mathcal{A}$.*

Proof. Let $c_i(q_i, \theta_i) = w\theta_i^2 + (1-w)(1-q_i)^2$ be the cost function of aircraft $i \in \mathcal{A}$. The first-order optimality conditions of $c_i(\theta_i, q_i)$ are:

$$\begin{aligned} \frac{\partial c_i(\theta_i, q_i)}{\partial q_i} &= (2q_i - 2)(1-w) = 0 \\ \frac{\partial c_i(\theta_i, q_i)}{\partial \theta_i} &= 2w\theta_i = 0 \end{aligned}$$

Recall that $w \in]0, 1[$, hence the first-order optimality conditions of this objective function yield $q_i = 1$ and $\theta_i = 0$ for all aircraft $i \in \mathcal{A}$.

Computing the Hessian matrix H of $c_i(q_i, \theta_i)$ yields:

$$H = \begin{bmatrix} 2(1-w) & 0 \\ 0 & 2w \end{bmatrix}. \quad (3.14)$$

Observe that H is symmetric. Let $\mathbf{c} \in \mathbb{R}^2$ be a vector with entries c_1 and c_2 .

$$\mathbf{c}^\top H \mathbf{c} = 2(1-w)c_1^2 + 2wc_2^2 \geq 0. \quad (3.15)$$

Thus, H is positive semi-definite and the 2D objective function (3.13) is convex. \square

3.2 Non-convex Quadratic Formulation

Based on the constraint 3.7, the model established by Cafieri and Rey (2017) can be replicated and it requires a single binary variable to define the disjunction presented in constraint 3.7. This can be defined as:

$$(v_{ij,x}^2(\hat{y}_{ij}^2 - d^2) + v_{ij,y}^2(\hat{x}_{ij}^2 - d^2) - 2v_{ij,x}v_{ij,y}\hat{x}_{ij}\hat{y}_{ij})(s_{ij}) \geq 0, \quad \forall(i, j) \in \mathcal{P}, \quad (3.16a)$$

$$-(v_{ij,x}\hat{x}_{ij} + v_{ij,y}\hat{y}_{ij})(2s_{ij} - 1) \geq 0, \quad \forall(i, j) \in \mathcal{P}. \quad (3.16b)$$

This model can be characterised by its simplicity and is easily understood. Due to non-linear constraints and the presence of trigonometric functions in the equation of motion, this model cannot be solved by commercial linear solvers and it cannot be used to solve larger instances in a reasonable amount of time. This formulation can be summarised as:

Model 1. *Non-convex 2D Formulation using Non-Linear Separation Conditions*

$$\text{Minimise} \quad \sum_{i \in \mathcal{A}} w\theta_i^2 + (1-w)(1-q_i)^2,$$

Subject to:

$$v_{ij,x} = q_i\hat{v}_i \cos(\hat{\theta}_i + \theta_i) - q_j\hat{v}_j \cos(\hat{\theta}_j + \theta_j), \quad \forall(i, j) \in \mathcal{P},$$

$$v_{ij,y} = q_i\hat{v}_i \sin(\hat{\theta}_i + \theta_i) - q_j\hat{v}_j \sin(\hat{\theta}_j + \theta_j), \quad \forall(i, j) \in \mathcal{P},$$

$$(v_{ij,x}^2(\hat{y}_{ij}^2 - d^2) + v_{ij,y}^2(\hat{x}_{ij}^2 - d^2) - 2v_{ij,x}v_{ij,y}\hat{x}_{ij}\hat{y}_{ij})(s_{ij}) \geq 0, \quad \forall(i, j) \in \mathcal{P},$$

$$-(v_{ij,x}\hat{x}_{ij} + v_{ij,y}\hat{y}_{ij})(2s_{ij} - 1) \geq 0, \quad \forall(i, j) \in \mathcal{P},$$

$$\underline{q}_i \leq q_i \leq \bar{q}_i, \quad \forall i \in \mathcal{A},$$

$$\underline{\theta}_i \leq \theta_i \leq \bar{\theta}_i, \quad \forall i \in \mathcal{A},$$

$$v_{ij,x}, v_{ij,y} \in \mathcal{B}_{ij}, \quad \forall(i, j) \in \mathcal{P},$$

$$s_{ij} \in \{0, 1\}, \quad \forall(i, j) \in \mathcal{P}.$$

3.3 Non-convex Disjunctive Formulation

To linearise the separation condition (3.6) with regards to variables $v_{ij,x}$ and $v_{ij,y}$, the same approach proposed by Rey and Hijazi (2017) is applied and the main steps are recalled hereafter. Observe that the solutions of the equation $g_{ij}(v_{ij,x}, v_{ij,y}) = 0$ can be identified by alternatively fixing variable $v_{ij,x}$ and $v_{ij,y}$, and calculating the

roots of the resulting single-variable quadratic equations. Isolating each variable, the discriminants can be obtained and expressed as:

$$\begin{cases} \Delta_{v_{ij,x}} = 4d^2 v_{ij,y}^2 (\hat{x}_{ij}^2 + \hat{y}_{ij}^2 - d^2), \\ \Delta_{v_{ij,y}} = 4d^2 v_{ij,x}^2 (\hat{x}_{ij}^2 + \hat{y}_{ij}^2 - d^2). \end{cases} \quad (3.18)$$

Assuming aircraft are initially separated, then $\hat{x}_{ij}^2 + \hat{y}_{ij}^2 - d^2 \geq 0$ holds and thus the discriminants are positive and the roots of equation $g_{ij}(v_{ij,x}, v_{ij,y}) = 0$ are the lines defined by the system of equations:

$$(\hat{y}_{ij}^2 - d^2)v_{ij,x} - (\hat{x}_{ij}\hat{y}_{ij} + d\sqrt{\hat{x}_{ij}^2 + \hat{y}_{ij}^2 - d^2})v_{ij,y} = 0, \quad (3.19a)$$

$$(\hat{y}_{ij}^2 - d^2)v_{ij,x} - (\hat{x}_{ij}\hat{y}_{ij} - d\sqrt{\hat{x}_{ij}^2 + \hat{y}_{ij}^2 - d^2})v_{ij,y} = 0, \quad (3.19b)$$

$$(\hat{x}_{ij}^2 - d^2)v_{ij,y} - (\hat{x}_{ij}\hat{y}_{ij} + d\sqrt{\hat{x}_{ij}^2 + \hat{y}_{ij}^2 - d^2})v_{ij,x} = 0, \quad (3.19c)$$

$$(\hat{x}_{ij}^2 - d^2)v_{ij,y} - (\hat{x}_{ij}\hat{y}_{ij} - d\sqrt{\hat{x}_{ij}^2 + \hat{y}_{ij}^2 - d^2})v_{ij,x} = 0. \quad (3.19d)$$

Let us emphasise that if all coefficients in (3.19a)-(3.19d) are non-zero, then (3.19a) is identical to (3.19c) and (3.19b) is identical to (3.19d). In addition, note that::

$$\begin{aligned} & \hat{x}_{ij}\hat{y}_{ij} \pm d\sqrt{\hat{x}_{ij}^2 + \hat{y}_{ij}^2 - d^2} = 0, \\ \Rightarrow & d^2(\hat{x}_{ij}^2 + \hat{y}_{ij}^2 - d^2) = \hat{x}_{ij}^2\hat{y}_{ij}^2, \\ \Leftrightarrow & \hat{x}_{ij}^2\hat{y}_{ij}^2 - d^2(\hat{x}_{ij}^2 + \hat{y}_{ij}^2 - d^2) = 0, \\ \Leftrightarrow & (\hat{x}_{ij}^2 - d^2)(\hat{y}_{ij}^2 - d^2) = 0. \end{aligned}$$

Hence, Eqs. (3.19a), (3.19b), (3.19c) and (3.19d) define two lines, denoted R_1 and R_2 , in the plane $\{(v_{ij,x}, v_{ij,y}) \in \mathbb{R}^2\}$ and the sign of $g_{ij}(v_{ij,x}, v_{ij,y})$ can be characterised based on the position of $(v_{ij,x}, v_{ij,y})$ relative to these lines. Recall that according to Eq. (3.4), the sign of the dot product $\hat{p}_{ij} \cdot v_{ij}$ indicates aircraft convergence or divergence. Let (P) be the equation of the line corresponding to the dot product $\hat{p}_{ij} \cdot v_{ij}$.

$$v_{ij,x}\hat{x}_{ij} + v_{ij,y}\hat{y}_{ij} = 0. \quad (P)$$

The line defined by (P) splits the plane $\{(v_{ij,x}, v_{ij,y}) \in \mathbb{R}^2\}$ in two half-planes, each of which representing converging and diverging trajectories, respectively. This is illustrated in Figure 3.2 which depicts a two-aircraft conflict in the plane $\{(v_{ij,x}, v_{ij,y}) \in \mathbb{R}^2\}$. The sign of $g_{ij}(v_{ij,x}, v_{ij,y})$ is shown by the + and - green symbols and the hashed pink region corresponds to $g_{ij}(v_{ij,x}, v_{ij,y}) \geq 0$. The hashed green half-plane delimited by (P) represents diverging trajectories, i.e. $t_{ij}^{\min}(v_{ij,x}, v_{ij,y}) \leq 0$.

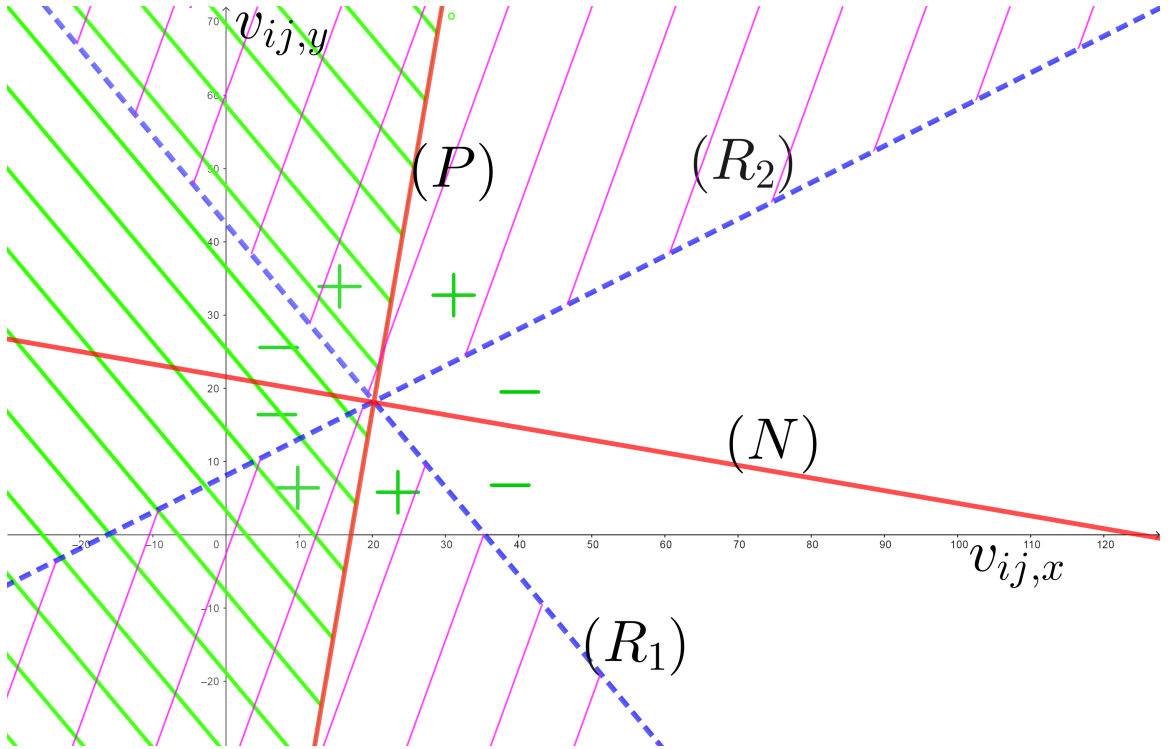


Figure 3.2: Illustration of a two-aircraft conflict in the plane $\{(v_{ij,x}, v_{ij,y}) \in \mathbb{R}^2\}$. The sign of $g_{ij}(v_{ij,x}, v_{ij,y})$ is shown by the + and - green symbols and the hashed pink region represents $g_{ij}(v_{ij,x}, v_{ij,y}) \geq 0$. The hashed green half-plane represents diverging trajectories, i.e. $t_{ij}^{\min}(v_{ij,x}, v_{ij,y}) \leq 0$. The dashed blue lines R_1 and R_2 correspond to the linear equations that are the roots of $g_{ij}(v_{ij,x}, v_{ij,y}) = 0$.

Consider the line normal to (P) , denoted (N) :

$$v_{ij,y}\hat{x}_{ij} - v_{ij,x}\hat{y}_{ij} = 0. \quad (N)$$

Recall that any point $(v_{ij,x}, v_{ij,y})$ such that $t_{ij}^{\min} \leq 0$ or $g_{ij}(v_{ij,x}, v_{ij,y}) \geq 0$ corresponds to a pair of conflict-free trajectories. Hence, the conflict-free region is non-convex and is represented by the union of the green and pink hashed regions in Figure 3.2. Reciprocally, the conflict region, corresponding to conflicting trajectories is convex and represented by the non-hashed region in Figure 3.2. An equivalent expression of Eq. (3.19) was proposed by Frazzoli et al. (2001) which observed that the set of conflict-free trajectories could be characterised by the union of two half-planes. However, the authors did not expand the formulation leading to the linear separation constraints (3.20) and (3.21) which require only a single binary variable for each disjunction.

Through Lemmas 1 and 2, it is shown that (N) is a bisector of the angle formed by lines R_1 and R_2 in the conflict zone ($g_{ij}(v_{ij,x}, v_{ij,y}) \leq 0$) and can be used to generate

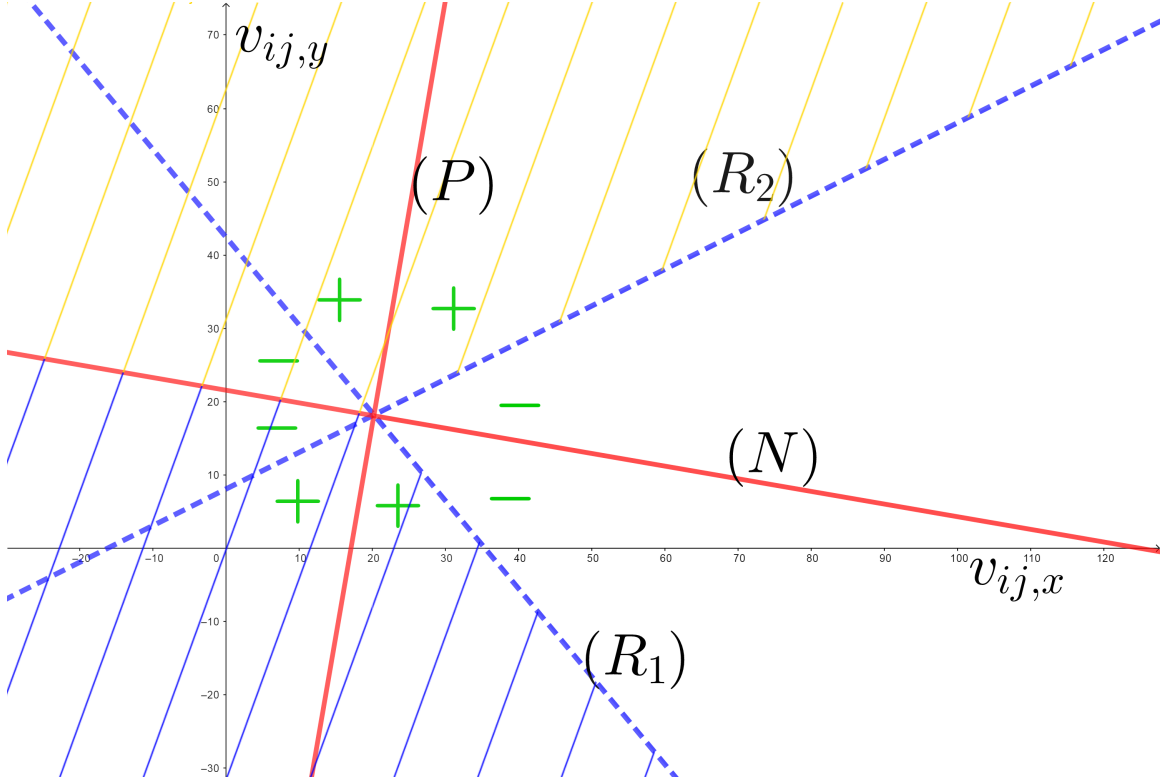


Figure 3.3: Illustration of a two-aircraft conflict in the plane $\{(v_{ij,x}, v_{ij,y}) \in \mathbb{R}^2\}$ highlighting the disjunctive convex regions: $z_{ij} = 1$ correspond to the region hashed in yellow and $z_{ij} = 0$ corresponds to the region hashed in blue. The dashed blue lines corresponds to the linear equations R_1 and R_2 that are the roots of $g_{ij}(v_{ij,x}, v_{ij,y}) = 0$.

two disjunctive but convex conflict-free regions.

Lemma 1. *The lines (P) and (N) are bisectors of the angles formed by the two lines R_1 and R_2 representing the solutions of $g_{ij}(v_{ij,x}, v_{ij,y}) = 0$.*

Proof. First, it is showed that (N) is the bisector of one of the two angles formed between R_1 and R_2 (see Figure 3.3). Note that the slope of the plane defined by (N) is $\frac{\hat{y}_{ij}}{\hat{x}_{ij}}$. Without any loss of generality, assume that $|\hat{x}_{ij}| > d$ (the case $|\hat{x}_{ij}| \leq d$ can be treated similarly).

Let $r_1 = \frac{\hat{x}_{ij}\hat{y}_{ij} + d\sqrt{\hat{x}_{ij}^2 + \hat{y}_{ij}^2 - d^2}}{\hat{x}_{ij}^2 - d^2}$ and $r_2 = \frac{\hat{x}_{ij}\hat{y}_{ij} - d\sqrt{\hat{x}_{ij}^2 + \hat{y}_{ij}^2 - d^2}}{\hat{x}_{ij}^2 - d^2}$ be the slopes of the lines defined by (3.19c) and (3.19d). The angle of the bisector of these lines is $\mu = \frac{1}{2}(\arctan r_1 + \arctan r_2)$ and its slope is:

$$\tan(\mu) = \tan\left(\frac{1}{2}(\arctan(r_1) + \arctan(r_2))\right) = \tan\left(\frac{1}{2}\left(\arctan\left(\frac{r_1 + r_2}{1 - r_1 r_2}\right)\right)\right).$$

If $r_1 r_2 = 1$, recall that $\lim_{X \rightarrow \pm\infty} \arctan(X) = \pm\pi/2$, thus $\tan(\mu) = \tan(\frac{1 \pm \pi}{2}) = \tan(\pm\pi/4) = \pm 1$. In addition, $r_1 r_2 = \frac{\hat{y}_{ij}^2 - d^2}{\hat{x}_{ij}^2 - d^2}$, hence $r_1 r_2 = 1 \Leftrightarrow \hat{y}_{ij}^2 = \hat{x}_{ij}^2$ and the slope of the plane defined by (N) is ± 1 .

Assume now $r_1 r_2 \neq 1$, using the half-angle formula, $\tan(\mu)$ can be written as:

$$\tan(\mu) = \frac{\sqrt{1 + \left(\frac{r_1 + r_2}{1 - r_1 r_2}\right)^2} - 1}{\left(\frac{r_1 + r_2}{1 - r_1 r_2}\right)}.$$

Since $\frac{r_1 + r_2}{1 - r_1 r_2} = \frac{2\hat{x}_{ij}\hat{y}_{ij}}{\hat{x}_{ij}^2 - \hat{y}_{ij}^2}$, this gives:

$$\tan(\mu) = \frac{\sqrt{(\hat{x}_{ij}^2 - \hat{y}_{ij}^2)^2 + 4\hat{x}_{ij}\hat{y}_{ij}} - (\hat{x}_{ij}^2 - \hat{y}_{ij}^2)}{2\hat{x}_{ij}\hat{y}_{ij}} = \frac{\hat{y}_{ij}}{\hat{x}_{ij}}.$$

Since (P) is orthogonal to (N) , the line (P) is the bisector of the other angle between the two linear equations represented by R_1 and R_2 . \square

Lemma 2. $g_{ij}(v_{ij,x}, v_{ij,y}) \leq 0$ for all points $(v_{ij,x}, v_{ij,y})$ of the normal line (N) .

Proof. Any point $(v_{ij,x}, v_{ij,y})$ of (N) verifies $v_{ij,y} = \frac{\hat{y}_{ij}}{\hat{x}_{ij}} v_{ij,x}$. Replacing $v_{ij,y}$ in (3.6) yields:

$$\begin{aligned} g_{ij}\left(v_{ij,x}, \frac{\hat{y}_{ij}}{\hat{x}_{ij}} v_{ij,x}\right) &= v_{ij,x}^2 (\hat{y}_{ij}^2 - d^2) + \left(\frac{\hat{y}_{ij}}{\hat{x}_{ij}} v_{ij,x}\right)^2 (\hat{x}_{ij}^2 - d^2) \\ &\quad - v_{ij,x} \frac{\hat{y}_{ij}}{\hat{x}_{ij}} v_{ij,x} (2\hat{x}_{ij}\hat{y}_{ij}). \end{aligned}$$

Simplifying the previous expression yields:

$$g_{ij}\left(v_{ij,x}, \frac{\hat{y}_{ij}}{\hat{x}_{ij}} v_{ij,x}\right) = -d^2 v_{ij,x}^2 \left(1 + \left(\frac{\hat{y}_{ij}}{\hat{x}_{ij}}\right)^2\right) \leq 0.$$

\square

Lemmas 1 and 2 assert that (N) can be used to split the conflict-free region into two convex but disjunctive regions. To model this disjunction, the variable $z_{ij} \in \{0, 1\}$ is defined as:

$$v_{ij,y}\hat{x}_{ij} - v_{ij,x}\hat{y}_{ij} \leq 0, \quad \text{if } z_{ij} = 1, \quad \forall (i, j) \in \mathcal{P}, \quad (3.20a)$$

$$v_{ij,y}\hat{x}_{ij} - v_{ij,x}\hat{y}_{ij} \geq 0, \quad \text{if } z_{ij} = 0, \quad \forall (i, j) \in \mathcal{P}. \quad (3.20b)$$

In each convex sub-region, the lines defined by (3.19a)-(3.19d) delineate the conflict-free region. The expressions of these lines depends on aircraft initial positions, i.e. \hat{x}_{ij} ,

\hat{y}_{ij} . Recall that R_1 and R_2 are denoted as the equation of these lines. Integer-linear separation conditions with regards to aircraft velocity components can be derived as follows:

$$v_{ij,y}\gamma_{ij}^l - v_{ij,x}\phi_{ij}^l \leq 0, \quad \text{if } z_{ij} = 1, \quad \forall(i, j) \in \mathcal{P}, \quad (3.21a)$$

$$v_{ij,y}\gamma_{ij}^u - v_{ij,x}\phi_{ij}^u \geq 0, \quad \text{if } z_{ij} = 0, \quad \forall(i, j) \in \mathcal{P}, \quad (3.21b)$$

where γ_{ij}^l , ϕ_{ij}^l and γ_{ij}^u , ϕ_{ij}^u are coefficients of the lines (3.19a)-(3.19d) corresponding to the roots of $g_{ij}(v_{ij,x}, v_{ij,y}) = 0$. The proposed linear disjunction is illustrated in Figure 3.3 which depicts the resulting convex sub-regions corresponding the disjunction $z_{ij} \in \{0, 1\}$ for a two-aircraft conflict. This leads to the following result.

Theorem 1. *The disjunctive linear separation conditions (3.20)-(3.21) fully characterise the set of aircraft pairwise conflict-free trajectories as given by Eq. (3.1)*

Proof. This statement is proved by showing that the conditions (3.20)-(3.21) are equivalent to the non-linear conditions (3.7) which are well-known to be equivalent to Eq. (3.1). As shown by Lemmas 1 and 2, the line (N) splits the $(v_{ij,x}, v_{ij,y})$ -plane into two disjunctive regions and the region in which lies the normal line (N) consists of conflicting trajectories. Thus, both half-planes induced by the normal plane (N) contain sub-regions corresponding to conflict-free and conflicting trajectories, and Eq. (3.20) defines variables z_{ij} accordingly. Consider the half-plane corresponding to $z_{ij} = 1$ (see Figure 3.3). This half-plane can be further split into two convex sub-regions and inequality (3.21a) characterises convex conflict-free region in which all pairs of aircraft trajectories verify $g_{ij}(v_{ij,x}, v_{ij,y}) \geq 0$ or $t_{ij}^{\min} \leq 0$. The same reasoning applies to the half-plane corresponding to $z_{ij} = 0$ if substituting (3.21a) by (3.21b). Hence, all pairs of future conflict-free trajectories for aircraft i and j are characterised by the separation conditions (3.20)-(3.21). \square

Theorem 1 asserts that the disjunctive separation conditions (3.20)-(3.21) is equivalent to the definition of the non-linear separation conditions. Further, these disjunctive separation conditions are linear with regards to aircraft velocity variables $v_{ij,x}$ and $v_{ij,y}$ and require a single binary variable per pair of aircraft. This is expected to improve on the so-called shadow separation conditions which are also linear with regards to aircraft velocity variables, but require four binary variables per pair of aircraft (Pallottino et al., 2002; Alonso-Ayuso et al., 2011, 2016). The remaining of this section discusses the aircraft trajectory control model and the objective functions

of the proposed formulations.

Model 2. *Non-convex 2D Formulation using Disjunctive Separation Conditions*

$$\begin{aligned}
& \text{Minimise} && \sum_{i \in \mathcal{A}} w\theta_i^2 + (1-w)(1-q_i)^2, \\
& \text{Subject to:} && \\
& v_{ij,x} = q_i \widehat{v}_i \cos(\widehat{\theta}_i + \theta_i) - q_j \widehat{v}_j \cos(\widehat{\theta}_j + \theta_j), && \forall (i, j) \in \mathcal{P}, \\
& v_{ij,y} = q_i \widehat{v}_i \sin(\widehat{\theta}_i + \theta_i) - q_j \widehat{v}_j \sin(\widehat{\theta}_j + \theta_j), && \forall (i, j) \in \mathcal{P}, \\
& v_{ij,y} \widehat{x}_{ij} - v_{ij,x} \widehat{y}_{ij} \leq 0, && \text{if } z_{ij} = 1, \quad \forall (i, j) \in \mathcal{P}, \\
& v_{ij,y} \widehat{x}_{ij} - v_{ij,x} \widehat{y}_{ij} \geq 0, && \text{if } z_{ij} = 0, \quad \forall (i, j) \in \mathcal{P}, \\
& v_{ij,y} \gamma_{ij}^l - v_{ij,x} \phi_{ij}^l \leq 0, && \text{if } z_{ij} = 1, \quad \forall (i, j) \in \mathcal{P}, \\
& v_{ij,y} \gamma_{ij}^u - v_{ij,x} \phi_{ij}^u \geq 0, && \text{if } z_{ij} = 0, \quad \forall (i, j) \in \mathcal{P}, \\
& \underline{q}_i \leq q_i \leq \bar{q}_i, && \forall i \in \mathcal{A}, \\
& \underline{\theta}_i \leq \theta_i \leq \bar{\theta}_i, && \forall i \in \mathcal{A}, \\
& v_{ij,x}, v_{ij,y} \in \mathcal{B}_{ij}, && \forall (i, j) \in \mathcal{P}, \\
& z_{ij} \in \{0, 1\}, && \forall (i, j) \in \mathcal{P}.
\end{aligned}$$

3.4 Non-convex Shadow Formulation

Another state-of-the-art formulation was initially proposed by Bilimoria (2000) and further discussed by Pallottino et al. (2002) where the authors created a model based on trigonometric projections of the conflict circle of two aircraft. The formulation is based on the projection of the circumference corresponding to one aircraft into the trajectory of the other, called shadow. In this formulation, a conflict occurs if two or more aircraft have an intersection between their respective shadows. One way to calculate those shadows segments is via the angle formed by each pair of aircraft given certain manoeuvres which are defined as l_{ij} and r_{ij} for $(i, j) \in \mathcal{P}$ and can be visualised in Figure 3.4. But first, it is required to define the angles w_{ij} and α_{ij} . In the figure, the segment \widehat{p}_i and \widehat{p}_j represent the initial trajectory vector. The resulting segment obtained by joining those vector has a slope equal to w_{ij} . In this same picture, the segment formed by the relative distance between \widehat{p}_i and \widehat{p}_j and the safety distance d can be used to calculate α_{ij} . Hence,

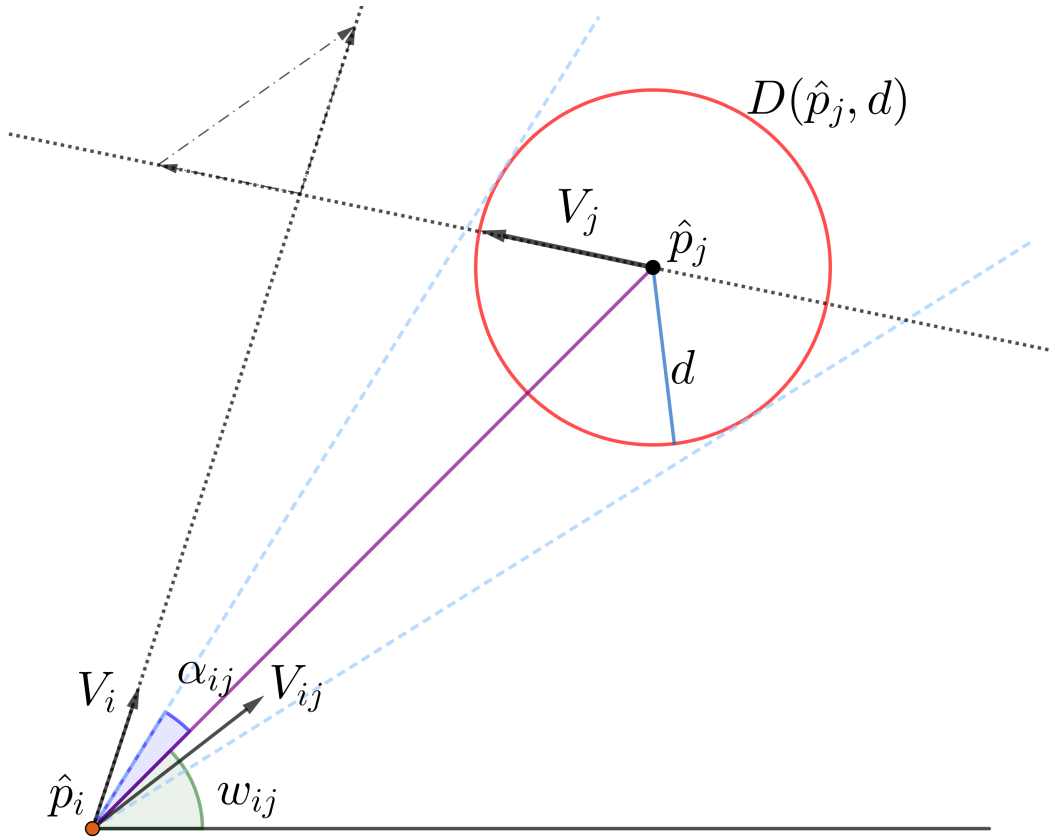


Figure 3.4: Geometrical analysis of conflict between two aircraft based on relative velocity

$$\tan(w_{ij}) = \frac{\hat{y}_{ij}}{\hat{x}_{ij}} \quad (3.23a)$$

$$\tan(\alpha_{ij}) = \frac{d}{\sqrt{\hat{x}_{ij}^2 + \hat{y}_{ij}^2 - d^2}} \quad (3.24a)$$

where d is the minimal separation between pairs of aircraft and d_{ij} is the initial distance between a pair of aircraft. Based on those definitions, the angle l_{ij} and r_{ij} can be calculated as:

$$l_{ij} = w_{ij} + \alpha_{ij}, \quad (3.25a)$$

$$r_{ij} = w_{ij} - \alpha_{ij}. \quad (3.25b)$$

Finally, no conflicts occur if:

$$\frac{v_{ij,y}}{v_{ij,x}} \geq \tan(l_{ij}) \quad \forall (i, j) \in \mathcal{P}, \quad (3.26a)$$

or

$$\frac{v_{ij,y}}{v_{ij,x}} \leq \tan(r_{ij}) \quad \forall (i, j) \in \mathcal{P}. \quad (3.26b)$$

Given that the sign of $v_{ij,x}$ changes the value of the tan function, this results in four cases and to check the existence of conflicts those four conditions need to be verified. Let $\sigma_{ij}^1, \sigma_{ij}^2, \sigma_{ij}^3, \sigma_{ij}^4 \in \{0, 1\}$ be binary decision variables for all aircraft pair $(i, j) \in \mathcal{P}$. The separation constraints for this so-called shadow formulation are defined as:

$$-v_{ij,x} \leq M_{ij}^s(1 - \sigma_{ij}^1), \quad \forall (i, j) \in \mathcal{P}, \quad (3.27a)$$

$$v_{ij,x} \tan(l_{ij}) - v_{ij,y} \leq (1 - \sigma_{ij}^1)M_{ij}^{tanl}, \quad \forall (i, j) \in \mathcal{P}, \quad (3.27b)$$

$$-v_{ij,x} \leq M_{ij}^s(1 - \sigma_{ij}^2), \quad \forall (i, j) \in \mathcal{P}, \quad (3.27c)$$

$$-v_{ij,x} \tan(r_{ij}) + v_{ij,y} \leq (1 - \sigma_{ij}^2)M_{ij}^{tanr}, \quad \forall (i, j) \in \mathcal{P}, \quad (3.27d)$$

$$v_{ij,x} \leq M_{ij}^s(1 - \sigma_{ij}^3), \quad \forall (i, j) \in \mathcal{P}, \quad (3.27e)$$

$$-v_{ij,x} \tan(l_{ij}) + v_{ij,y} \leq (1 - \sigma_{ij}^3)M_{ij}^{tanl}, \quad \forall (i, j) \in \mathcal{P}, \quad (3.27f)$$

$$v_{ij,x} \leq M_{ij}^s(1 - \sigma_{ij}^4), \quad \forall (i, j) \in \mathcal{P}, \quad (3.27g)$$

$$v_{ij,x} \tan(r_{ij}) - v_{ij,y} \leq (1 - \sigma_{ij}^4)M_{ij}^{tanr}, \quad \forall (i, j) \in \mathcal{P}, \quad (3.27h)$$

$$\sigma_{ij}^1 + \sigma_{ij}^2 + \sigma_{ij}^3 + \sigma_{ij}^4 \geq 1, \quad \forall (i, j) \in \mathcal{P}, \quad (3.27i)$$

where M_{ij}^{tanr} and M_{ij}^{tanl} are big-M constants. This formulation was further implemented and expanded for speed and altitude control by Alonso-Ayuso et al. (2011) and to incorporate heading control in Alonso-Ayuso et al. (2016). The main contribution of this model is the way the author defined their separation condition as described in details in Pallottino et al. (2002).

The non-convex formulation for the 2D ACRP based on the shadow separation conditions can be summarised as follows:

Model 3. *Non-convex 2D Formulation using Shadow Separation Conditions*

$$\text{Minimise} \quad \sum_{i \in \mathcal{A}} w\theta_i^2 + (1 - w)(1 - q_i)^2,$$

Subject to:

$$\begin{aligned}
v_{ij,x} &= q_i \widehat{v}_i \cos(\widehat{\theta}_i + \theta_i) - q_j \widehat{v}_j \cos(\widehat{\theta}_j + \theta_j), & \forall (i, j) \in \mathcal{P}, \\
v_{ij,y} &= q_i \widehat{v}_i \sin(\widehat{\theta}_i + \theta_i) - q_j \widehat{v}_j \sin(\widehat{\theta}_j + \theta_j), & \forall (i, j) \in \mathcal{P}, \\
-v_{ij,x} &\leq M_{ij}^s (1 - \sigma_{ij}^1), & \forall (i, j) \in \mathcal{P}_S, \\
v_{ij,x} \tan(l_{ij}) - v_{ij,y} &\leq (1 - \sigma_{ij}^1) M_{ij}^{tanl}, & \forall (i, j) \in \mathcal{P}, \\
-v_{ij,x} &\leq M_{ij}^s (1 - \sigma_{ij}^2), & \forall (i, j) \in \mathcal{P}, \\
-v_{ij,x} \tan(r_{ij}) + v_{ij,y} &\leq (1 - \sigma_{ij}^2) M_{ij}^{tanr}, & \forall (i, j) \in \mathcal{P}, \\
v_{ij,x} &\leq M_{ij}^s (1 - \sigma_{ij}^3), & \forall (i, j) \in \mathcal{P}, \\
-v_{ij,x} \tan(l_{ij}) + v_{ij,y} &\leq (1 - \sigma_{ij}^3) M_{ij}^{tanl}, & \forall (i, j) \in \mathcal{P}, \\
v_{ij,x} &\leq M_{ij}^s (1 - \sigma_{ij}^4), & \forall (i, j) \in \mathcal{P}, \\
v_{ij,x} \tan(r_{ij}) - v_{ij,y} &\leq (1 - \sigma_{ij}^4) M_{ij}^{tanr}, & \forall (i, j) \in \mathcal{P}, \\
\sigma_{ij}^1 + \sigma_{ij}^2 + \sigma_{ij}^3 + \sigma_{ij}^4 &\geq 1, & \forall (i, j) \in \mathcal{P}, \\
\underline{q}_i &\leq q_i \leq \overline{q}_i, & \forall i \in \mathcal{A}, \\
\underline{\theta}_i &\leq \theta_i \leq \overline{\theta}_i, & \forall i \in \mathcal{A}, \\
v_{ij,x}, v_{ij,y} &\in \mathcal{B}_{ij}, & \forall (i, j) \in \mathcal{P}, \\
\sigma_{ij}^1, \sigma_{ij}^2, \sigma_{ij}^3, \sigma_{ij}^4 &\in \{0, 1\}, & \forall (i, j) \in \mathcal{P}.
\end{aligned}$$

3.5 Equivalence Between Formulations

Models 1 and 2 have the same derivation, whereas the second corresponds to the linearisation of the non-linear separation conditions presented in the first model. Therefore, the equivalence between those two models is easily explained.

However, although Models 2 and 3 are initially different, because their basic premises and constraint format, as proved by Pelegrín and d'Ambrosio (2020), both present the same constraints that are only represented differently.

Recalling that the angles l_{ij} and r_{ij} are used to verify conflicts in Model 3. Those angles are based, among other parameters, on the value of α_{ij} and β_{ij} . In addition, recalling the equation in 3.26, the tangents of such angles are used in the separation conditions. Calculating those values:

$$\tan(w_{ij} + \alpha_{ij}) = \frac{\tan(w_{ij}) + \tan(\alpha_{ij})}{1 - \tan(w_{ij}) \tan(\alpha_{ij})} = \frac{\widehat{y}_{ij} \sqrt{\widehat{x}_{ij}^2 + \widehat{y}_{ij}^2 - d^2} + d\widehat{x}_{ij}}{\widehat{x}_{ij} \sqrt{\widehat{x}_{ij}^2 + \widehat{y}_{ij}^2 - d^2} - d\widehat{y}_{ij}} \quad (3.29a)$$

$$\tan(w_{ij} - \alpha_{ij}) = \frac{\tan(w_{ij}) - \tan(\alpha_{ij})}{1 - \tan(w_{ij}) \tan(\alpha_{ij})} = \frac{\widehat{y}_{ij} \sqrt{\widehat{x}_{ij}^2 + \widehat{y}_{ij}^2 - d^2} - d\widehat{x}_{ij}}{\widehat{x}_{ij} \sqrt{\widehat{x}_{ij}^2 + \widehat{y}_{ij}^2 - d^2} + d\widehat{y}_{ij}} \quad (3.29b)$$

Those expressions can be further simplified by multiplying both numerator and denominator by the "conjugate" of their respective denominator. The following expression is obtained:

$$\tan(w_{ij} + \alpha_{ij}) = \frac{\widehat{x}_{ij}\widehat{y}_{ij} + d\sqrt{\widehat{x}_{ij}^2 + \widehat{y}_{ij}^2 - d^2}}{\widehat{x}_{ij}^2 - d^2} \quad (3.29ca)$$

$$\tan(w_{ij} - \alpha_{ij}) = \frac{\widehat{x}_{ij}\widehat{y}_{ij} - d\sqrt{\widehat{x}_{ij}^2 + \widehat{y}_{ij}^2 - d^2}}{\widehat{x}_{ij}^2 - d^2} \quad (3.29cb)$$

Now replacing this equation in (3.26):

$$\frac{v_{ij,y}}{v_{ij,x}} \geq \frac{\widehat{x}_{ij}\widehat{y}_{ij} + d\sqrt{\widehat{x}_{ij}^2 + \widehat{y}_{ij}^2 - d^2}}{\widehat{x}_{ij}^2 - d^2} \rightarrow (\widehat{x}_{ij}^2 - d^2)v_{ij,y} - (\widehat{x}_{ij}\widehat{y}_{ij} + d\sqrt{\widehat{x}_{ij}^2 + \widehat{y}_{ij}^2 - d^2})v_{ij,x} \geq 0, \quad (3.29da)$$

$$\frac{v_{ij,y}}{v_{ij,x}} \geq \frac{\widehat{x}_{ij}\widehat{y}_{ij} - d\sqrt{\widehat{x}_{ij}^2 + \widehat{y}_{ij}^2 - d^2}}{\widehat{x}_{ij}^2 - d^2} \rightarrow (\widehat{x}_{ij}^2 - d^2)v_{ij,y} - (\widehat{x}_{ij}\widehat{y}_{ij} - d\sqrt{\widehat{x}_{ij}^2 + \widehat{y}_{ij}^2 - d^2})v_{ij,x} \geq 0, \quad (3.29db)$$

where those constraints are exactly the same as 3.19c and 3.19d presented in Section 3.3. The remaining constraint 3.19a and 3.19b can be obtained via the same process with the difference that 3.29 should be multiplied by the "conjugate" of the numerator instead.

This comes to show that the combinatorial nature of this problem, the different formulation can look completely apart from a first glance but represent the same approach in close analysis. However, it is important to emphasise that the disjunctive formulation requires a single binary variable as a single representation of the disjunction in its feasible region while the shadow formulation requires four different binary variables to represent all four possibilities.

3.6 Data For Numerical Experiments

The performance of the proposed mixed-integer formulations and algorithms is tested using four benchmark problems from the literature: the Circle Problem (CP), the Flow Problem (FP), the Grid Problem (GP) and the Random Circle Problem (RCP). The four types of benchmarking instances are illustrated in Figure 3.5. For all instances, it is assumed that the aircraft obey uniform motion laws and there is no randomness effect. Their trajectory is traceable throughout the whole process. In addition, they represent enclosed air space, which means that there are not additional aircraft leaving or entering that region.

The CP consists of a set of aircraft uniformly positioned on the circle, heading towards its centre. Aircraft speeds are assumed to be identical, hence the problem is highly symmetric (see Fig. 3.5a). The CP is notoriously difficult due to the geometry of aircraft initial configuration and it has been widely used for benchmarking CD&R algorithms in the literature (Durand and Alliot, 2009; Rey et al., 2015; Cafieri and Omhenni, 2017; Cafieri and Rey, 2017; Rey and Hijazi, 2017). Those instances represent a more ideal scenario where all the aircraft are believed to move at the same initial speed, therefore leading to conflicts in the centre of the circle. In those cases, the number of conflicts can be easily pre-calculated based on the number of aircraft in the instances. The main benefit of this instance is that they provide a significant number of conflicts in each instance, which is ideal to test whether the models are robust and scalable enough. However, the main drawback is their symmetry which does not represent real air traffic scenarios.

To break the symmetry of CP benchmarking instances, Vanaret et al. (2012) introduced the RCP which builds on the same framework, but aircraft initial speeds and headings are randomly deviated within specified ranges to create randomised instances with less structure (see Figure 3.5b). CP and RCP instances are named CP-N and RCP-N, respectively, where N is the total number of aircraft. Different from the CP instances, RCP instances provide a more realistic scenario where aircraft have more autonomy in which direction that will take. Even though those instances have more aircraft, the number of conflicts is not fixed and is normally small compared to their density, which reflects the real scenarios. Because of their random aspects, 100 unique copies of each of those instances are tested.

Both CP and RCP instances do not account for the sequences of aircraft which is a very common phenomenon due to the way airways are organised and the consequently

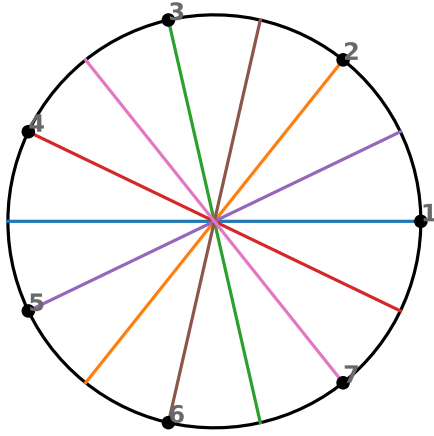
queuing of aircraft. Lehouillier et al. (2017) formally introduced two additional structured problems which aim to represent more realistic air traffic configurations: the FP and the GP. The FP consists of two streams of aircraft separated by an angle α and anchored on the circumference of a circle. In each stream, aircraft are separated by at least 5 NM (15 NM is used in these experiments) from each other (see Figure 3.5c). The GP consists of two FP instances separated by 15 NM diagonally (see Figure 3.5d). FP and GP instances are named FP-N and GP-N, respectively, where N denotes the number of aircraft per stream. In these instances, the initial distance between aircraft (or frequency) can be manipulated and therefore used to reproduce any type of scenario and therefore cover the most common occurrences in real airspace applications.

In all experiments, a circle of radius 200NM is used. For CP, FP and GP instances, all aircraft have an initial speed of 500 NM/h. For RCP instances, aircraft initial speeds are randomly chosen in the range 486-594 NM/h and their initial headings are deviated from a radial trajectory (i.e. towards the centre of the circle) by adding a randomly chosen angle between $-\frac{\pi}{6}$ and $+\frac{\pi}{6}$. For FP and GP instances, the values for α are $\alpha = \frac{\pi}{6}$ and $\alpha = \frac{\pi}{2}$, respectively, as proposed by Lehouillier et al. (2017). Those four sets of instances represent collectively the most used instances to test ATC models. They represent a viable replacement of real data, due to the difficulty in acquiring real information, which is mostly classified or limited to specific geographic regions. Nevertheless, the main objective is to extensively study and analyse the behaviour of the models in extreme circumstances.

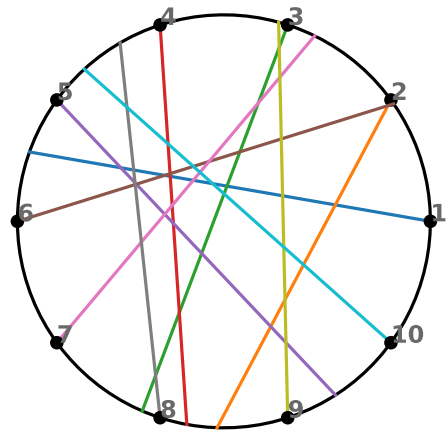
3.7 Numerical Results

In this section, the three classical formulations are compared using the instances presented in the previous section. Report of numerical results for problems with a subliminal speed control range of $[-6\%, +3\%]$ (Bonini et al., 2009) and the heading angle range of $[-\frac{\pi}{6}, \frac{\pi}{6}]$ as commonly used in the literature (Cafieri and Omheni, 2017; Rey and Hijazi, 2017) are presented. As setting conditions, it is assumed that there is only one flight level available and all aircraft is at that level. For the parameter w , it is used $w = 0.5$ to guarantee balance both types of manoeuvres.

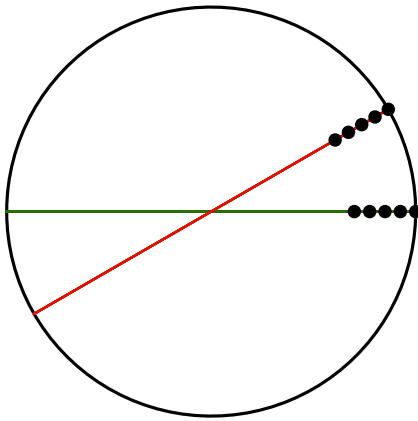
For this testing, the same formulation is used for all models with the difference of the separation conditions that is specific for each model. All models are implemented using PYTHON on a personal computer with 16 GB of RAM and an Intel i7 processor at 2.9GHz. The MIQPs and MIQCPs are solved with AMPL (Fourer et al. (1987))



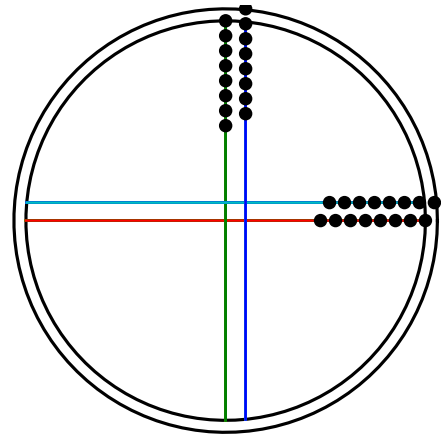
(a) CP-7: circle problem with 7 aircraft



(b) RCP-10: random circle problem with 10 aircraft



(c) FP-5: flow problem with 10 aircraft and $\alpha = \frac{\pi}{6}$



(d) GP-8: grid problem with 32 aircraft and $\alpha = \frac{\pi}{2}$

Figure 3.5: Example of 2D benchmarking instances for the Circle Problem (CP), Random Circle Problem (RCP), Flow Problem (FP) and Grid Problem (GP).

using default options. For reproducibility purposes, all formulations and instances used are available at <https://github.com/acrp-lib/acrp-lib>.

To report the performances of the proposed formulations on 2D ACRPs, four groups of numerical experiments are used, one per instance type. The results for 5 CP instances ranging from 4 to 8 aircraft are presented in Table 3.1. Results for FP and GP instances are reported in Tables 3.2-3.3, respectively, for 5 instances with 6 to 14 aircraft per stream and 3 instances with 12 to 28 aircraft. Results for RCP instances are reported in Tables 3.4 and 3.5 for five instance sizes with 10 and 20 and

the average performance along with the standard deviation in parenthesis are also reported. A time limit of 10 minutes was set for all instances.

Each row in the results tables represents an instance. The header of the results tables is presented from left to right. The left-most column, Instance, identifies the instance; $|\mathcal{A}|$ is the number of aircraft and n_c is the number of the conflicts. The next three sections correspond to the performance of three classical formulations: the first one corresponds to Model 1 using the non-linear formulation for the separation conditions and the header are: LB and UB are the lower and upper bound; Gap is the optimality gap in percent calculated using LB and UB; Time is the total runtime in seconds and n_t represents whether the instance could not be solved within the time limit (10 minutes), i.e. reports instances that time-out. The second section corresponds to the same value but for the Model 2 using the disjunctive formulation. The third section is the results from the Model 3 using the shadow formulation.

Instance	$ \mathcal{A} $	n_c	Non-convex Quadratic			Non-convex Disjunctive			Non-convex Shadow		
			UB	Time	n_t	UB	Time	n_t	UB	Time	n_t
CP-4	4	6	6.25e-4	9.59	no	6.25e-4	1.21	no	6.24e-4	2.27	no
CP-5	5	10	1.13e-3	600	yes	1.13e-3	5.27	no	1.13e-3	10.7	no
CP-6	6	15	1.91e-3	600	yes	1.81e-3	15.7	no	1.80e-3	16.1	no
CP-7	7	21	5.12e-3	600	yes	2.37e-3	42.5	no	2.37e-3	76.1	no
CP-8	8	28	4.16e-3	600	yes	3.46e-3	293	no	3.46e-3	600	yes

Table 3.1: Summary of Results for 2D CP instances with a speed control range of $[-6\%, +3\%]$ and a heading control range of $[-30^\circ, +30^\circ]$. All runtimes (Time) are reported in seconds. The optimality gaps (Gap) are the proportion of time-outs (n_t) are reported in percentage.

The experiments on the CP instances (Table 3.1 show that the upper bound increases with the number of aircraft. Using both disjunctive and shadow formulation, instances up to 7 aircraft were solved within the available time limit. For the non-linear formulation, it is observed that instances with more than 5 aircraft could not be solved. For all three formulations, the runtime increases exponentially with the number of aircraft and as the number of conflict increases. For the non-linear model, the only instances that can be solved are CP-5 in less than 10s. For disjunctive, all instances can be solved up to roughly 300s. For the shadow formulation, all instances except CP-8 (out of the five tested) could be solved within the time limit and the runtime is up to 76s. However, for all instances that could be solved by both disjunctive and shadow, the former outperforms the latter in all instances by an average of 62.6%.

Instance	$ \mathcal{A} $	n_c	Non-convex Quadratic			Non-convex Disjunctive			Non-convex Shadow		
			UB	Time	n_t	UB	Time	n_t	UB	Time	n_t
FP-3	6	3	3.90e-4	600	yes	3.42e-4	2.41	no	3.39e-4	7.03	no
FP-4	8	4	8.62e-4	600	yes	8.15e-4	122	no	8.14e-4	600	yes
FP-5	10	5	1.44e-3	600	yes	1.13e-3	600	yes	1.13e-3	600	yes
FP-6	12	6	3.70e-1	600	yes	1.53e-3	600	yes	3.40e-2	600	yes
FP-7	14	7	4.79e-1	600	yes	2.05e-3	600	yes	3.85e-1	600	yes

Table 3.2: Summary of Results for 2D FP instances with a speed control range of $[-6\%, +3\%]$ and a heading control range of $[-30^\circ, +30^\circ]$. All runtimes (Time) are reported in seconds. The optimality gaps (Gap) are the proportion of time-outs (n_t) are reported in percentage.

In Table 3.2, the results from FP instances are presented. In a similar manner as in the CP results, the upper bound increases with the number of the aircraft as the runtime. However, given the difficulty and density of those instances, the results show that those formulations cannot solve the majority of the instances tested. For the non-linear formulation, all the instances could not be solved within 10 minutes of the time limit. However, by comparison with the remaining formulations, the optimality gap is relatively small. The disjunctive formulation performs the best between the three tested and it can solve 2 out of the 5 tested instances within 2 minutes. Lastly, the shadow formulation can solve only 1 instance (FP-3) within the time limit imposed.

Instance	$ \mathcal{A} $	n_c	Non-convex Quadratic			Non-convex Disjunctive			Non-convex Shadow		
			UB	Time	n_t	UB	Time	n_t	UB	Time	n_t
GP-3	12	8	8.49e-4	600	yes	8.25e-4	600	yes	8.34e-4	600	yes
GP-4	16	16	3.18e-2	600	yes	9.17e-4	600	yes	9.17e-4	600	yes
GP-5	20	20	2.82e-2	600	yes	1.29e-3	600	yes	1.29e-3	600	yes
GP-6	24	24	1.20e+1	600	yes	1.20e+1	600	yes	1.20e+1	600	yes
GP-7	28	28	1.40e+1	600	yes	1.40e+1	600	yes	1.40e+1	600	yes

Table 3.3: Summary of Results for 2D GP instances with a speed control range of $[-6\%, +3\%]$ and a heading control range of $[-30^\circ, +30^\circ]$. All runtimes (Time) are reported in seconds. The optimality gaps (Gap) are the proportion of time-outs (n_t) are reported in percentage.

For GP instances, the results in Table 3.3 show that all three formulations cannot solve any of the five instances tested. Similarly as expressed in the CP instances, there is no correlation between the number of aircraft and number of conflict and the former is calculated in pre-processing. As in previous results, the upper bound increases proportionally to the number of aircraft and the number of conflict per instance. For

smaller instances, the best possible upper bound found within the time limit is the same for disjunctive and shadow formulation. However, it is slightly larger for the non-linear formulation, especially for GP-4. However, for larger instances (GP-5 and above) all the formulation found the same upper bound after 10 minutes of runtime.

Instance	$ \mathcal{A} $	n_c	Non-convex Quadratic			Non-convex Disjunctive			Non-convex Shadow		
			UB	Time	n_t	UB	Time	n_t	UB	Time	n_t
RCP-10-1	10	6	2.78e-4	600	yes	2.13e-4	15.9	no	2.12e-4	39.7	no
RCP-10-2	10	10	3.28e-5	600	yes	3.45e-5	13.6	no	3.22e-5	37.6	no
RCP-10-3	10	15	1.54e-4	600	yes	1.54e-4	14.5	no	1.54e-4	33.2	no
RCP-10-4	10	21	7.53e-6	101	no	5.53e-6	14.1	no	7.23e-6	23.1	no
RCP-10-5	10	28	1.43e-4	600	yes	6.31e-5	17.4	no	5.73e-5	38.0	no

Table 3.4: Summary of Results for 2D RCP-10 instances with a speed control range of $[-6\%, +3\%]$ and a heading control range of $[-30^\circ, +30^\circ]$. All runtimes (Time) are reported in seconds. The optimality gaps (Gap) are the proportion of time-outs (n_t) are reported in percentage.

In RCP-10, the result for different versions of the same instance generated by its randomness nature is reported. In these results, it is observed that the number of conflicts is not proportional to number to aircraft (differently from CP instances) and it is calculated separately. In average, it is no more than 4 conflicts per instances. The runtime is roughly similar for all instances as the value for the upper bound. The results also reveal that only one instance (RCP-10-4) could be solved by the non-linear formulation and it took less than 2 minutes. Using the disjunctive formulation, all instances were solved in less than 20s while the shadow formulation took approximately the double of this amount on average. For disjunctive formulation, the runtime is on average around 15s seconds with RCP-10-2 taking only 13.6s while RCP-10-5 taking up to 17.4s. For the shadow formulation, the average is 35s (133% higher than disjunctive), with RCP-10-4 as the quickest instances to be solved in only 23s while RCP-10-1 took almost 40s.

Table 3.5 reveals the results for RCP instances with 20 aircraft. In this table, the results for different versions of the same instance generated by its randomness nature are reported and in this case, it is with 20 aircraft per instances. In these results, it is observed that the number of conflicts is not proportional to number to aircraft (similarly as in RCP-10 instances) and it is calculated separately. In average, it is no more than 8 conflicts per instances. In addition, it can be noticed that for all instance, all three models could not find a solution within the time limit. For

Instance	$ \mathcal{A} $	n_c	Non-convex Quadratic			Non-convex Disjunctive			Non-convex Shadow		
			UB	Time	n_t	UB	Time	n_t	UB	Time	n_t
RCP-20-1	4	6	2.04e-2	600	yes	2.04e-2	600	yes	2.04e-2	600	yes
RCP-20-2	5	10	-	600	-	-	600	-	-	600	-
RCP-20-3	6	15	-	600	-	-	600	-	-	600	-
RCP-20-4	7	21	-	600	-	-	600	-	-	600	-
RCP-20-5	8	28	-	600	-	-	600	-	-	600	-

Table 3.5: Summary of Results for 2D RCP-20 instances with a speed control range of $[-6\%, +3\%]$ and a heading control range of $[-30^\circ, +30^\circ]$. All runtimes (Time) are reported in seconds. The optimality gaps (Gap) are the proportion of time-outs (n_t) are reported in percentage.

RCP-20-1, all model found the same upper bound, but the time limit was reached. For the four remaining instances, an upper bound could not be found.

3.8 Summary of Findings

In this chapter, the three classic formulations to solve the aircraft conflict resolution problem were presented and reviewed. It started by defining the equation of motions that are necessary to establish such models. Considering the two-dimensional problem with continuous speed and heading control, the three formulations are formally revised. It is also showed how the non-linear formulation can be linearised and that is the premise to obtain the disjunctive separation constraints. Further, the shadow separation constraint is revised and reproducing the proof shown by Pelegrín and d’Ambrosio (2020), it is showed that the disjunctive and the shadow formulation are equivalent. This solidifies the fact that all formulations are, at their core, equivalent. The difference relies upon the non-linearity with respect to the number of binaries variables required to implement and the non-linear components in the separation constraints.

The data necessary to test those three classical formulations were also introduced and it is composed of four different sets of instances: Circle Problem (CP), Flow Problem (FP), Grid Problem (GP) and Random Circle Problem (RCP). As an illustration, a smaller subset of those instances was used as a test. The performance of those models highlights the scalability issues that exist in those formulations given the trigonometric and quadratic constraints present in those models. In addition, the results in Section 3.7 show that the CP instances are the easiest to solve using disjunctive and shadow. However, due to the number of conflicts, the runtime increases

exponentially, which will ultimately hinder their performance. For FP instances, only disjunctive can solve more than one instance while GP instances cannot be solved by any of those formulations. These results highlight the difficulty of such format of instances (aircraft lineup in a stream), especially when comparing the disjunctive and shadow formulations. Finally, for RCP instances with 10 aircraft, the non-linear formulation cannot handle instance with such number of aircraft while the disjunctive and shadow formulation shows competitive results, with the former outperforming the latter where the runtime is reduced by half.

This could be easily justified by the number of binary variables used in each formulation. Nevertheless, due to the amount of aircraft per instances and the actual number of conflicts, the runtime for those instances is quite larger and it is expected that increasing the number of aircraft can cause violation of runtime limit. This is further evidenced in the results for RCP instances with 20 aircraft, that, even though many instances have a relatively small number of conflicts (in comparison to CP-7), a feasible solution cannot be found within 10 limits due to the dimension and difficulty of such instances. This highlights the fact that such formulations, although competitive and useful, can be improved. Nevertheless, earlier results show that the disjunctive model slightly outperforms the remaining formulations.

In the numerical experiments, it is showed the performance of the proposed models with different separation conditions by testing 5 CP instances, 5 FP instances, 5 GP instances and 5 RCP-10 and RCP-20 instances. The results reveal that the disjunctive formulation is able to solve 48% of the benchmarking instances compared to 40% using the shadow formulation and 4% using the non-linear formulation. Upon examining all instances that were solved by the disjunctive formulation and by the shadow formulation, it is observed that the former is systematically faster in all instances as well as than the non-linear formulation. For reproducibility purposes, all formulations and instances are made available at the public repository <https://github.com/acrp-lib/acrp-lib>.

3.9 Conclusion

As presented in this chapter, the basis of aircraft conflict resolution can be summarised in finding optimal routes based on the available manoeuvres regarding a set of aircraft in a limited airspace. The three state-of-the-art formulations established in the literature are presented and reported numerical results to illustrate their behaviour. The results showed that those formulations cannot be easily implemented.

Although they serve as a solid standpoint, they have many issues that limit their usage in terms of scalability and complexity. Between those issues, three main can be highlighted: 1) non-linearity. Because of the quadratic terms (present in Model 1) and trigonometric terms (in Model 2 and 3, the formulation is non-linear and non-convex which makes them very difficult to solve on large scale instances. Even for smaller or medium instances, those models cannot solve many instances, showing that cases hinder the potential of those formulations. In addition, to solve them, commercial solver such as CPLEX and GUROBI cannot be used. 2) weather events and measurements errors. In the vast literature review, it is noticeable the lack of models accounting for randomness. In these formulations and their performance, it is evident that they are challenging to solve. Therefore, it is expected that incorporating stochastic creates even more difficult cases to solve. Although there has been an effective effort into calculating conflict probabilities and how impactful such events can be in an already packed airspace, there are very fewer models where a solution algorithm is proposed to ACRP under uncertainty. 3) trajectory recovery. Avoidance is considered as the stage where manoeuvres are performed to avoid potential conflict. Those manoeuvres will eventually change the aircraft speed, heading and/or altitude. Although the latter does not interfere with the aircraft destination, speed and heading angle can cause the final trajectory to be very deviated from its nominal trajectory, which does not solve the original problem. For speed recovery, this task is slightly simpler, but heading changes represents a significant challenge. This is an area that has not been extensively covered and integrating trajectory recovery in mathematical programming approaches is a very challenging task that makes the problem even harder. Many attempts have been done in these are but there still an open question to provide a complete solution for such problem.

Chapter 4

Exact Solution Methods for the Deterministic Aircraft Conflict Resolution Problem

As explored in the literature review, automation is key component to perform and assist air traffic control. Higher and more reliable levels of automation can be achieved by the presence of efficient methods capable of detecting and proposing solutions for conflicts. Those solutions are required to be quick, free of error and precise. Between the myriad of solutions available, deterministic methods are a vital solution. In this chapter, the focus is on the deterministic ACRP approach, which is the version of the aircraft conflict resolution problem which does not allow any randomness and all variables are considered deterministic. This novel method is a constraint generation algorithm for the aircraft conflict resolution problem using the complex number formulation. It starts by presenting a linear programming to pre-process the set of aircraft based on the existence of potential conflicts in Section 4.1, followed by review of the complex number formulation introduced by Rey and Hijazi (2017) in Section 4.2. This formulation is extended to incorporate altitude changes in Section 4.3. Further quadratic relaxations are presented in Section 4.4 and the constraint generation is finally in Section 4.5. A decomposition algorithm comprehending all the steps above is described in Section 4.6, numerical results are described in Section 4.7 and the proposed formulation is tested against the convex and linearised version of the complex number formulation and the shadow formulation. An analytical solution of the two-aircraft conflict resolution problem is proposed in Section 4.8. In the conclusion, the summary of findings is presented in Section 4.9.1. This chapter is based on a paper accepted for publication in the European Journal of Operational Research (Dias et al., 2021).

Based on the definition of the aircraft conflict resolution problem established in Chapter 3, it is noticed that those formulations are non-linear and non-convex. In order to guarantee that feasible solutions are precise, quick and always possible to be achieved, some adjustments are necessary and more than often those adjustments end up hindering the quality of such methods. In this chapter addresses the deterministic ACRP, which presents a novel solution for the ACRP problem that guarantee optimality under deterministic conditions. In this, for the two-dimensional (2D) formulation, only speed and heading control are the manoeuvres available, while, For the 2D+FL formulation, it incorporate flight levels (FL) control to manage the altitude changes.

4.1 Pre-processing

Considering the conflict region of pair of aircraft represents the set of relative velocity vectors which correspond to a conflict. The relative positions of the relative velocity box \mathcal{B}_{ij} and the conflict region \mathcal{C}_{ij} can be examined to determine the existence or not of a potential conflict. For any pair $(i, j) \in \mathcal{P}$, if $\mathcal{B}_{ij} \cap \mathcal{C}_{ij} = \emptyset$, then aircraft i and j are separated for any combination of controls; conversely if $\mathcal{B}_{ij} \subset \mathcal{C}_{ij}$ then i and j cannot be separated via speed or heading control within the assumed control bounds; otherwise, \mathcal{B}_{ij} and \mathcal{C}_{ij} intersect but do not completely overlap. This is illustrated in Figure 3.1 which illustrates the three possible cases. Figure 3.1a illustrates the case where aircraft i and j are separated for any combination of speed and heading control— which means that such pairs are conflict-free. Figure 3.1b depicts the case where \mathcal{B}_{ij} and \mathcal{C}_{ij} only partially intersect— which means that such pairs are separable. Last, Figure 3.1c illustrates the case where $\mathcal{B}_{ij} \subset \mathcal{C}_{ij}$ — which means that such pairs are non-separable. The following propositions provide methods to efficiently determine if, given controls bounds on speed and heading, a pair of aircraft is either conflict-free or non-separable.

Proposition 2 (Conflict-free aircraft pair). *Consider a pair of aircraft $(i, j) \in \mathcal{P}$, and let $LP(i, j)$ be the feasibility problem defined as:*

$$LP(i, j) : \begin{cases} v_{ij,y}\gamma_{ij}^l - v_{ij,x}\phi_{ij}^l \geq 0, \\ v_{ij,y}\gamma_{ij}^u - v_{ij,x}\phi_{ij}^u \leq 0, \\ (v_{ij,x}, v_{ij,y}) \in \mathcal{B}_{ij}. \end{cases}$$

The pair of aircraft (i, j) is conflict-free for any 2D control if and only if the feasibility problem $LP(i, j)$ is infeasible.

Proof. For any pair $(i, j) \in \mathcal{P}$, the relative velocity box \mathcal{B}_{ij} and the conflict region \mathcal{C}_{ij} are both convex sets, and $\mathcal{B}_{ij} \cap \mathcal{C}_{ij}$ can be fully characterised by linear inequalities. The feasible region of the proposed feasibility linear program $LP(i, j)$ represents the set $\{(v_{ij,x}, v_{ij,y}) \in \mathcal{B}_{ij} \cap \mathcal{C}_{ij}\}$. If this set is empty, then there exists no pair of feasible trajectories for aircraft i and j which correspond to a conflict, hence the pair of aircraft $(i, j) \in \mathcal{P}$ is conflict-free. \square

Proposition 3 (Non-separable aircraft pair). *Consider a pair of aircraft $(i, j) \in \mathcal{P}$. The pair of aircraft (i, j) is non-separable if and only if each of the four extreme points of \mathcal{B}_{ij} corresponds to a conflict.*

Proof. Since the conflict region \mathcal{C}_{ij} is the convex, if all four extreme points of \mathcal{B}_{ij} are inside \mathcal{C}_{ij} , i.e. each extreme points of $E(\mathcal{B}_{ij})$ corresponds to a conflict, then the aircraft pair $(i, j) \in \mathcal{P}$ is non-separable for any controls. \square

Using Propositions 2 and 3, an efficient pre-processing algorithm to partition can be designed the set of aircraft pairs \mathcal{P} of a 2D ACRP instance into three categories: conflict-free pairs denoted \mathcal{P}_F , separable pairs denoted \mathcal{P}_S and non-separable pairs \mathcal{P}_I . To identify conflict-free pairs, $LP(i, j)$ is solved and a pair of aircraft is conflict-free if and only if the LP is infeasible. Observe that the feasibility linear program $LP(i, j)$ can be solved by enumerating all extreme points of its feasible region and tests if this corresponds to a conflict or not. Since the $LP(i, j)$ consists of four bound constraints and two shared constraints, there is a total of 13 extreme points to test (the combinations of the bound constraints of a variable can be excluded). To identify non-separable pairs, let denote $E(\mathcal{B}_{ij})$ the set of extreme points of the relative velocity box \mathcal{B}_{ij} for any pair $(i, j) \in \mathcal{P}$ and use the separation condition (3.3) to determine if all extreme points are conflicts or not. This procedure is summarised in Algorithm 1 (boldface is used to denote vectors). Observe that pairwise variables and constraints need only to be indexed by the set of separable pairs \mathcal{P}_S since pairs in \mathcal{P}_F are always conflict-free. Further, any 2D conflict resolution problem such that $|\mathcal{P}_I| > 0$ is infeasible.

Algorithm 1 Pre-processing of aircraft pairs

Input: $\mathcal{A}, \hat{\theta}, \hat{v}, \underline{q}, \bar{q}, \underline{\theta}, \bar{\theta}$ **Output:** $\mathcal{P}, \mathcal{P}_F, \mathcal{P}_S, \mathcal{P}_I$ $\mathcal{P} \leftarrow \{i, j \in \mathcal{A} : i < j\}$ $\mathcal{P}_F, \mathcal{P}_S, \mathcal{P}_I \leftarrow \emptyset$ **for** $(i, j) \in \mathcal{P}$ **do** Solve $LP(i, j)$ **if** $LP(i, j)$ is infeasible **then** $\mathcal{P}_F \leftarrow \mathcal{P}_F \cup \{(i, j)\}$ **else** $k \leftarrow 0$ **for** $(v_{ij,x}, v_{ij,y}) \in E(\mathcal{B}_{ij})$ **do** **if** $g_{ij}(v_{ij,x}, v_{ij,y}) < 0 \wedge t_{ij}^{min}(v_{ij,x}, v_{ij,y}) > 0$ **then** $k \leftarrow k + 1$ **if** $k = 4$ **then** $\mathcal{P}_I \leftarrow \mathcal{P}_I \cup \{(i, j)\}$ **else** $\mathcal{P}_S \leftarrow \mathcal{P}_S \cup \{(i, j)\}$

4.2 Complex Number Formulation for the 2D Aircraft Conflict Resolution Problem

An alternative way to represent aircraft motion equation is via the complex number formulation introduced by Rey and Hijazi (2017). Let V_i be the complex number defined as:

$$V_i = q_i(\cos(\theta_i) + i \sin(\theta_i)), \quad \forall i \in \mathcal{A}. \quad (4.1)$$

Representing V_i in its polar form with $\delta_{i,x} = q_i \cos(\theta_i)$ and $\delta_{i,y} = q_i \sin(\theta_i)$, yield:

$$V_i = \delta_{i,x} + i\delta_{i,y}, \quad \forall i \in \mathcal{A}. \quad (4.2)$$

The magnitude of V_i is $|V_i| = \sqrt{\delta_{i,x}^2 + \delta_{i,y}^2} = q_i$ and its argument is $\arg(V_i) = \arctan \frac{\delta_{i,x}}{\delta_{i,y}} = \theta_i$. This approach is inspired by complex number formulation for the optimal power flow problem in power systems, such as in Hijazi et al. (2017) and Coffrin et al. (2015). Accordingly, the relative motion equations of a pair of aircraft

can be rewritten as:

$$v_{ij,x} = \delta_{i,x} \hat{v}_i \cos(\hat{\theta}_i) - \delta_{i,y} \hat{v}_i \sin(\hat{\theta}_i) - \delta_{j,x} \hat{v}_j \cos(\hat{\theta}_j) + \delta_{j,y} \hat{v}_j \sin(\hat{\theta}_j), \quad \forall (i, j) \in \mathcal{P}_S, \quad (4.3a)$$

$$v_{ij,y} = \delta_{i,y} \hat{v}_i \cos(\hat{\theta}_i) - \delta_{i,x} \hat{v}_i \sin(\hat{\theta}_i) - \delta_{j,y} \hat{v}_j \cos(\hat{\theta}_j) + \delta_{j,x} \hat{v}_j \sin(\hat{\theta}_j), \quad \forall (i, j) \in \mathcal{P}_S. \quad (4.3b)$$

The variables $\delta_{i,x}$ and $\delta_{i,y}$ are used as the main control variables in this formulation and their bounds are derived from the bounds of the original control variables q_i and θ_i :

$$\underline{q}_i \cos(\max\{|\overline{\theta}_i|, |\underline{\theta}_i|\}) \leq \delta_{i,x} \leq \overline{q}_i, \quad \forall i \in \mathcal{A}, \quad (4.4a)$$

$$\overline{q}_i \sin(\underline{\theta}_i) \leq \delta_{i,y} \leq \overline{q}_i \sin(\overline{\theta}_i), \quad \forall i \in \mathcal{A}. \quad (4.4b)$$

The speed control constraint (3.8) can be reformulated in quadratic form as:

$$\underline{q}_i^2 \leq \delta_{i,x}^2 + \delta_{i,y}^2, \quad \forall i \in \mathcal{A}, \quad (4.5a)$$

$$\overline{q}_i^2 \geq \delta_{i,x}^2 + \delta_{i,y}^2, \quad \forall i \in \mathcal{A}. \quad (4.5b)$$

The heading control constraint (3.9) can be reformulated in linear form as:

$$\delta_{i,y} \geq \delta_{i,x} \tan(\underline{\theta}_i), \quad \forall i \in \mathcal{A}, \quad (4.6a)$$

$$\delta_{i,y} \leq \delta_{i,x} \tan(\overline{\theta}_i), \quad \forall i \in \mathcal{A}. \quad (4.6b)$$

To design the objective function, let introduce a preference weight $w \in]0, 1[$ to balance the trade-offs among velocity controls, i.e. speed and heading. The objective function proposed by Rey and Hijazi (2017) can be extended as follows:

$$\text{minimise } \sum_{i \in \mathcal{A}} w \delta_{i,y}^2 + (1 - w)(1 - \delta_{i,x})^2. \quad (4.7)$$

Next, is showed that the objective function (4.7) attains its minimum value when aircraft have deviation-free trajectories, i.e. $q_i = 1$ and $\theta_i = 0$ for all $i \in \mathcal{A}$.

Proposition 4. *The 2D objective function (4.7) is convex with regards to decision variables $\delta_{i,x}$ and $\delta_{i,y}$ for any value $w \in]0, 1[$, and is minimal for $q_i = 1$ and $\theta_i = 0$ for all aircraft $i \in \mathcal{A}$.*

Proof. Let $c_i(\delta_{i,x}, \delta_{i,y}) = w\delta_{i,y}^2 + (1-w)(1-\delta_{i,x})^2$ be the cost function of aircraft $i \in \mathcal{A}$. The first-order optimality conditions of $c_i(\delta_{i,x}, \delta_{i,y})$ are:

$$\begin{aligned}\frac{\partial c_i(\delta_{i,x}, \delta_{i,y})}{\partial \delta_{i,x}} &= (2\delta_{i,x} - 2)(1-w) = 0 \\ \frac{\partial c_i(\delta_{i,x}, \delta_{i,y})}{\partial \delta_{i,y}} &= 2w\delta_{i,y} = 0\end{aligned}$$

Recall that $w \in]0, 1[$, hence the first-order optimality conditions of this objective function yield $\delta_{i,x} = 1$ and $\delta_{i,y} = 0$ for all aircraft $i \in \mathcal{A}$. Since $\delta_{i,y} = q_i \sin(\theta_i)$, and $q_i > 0$, this implies $\delta_{i,y} = 0$ which is equivalent to $\theta_i = 0$ if $\theta_i \in]-\pi, \pi[$. Further, since $\delta_{i,x} = q_i \cos(\theta_i)$ and $\theta_i = 0$, $\delta_{i,x} = 1$ implies $q_i = 1$. It is trivial to show that $c_i(\delta_{i,x}, \delta_{i,y})$ is convex, thus the 2D objective function (4.7) is also convex.

Computing the Hessian matrix H of $c_i(\delta_{i,x}, \delta_{i,y})$ yields:

$$H = \begin{bmatrix} 2(1-w) & 0 \\ 0 & 2w \end{bmatrix}. \quad (4.8)$$

Observe that H is symmetric. Let $\mathbf{c} \in \mathbb{R}^2$ be a vector with entries c_1 and c_2 .

$$\mathbf{c}^\top H \mathbf{c} = 2(1-w)c_1^2 + 2wc_2^2 \geq 0. \quad (4.9)$$

Thus, H is positive semi-definite and the 2D objective function (4.7) is convex. \square

Proposition 4 shows that the proposed 2D objective function achieves an optimal value for deviation-free aircraft trajectories for any preference weight $w \in]0, 1[$. In Section 4.7.2, it is showed that the preference weight w can be used to prioritise speed deviation manoeuvres over heading deviation manoeuvres or vice-versa. Specifically, increasing w increases the penalisation of heading deviations whereas decreasing w increases the penalisation of speed deviations. Note that Pallottino et al. (2002) proposed MILP formulations for two conflict resolution problems which can be viewed as extreme case of the proposed 2D ACRP. Specifically, the authors introduced MILP constraints for the cases of speed-only control or heading-only control. Instead, let focus on the case of velocity control, i.e. simultaneous optimisation of aircraft speed and heading, thus justifying the range of the preference weight $w \in]0, 1[$.

The resulting formulation is summarised in Model 4. Model 4 provides a compact formulation for the 2D ACRP with speed and heading control which requires a single binary variable per pair of aircraft. This formulation is non-convex due to the speed lower bound constraint (4.5a) which is non-convex quadratic. Note that, the convex hull reformulation of the linear On/Off constraints (3.20) and (3.21) as derived in

Hijazi et al. (2014) is used. This reformulation does not require the introduction of auxiliary variables and is proved to provide the tightest continuous relaxation for each On/Off constraint. Note that coefficients $\gamma_{ij}^l, \phi_{ij}^l$ and $\gamma_{ij}^u, \phi_{ij}^u$ (present in (3.20) and (3.21)) can be pre-processed based on the sign of \hat{x}_{ij} and \hat{y}_{ij} . For implementation details, a fully reproducible formulation can be found at: <https://github.com/acrp-lib/acrp-lib>.

Model 4. Non-convex Complex Number Formulation

$$\text{Minimise } \sum_{i \in \mathcal{A}} w \delta_{i,y}^2 + (1-w)(1 - \delta_{i,x})^2,$$

Subject to:

$$\begin{aligned} v_{ij,x} &= \delta_{i,x} \hat{v}_i \cos(\hat{\theta}_i) - \delta_{i,y} \hat{v}_i \sin(\hat{\theta}_i) - \delta_{j,x} \hat{v}_j \cos(\hat{\theta}_j) + \delta_{j,y} \hat{v}_j \sin(\hat{\theta}_j), & \forall (i,j) \in \mathcal{P}_S, \\ v_{ij,y} &= \delta_{i,x} \hat{v}_i \sin(\hat{\theta}_i) + \delta_{i,y} \hat{v}_i \cos(\hat{\theta}_i) - \delta_{j,x} \hat{v}_j \sin(\hat{\theta}_j) - \delta_{j,y} \hat{v}_j \cos(\hat{\theta}_j), & \forall (i,j) \in \mathcal{P}_S, \\ v_{ij,y} \hat{x}_{ij} - v_{ij,x} \hat{y}_{ij} &\leq 0, & \text{if } z_{ij} = 1, & \forall (i,j) \in \mathcal{P}_S, \\ v_{ij,y} \hat{x}_{ij} - v_{ij,x} \hat{y}_{ij} &\geq 0, & \text{if } z_{ij} = 0, & \forall (i,j) \in \mathcal{P}_S, \\ v_{ij,y} \gamma_{ij}^l - v_{ij,x} \phi_{ij}^l &\leq 0, & \text{if } z_{ij} = 1, & \forall (i,j) \in \mathcal{P}_S, \\ v_{ij,y} \gamma_{ij}^u - v_{ij,x} \phi_{ij}^u &\geq 0, & \text{if } z_{ij} = 0, & \forall (i,j) \in \mathcal{P}_S, \\ \underline{q}_i^2 &\leq \delta_{i,x}^2 + \delta_{i,y}^2 \leq \bar{q}_i^2, & \forall i \in \mathcal{A}, \\ \delta_{i,x} \tan(\underline{\theta}_i) &\leq \delta_{i,y} \leq \delta_{i,x} \tan(\bar{\theta}_i), & \forall i \in \mathcal{A}, \\ \underline{q}_i \cos(\max\{|\bar{\theta}_i|, |\underline{\theta}_i|\}) &\leq \delta_{i,x} \leq \bar{q}_i, & \forall i \in \mathcal{A}, \\ \bar{q}_i \sin(\underline{\theta}_i) &\leq \delta_{i,y} \leq \bar{q}_i \sin(\bar{\theta}_i), & \forall i \in \mathcal{A}, \\ \underline{v}_{ij,x} &\leq v_{ij,x} \leq \bar{v}_{ij,x}, & \forall (i,j) \in \mathcal{P}_S, \\ \underline{v}_{ij,y} &\leq v_{ij,y} \leq \bar{v}_{ij,y}, & \forall (i,j) \in \mathcal{P}_S, \\ z_{ij} &\in \{0, 1\}, & \forall (i,j) \in \mathcal{P}_S, \\ \delta_{i,x}, \delta_{i,y} &\in \mathbb{R}, & \forall i \in \mathcal{A}. \end{aligned}$$

4.3 Complex Number Formulation for the 2D+FL Aircraft Conflict Resolution Problem

To model flight level changes, it is assumed that each aircraft $i \in \mathcal{A}$ is initially assigned to a base FL denoted $\hat{\rho}_i$. In addition, it is assumed that adjacent FLs are vertically separated (e.g. by 1000 ft.). Thus, the only needs to impose separation constraints on pairs of aircraft are on those which share the same FL.

Let \mathcal{Z}_i denote the set of available FLs for each aircraft $i \in \mathcal{A}$, and consider the binary variable ρ_{ik} defined as:

$$\rho_{ik} = \begin{cases} 1 & \text{if aircraft } i \in \mathcal{A} \text{ is on FL } k \in \mathcal{Z}_i, \\ 0 & \text{otherwise.} \end{cases} \quad (4.11)$$

By design, $\hat{\rho}_i \in \mathcal{Z}_i$ and it is required that each aircraft $i \in \mathcal{A}$ to be assigned to exactly one FL in its reachable set \mathcal{Z}_i via constraint (4.12):

$$\sum_{k \in \mathcal{Z}_i} \rho_{ik} = 1, \quad \forall i \in \mathcal{A}. \quad (4.12)$$

For each pair of aircraft, it is necessary to identify if they share or may be sharing the same FL. Let \mathcal{P}_S^3 be the set of such aircraft pairs which are not conflict-free, i.e. $\mathcal{P}_S^3 = \{(i, j) \in \mathcal{P}_S \cup \mathcal{P}_I : \mathcal{Z}_i \cap \mathcal{Z}_j \neq \emptyset\}$. Let φ_{ij} be the binary variable defined as:

$$\varphi_{ij} = \begin{cases} 1 & \text{if aircraft } i \text{ and } j \text{ are assigned to the same FL,} \\ 0 & \text{otherwise.} \end{cases} \quad (4.13)$$

Variable φ_{ij} can be linked to binary variables ρ_{ik} and ρ_{jk} via the constraint:

$$\rho_{ik} + \rho_{jk} \leq \varphi_{ij} + 1, \quad \forall (i, j) \in \mathcal{P}_S^3, \forall k \in \mathcal{Z}_i \cap \mathcal{Z}_j. \quad (4.14)$$

The separation conditions determined by (3.20)-(3.21) can be rewritten to account for altitude separation as follows:

$$v_{ij,x}\hat{x}_{ij} - v_{ij,y}\hat{y}_{ij} \leq 0, \quad \text{if } z_{ij} = 1 \quad \text{and} \quad \varphi_{ij} = 1, \quad \forall (i, j) \in \mathcal{P}_S^3, \quad (4.15a)$$

$$v_{ij,x}\hat{x}_{ij} - v_{ij,y}\hat{y}_{ij} \geq 0, \quad \text{if } z_{ij} = 0 \quad \text{and} \quad \varphi_{ij} = 1, \quad \forall (i, j) \in \mathcal{P}_S^3, \quad (4.15b)$$

$$v_{ij,x}\gamma_{ij}^l - v_{ij,y}\phi_{ij}^l \leq 0, \quad \text{if } z_{ij} = 1 \quad \text{and} \quad \varphi_{ij} = 1, \quad \forall (i, j) \in \mathcal{P}_S^3, \quad (4.15c)$$

$$v_{ij,x}\gamma_{ij}^u - v_{ij,y}\phi_{ij}^u \geq 0, \quad \text{if } z_{ij} = 0 \quad \text{and} \quad \varphi_{ij} = 1, \quad \forall (i, j) \in \mathcal{P}_S^3. \quad (4.15d)$$

FL changes are typically less desirable compared to other deconfliction manoeuvres such as speed or heading control (Bilimoria et al., 1996; Hu et al., 2002; Alonso-Ayuso et al., 2011). This is due to a number of practical considerations including an increase in fuel consumption, passenger discomfort due to climbing or descending and the need for extended monitoring (Wiener, 1989).

Under these considerations, a lexicographic optimisation approach for the 2D+FL ACRP is proposed. The number of FL changes is first minimised; before the total 2D deviation of flights is minimised. The proposed objective function for minimising the number of FL changes is:

$$\text{minimise } \sum_{i \in \mathcal{A}} \left| \sum_{k \in \mathcal{Z}_i} k \rho_{ik} - \hat{\rho}_i \right|. \quad (4.16)$$

The resulting model is summarised in Model 5 and hereby referred to as the non-convex lexicographic 2D+FL formulation.

Model 5. *Non-convex Lexicographic 2D+FL Complex Number Formulation*

1. Minimise $\sum_{i \in \mathcal{A}} \left| \sum_{k \in \mathcal{Z}_i} k \rho_{ik} - \hat{\rho}_i \right|$,
2. Minimise $\sum_{i \in \mathcal{A}} w \delta_{i,y}^2 + (1-w)(1 - \delta_{i,x})^2$,

Subject to:

$$\begin{aligned}
v_{i,j,x} &= \delta_{i,x} \hat{v}_i \cos(\hat{\theta}_i) - \delta_{i,y} \hat{v}_i \sin(\hat{\theta}_i) - \delta_{j,x} \hat{v}_j \cos(\hat{\theta}_j) + \delta_{j,y} \hat{v}_j \sin(\hat{\theta}_j), & \forall (i,j) \in \mathcal{P}_S^3, \\
v_{i,j,y} &= \delta_{i,y} \hat{v}_i \cos(\hat{\theta}_i) - \delta_{i,x} \hat{v}_i \sin(\hat{\theta}_i) - \delta_{j,y} \hat{v}_j \cos(\hat{\theta}_j) + \delta_{j,x} \hat{v}_j \sin(\hat{\theta}_j), & \forall (i,j) \in \mathcal{P}_S^3, \\
v_{i,j,y} \hat{x}_{ij} - v_{i,j,x} \hat{y}_{ij} &\leq 0, & \text{if } z_{ij} = 1 \text{ and } \varphi_{ij} = 1, & \forall (i,j) \in \mathcal{P}_S^3, \\
v_{i,j,y} \hat{x}_{ij} - v_{i,j,x} \hat{y}_{ij} &\geq 0, & \text{if } z_{ij} = 0 \text{ and } \varphi_{ij} = 1, & \forall (i,j) \in \mathcal{P}_S^3, \\
v_{i,j,y} \gamma_{ij}^l - v_{i,j,x} \phi_{ij}^l &\leq 0, & \text{if } z_{ij} = 1 \text{ and } \varphi_{ij} = 1, & \forall (i,j) \in \mathcal{P}_S^3, \\
v_{i,j,y} \gamma_{ij}^u - v_{i,j,x} \phi_{ij}^u &\geq 0, & \text{if } z_{ij} = 0 \text{ and } \varphi_{ij} = 1, & \forall (i,j) \in \mathcal{P}_S^3, \\
\underline{q}_i^2 &\leq \delta_{i,x}^2 + \delta_{i,y}^2 \leq \bar{q}_i^2, & \forall i \in \mathcal{A}, \\
\delta_{i,x} \tan(\underline{\theta}_i) &\leq \delta_{i,y} \leq \delta_{i,x} \tan(\bar{\theta}_i), & \forall i \in \mathcal{A}, \\
\underline{q}_i \cos(\max\{|\bar{\theta}_i|, |\underline{\theta}_i|\}) &\leq \delta_{i,x} \leq \bar{q}_i, & \forall i \in \mathcal{A}, \\
\bar{q}_i \sin(\underline{\theta}_i) &\leq \delta_{i,y} \leq \bar{q}_i \sin(\bar{\theta}_i), & \forall i \in \mathcal{A}, \\
\sum_{k \in \mathcal{Z}_i} \rho_{ik} &= 1, & \forall i \in \mathcal{A}, \\
\rho_{ik} + \rho_{jk} &\leq \varphi_{ij} + 1, & \forall (i,j) \in \mathcal{P}_S^3, k \in \mathcal{Z}_i \cap \mathcal{Z}_j, \\
\underline{v}_{i,j,x} &\leq v_{i,j,x} \leq \bar{v}_{i,j,x}, & \forall (i,j) \in \mathcal{P}_S^3, \\
\underline{v}_{i,j,y} &\leq v_{i,j,y} \leq \bar{v}_{i,j,y}, & \forall (i,j) \in \mathcal{P}_S^3, \\
z_{ij} &\in \{0, 1\}, & \forall (i,j) \in \mathcal{P}_S^3, \\
\delta_{i,x}, \delta_{i,y} &\in \mathbb{R}, & \forall i \in \mathcal{A}, \\
\rho_{ik} &\in \{0, 1\}, & \forall i \in \mathcal{A}, k \in \mathcal{Z}_i.
\end{aligned}$$

Compared to Model 4, Model 5 requires additional binary decision variables ρ_{ik} and φ_{ij} . The former are used to assign aircraft to separated flight levels and the latter ensures that aircraft sharing the same flight level are separated via the 2D separation conditions. Next, the exact solution methods for these 2D and 2D+FL non-convex aircraft conflict formulations are proposed.

The exact solution methods for the 2D and the 2D+FL ACRPs are built on and extended from the convex relaxations presented by Rey and Hijazi (2017). First, a convex relaxation of the 2D ACRP that fully relaxes the speed control constraint in the complex number formulation is presented in Section 4.4. This relaxation yields a Mixed-Integer Quadratic Program (MIQP) which solution may violate the speed control bounds of the problem. To eliminate these potential violations, convex quadratic constraints and piecewise linear outer approximations are introduced in a Mixed-Integer Quadratically Constrained Program (MIQCP). This culminates in the proposed constraint generation algorithm to iteratively refine the piece-wise linear approximation and show that this approach converges to optimal solutions of the 2D ACRP (Section 4.5).

To solve the lexicographic optimisation formulation for the 2D+FL ACRP, a two-step decomposition approach is proposed. At first, it solves a restricted flight assignment problem that only implicitly accounts for aircraft trajectories and yields an optimal solution with regards to the first objective function (total FL deviation). Then, it uses the optimal solution of the flight assignment formulation to assign aircraft to FLs and solve a series of 2D problems (one per FL) to construct an optimal solution with regards to the second objective function (total 2D deviation). Both steps are iterated until a global solution is found (Section 4.6). The proposed exact solution methods are presented in detail the next sections.

4.4 Mixed-Integer Quadratic Relaxation for the 2D Aircraft Conflict Resolution Problem

An initial convex relaxation of Model 4 was proposed by Rey and Hijazi (2017) by relaxing the speed control constraint (4.5). The resulting formulation is a MIQP summarised in Model 6.

Model 6. *MIQP 2D Formulation*

$$\text{Minimise} \quad \sum_{i \in \mathcal{A}} w \delta_{i,y}^2 + (1 - w)(1 - \delta_{i,x})^2,$$

Subject to:

$$\begin{aligned} v_{ij,x} &= \delta_{i,x} \hat{v}_i \cos(\hat{\theta}_i) - \delta_{i,y} \hat{v}_i \sin(\hat{\theta}_i) - \delta_{j,x} \hat{v}_j \cos(\hat{\theta}_j) + \delta_{j,y} \hat{v}_j \sin(\hat{\theta}_j), \quad \forall (i, j) \in \mathcal{P}_S, \\ v_{ij,y} &= \delta_{i,y} \hat{v}_i \cos(\hat{\theta}_i) - \delta_{i,x} \hat{v}_i \sin(\hat{\theta}_i) - \delta_{j,y} \hat{v}_j \cos(\hat{\theta}_j) + \delta_{j,x} \hat{v}_j \sin(\hat{\theta}_j), \quad \forall (i, j) \in \mathcal{P}_S, \\ v_{ij,y} \hat{x}_{ij} - v_{ij,x} \hat{y}_{ij} &\leq 0, \quad \text{if } z_{ij} = 1, \quad \forall (i, j) \in \mathcal{P}_S, \end{aligned}$$

$$\begin{aligned}
v_{ij,y}\hat{x}_{ij} - v_{ij,x}\hat{y}_{ij} &\geq 0, & \text{if } z_{ij} = 0, & \forall (i,j) \in \mathcal{P}_S, \\
v_{ij,y}\gamma_{ij}^l - v_{ij,x}\phi_{ij}^l &\leq 0, & \text{if } z_{ij} = 1, & \forall (i,j) \in \mathcal{P}_S, \\
v_{ij,y}\gamma_{ij}^u - v_{ij,x}\phi_{ij}^u &\geq 0, & \text{if } z_{ij} = 0, & \forall (i,j) \in \mathcal{P}_S, \\
\delta_{i,x} \tan(\underline{\theta}_i) &\leq \delta_{i,y} \leq \delta_{i,x} \tan(\bar{\theta}_i), & & \forall i \in \mathcal{A}, \\
\underline{q}_i \cos(\max\{|\bar{\theta}_i|, |\underline{\theta}_i|\}) &\leq \delta_{i,x} \leq \bar{q}_i, & & \forall i \in \mathcal{A}, \\
\bar{q}_i \sin(\underline{\theta}_i) &\leq \delta_{i,y} \leq \bar{q}_i \sin(\bar{\theta}_i), & & \forall i \in \mathcal{A}, \\
\underline{v}_{ij,x} &\leq v_{ij,x} \leq \bar{v}_{ij,x}, & & \forall (i,j) \in \mathcal{P}_S, \\
\underline{v}_{ij,y} &\leq v_{ij,y} \leq \bar{v}_{ij,y}, & & \forall (i,j) \in \mathcal{P}_S, \\
z_{ij} &\in \{0, 1\}, & & \forall (i,j) \in \mathcal{P}_S, \\
\delta_{i,x}, \delta_{i,y} &\in \mathbb{R}, & & \forall i \in \mathcal{A}.
\end{aligned}$$

Model 6 yields a lower bound on the optimal objective value of Model 4 and a solution which is a global optimum if the relaxed constraint (4.5) is not violated. Since speed deviations are penalised in the objective function, the empirical performance of Model 6 is competitive for low to medium density (in terms of number of aircraft and conflicts) 2D problems with several such instances solved to global optimality via this relaxation (see Section 4.7.3).

4.5 Mixed-Integer Quadratically Constrained Relaxation and Constraint Generation Algorithm

To tighten the MIQP relaxation given in Section 4.4, the MIQCP relaxation proposed by Rey and Hijazi (2017) is built on and extended by incorporating the speed control constraint (4.5) using convex quadratic and piecewise linear constraints.

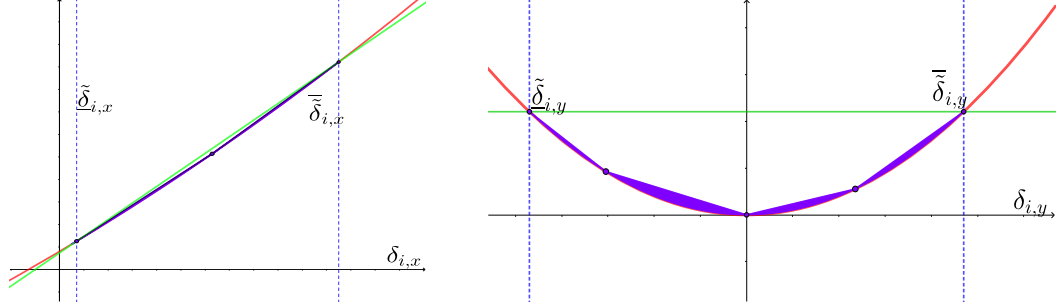
Observe that the speed upper bound constraint (4.5b) is convex quadratic, hence it can be incorporated directly in the MIQCP formulation. To incorporate the speed lower bound constraint (4.5a), auxiliary real variables $\tilde{\delta}_{i,x}$ and $\tilde{\delta}_{i,y}$ defined as $\tilde{\delta}_{i,x} \equiv \delta_{i,x}^2$ and $\tilde{\delta}_{i,y} \equiv \delta_{i,y}^2$ for each aircraft $i \in \mathcal{A}$ are introduced. These variables can be incorporated in relaxed form via convex quadratic constraints:

$$\tilde{\delta}_{i,x} \geq \delta_{i,x}^2, \quad \forall i \in \mathcal{A}, \quad (4.19a)$$

$$\tilde{\delta}_{i,y} \geq \delta_{i,y}^2, \quad \forall i \in \mathcal{A}. \quad (4.19b)$$

Accordingly, it is required that:

$$\underline{q}_i^2 \leq \tilde{\delta}_{i,x} + \tilde{\delta}_{i,y}, \quad \forall i \in \mathcal{A}. \quad (4.20)$$



(a) Graph of $\delta_{i,x}^2$ (in red) over the domain given by Eq. (4.4a). The mixed-integer cuts (4.22a) are illustrated for a partition of $|\Gamma_{i,x}| = 2$ segments.

(b) Graph of $\delta_{i,y}^2$ (in red) over the domain given by Eq. (4.4b). The mixed-integer cuts (4.22b) are illustrated for a partition of $|\Gamma_{i,y}| = 4$ segments.

Figure 4.1: Piece-wise linear approximation of $\delta_{i,x}^2$ and $\delta_{i,y}^2$ (in red). The green lines represent the initial McCormick relaxation given by (4.21). The purple shaded regions represent the refined feasible region of $\delta_{i,x}$ and $\delta_{i,y}$ after imposing the mixed-integer cuts (4.22). The speed control bounds are $\underline{q}_i = 0.94$, $\bar{q}_i = 1.03$ and the heading control bounds are $\underline{\theta}_i = -\frac{\pi}{6}$ and $\bar{\theta}_i = +\frac{\pi}{6}$.

To impose upper bounds on $\tilde{\delta}_{i,x}$ and $\tilde{\delta}_{i,y}$, their McCormick envelopes (McCormick, 1976) are introduced as:

$$\tilde{\delta}_{i,x} \leq (\bar{q}_i + \underline{q}_i \cos(\max\{|\underline{\theta}_i|, |\bar{\theta}_i|\}))\delta_{i,x} - \bar{q}_i \underline{q}_i \cos(\max\{|\underline{\theta}_i|, |\bar{\theta}_i|\}), \quad \forall i \in \mathcal{A}, \quad (4.21a)$$

$$\tilde{\delta}_{i,y} \leq \bar{q}_i (\sin(\underline{\theta}_i) + \sin(\bar{\theta}_i))\delta_{i,y} - \bar{q}_i^2 \sin(\bar{\theta}_i) \sin(\underline{\theta}_i), \quad \forall i \in \mathcal{A}. \quad (4.21b)$$

Constraints (4.19)-(4.21) restrict variables $\tilde{\delta}_{i,x}$ and $\tilde{\delta}_{i,y}$ to convex regions thus providing an initial relaxation of the speed lower bound constraint (4.5a). This initial relaxation is illustrated in Figure 4.1 which depicts the variation of $\delta_{i,x}^2$ and $\delta_{i,y}^2$ (in red) over the domain of $\delta_{i,x}$ and $\delta_{i,y}$ for realistic speed and heading control bounds. The green lines in Figures 4.1a and 4.1b represent the initial McCormick envelopes. This relaxation may still yield infeasible aircraft speeds. To refine this convex relaxation, mixed-integer cuts are introduced and they are generated on-the-fly in a constraint generation algorithm.

The general structure of the proposed mixed-integer cuts is presented next before discussing how these cuts are generated iteratively. Let $\Gamma_{i,x}$ and $\Gamma_{i,y}$ be partitions of the domain of variables $\delta_{i,x}$ and $\delta_{i,y}$, respectively. Since $\delta_{i,x}^2$ and $\delta_{i,y}^2$ are convex, any line joining two extremities of a segment in $\Gamma_{i,x}$ and $\Gamma_{i,y}$ refines the initial McCormick upper envelopes. Let $\alpha_{i,x}^k$ (resp. $\alpha_{i,y}^k$) and $\beta_{i,x}^k$ (resp. $\beta_{i,y}^k$) be the slope and the intercept corresponding to segment $k \in \Gamma_{i,x}$ (resp. $k \in \Gamma_{i,y}$). Further, let $s_{i,x}^k$ (resp.

$s_{i,y}^k$) be a binary variable taking value 1 if $\delta_{i,x}$ (resp. $\delta_{i,y}$) belongs to segment k of partition $\Gamma_{i,x}$ (resp. $\Gamma_{i,y}$). The proposed mixed-integer cuts take the form of:

$$\tilde{\delta}_{i,x} \leq \alpha_{i,x}^k \delta_{i,x} + \beta_{i,x}^k, \quad \text{if } s_{i,x}^k = 1, \quad \forall i \in \mathcal{A}, k \in \Gamma_{i,x}, \quad (4.22a)$$

$$\tilde{\delta}_{i,y} \leq \alpha_{i,y}^k \delta_{i,y} + \beta_{i,y}^k, \quad \text{if } s_{i,y}^k = 1, \quad \forall i \in \mathcal{A}, k \in \Gamma_{i,y}. \quad (4.22b)$$

Let $\underline{\delta}_{i,x}^k$ and $\bar{\delta}_{i,x}^k$ (resp. $\underline{\delta}_{i,y}^k$ and $\bar{\delta}_{i,y}^k$) be the extremities of segment $k \in \Gamma_{i,x}$ (resp. $k \in \Gamma_{i,y}$). Binary variables $s_{i,x}^k$ and $s_{i,y}^k$ are defined as:

$$s_{i,x}^k = \begin{cases} 1 & \text{if } \delta_{i,x} \in [\underline{\delta}_{i,x}^k, \bar{\delta}_{i,x}^k], \\ 0 & \text{otherwise,} \end{cases} \quad \forall i \in \mathcal{A}, k \in \Gamma_{i,x}, \quad (4.23a)$$

$$s_{i,y}^k = \begin{cases} 1 & \text{if } \delta_{i,y} \in [\underline{\delta}_{i,y}^k, \bar{\delta}_{i,y}^k], \\ 0 & \text{otherwise.} \end{cases} \quad \forall i \in \mathcal{A}, k \in \Gamma_{i,y}. \quad (4.23b)$$

The following cut selection constraints are also required:

$$\sum_{k \in \Gamma_{i,x}} s_{i,x}^k = 1 \quad \forall i \in \mathcal{A}, \quad (4.24a)$$

$$\sum_{k \in \Gamma_{i,y}} s_{i,y}^k = 1 \quad \forall i \in \mathcal{A}. \quad (4.24b)$$

The proposed mixed-integer cuts are illustrated in Figures 4.1a and 4.1b for the case of $|\Gamma_{i,x}| = 2$ and $|\Gamma_{i,y}| = 4$ segments, respectively. The shaded purple region represents the feasible region of $\tilde{\delta}_{i,x}$ and $\tilde{\delta}_{i,y}$ after imposing the mixed-integer cuts.

The resulting formulation is an MIQCP with mixed-integer cuts summarised in Model 7. This formulation can be solved by off-the-shelf commercial optimisation software and provides a relaxation of the Model 4 which can be tightened as desired by refining the partitions $\Gamma_{i,x}$ and $\Gamma_{i,y}$ of the domain of variables $\delta_{i,x}$ and $\delta_{i,y}$, respectively.

Model 7. MIQCP 2D Formulation

$$\text{Minimise} \quad \sum_{i \in \mathcal{A}} w \delta_{i,y}^2 + (1-w)(1 - \delta_{i,x})^2,$$

Subject to:

$$v_{i,j,x} = \delta_{i,x} \hat{v}_i \cos(\hat{\theta}_i) - \delta_{i,y} \hat{v}_i \sin(\hat{\theta}_i) - \delta_{j,x} \hat{v}_j \cos(\hat{\theta}_j) + \delta_{j,y} \hat{v}_j \sin(\hat{\theta}_j), \quad \forall (i,j) \in \mathcal{P}_S,$$

$$v_{i,j,y} = \delta_{i,y} \hat{v}_i \cos(\hat{\theta}_i) - \delta_{i,x} \hat{v}_i \sin(\hat{\theta}_i) - \delta_{j,y} \hat{v}_j \cos(\hat{\theta}_j) + \delta_{j,x} \hat{v}_j \sin(\hat{\theta}_j), \quad \forall (i,j) \in \mathcal{P}_S,$$

$$\begin{aligned}
v_{i,j,y}\hat{x}_{ij} - v_{i,j,x}\hat{y}_{ij} &\leq 0, & \text{if } z_{ij} = 1, & \forall (i,j) \in \mathcal{P}_S, \\
v_{i,j,y}\hat{x}_{ij} - v_{i,j,x}\hat{y}_{ij} &\geq 0, & \text{if } z_{ij} = 0, & \forall (i,j) \in \mathcal{P}_S, \\
v_{i,j,y}\gamma_{ij}^l - v_{i,j,x}\phi_{ij}^l &\leq 0, & \text{if } z_{ij} = 1, & \forall (i,j) \in \mathcal{P}_S, \\
v_{i,j,y}\gamma_{ij}^u - v_{i,j,x}\phi_{ij}^u &\geq 0, & \text{if } z_{ij} = 0, & \forall (i,j) \in \mathcal{P}_S, \\
\delta_{i,x} \tan(\underline{\theta}_i) &\leq \delta_{i,y} \leq \delta_{i,x} \tan(\bar{\theta}_i), & & \forall i \in \mathcal{A}, \\
\tilde{\delta}_{i,x} &\geq \delta_{i,x}^2, & & \forall i \in \mathcal{A}, \\
\tilde{\delta}_{i,y} &\geq \delta_{i,y}^2, & & \forall i \in \mathcal{A}, \\
\underline{q}_i^2 &\leq \tilde{\delta}_{i,x} + \tilde{\delta}_{i,y}, & & \forall i \in \mathcal{A}, \\
\tilde{\delta}_{i,x} &\leq (\bar{q}_i + \underline{q}_i \cos(\max\{|\underline{\theta}_i|, |\bar{\theta}_i|\}))\delta_{i,x} - \bar{q}_i \underline{q}_i \cos(\max\{|\underline{\theta}_i|, |\bar{\theta}_i|\}), & & \forall i \in \mathcal{A}, \\
\tilde{\delta}_{i,y} &\leq \bar{q}_i (\sin(\underline{\theta}_i) + \sin(\bar{\theta}_i))\delta_{i,y} - \bar{q}_i^2 \sin(\bar{\theta}_i) \sin(\underline{\theta}_i), & & \forall i \in \mathcal{A}, \\
\tilde{\delta}_{i,x} &\leq \alpha_{i,x}^k \delta_{i,x} + \beta_{i,x}^k, & \text{if } s_{i,x}^k = 1, & \forall i \in \mathcal{A}, k \in \Gamma_{i,x}, \\
\tilde{\delta}_{i,y} &\leq \alpha_{i,y}^k \delta_{i,y} + \beta_{i,y}^k, & \text{if } s_{i,y}^k = 1, & \forall i \in \mathcal{A}, k \in \Gamma_{i,y}, \\
s_{i,x}^k &= 1 \text{ if } \delta_{i,x} \in [\underline{\delta}_{i,x}^k, \bar{\delta}_{i,x}^k], & & \forall i \in \mathcal{A}, k \in \Gamma_{i,x}, \\
s_{i,y}^k &= 1 \text{ if } \delta_{i,y} \in [\underline{\delta}_{i,y}^k, \bar{\delta}_{i,y}^k], & & \forall i \in \mathcal{A}, k \in \Gamma_{i,y}, \\
\sum_{k \in \Gamma_{i,x}} s_{i,x}^k &= 1 & & \forall i \in \mathcal{A}, \\
\sum_{k \in \Gamma_{i,y}} s_{i,y}^k &= 1 & & \forall i \in \mathcal{A}, \\
\underline{q}_i^2 &\leq \delta_{i,x}^2 + \delta_{i,y}^2, & & \forall i \in \mathcal{A}, \\
\underline{q}_i \cos(\max\{|\bar{\theta}_i|, |\underline{\theta}_i|\}) &\leq \delta_{i,x} \leq \bar{q}_i, & & \forall i \in \mathcal{A}, \\
\bar{q}_i \sin(\underline{\theta}_i) &\leq \delta_{i,y} \leq \bar{q}_i \sin(\bar{\theta}_i), & & \forall i \in \mathcal{A}, \\
\underline{v}_{i,j,x} &\leq v_{i,j,x} \leq \bar{v}_{i,j,x}, & & \forall (i,j) \in \mathcal{P}_S, \\
\underline{v}_{i,j,y} &\leq v_{i,j,y} \leq \bar{v}_{i,j,y}, & & \forall (i,j) \in \mathcal{P}_S, \\
z_{ij} &\in \{0, 1\}, & & \forall (i,j) \in \mathcal{P}_S, \\
\delta_{i,x}, \delta_{i,y} &\in \mathbb{R}, & & \forall i \in \mathcal{A}, \\
\tilde{\delta}_{i,x}, \tilde{\delta}_{i,y} &\in \mathbb{R}, & & \forall i \in \mathcal{A}, \\
s_{i,x}^k &\in \{0, 1\}, & & \forall i \in \mathcal{A}, k \in \Gamma_{i,x}, \\
s_{i,y}^k &\in \{0, 1\}, & & \forall i \in \mathcal{A}, k \in \Gamma_{i,y}.
\end{aligned}$$

A constraint generation algorithm is proposed and it starts from a relaxed formulation and iteratively refines the piecewise linear outer approximation of the quadratic terms $\delta_{i,x}^2$ and $\delta_{i,y}^2$ via mixed-integer cuts (4.22). At each iteration, the proposed constraint generation algorithm examines the solution $(\delta_{i,x}, \delta_{i,y})$ of each aircraft $i \in \mathcal{A}$

for speed lower bound violations. If $\delta_{i,x}^2 + \delta_{i,y}^2 < \underline{q}_i^2$, then at least one of the relaxed auxiliary variables $\tilde{\delta}_{i,x}$ or $\tilde{\delta}_{i,y}$ must be such that $\tilde{\delta}_{i,x} > \delta_{i,x}^2$ or $\tilde{\delta}_{i,y} > \delta_{i,y}^2$. To eliminate the current infeasible solution, the partition(s) $\Gamma_{i,x}$ or $\Gamma_{i,y}$ of the violating variable(s) is augmented by dividing the segment(s) corresponding to $\delta_{i,x}$ or $\delta_{i,y}$ into two segments which meet at $\delta_{i,x}$ or $\delta_{i,y}$ and corresponding binary variable(s) $s_{i,x}^k$ or $s_{i,y}^k$ are added to the formulation. The process is repeated until all aircraft have feasible speed profiles which correspond to a global optimum of Model 4. To further improve the convergence of the solution algorithm, the heuristic procedure outlined by Rey and Hijazi (2017) is used to attempt to find improving upper bounds. After each solve of the relaxed formulation 7, Model 4 is solved as a non-linear program (NLP) by fixing variable z_{ij} . The pseudo-code of the resulting algorithm is summarised in Algorithm 2.

4.6 Decomposition Algorithm for the 2D+FL Aircraft Conflict Resolution Problem

Next, a two-step decomposition approach for the non-convex lexicographic 2D+FL conflict resolution problem represented by Model 5 is introduced. The first objective function (4.16) focuses on minimising the number of FL changes. Observe that this objective function is null and minimal if all aircraft $i \in \mathcal{A}$ can remain at their initial FL $\hat{\rho}_i$. Since minimising aircraft FL re-assignment is the highest priority objective function, it is only necessary to identify combinations of aircraft which are non-separable in 2D and ensure that such combinations are not assigned to the same FL.

To address this first step, a compact aircraft FL assignment model is introduced and it implicitly accounts for 2D non-separable aircraft combinations. Let $\Omega_I \subseteq 2^{\mathcal{A}}$ be the set of aircraft combinations which are 2D non-separable, i.e. for any $\omega \in \Omega_I$, the subset of aircraft ω cannot be separated in 2D. To ensure that all aircraft are assigned to 2D separable FLs, it is required:

$$\sum_{i \in \omega} \rho_{ik} \leq |\omega| - 1, \quad \forall \omega \in \Omega_I, \forall k \in \bigcap_{i \in \omega} \mathcal{Z}_i. \quad (4.26)$$

Although the number of constraints (4.26) is exponential in the number of aircraft, the numerical experiments show that dense traffic scenarios can be solved to optimality by restricting Ω_I to aircraft pairs (see Section 4.7.4), thus motivating a relaxation and constraint generation approach.

Algorithm 2 Solution algorithm for the 2D ACRP

Input: $\mathcal{A}, \hat{\theta}, \hat{v}, \underline{q}, \bar{q}, \underline{\theta}, \bar{\theta}, \epsilon$

Output: $q^*, \theta^*, \text{LB}, \text{UB}$

$\mathcal{P}, \mathcal{P}_I, \mathcal{P}_F, \mathcal{P}_S \leftarrow$ Algorithm 1

LB \leftarrow 0

UB $\leftarrow +\infty$

$q, \theta, \delta_x, \delta_y, z, \text{LB} \leftarrow$ Solve MIQP 6 and calculate q and θ from δ_x and δ_y

if MIQP 6 is infeasible **then**

└ Return INFEASIBLE

if q is feasible (no speed violation) **then**

└ UB \leftarrow LB

└ $q^* \leftarrow q$

└ $\theta^* \leftarrow \theta$

else

└ CONVERGED \leftarrow False

└ **while** CONVERGED = False **do**

└ └ $q', \theta', \text{UB-NLP} \leftarrow$ Solve Model 4 as NLP with fixed z

└ └ **if** UB-NLP < UB **then**

└ └ └ UB \leftarrow UB-NLP

└ └ └ $q^* \leftarrow q'$

└ └ └ $\theta^* \leftarrow \theta'$

└ └ **for** $i \in \mathcal{A}$ **do**

└ └ └ **if** $\delta_{i,x}^2 + \delta_{i,y}^2 > \bar{q}_i^2$ **then**

└ └ └ └ Add constraint (4.5b)

└ └ └ **else if** $\delta_{i,x}^2 + \delta_{i,y}^2 < \underline{q}_i^2$ **then**

└ └ └ └ **if** $\tilde{\delta}_{i,x} > \delta_{i,x}^2$ **then**

└ └ └ └ └ Add segment to $\Gamma_{i,x}$ at $\delta_{i,x}$, variable $s_{i,x}^k$, constraints (4.22a), (4.23a),
└ └ └ └ └ and update (4.24a)

└ └ └ └ **if** $\tilde{\delta}_{i,y} > \delta_{i,y}^2$ **then**

└ └ └ └ └ Add segment to $\Gamma_{i,y}$ at $\delta_{i,y}$, variable $s_{i,y}^k$, constraints (4.22b), (4.23b),
└ └ └ └ └ and update (4.24b)

└ └ $q, \theta, \delta_x, \delta_y, \tilde{\delta}_x, \tilde{\delta}_y, z, \text{LB} \leftarrow$ Solve MIQCP 7 and calculate q and θ from δ_x and δ_y

└ └ **if** MIQCP 7 is infeasible **then**

└ └ └ Return INFEASIBLE

└ └ **if** q is feasible (no speed violation) **then**

└ └ └ UB \leftarrow LB

└ └ └ $q^* \leftarrow q$

└ └ └ $\theta^* \leftarrow \theta$

└ └ └ CONVERGED \leftarrow True

└ └ **if** (UB-LB)/UB $\leq \epsilon$ **then**

└ └ └ CONVERGED \leftarrow True

Let $\Delta\rho_i \geq 0$ be a variable representing the absolute flight level deviation for aircraft $i \in \mathcal{A}$. Objective function (4.16) can be linearised as:

$$\text{minimise } \sum_{i \in \mathcal{A}} \Delta\rho_i, \quad (4.27)$$

subject to the constraints:

$$\Delta\rho_i \geq \sum_{k \in \mathcal{Z}_i} k\rho_{ik} - \hat{\rho}_i, \quad \forall i \in \mathcal{A}, \quad (4.28a)$$

$$\Delta\rho_i \geq \hat{\rho}_i - \sum_{k \in \mathcal{Z}_i} k\rho_{ik}, \quad \forall i \in \mathcal{A}. \quad (4.28b)$$

Combining the FL separation constraint (4.26) and the above linearised objective function, yields a compact FL assignment formulation summarised in Model 8 which is a MILP with an exponential number of constraints.

Model 8. *FL Assignment Formulation*

$$\text{Minimise } \sum_{i \in \mathcal{A}} \Delta\rho_i$$

Subject to:

$$\sum_{k \in \mathcal{Z}_i} \rho_{ik} = 1, \quad \forall i \in \mathcal{A},$$

$$\sum_{i \in \omega} \rho_{ik} \leq |\omega| - 1, \quad \forall \omega \in \Omega_I, \forall k \in \bigcap_{i \in \omega} \mathcal{Z}_i,$$

$$\Delta\rho_i \geq \sum_{k \in \mathcal{Z}_i} k\rho_{ik} - \hat{\rho}_i, \quad \forall i \in \mathcal{A},$$

$$\Delta\rho_i \geq \hat{\rho}_i - \sum_{k \in \mathcal{Z}_i} k\rho_{ik}, \quad \forall i \in \mathcal{A},$$

$$\rho_{ik} \in \{0, 1\}, \quad \forall i \in \mathcal{A}, k \in \mathcal{Z}_i,$$

$$\Delta\rho_i \geq 0, \quad \forall i \in \mathcal{A}.$$

Initially, to solve Model 8, it is done by first restricting Constraint (4.26) to subsets of size two, i.e. 2D non-separable aircraft pairs, which can be efficiently identified using Algorithm 1 as a pre-processing step. Then, the 2D+FL problem is decomposed into a series of 2D conflict resolution problems, one per FL, based on the optimal solution $\boldsymbol{\rho}^*$ of the relaxed Model 8. For each FL, the corresponding 2D problem is solved using the exact constraint generation approach of Algorithm 2 with the aircraft set $\mathcal{A}_k = \{i \in \mathcal{A} : \rho_{ik}^* = 1\}$. If Algorithm 2 returns INFEASIBLE for FL k , then the corresponding FL separation constraint (4.26) with $\omega = \mathcal{A}_k$ is generated and

Model 8 is re-solved with the additional constraint(s). The process is repeated until all 2D problems are feasible. Let \mathcal{Z} be the set of all FLs, i.e. $\mathcal{Z} = \cup_{k \in \mathcal{Z}_i: i \in \mathcal{A}} \mathcal{Z}_i$, \mathbf{q}_k and $\boldsymbol{\theta}_k$ can be denoted as the vectors of speed and heading controls for aircraft assigned to FL $k \in \mathcal{Z}$, respectively. The proposed exact solution method for the lexicographic 2D+FL conflict resolution problem is summarised in Algorithm 3. Note that this decomposition approach provides an opportunity to solve all 2D problems in parallel, i.e. by parallelising the **for** loop at Line 8.

Algorithm 3 Solution algorithm for the lexicographic 2D+FL conflict resolution problem

Input: \mathcal{A} , $[\mathcal{Z}_i]_{i \in \mathcal{A}}$, $\hat{\boldsymbol{\theta}}$, \hat{v} , $\hat{\rho}$, $\underline{\mathbf{q}}$, $\bar{\mathbf{q}}$, $\underline{\boldsymbol{\theta}}$, $\bar{\boldsymbol{\theta}}$

Output: \mathbf{q}^* , $\boldsymbol{\theta}^*$, ρ^*

\mathcal{P} , \mathcal{P}_F , \mathcal{P}_S , $\mathcal{P}_I \leftarrow$ Algorithm 1

$\Omega_I \leftarrow \{(i, j) \in \mathcal{P}_I : \mathcal{Z}_i \cap \mathcal{Z}_j \neq \emptyset\}$

$\mathcal{Z} \leftarrow \cup_{k \in \mathcal{Z}_i: i \in \mathcal{A}} \mathcal{Z}_i$

CONVERGED \leftarrow False

while CONVERGED = False **do**

$\rho^* \leftarrow$ Solve MILP 8

 CONVERGED \leftarrow True

for $k \in \mathcal{Z}$ **do**

$\mathcal{A}_k \leftarrow \{i \in \mathcal{A} : \rho_{ik}^* = 1\}$

$\mathbf{q}_k^*, \boldsymbol{\theta}_k^* \leftarrow$ Algorithm 2 with $\mathcal{A} = \mathcal{A}_k$

if Algorithm 2 returns INFEASIBLE **then**

$\Omega_I \leftarrow \Omega_I \cup \mathcal{A}_k$

 CONVERGED \leftarrow False

$\mathbf{q}^*, \boldsymbol{\theta}^* \leftarrow [\mathbf{q}_k^*]_{k \in \mathcal{Z}}, [\boldsymbol{\theta}_k^*]_{k \in \mathcal{Z}}$

4.7 Numerical Results

First, the experimental framework that is used to test the proposed mixed-integer formulations and algorithms are introduced in Section 4.7.1. Then, the behaviour of the proposed 2D objective function is explored in Section 4.7.2. Numerical results for the 2D ACRP are presented in Section 4.7.3, and results for the 2D+FL problem are presented in Section 4.7.4.

4.7.1 Experiments Design

The performance of the proposed mixed-integer formulations and algorithms is tested using four benchmarking problems from the literature: the Circle Problem (CP), the Flow Problem (FP), the Grid Problem (GP) and the Random Circle Problem (RCP). Numerical results for problems with a subliminal speed control range of. $[-6\%, +3\%]$ (Bonini et al., 2009) are reported. Two heading control ranges are considered, first assuming that aircraft can modify their heading within the range $[-30^\circ, +30^\circ]$ as commonly used in the literature (Cafieri and Omheni, 2017; Rey and Hijazi, 2017), and considering a reduced heading control range of $[-15^\circ, +15^\circ]$. For conflict resolution problems with altitude control, each aircraft $i \in \mathcal{A}$ is randomly assigned to a FL $\hat{\rho}_i \in \mathcal{Z}$, and it is assumed that only adjacent FLs are available for aircraft, i.e. $\mathcal{Z}_i = \{\hat{\rho}_i - 1, \hat{\rho}_i, \hat{\rho}_i + 1\}$.

The proposed approach is referred to as **Disjunctive** and is compared to two benchmarks from the literature: the method proposed by Rey and Hijazi (2017) named **Disjunctive-2017** and an implementation based on the so-called shadow separation constraints named **Shadow**. The method **Disjunctive** corresponds to Algorithm 2 for 2D ACRP instances and to Algorithm 3 for 2D+FL ACRP instances. The method **Disjunctive-2017** is based on the same disjunctive linear separation conditions as **Disjunctive** but uses the algorithm proposed by Rey and Hijazi (2017). This algorithm has 3 steps: i) solve the MIQP relaxation (Model 6), ii) solve the MIQCP relaxation (Model 7) without any mixed-integer cuts (4.22), and, if a feasible solution has not been obtained, iii) solve Model 4 as NLP for fixed \mathbf{z} . Compared to **Disjunctive**, the method **Disjunctive-2017** is identical in the first step only. In step ii) of **Disjunctive-2017**, the MIQCP relaxation is solved without any constraint generation, thus all convex quadratic cuts (4.19) are added for all aircraft simultaneously and no mixed-integer cuts are generated. In addition, if the NLP fails to find a feasible solution in step iii), then the method fails to yield a feasible solution whereas the method **Disjunctive** is guaranteed to converge to a global optimal solution if it exists. In the implementation of the method **Shadow**, the control variables and the algorithm are identical to that of the method **Disjunctive**, and the only difference between both methods is the set of separation constraints used, i.e. Constraints (3.20) and (3.21) are replaced with the shadow separation conditions and the number of binary variables required to express these On/Off constraints. Specifically, for the 2D ACRP, **Disjunctive** only requires a single binary variable per aircraft pair (z_{ij}) whereas **Shadow** requires four binary variables per aircraft pair (Pallottino et al., 2002; Alonso-Ayuso et al., 2011, 2016). Details of the implementation of **Shadow** are

provided in the supplementary material. All three methods are implemented using the same pre-processing procedure (Algorithm 1) to eliminate conflict-free aircraft pairs.

All 2D ACRPs are solved by implementing Algorithm 2 with an optimality gap $\epsilon = 0.01$ and a time limit of 10 minutes. All 2D+FL problems are solved by implementing Algorithm 3 which calls Algorithm 2 using the same optimality gap as for the 2D problems, and a time limit of 10 minutes per FL is allocated. All models are implemented using PYTHON on a personal computer with 16 GB of RAM and an Intel i7 processor at 2.9GHz. The MIQPs and MIQCPs are solved with CPLEX v12.10 (Cplex, 2009) API for PYTHON using default options. Next, a sensitivity analysis on the preference weight w is conducted in the 2D objective function to explore its impact on aircraft trajectories in Section 4.7.2. Results on 2D problems are presented in Section 4.7.3 and results on 2D+FL problems in Section 4.7.4.

4.7.2 Sensitivity Analysis on the Preference Weight w

To quantify the impact of the preference weight w in the proposed 2D objective function (4.7), numerical experiments are conducted on one instance of each of the four types of benchmarking instances for varying values of w . For this experiment, the focus is on the typical heading control range $[-30^\circ, +30^\circ]$. The total speed deviation $\Sigma_q = \sum_{i \in \mathcal{A}} (1 - q_i)^2$, and the total heading deviation $\Sigma_\theta = \sum_{i \in \mathcal{A}} \theta_i^2$ are reported. The goal is to show that by varying the preference weight $w \in]0, 1[$, the decision-maker can control the desired level of trade-off between total speed deviation and total heading deviation. Recall that in objective function (4.7), w is the coefficient of $\delta_{i,y}^2 = (q_i \sin(\theta_i))^2$ which is minimal for $\theta_i = 0$; while $(1 - w)$ is the coefficient of $(1 - \delta_{i,x})^2 = (1 - q_i \cos(\theta_i))^2$ which is minimal for $q_i = 1$ and $\theta_i = 0$. Hence, one can expect that increasing (resp. decreasing) w will tend to penalise heading (resp. speed) deviations more than speed (resp. heading) deviations.

This behaviour is confirmed in the numerical experiments. Specifically, when observing the solution for the 2D instances CP-8, FP-10, GP-10 and one RCP-30 instance for $w = 0.1, \dots, 0.9$ in steps of size 0.1, i.e. for a total of 9 values of w per instance. All instances are solved to optimality using Algorithm 2 with no MIQCP iterations, i.e. the MIQP returned a global optimal solution for all tests. The change in the total speed deviation Σ_q and in the total heading deviation Σ_θ are reported in Figure 4.2. For all four instances tested, it is observed that increasing w monotonically decreases the total heading deviation and monotonically increases the

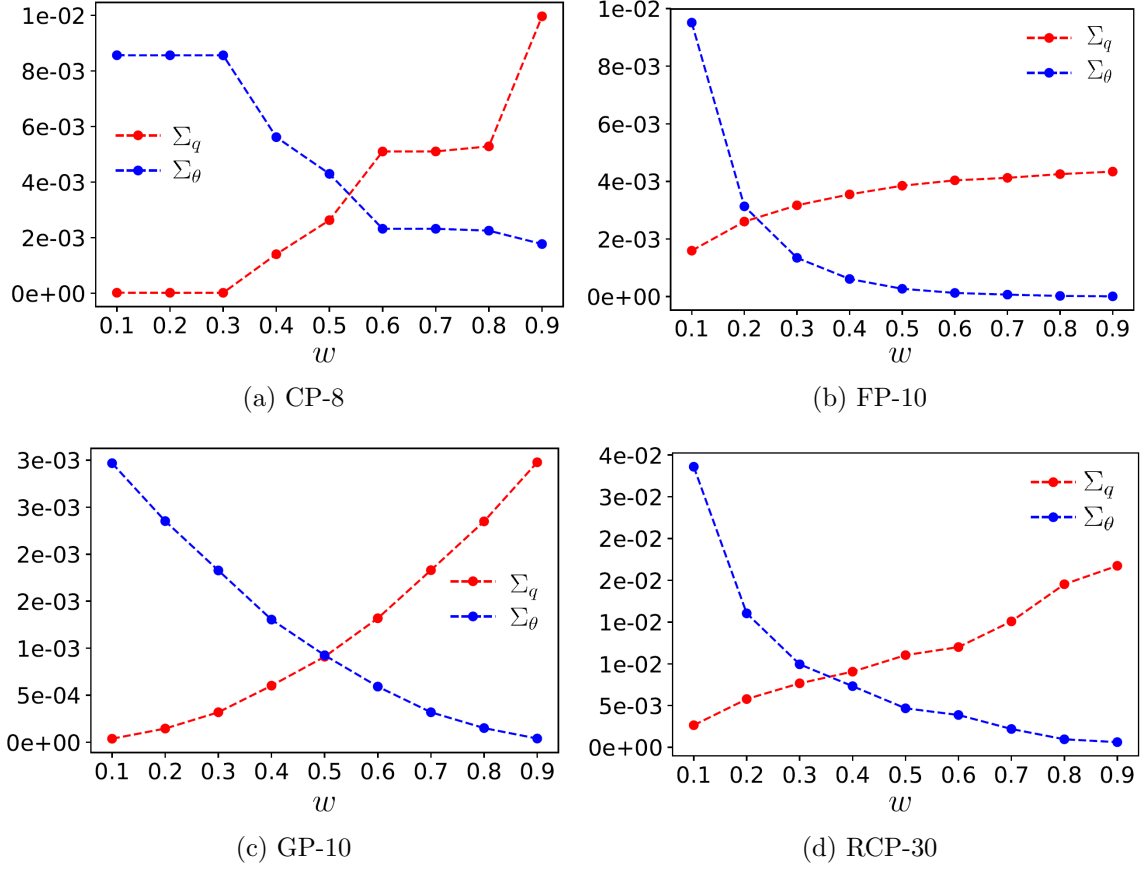


Figure 4.2: Sensitivity analysis on the preference weight w of the 2D objective function (4.7). For all figures, Σ_q represents the total speed deviation defined as $\sum_{i \in \mathcal{A}} (1 - q_i)^2$ (in red) and Σ_θ represents the total heading deviation defined as $\sum_{i \in \mathcal{A}} \theta_i^2$ (in blue).

total speed deviation. Further, it is noticed that in all cases both the total speed and heading deviations are of similar order of magnitudes.

This sensitivity analysis shows that using the proposed 2D objective function, the decision-maker can control which manoeuvre is prioritised by scaling up or down the preference weight w accordingly. Higher values of w will minimise the total heading deviation while lower values of w will minimise the total speed deviation. Based on these results, $w = 0.5$ is used in the numerical experiments presented in the remaining of the paper.

4.7.3 Results on 2D instances

To report the performances of the proposed formulations on 2D ACRPs, four groups of numerical experiments are used, one per instance type. The results for 12 CP instances are presented ranging from 4 to 15 aircraft in Tables 4.1 and 4.2. Results

for FP and GP instances are reported in Tables 4.3-4.6, respectively, for 12 instances each with 4 to 15 aircraft per stream. Results for RCP instances are reported in Tables 4.7 and 4.8 for four instance sizes with 10, 20, 30 and 40 aircraft per group. For each instance size, 100 RCP instances are randomly generated and it is reported the average performance along with the standard deviation in parenthesis. The performances of the proposed formulations are compared for both the standard and reduced heading control ranges.

Each row in the results tables represents an instance (CP, FP and GP) or a group of instances (RCP). The header of the results tables is presented from left to right. The left-most column, Instance, identifies the instance; $|A|$ is the number of aircraft and n_c is the number of the conflicts. The next three columns summarise the performance of the pre-processing algorithm: $|\mathcal{P}_F|/|\mathcal{P}|$ is the proportion of conflict-free aircraft pairs; $|\mathcal{P}_I|/|\mathcal{P}|$ is the proportion of non-separable aircraft pairs; and Time is the runtime of Algorithm 1 in seconds. The next six columns summarise the performance of **Disjunctive**: LB and UB are the lower and upper bound; Gap is the optimality gap in percent calculated using LB and UB; Time is the total runtime in seconds; n_i is the number of iterations of the **while** loop in Algorithm 2, and n_t represents the proportion of instances that could not be solved within the time limit (10 minutes), i.e. the number of time-outs. The next five columns summarise the performance of **Disjunctive-2017**: Δ UB is the upper bound of **Disjunctive-2017** minus that of **Disjunctive**; Gap is the optimality gap, Time is the total runtime, n_t is the proportion of time-outs, and Gain is the performance gain in runtime for instances solved within the time limit calculated as the runtime of **Disjunctive-2017** minus that of **Disjunctive** in percentage: a positive value indicates that **Disjunctive** is faster. The right-most five columns summarise the performance of **Shadow** relative to **Disjunctive**, similarly to the five previous columns. For RCP instances, it is also reported the number of times each method failed to find a feasible solution in columns named n_f . This value is always zero for CP, FP and GP instances hence this is not reported in their corresponding results tables.

The implementation of the pre-processing procedure (Algorithm 1) across CP, FP and GP instances with both the standard heading control range of $[-30^\circ, +30^\circ]$ and the reduced range of $[-15^\circ, +15^\circ]$ reveal that no aircraft pair can be eliminated (i.e. is conflict-free) or is non-separable. It is also noted that the runtime of Algorithm 1 on all these instances grows quadratically with the number of aircraft and evolve under from 0.01 s to 1.23 s. The experiments on the CP instances (Tables 4.1 and 4.2) show that, as expected, the upper bound (UB) and the lower bound (LB) increase with

the number of aircraft. Using a heading control range of $[-30^\circ, +30^\circ]$ (Table 4.1), all three methods are able to solve CP instances with 4 to 10 aircraft within the available time limit. In both cases, runtime increases exponentially with the number of aircraft. For CP instances with 11 to 15 aircraft, the MIQP iteration of Algorithm 2 is unable to converge. Since no MIQCP iterations are performed ($n_i = 0$), the results obtained using *Disjunctive-2017* are identical to those obtained using *Disjunctive*. *Disjunctive* outperforms *Shadow* for instances solved but both formulations return comparable optimality gaps for instances that timed-out. Notably, the optimality gap of CP-15 is 73.5% and 74.1% using *Disjunctive* and *Shadow*, respectively, which highlights the difficulty of CP instances. Using a reduced heading control range of $[-15^\circ, +15^\circ]$ (Table 4.2), yields a comparable performance, although the proposed formulations are able to achieve slightly better UB values for CP-11 and CP-15, suggesting that the reduction of the solution space may help performance.

The numerical results obtained for FP instances (Tables 4.3 and 4.4) for both heading control ranges reveal that all corresponding 24 ACRPs can be solved to optimality within the available time limit by *Disjunctive* and *Disjunctive-2017*. In turn, *Shadow* fails to solve FP-15 with a reduced heading control range (Table 4.4). All three methods find the same optimal objective value, i.e. $\Delta\text{UB} = 0$ for all FP instances tested. *Disjunctive* and *Disjunctive-2017* are able to solve all FP instances in less than a minute, which contrasts with the performance of *Shadow* which requires significantly more time to solve FP instances with 9 or more aircraft per stream. This corresponds to an average performance gain of 90.9% across all FP instances solved to optimality by both methods. The outcome of the numerical experiments for GP instances (Tables 4.5 and 4.6) reveal a similar trend. *Disjunctive* and *Disjunctive-2017* can solve all GP instances with average runtimes of 125 s and 132 s for GP-15, which corresponds to a total of 60 aircraft, with a standard and a reduced heading control range, respectively. *Shadow* is able to solve all but three GP instances across all 24 GPs tested. The average performance gain for GP instances solved to optimality by all three formulations is 68.0%. It is also observed that reducing the heading control range does not affect the optimal solution of these problems and *Shadow* is consistently able to find the same best UB as *Disjunctive*.

The experiments performed on RCP instances reveal that the pre-processing procedure (Algorithm 1) can eliminate approximately 8% of aircraft pairs when using a reduced heading control range (Table 4.8), whereas no aircraft pairs are conflict-free using a standard heading control range (Table 4.7). The implementation of *Disjunctive* on RCP instances (Tables 4.7 and 4.8) reveals that while all 10- and 20-aircraft RCP

instances can be solved via the MIQP iteration, 30- and 40-aircraft RCP instances may require additional MIQCP iterations. Since no MIQCP iterations are performed ($n_i = 0$) for RCP-10 and RCP-20, the results obtained using *Disjunctive-2017* are identical to those obtained using *Disjunctive*. Using the standard heading control range (Table 4.7), on average, RCP-10 instances can be solved in 0.05 s and 0.14 s using *Disjunctive* and *Shadow*, respectively. RCP-20 instances require 0.26 s and 2.52 s, on average, using *Disjunctive* and *Shadow*, respectively, under the standard heading control range. The performance of the proposed formulations on RCP-10 and RCP-20 using a reduced heading control range (Table 4.8) is of similar order of magnitude due to the relatively low average number of conflicts per instance, i.e. 3.1 and 13.1, respectively. Those values lead to a performance gain of *Disjunctive* over *Shadow* of 71.8% and 62.6% for standard and reduced ranges, respectively, for RCP-10 instances; and of 89.6% and 81.3% for RCP-20 instances.

RCP-30 and RCP-40 instances have on average 32.9 and 59.3 conflicts, respectively, and present considerable computing challenges, notably the latter. Overall, it is noted that reducing the heading control range tends to improve the performance while retaining comparable optimal solutions, as indicated by the similar UB values obtained. *Disjunctive* requires an average of 0.4 MIQCP iterations for RCP-30 instances using a standard heading control range (Table 4.7) compared to 1.4 when using a reduced heading control range (Table 4.8). These figures increase to 0.8 and 1.6 in RCP-40 instances. For RCP-30 instances, the average optimality gaps are 0.17%, 4.60% and 2.36% using *Disjunctive*, *Disjunctive-2017* and *Shadow*, respectively using the standard heading control range (Table 4.7). These figures are reduced to 0.01%, 3.13% and 0.89% using the reduced heading control range (Table 4.8). For RCP-40 instances, the average optimality gaps values are significantly greater: 15%, 51.2% and 29.8% for a standard heading control (Table 4.7); and 13.1%, 52.0% and 25.8% for a reduced heading control range (Table 4.8). This shows that *Shadow* tends to double the optimality gap compared to *Disjunctive*, while *Disjunctive-2017* tends to triple this figure compared to *Disjunctive*. Using a standard heading control range (Table 4.7), *Disjunctive* is able to solve all but 3% of the RCP-30 instances whereas *Disjunctive-2017* and *Shadow* time out on 26% and 20% of these instances, respectively. The performance gain of *Disjunctive* compared to *Disjunctive-2017* and *Shadow* in terms of runtime are 21.0% and 41.7%, respectively. For RCP-40 instances, *Disjunctive* can solve 28% of the problems (72% of time-outs), while *Disjunctive-2017* and *Shadow* time out on 73% and 100% of the instances, respectively. It is also observed that *Disjunctive-2017* and *Shadow* may occasionally fail to find a UB as competitive as

that found by the **Disjunctive** on RCP-40 instances. The runtime performance gains of **Disjunctive** on RCP-30 instances are 21.0% and 41.7% compared to **Disjunctive-2017** and **Shadow**, respectively, using standard heading control range; and increase to 57.2% and 60.5% using the reduced heading control range. For RCP-40 instances, the gains of **Disjunctive** compared to **Disjunctive-2017** are 3.73% and 24.6% for standard and reduced heading control ranges, respectively; while **Shadow** is unable to solve any RCP-40 instances to optimality (100% of time-outs). The method **Disjunctive-2017** fails to find a feasible solution for 19% and 48% of the RCP-40 instances using the standard and reduced heading control ranges, respectively.

Table 4.1: Results for 2D CP instances with a speed control range of $[-6\%, +3\%]$ and a heading control range of $[-30^\circ, +30^\circ]$. Times (Time) are reported in seconds. The proportions of conflict-free ($\frac{|\mathcal{P}_F|}{|\mathcal{P}|}$) and non-separable ($\frac{|\mathcal{P}_I|}{|\mathcal{P}|}$) pairs, optimality gaps (Gap), proportions of time-outs (n_t) and the performance gain (Gain) are reported in %.

Instance	$ \mathcal{A} $	n_c	Pre-processing			Disjunctive						Disjunctive-2017					Shadow				
			$\frac{ \mathcal{P}_F }{ \mathcal{P} }$	$\frac{ \mathcal{P}_I }{ \mathcal{P} }$	Time	LB	UB	Gap	Time	n_i	n_t	Δ UB	Gap	Time	n_t	Gain	Δ UB	Gap	Time	n_t	Gain
CP-4	4	6	0	0	0.01	6.2E-4	6.2E-4	0.00	0.20	0	0	0.00	0.00	0.20	0	0.00	0.00	0.00	1.31	0	84.5
CP-5	5	10	0	0	0.03	1.1E-3	1.1E-3	0.00	0.40	0	0	0.00	0.00	0.40	0	0.00	0.00	0.00	1.02	0	60.1
CP-6	6	15	0	0	0.07	1.8E-3	1.8E-3	0.00	0.64	0	0	0.00	0.00	0.64	0	0.00	0.00	0.00	1.17	0	45.3
CP-7	7	21	0	0	0.12	2.4E-3	2.4E-3	0.00	0.39	0	0	0.00	0.00	0.39	0	0.00	0.00	0.00	1.28	0	69.5
CP-8	8	28	0	0	0.18	3.5E-3	3.5E-3	0.02	3.04	0	0	0.00	0.02	3.04	0	0.00	0.00	0.02	4.23	0	28.0
CP-9	9	36	0	0	0.24	4.3E-3	4.3E-3	0.02	7.97	0	0	0.00	0.02	7.97	0	0.00	0.00	0.02	11.2	0	29.3
CP-10	10	45	0	0	0.31	5.6E-3	5.6E-3	0.02	72.3	0	0	0.00	0.02	72.3	0	0.00	0.00	0.02	73.1	0	1.10
CP-11	11	55	0	0	0.37	6.8E-3	6.9E-3	1.99	600	0	100	0.00	1.99	600	100	-	0.00	15.6	600	100	-
CP-12	12	66	0	0	0.48	5.0E-3	8.4E-3	40.2	600	0	100	0.00	40.2	600	100	-	0.00	37.6	600	100	-
CP-13	13	78	0	0	0.63	4.4E-3	9.9E-3	55.2	600	0	100	0.00	55.2	600	100	-	0.00	53.1	600	100	-
CP-14	14	91	0	0	0.72	3.8E-3	1.1E-2	66.8	600	0	100	0.00	66.8	600	100	-	0.00	63.0	600	100	-
CP-15	15	105	0	0	0.89	3.6E-3	1.5E-2	73.5	600	0	100	0.00	73.5	600	100	-	0.00	74.1	600	100	-

Table 4.2: Results for 2D CP instances with a speed control range of $[-6\%, +3\%]$ and a heading control range of $[-15^\circ, +15^\circ]$. Times (Time) are reported in seconds. The proportions of conflict-free ($\frac{|\mathcal{P}_F|}{|\mathcal{P}|}$) and non-separable ($\frac{|\mathcal{P}_I|}{|\mathcal{P}|}$) pairs, optimality gaps (Gap), proportions of time-outs (n_t) and the performance gain (Gain) are reported in %.

Instance	$ \mathcal{A} $	n_c	Pre-processing			Disjunctive						Disjunctive-2017						Shadow			
			$\frac{ \mathcal{P}_F }{ \mathcal{P} }$	$\frac{ \mathcal{P}_I }{ \mathcal{P} }$	Time	LB	UB	Gap	Time	n_i	n_t	Δ UB	Gap	Time	n_t	Gain	Δ UB	Gap	Time	n_t	Gain
CP-4	4	6	0	0	0.01	6.2E-4	6.2E-4	0.00	0.25	0	0	0.00	0.01	0.25	0	0.00	0.00	0.00	1.27	0	80.2
CP-5	5	10	0	0	0.03	1.1E-3	1.1E-3	0.00	0.03	0	0	0.00	0.03	0.03	0	0.00	0.00	0.00	1.16	0	97.3
CP-6	6	15	0	0	0.11	1.8E-3	1.8E-3	0.00	0.23	0	0	0.00	0.11	0.23	0	0.00	0.00	0.00	1.24	0	81.4
CP-7	7	21	0	0	0.18	2.4E-3	2.4E-3	0.00	0.19	0	0	0.00	0.18	0.19	0	0.00	0.00	0.01	1.20	0	84.4
CP-8	8	28	0	0	0.25	3.5E-3	3.5E-3	0.02	3.17	0	0	0.00	0.25	3.17	0	0.00	0.00	0.00	3.72	0	14.7
CP-9	9	36	0	0	0.31	4.3E-3	4.3E-3	0.02	8.11	0	0	0.00	0.31	8.11	0	0.00	0.00	0.02	8.80	0	7.80
CP-10	10	45	0	0	0.42	5.6E-3	5.6E-3	0.02	75.1	0	0	0.00	0.42	75.1	0	0.00	0.00	0.02	85.1	0	11.7
CP-11	11	55	0	0	0.52	6.6E-3	6.8E-3	5.25	600	0	100	0.00	0.52	600	100	-	0.00	10.2	600	100	-
CP-12	12	66	0	0	0.62	4.9E-3	8.4E-3	40.7	600	0	100	0.00	0.62	600	100	-	0.00	39.9	600	100	-
CP-13	13	78	0	0	0.72	4.4E-3	9.9E-3	55.5	600	0	100	0.00	0.72	600	100	-	0.00	50.1	600	100	-
CP-14	14	91	0	0	0.80	3.8E-3	1.1E-2	66.5	600	0	100	0.00	0.80	600	100	-	0.00	65.7	600	100	-
CP-15	15	105	0	0	0.88	3.7E-3	1.4E-2	72.9	600	0	100	0.00	0.88	600	100	-	0.00	70.6	600	100	-

Table 4.3: Results for 2D FP instances with a speed control range of $[-6\%, +3\%]$ and a heading control range of $[-30^\circ, +30^\circ]$. Times (Time) are reported in seconds. The proportions of conflict-free ($\frac{|\mathcal{P}_F|}{|\mathcal{P}|}$) and non-separable ($\frac{|\mathcal{P}_I|}{|\mathcal{P}|}$) pairs, optimality gaps (Gap), proportions of time-outs (n_t) and the performance gain (Gain) are reported in %.

Instance	$ \mathcal{A} $	n_c	Pre-processing			Disjunctive						Disjunctive-2017					Shadow				
			$\frac{ \mathcal{P}_F }{ \mathcal{P} }$	$\frac{ \mathcal{P}_I }{ \mathcal{P} }$	Time	LB	UB	Gap	Time	n_i	n_t	Δ UB	Gap	Time	n_t	Gain	Δ UB	Gap	Time	n_t	Gain
FP-4	8	4	0	0	0.17	8.1E-4	8.2E-4	0.10	0.05	0	0	0.00	0.10	0.05	0	0.00	0.00	0.10	0.26	0	80.7
FP-5	10	5	0	0	0.28	1.1E-3	1.1E-3	0.03	0.05	0	0	0.00	0.03	0.05	0	0.00	0.00	0.08	4.17	0	98.8
FP-6	12	6	0	0	0.36	1.5E-3	1.5E-3	0.05	0.16	0	0	0.00	0.05	0.16	0	0.00	0.00	0.72	6.00	0	97.3
FP-7	14	7	0	0	0.40	2.1E-3	2.1E-3	0.05	0.44	0	0	0.00	0.05	0.44	0	0.00	0.00	0.32	6.80	0	93.5
FP-8	16	8	0	0	0.45	2.8E-3	2.7E-3	0.04	2.31	0	0	0.00	0.04	2.31	0	0.00	0.00	0.04	7.66	0	69.8
FP-9	18	9	0	0	0.52	3.7E-3	3.7E-3	0.03	2.28	0	0	0.00	0.03	2.28	0	0.00	0.00	0.15	126	0	98.1
FP-10	20	10	0	0	0.61	5.2E-3	5.2E-3	0.02	8.41	0	0	0.00	0.02	8.41	0	0.00	0.00	0.23	138	0	93.9
FP-11	22	12	0	0	0.71	5.8E-3	5.8E-3	0.14	12.3	0	0	0.00	0.14	12.3	0	0.00	0.00	0.05	126	0	90.2
FP-12	24	14	0	0	0.82	6.6E-3	6.6E-3	0.03	16.2	0	0	0.00	0.03	16.2	0	0.00	0.00	0.25	261	0	93.7
FP-13	26	16	0	0	0.94	7.4E-3	4.5E-3	0.12	21.4	0	0	0.00	0.12	21.4	0	0.00	0.00	0.12	342	0	93.7
FP-14	25	18	0	0	1.05	2.7E-2	2.7E-2	0.14	25.3	0	0	0.00	0.14	25.3	0	0.00	0.00	0.16	465	0	94.5
FP-15	30	22	0	0	1.15	3.5E-2	3.5E-2	0.13	42.2	0	0	0.00	0.13	42.2	0	0.00	0.00	0.24	576	0	92.6

Table 4.4: Results for 2D FP instances with a speed control range of $[-6\%, +3\%]$ and a heading control range of $[-15^\circ, +15^\circ]$. Times (Time) are reported in seconds. The proportions of conflict-free ($\frac{|\mathcal{P}_F|}{|\mathcal{P}|}$) and non-separable ($\frac{|\mathcal{P}_I|}{|\mathcal{P}|}$) pairs, optimality gaps (Gap), proportions of time-outs (n_t) and the performance gain (Gain) are reported in %.

Instance	$ \mathcal{A} $	n_c	Pre-processing			Disjunctive						Disjunctive-2017						Shadow			
			$\frac{ \mathcal{P}_F }{ \mathcal{P} }$	$\frac{ \mathcal{P}_I }{ \mathcal{P} }$	Time	LB	UB	Gap	Time	n_i	n_t	Δ UB	Gap	Time	n_t	Gain	Δ UB	Gap	Time	n_t	Gain
FP-4	8	4	0	0	0.09	8.1E-4	8.2E-4	0.11	0.06	0	0	0.00	0.11	0.06	0	0.00	0.00	0.09	0.20	0	70.0
FP-5	10	5	0	0	0.22	1.1E-3	1.1E-3	0.03	0.07	0	0	0.00	0.03	0.07	0	0.00	0.00	0.10	4.57	0	98.4
FP-6	12	6	0	0	0.29	1.5E-3	1.5E-3	0.03	0.21	0	0	0.00	0.03	0.21	0	0.00	0.00	0.67	6.23	0	96.6
FP-7	14	7	0	0	0.41	2.1E-3	2.1E-3	0.06	0.47	0	0	0.00	0.06	0.47	0	0.00	0.00	0.30	6.81	0	93.1
FP-8	16	8	0	0	0.45	2.8E-3	2.7E-3	0.04	2.56	0	0	0.00	0.04	2.56	0	0.00	0.00	0.41	7.66	0	66.5
FP-9	18	9	0	0	0.62	3.7E-3	3.7E-3	0.03	2.76	0	0	0.00	0.03	2.76	0	0.00	0.00	0.15	156	0	98.2
FP-10	20	10	0	0	0.72	5.2E-3	5.2E-3	0.02	9.52	0	0	0.00	0.02	9.52	0	0.00	0.00	0.24	143	0	93.3
FP-11	22	12	0	0	0.85	5.8E-3	5.8E-3	0.04	10.3	0	0	0.00	0.04	10.3	0	0.00	0.00	0.04	176	0	94.4
FP-12	24	14	0	0	0.92	6.6E-3	6.6E-3	0.13	12.2	0	0	0.00	0.13	12.2	0	0.00	0.00	0.14	226	0	94.6
FP-13	26	16	0	0	0.99	7.4E-3	4.5E-3	0.12	18.4	0	0	0.00	0.12	18.4	0	0.00	0.00	0.01	338	0	94.5
FP-14	25	18	0	0	1.02	2.7E-2	2.7E-2	0.04	22.3	0	0	0.00	0.04	22.3	0	0.00	0.00	0.04	476	0	95.3
FP-15	30	22	0	0	1.23	3.5E-2	3.5E-2	0.23	32.2	0	0	0.00	0.23	32.2	0	0.00	0.00	0.14	600	100	-

Table 4.5: Results for 2D GP instances with a speed control range of $[-6\%, +3\%]$ and a heading control range of $[-30^\circ, +30^\circ]$. Times (Time) are reported in seconds. The proportions of conflict-free ($\frac{|\mathcal{P}_F|}{|\mathcal{P}|}$) and non-separable ($\frac{|\mathcal{P}_I|}{|\mathcal{P}|}$) pairs, optimality gaps (Gap), proportions of time-outs (n_t) and the performance gain (Gain) are reported in %.

Instance	$ \mathcal{A} $	n_c	Pre-processing			Disjunctive						Disjunctive-2017						Shadow			
			$\frac{ \mathcal{P}_F }{ \mathcal{P} }$	$\frac{ \mathcal{P}_I }{ \mathcal{P} }$	Time	LB	UB	Gap	Time	n_i	n_t	Δ UB	Gap	Time	n_t	Gain	Δ UB	Gap	Time	n_t	Gain
GP-4	16	12	0	0	0.03	9.2E-4	9.2E-4	0.01	0.16	0	0	0.00	0.01	0.16	0	0.00	0.00	0.11	1.22	0	86.8
GP-5	20	16	0	0	0.10	1.3E-3	1.3E-3	0.02	0.98	0	0	0.00	0.02	0.98	0	0.00	0.00	0.25	2.34	0	58.1
GP-6	24	20	0	0	0.21	1.8E-3	1.8E-3	0.04	2.85	0	0	0.00	0.04	2.85	0	0.00	0.00	0.26	12.1	0	76.4
GP-7	28	24	0	0	0.32	2.4E-3	2.4E-3	0.03	11.3	0	0	0.00	0.03	11.3	0	0.00	0.00	0.33	14.4	0	21.5
GP-8	32	28	0	0	0.44	3.2E-3	3.2E-3	0.02	20.7	0	0	0.00	0.02	20.7	0	0.00	0.00	0.12	59.5	0	65.2
GP-9	36	32	0	0	0.58	4.3E-3	4.3E-3	0.04	46.2	0	0	0.00	0.04	46.2	0	0.00	0.00	0.24	165	0	72.0
GP-10	40	36	0	0	0.69	6.1E-3	6.1E-3	0.02	47.5	0	0	0.00	0.02	47.5	0	0.00	0.00	0.82	194	0	75.5
GP-11	44	40	0	0	0.72	7.9E-3	7.9E-3	0.24	52.3	0	0	0.00	0.24	52.3	0	0.00	0.00	0.12	225	0	77.6
GP-12	48	44	0	0	0.89	8.3E-3	8.3E-3	0.31	61.2	0	0	0.00	0.31	61.2	0	0.00	0.00	0.13	383	0	83.7
GP-13	52	48	0	0	0.98	9.5E-3	9.5E-3	0.12	75.3	0	0	0.00	0.12	75.3	0	0.00	0.00	0.21	476	0	83.5
GP-14	56	52	0	0	1.09	3.4E-2	3.4E-2	0.56	92.8	0	0	0.00	0.56	92.8	0	0.00	0.00	0.24	600	100	-
GP-15	60	54	0	0	1.24	3.8E-2	3.8E-2	0.45	125	0	0	0.00	0.45	125	0	0.00	0.00	0.25	600	100	-

Table 4.6: Results for 2D GP instances with a speed control range of $[-6\%, +3\%]$ and a heading control range of $[-15^\circ, +15^\circ]$. Times (Time) are reported in seconds. The proportions of conflict-free ($\frac{|\mathcal{P}_F|}{|\mathcal{P}|}$) and non-separable ($\frac{|\mathcal{P}_I|}{|\mathcal{P}|}$) pairs, optimality gaps (Gap), proportions of time-outs (n_t) and the performance gain (Gain) are reported in %.

Instance	$ \mathcal{A} $	n_c	Pre-processing			Disjunctive						Disjunctive-2017						Shadow			
			$\frac{ \mathcal{P}_F }{ \mathcal{P} }$	$\frac{ \mathcal{P}_I }{ \mathcal{P} }$	Time	LB	UB	Gap	Time	n_i	n_t	Δ UB	Gap	Time	n_t	Gain	Δ UB	Gap	Time	n_t	Gain
GP-4	16	12	0	0	0.05	9.2E-4	9.2E-4	0.03	0.24	0	0	0.00	0.03	0.24	0	0.00	0.00	0.18	1.58	0	84.6
GP-5	20	16	0	0	0.05	1.3E-3	1.3E-3	0.02	1.81	0	0	0.00	0.02	1.81	0	0.00	0.00	0.21	2.16	0	16.2
GP-6	24	20	0	0	0.15	1.8E-3	1.8E-3	0.05	3.91	0	0	0.00	0.05	3.91	0	0.00	0.00	0.24	11.3	0	65.3
GP-7	28	24	0	0	0.24	2.4E-3	2.4E-3	0.03	11.2	0	0	0.00	0.03	11.2	0	0.00	0.00	0.65	18.6	0	39.7
GP-8	32	28	0	0	0.34	3.2E-3	3.2E-3	0.02	21.5	0	0	0.00	0.02	21.5	0	0.00	0.00	0.12	59.5	0	63.8
GP-9	36	32	0	0	0.48	4.3E-3	4.3E-3	0.05	46.5	0	0	0.00	0.05	46.5	0	0.00	0.00	0.24	136	0	65.8
GP-10	40	36	0	0	0.56	6.1E-3	6.1E-3	0.04	49.2	0	0	0.00	0.04	49.2	0	0.00	0.00	0.89	188	0	73.8
GP-11	44	40	0	0	0.67	7.9E-3	7.9E-3	0.14	50.3	0	0	0.00	0.14	50.3	0	0.00	0.00	0.32	205	0	75.4
GP-12	48	44	0	0	0.78	8.3E-3	8.3E-3	0.23	62.2	0	0	0.00	0.23	62.2	0	0.00	0.00	0.43	352	0	82.2
GP-13	52	48	0	0	0.81	9.5E-3	9.5E-3	0.22	78.3	0	0	0.00	0.22	78.3	0	0.00	0.00	0.31	421	0	81.4
GP-14	56	52	0	0	0.95	3.4E-2	3.4E-2	0.24	102	0	0	0.00	0.24	102	0	0.00	0.00	0.42	525	0	80.5
GP-15	60	54	0	0	1.03	3.8E-2	3.8E-2	0.33	132	0	0	0.00	0.33	132	0	0.00	0.00	0.51	600	100	-

Table 4.7: Results for 2D RCP instances with a speed control range of $[-6\%, +3\%]$ and a heading control range of $[-30^\circ, +30^\circ]$. Times (Time) are reported in seconds. The proportions of conflict-free ($\frac{|\mathcal{P}_F|}{|\mathcal{P}|}$) and non-separable ($\frac{|\mathcal{P}_I|}{|\mathcal{P}|}$) pairs, optimality gaps (Gap), time-outs (n_t), infeasible solutions (n_f) and the performance gain (Gain) are reported in %.

Instance	\mathcal{A}	Pre-processing				Disjunctive								
		n_c	$\frac{ \mathcal{P}_F }{ \mathcal{P} }$	$\frac{ \mathcal{P}_I }{ \mathcal{P} }$	Time	LB			UB		Gap	Time	n_i	n_t
RCP-10	10	3.10 (1.6)	0	0	0.12	2.2E-4 (2E-4)	2.2E-4 (2E-4)	2.2E-4 (2E-4)	0.00 (0.0)	0.05 (0.01)	0.0 (0.0)	0	0	
RCP-20	20	13.1 (3.5)	0	0	0.23	1.7E-3 (9E-4)	1.7E-3 (9E-4)	1.7E-3 (9E-4)	0.00 (0.0)	0.26 (0.10)	0.0 (0.0)	0	0	
RCP-30	30	32.9 (5.6)	0	0	0.45	7.1E-3 (2E-3)	7.1E-3 (2E-3)	7.1E-3 (2E-3)	0.17 (0.7)	135 (239)	0.4 (0.6)	3	0	
RCP-40	40	59.3 (7.1)	0	0	0.60	1.8E-2 (5E-3)	2.4E-2 (1E-2)	15.0 (25)	516 (194)	0.8 (0.5)	72	0		

Instance	Disjunctive-2017							Shadow					
	Δ UB	Gap	Time	n_t	n_f	Gain	Δ UB	Gap	Time	n_t	n_f	Gain	
RCP-10	0.00 (0.0)	0.00 (0.0)	0.05 (0.01)	0	0	0.00	0.00 (0.0)	0.02 (0.1)	0.14 (0.10)	0	0	71.8	
RCP-20	0.00 (0.0)	0.00 (0.0)	0.26 (0.10)	0	0	0.00	0.00 (0.0)	0.01 (0.0)	2.52 (0.60)	0	0	89.6	
RCP-30	0.00 (0.0)	4.60 (11)	171 (266)	26	0	21.0	0.00 (0.0)	2.36 (4.9)	231 (218)	20	0	41.7	
RCP-40	0.01 (0.1)	51.2 (12)	536 (200)	77	19	3.73	0.02 (0.1)	29.8 (25)	600 (0.0)	100	0	-	

Table 4.8: Results for 2D RCP instances with a speed control range of $[-6\%, +3\%]$ and a heading control range of $[-15^\circ, +15^\circ]$. Times (Time) are reported in seconds. The proportions of conflict-free ($\frac{|\mathcal{P}_F|}{|\mathcal{P}|}$) and non-separable ($\frac{|\mathcal{P}_I|}{|\mathcal{P}|}$) pairs, optimality gaps (Gap), time-outs (n_t), infeasible solutions (n_f) and the performance gain (Gain) are reported in %.

Instance	$ \mathcal{A} $	Pre-processing					Disjunctive								
		n_c	$\frac{ \mathcal{P}_F }{ \mathcal{P} }$	$\frac{ \mathcal{P}_I }{ \mathcal{P} }$	Time	LB	UB	Gap	Time	n_i	n_t	n_f			
RCP-10	10	3.10 (1.6)	8.2	0	0.33	2.2E-4 (2E-4)	2.2E-4 (2E-4)	0.03 (0.2)	0.04 (0.0)	0.0 (0.0)	0	0			
RCP-20	20	13.1 (3.5)	7.7	0	0.51	1.7E-3 (9E-4)	1.7E-3 (9E-4)	0.01 (0.0)	0.24 (0.1)	0.0 (0.0)	0	0			
RCP-30	30	32.9 (5.6)	7.7	0	0.62	7.2E-3 (2E-3)	7.2E-3 (2E-3)	0.01 (0.1)	66.3 (135)	1.4 (0.8)	3	0			
RCP-40	40	59.3 (7.1)	7.9	0	0.75	1.8E-2 (5E-3)	2.2E-2 (1E-2)	13.1 (20.7)	389 (261)	1.6 (0.5)	59	0			

Instance	Disjunctive-2017							Shadow					
	Δ UB	Gap	Time	n_t	n_f	Gain	Δ UB	Gap	Time	n_t	n_f	Gain	
RCP-10	0.00 (0.0)	0.03 (0.2)	0.04 (0.0)	0	0	0.00	0.00 (0.0)	0.03 (0.1)	0.11 (0.1)	0	0	62.6	
RCP-20	0.00 (0.0)	0.01 (0.0)	0.24 (0.1)	0	0	0.00	0.00 (0.0)	0.01 (0.0)	1.39 (1.1)	0	0	81.3	
RCP-30	0.00 (0.0)	3.13 (8.8)	155 (256)	22	0	57.2	0.00 (0.0)	0.89 (2.9)	167 (181)	10	0	60.5	
RCP-40	0.01 (0.1)	52.0 (41)	516 (200)	78	48	24.6	0.02 (0.1)	25.8 (24)	600 (0.0)	100	0	-	

4.7.4 Results on 2D+FL instances

Results on 2D+FL instances are reported using similar tables as in Section 4.7.3. Instead of reporting the number of aircraft and the number of conflicts, the average number of aircraft and conflicts per FL is reported, i.e. $\frac{|A|}{|Z|}$, $\frac{n_c}{|Z|}$ respectively. In addition, there is the inclusion of a section corresponding to the FL assignment formulation. In all the numerical experiments on 2D+FL instances, only a single pass through the **while** loop of Algorithm 3 is required. Hence, it is only reported the Obj which is the objective function value of MILP 8; and Time which is the corresponding computing runtime in seconds. For the numerical experiment on 2D+FL problems, the focus is on RCP instances named RCP-N-Z where N is the number of aircraft and Z is the number of FLs. Three numbers of aircraft are considered: 50, 100 and 150; and two numbers of FLs: 3 and 5. In terms of conflict density, for the same number of aircraft, instances with 3 FLs have a greater number of conflicts compared to instances with 5 FLs and are more computationally challenging. The results are reported in Table 4.9 for the standard heading control range, and in Table 4.10 for the reduced heading control range.

Using the standard heading control range ($[-30^\circ, +30^\circ]$, see Table 4.9), the numerical experiments reveal that among all six groups of 2D+FL instances, only some RCP-150-3 and RCP-150-5 instances may require aircraft to change FLs. That is, for all other 2D+FL instances, all conflicts can be resolved using 2D trajectory control only and thus aircraft do not require performing any FL change. This can be explained by observing that for instances RCP-150-3, the average number of aircraft per FL is 50 which corresponds to a denser aircraft configuration compared to the 2D RCP-40 instances, which all admit feasible solutions. In comparison, only a single RCP-150-5 instance required a FL change for a single aircraft. For RCP-150-5, even though the average density per FL is 30, some instances may have denser FL requiring FL separation. Among all 100 RCP-150-3 instances, 35% of the instances requires a FL change. The maximum number of non-separable pairs ($|\mathcal{P}_I|$) is 2 and the maximum objective value of Model 8 is 1, indicating that only a single aircraft deviated from its initial FL.

Comparing the methods, it is observed that **Disjunctive** slightly outperforms the two benchmarks in terms of solution quality by occasionally finding better UBs than **Disjunctive-2017** or **Shadow**. For instances with 3 FLs, the optimality gaps are relatively small, i.e. less than 1.0% for RCP-50-3 and RCP-100-3 using **Disjunctive** (with a standard deviation below 0.5%) and around 10% for RCP-150-3 (with a standard deviation around 23%). However, using **Disjunctive-2017** and **Shadow**, the optimality

gaps are considerably larger. Especially in the former where the average gap (standard deviation in parenthesis) is 15.7% (18.6%) for RCP-50-3 and with RCP-100-3 and RCP-150-3, this difference is even larger, i.e. 42.0% (60.8%) and 61.6% (21.3%) of gap, respectively. For **Shadow**, those values are less than 1.0% (0.1% of standard deviation) for RCP-50-3, 53.2% (0.7%) for RCP-100-3 and 56.6% (24%) for RCP-150-3. From a computational standpoint, the average runtime of Model 8 on RCP-150-3 instances is 4.56 s. For RCP-50-3, **Disjunctive**, **Disjunctive-2017** and **Shadow** can solve all instances in an average time of 0.88 s, 2.81 s and 10.2 s, respectively. For RCP-100-3, which corresponds to an average number of 33.3 aircraft per FL, **Disjunctive** solves all instances in an average time of 3.3 minutes, whereas using **Disjunctive-2017** there is a total of 64 % instances that time out and for the remaining instances that can be solved, the runtime is 411 s. **Shadow** times out on 46% of the instances and requires an average runtime of 9.5 minutes for the instances solved. The denser RCP-150-3 instances, with an average of 50 aircraft per FL, present substantial computational challenges. **Disjunctive** is able to solve only 40% of these instances (60% of time-outs) and an average of 2.8 MIQCP iterations are required with a standard deviation of 1.5. In comparison, **Disjunctive-2017** is unable to solve most of these instances (95% of time-outs) and fails to find a feasible solution for 5% of them. The method **Shadow** is unable to solve any of these instances within the available time limit. The performance gain using 3 FLs shows that a gain of 87.8% and 51.8% can be obtained using **Disjunctive** over **Disjunctive-2017** and 91.3% and 61.9% using **Disjunctive** over **Shadow** for RCP-50-3 and RCP-100-3, respectively.

Increasing the number of FLs from 3 to 5 reduces the density of aircraft per FL which translates into better computational performance for all three methods. The UB value obtained by those instances using **Disjunctive-2017** is relatively close to the UB obtained with **Disjunctive** yielding deviations of 0.08, 0.09 and 0.10 in RCP-50-5, RCP-100-5 and RCP-150-5, respectively (see Table 4.9). **Shadow** only deviates from the UB found by **Disjunctive** by 0.08 for RCP-150-5 instances. All RCP-50-5 and RCP-100-5 instances are solved to optimality within the time limit using all three methods. The optimality gap is relatively small for **Disjunctive** and **Shadow**, and does not exceed 0.2% in those instances. Using **Disjunctive-2017**, it reaches 13.4% for RCP-50-5 and 45.5% for RCP-100-5. For RCP-150-5, using **Disjunctive** solves all instances with optimality gap of 0.05%. However, **Disjunctive-2017** fails to solve all RCP-150-5 instances and yields an average optimality gap of 45.1%. The method **Shadow** also fails to solve all RCP-150-5 instances and yields an average optimality gap of 1.56%. In terms of runtime, it is noticed that **Disjunctive** solves all instances with 5 FLs in less

than 142 s (see Table 4.9). The performance of the methods on 2D+FL instances with 5 FLs reveal that gains of 75.6% and 42.7% can be obtained using **Disjunctive** over **Disjunctive-2017**, and 81.8% and 98.8% using **Disjunctive** over **Shadow** for RCP-50-5 and RCP-100-5, respectively.

Reducing the heading control range (see Table 4.10), yields an overall similar performance. The main differences relative to the results obtained using the standard heading control range are observed in the pre-processing procedure which, as in the 2D RCP instances, eliminates on average 8% of the aircraft pairs. It is also observed that reducing the heading control range increases the number of non-separable pairs to 1.45% for RCP-150-3 instances and to 0.03% for RCP-150-5 instances. This increase in the proportion of non-separable aircraft pairs is reflected in the solution of the flight assignment formulation (MILP 8) which has an average value of 1.62 on RCP-150-3 instances and 0.02 on RCP-150-5 instances, respectively. For RCP-150-3, 67% of the instances required a FL change, the maximum number of non-separable pairs ($|\mathcal{P}_1|$) is 6 and the maximum objective value of Model 8 is 3, indicating that three aircraft deviated from their initial FL. Same UB for and RCP-50-5 and RCP-100-5, whereas for RCP-150-5 instances it is observed an average deviation of 0.05 using **Disjunctive-2017** and 0.02 using **Shadow**. The optimality gap is below 1% for all instances using **Disjunctive**, while it ranges from 13.3% in RCP-50-3 to 40.1% in RCP-150-3 using **Disjunctive-2017**, and from 0.01% to 42.1% using **Shadow**. In terms of runtime, all three methods are able to solve all RCP-50-3 instances in on average 0.88 s, 2.37 s and 11.3 s using **Disjunctive**, **Disjunctive-2017** and **Shadow**, respectively. For RCP-100-3, it is noted that all instances are solved by **Disjunctive** in 168 s, while 26% and 39% of them time out using **Disjunctive-2017** and **Shadow**, respectively. In addition, **Disjunctive-2017** fails to find a feasible solution in 10% of the instances. For those instances that can be solved, the average runtime is 474 s for **Disjunctive-2017** and 453 s for **Shadow**. For RCP-150-3 instances, **Disjunctive**, **Disjunctive-2017** and **Shadow** time out on 46%, 74% and 100% of the instances, respectively; and **Disjunctive-2017** fails to find a feasible solution in 14% of the instances. For the remaining instances, the runtime is around 420 for **Disjunctive** and 587 s for **Disjunctive-2017**. The performance gains of **Disjunctive** compared to both benchmarks are above 62% for RCP-50-3 and RCP-100-3 instances, and near 40% compared to **Disjunctive-2017** for RCP-150-3 instances. All RCP-50-5 and RCP-100-5 instances are solved to optimality by all methods. The runtime for those instances is less than 1 s for RCP-50-5 and 35.1 for RCP-100-5 for RCP-100-5 using **Disjunctive**, while **Disjunctive-2017** and **Shadow** yield larger runtimes but of the same order of magnitude. These figures

do not carry over to RCP-150-5 instances. Using **Disjunctive**, all RCP-150-5 instances can be solved with an average runtime of 152 s. However, using **Disjunctive-2017** all instances time out and this fails to find a feasible solution in 15% of the cases. Further, the average UB deviation is 0.12 using **Disjunctive-2017** and the average optimality gap 42.3%. Using **Shadow**, all RCP-150-5 instances also time out, the average UB deviation is 0.09 and the average optimality gap is 12.3%.

Table 4.9: Results for 2D+FL RCP instances with a speed control range of $[-6\%, +3\%]$ and a heading control range of $[-30^\circ, +30^\circ]$. Times (Time) are reported in seconds. The proportions of conflict-free ($\frac{|\mathcal{P}_F|}{|\mathcal{P}|}$) and non-separable ($\frac{|\mathcal{P}_I|}{|\mathcal{P}|}$) pairs, optimality gaps (Gap), time-outs (n_t), infeasible solutions (n_f) and the performance gain (Gain) are reported in %.

Instance	$\frac{ A }{ Z }$	Pre-processing				FL assignment				Disjunctive					
		$\frac{n_c}{ Z }$	$\frac{ \mathcal{P}_F }{ \mathcal{P} }$	$\frac{ \mathcal{P}_I }{ \mathcal{P} }$	Time	Obj.	Time	LB	UB	Gap	Time	n_i	n_t	n_f	
RCP-50-3	15	3.15 (1.50)	0	0.00	0.42	0.00 (0.0)	0.00 (0.0)	1.2E-2 (6E-3)	1.3E-2 (6E-3)	0.02 (0.0)	0.88 (0.2)	0.0 (0.0)	0	0	
RCP-100-3	33	35.6 (1.12)	0	0.00	0.86	0.00 (0.0)	0.00 (0.0)	1.4E-1 (3E-2)	1.4E-1 (3E-2)	0.12 (0.3)	198 (123)	1.2 (2.0)	0	0	
RCP-150-3	50	64.1 (5.26)	0	0.55	1.02	0.62 (0.08)	4.56 (0.8)	4.5E-2 (5E-3)	5.2E-2 (1E-2)	10.2 (23)	520 (136)	2.8 (1.5)	60	0	
RCP-50-5	10	3.11 (1.52)	0	0.00	0.62	0.00 (0.0)	0.00 (0.0)	9.4E-3 (5E-3)	9.4E-3 (5E-3)	0.00 (0.0)	0.26 (0.1)	0.0 (0.0)	0	0	
RCP-100-5	20	14.1 (3.52)	0	0.00	1.25	0.00 (0.0)	0.00 (0.0)	8.3E-3 (3E-2)	8.3E-2 (3E-2)	0.00 (0.0)	2.51 (2.4)	0.0 (0.0)	0	0	
RCP-150-5	30	34.2 (2.56)	0	0.01	1.92	0.01 (0.1)	0.11 (1.1)	3.3E-1 (8E-2)	3.3E-1 (8E-2)	0.05 (0.2)	142 (185)	2.3 (0.6)	0	0	

Instance	Disjunctive-2017							Shadow					
	Δ UB	Gap	Time	n_t	n_f	Gain	Δ UB	Gap	Time	n_t	n_f	Gain	
RCP-50-3	0.02 (0.0)	15.7 (18.6)	2.81(2.52)	0	0	87.8	0.00 (0.0)	0.01 (0.0)	10.2 (14.8)	0	0	91.3	
RCP-100-3	0.02 (0.1)	42.0 (60.8)	411 (136)	64	0	51.8	0.05 (0.1)	53.2 (0.7)	572 (17.5)	46	0	61.9	
RCP-150-3	0.10 (0.0)	61.6 (21.3)	600 (0.0)	95	5	-	0.03 (0.0)	56.6 (24)	600 (0.0)	100	0	-	
RCP-50-5	0.08 (0.0)	13.4 (16.6)	2.17 (1.98)	0	0	75.6	0.00 (0.0)	0.00 (0.0)	1.43 (1.0)	0	0	81.8	
RCP-100-5	0.09 (0.0)	45.5 (12.6)	67.2 (70.5)	0	0	42.7	0.00 (0.0)	0.13 (0.1)	126 (163)	0	0	98.0	
RCP-150-5	0.10 (0.0)	45.1 (10.3)	600 (0.0)	100	0	-	0.08 (0.0)	1.56 (0.6)	600 (0.0)	100	0	-	

Table 4.10: Results for 2D+FL RCP instances with a speed control range of $[-6\%, +3\%]$ and a heading control range of $[-15^\circ, +15^\circ]$. Times (Time) are reported in seconds. The proportions of conflict-free ($\frac{|\mathcal{P}_F|}{|\mathcal{P}|}$) and non-separable ($\frac{|\mathcal{P}_I|}{|\mathcal{P}|}$) pairs, optimality gaps (Gap), time-outs (n_t), infeasible solutions (n_f) and the performance gain (Gain) are reported in %.

Instance	$\frac{ A }{ Z }$	Pre-processing				FL assignment				Disjunctive				
		$\frac{n_c}{ Z }$	$\frac{ \mathcal{P}_F }{ \mathcal{P} }$	$\frac{ \mathcal{P}_I }{ \mathcal{P} }$	Time	Obj.	Time	LB	UB	Gap	Time	n_i	n_t	n_f
RCP-50-3	15	3.15 (1.5)	7.0	0.00	0.52	0.00 (0.0)	0.00 (0.0)	1.2E-2 (6E-3)	1.2E-2 (6E-3)	0.02 (0.0)	0.88 (0.2)	0.0 (0.0)	0	0
RCP-100-3	33	35.6 (1.12)	7.2	0.00	0.62	0.00 (0.0)	0.00 (0.0)	1.4E-1 (3E-2)	1.4E-1 (3E-2)	0.15 (0.3)	168 (103)	2.2 (2.0)	0	0
RCP-150-3	50	64.1 (5.26)	8.1	1.45	1.22	1.62 (0.1)	5.62 (0.8)	4.5E-2 (5E-3)	5.2E-2 (1E-2)	8.60 (12)	420 (102)	4.8 (1.5)	46	0
RCP-50-5	10	3.11 (1.52)	8.6	0.00	0.52	0.00 (0.0)	0.00 (0.0)	9.4E-3 (5E-3)	9.4E-3 (5E-3)	0.00 (0.0)	0.26 (0.1)	0.0 (0.0)	0	0
RCP-100-5	20	14.1 (3.52)	7.8	0.00	1.22	0.00 (0.0)	0.00 (0.0)	8.3E-3 (3E-2)	8.3E-2 (3E-2)	0.00 (0.0)	35.1 (2.4)	0.0 (0.0)	0	0
RCP-150-5	30	34.2 (2.56)	8.0	0.03	1.86	0.02 (0.2)	0.21 (1.1)	3.3E-1 (8E-2)	3.3E-1 (8E-2)	0.51 (0.3)	152 (78.2)	4.3 (1.0)	0	0

Instance	Disjunctive-2017							Shadow					
	Δ UB	Gap	Time	n_t	n_f	Gain	Δ UB	Gap	Time	n_t	n_f	Gain	
RCP-50-3	0.00 (0.0)	13.3 (15.3)	2.37 (1.79)	0	0	62.9	0.00 (0.0)	0.01 (0.0)	11.3 (15)	0	0	91.3	
RCP-100-3	0.00 (0.1)	37.4 (51.7)	474 (118)	26	10	64.6	0.08 (0.1)	43.5 (0.7)	453 (125)	39	0	62.4	
RCP-150-3	0.05 (0.1)	40.1 (13.6)	587 (14.2)	74	14	39.7	0.02 (0.0)	42.1 (20)	600 (0.0)	100	0	-	
RCP-50-5	0.00 (0.0)	11.6 (14.3)	1.22 (1.11)	0	0	78.6	0.00 (0.0)	0.00 (0.0)	1.43 (1.0)	0	0	81.8	
RCP-100-5	0.00 (0.0)	36.3 (3.68)	54.1 (61.5)	0	0	35.1	0.00 (0.0)	0.13 (0.1)	186 (163)	0	0	81.2	
RCP-150-5	0.12 (0.0)	42.3 (45.4)	600 (0.0)	100	15	-	0.09 (0.0)	12.3 (1.6)	600 (0.0)	100	0	-	

4.8 Analytical Solution for the Two-Aircraft Conflict Resolution Problem

Based on the results presented in Section 4.7, it is observed that dense instances are feasible even with reduced heading control and speed violations were observed only on RCP instances with 30 or more aircraft. Therefore, it is a reasonable assumption that instances with lower conflict density can be solved without bounds on heading and speed deviation. Considering a two-aircraft conflict configuration, the optimisation problem can be simplified and therefore solved analytically. In this section, an analytical solution for two-aircraft instances is proposed based on the decomposition of the non-convex two-aircraft conflict resolution problem into two convex sub-problems using the first order optimality conditions.

4.8.1 Analytical Problem Definition

Recalling the complex number formulation presented in Section 4.2, the relative motion equations of a pair of aircraft can be rewritten as:

$$v_{ij,x} = \delta_{i,x}\hat{v}_{i,x} - \delta_{i,y}\hat{v}_{i,y} - \delta_{j,x}\hat{v}_{j,x} + \delta_{j,y}\hat{v}_{j,y}, \quad (4.30a)$$

$$v_{ij,y} = \delta_{i,y}\hat{v}_{i,x} + \delta_{i,x}\hat{v}_{i,y} - \delta_{j,y}\hat{v}_{j,x} - \delta_{j,x}\hat{v}_{j,y}, \quad (4.30b)$$

where $v_{i,x}, v_{i,y}, v_{j,x}, v_{j,y}$ are defined as:

$$\hat{v}_{i,x} = \hat{v}_i \cos(\hat{\theta}_i), \quad (4.31a)$$

$$\hat{v}_{i,y} = \hat{v}_i \sin(\hat{\theta}_i), \quad (4.31b)$$

$$\hat{v}_{j,x} = \hat{v}_j \cos(\hat{\theta}_j), \quad (4.31c)$$

$$\hat{v}_{j,y} = \hat{v}_j \sin(\hat{\theta}_j). \quad (4.31d)$$

The objective function for a two-aircraft problem as described in 4.7 can be rewritten as:

$$\min f(\boldsymbol{\delta}) = (1-w)(1-\delta_{i,x})^2 + w\delta_{i,y}^2 + (1-w)(1-\delta_{j,x})^2 + w\delta_{j,y}^2, \quad (4.32)$$

where $\boldsymbol{\delta} = [\delta_{i,x}, \delta_{i,y}, \delta_{j,x}, \delta_{j,y}]^\top$ represents the solution vector containing all decision variables for the two-aircraft problem. As it was discussed in Section 4.7.2, the value adopted for w is 0.5 which assumes equal importance for both speed and heading angle

control. Without loss of generality and to simplify the exposition, this parameter is omitted in this section.

The separation constraints can be rewritten using the vector $\boldsymbol{\delta}$. This can be achieved by replacing Eq. (4.31) into the separation conditions in (3.20)-eq3.21. This results in:

$$h_1(\boldsymbol{\delta}) = a_{i,x}^1 \delta_{i,x} + a_{i,y}^1 \delta_{i,y} + a_{j,x}^1 \delta_{j,x} + a_{j,y}^1 \delta_{j,y} \leq 0, \quad \text{if } z_{ij} = 1, \quad (4.33a)$$

$$h_2(\boldsymbol{\delta}) = a_{i,x}^2 \delta_{i,x} + a_{i,y}^2 \delta_{i,y} + a_{j,x}^2 \delta_{j,x} + a_{j,y}^2 \delta_{j,y} \geq 0, \quad \text{if } z_{ij} = 0, \quad (4.33b)$$

$$h_3(\boldsymbol{\delta}) = a_{i,x}^3 \delta_{i,x} + a_{i,y}^3 \delta_{i,y} + a_{j,x}^3 \delta_{j,x} + a_{j,y}^3 \delta_{j,y} \leq 0, \quad \text{if } z_{ij} = 1, \quad (4.33c)$$

$$h_4(\boldsymbol{\delta}) = a_{i,x}^4 \delta_{i,x} + a_{i,y}^4 \delta_{i,y} + a_{j,x}^4 \delta_{j,x} + a_{j,y}^4 \delta_{j,y} \geq 0, \quad \text{if } z_{ij} = 0, \quad (4.33d)$$

where $a_{i,x}^1, a_{i,y}^1, a_{j,x}^1, a_{j,y}^1, a_{i,x}^2, a_{i,y}^2, a_{j,x}^2, a_{j,y}^2, a_{i,x}^3, a_{i,y}^3, a_{j,x}^3, a_{j,y}^3, a_{i,x}^4, a_{i,y}^4, a_{j,x}^4, a_{j,y}^4$ are constants based on the initial configuration of the two-aircraft problem. Considering that the disjunction represented by variable z divides the non-convex feasible region into two convex feasible regions, the problem can be decomposed into two sub-problems named \mathcal{SP}_0 and \mathcal{SP}_1 :

$$\mathcal{SP}_0 : \begin{cases} \text{Minimise } f(\boldsymbol{\delta}), \\ \text{Subject to:} \\ h_1(\boldsymbol{\delta}) \geq 0, \\ h_3(\boldsymbol{\delta}) \geq 0, \\ \boldsymbol{\delta} \in \mathbb{R}^4. \end{cases} \quad \mathcal{SP}_1 : \begin{cases} \text{Minimise } f(\boldsymbol{\delta}), \\ \text{Subject to:} \\ h_2(\boldsymbol{\delta}) \leq 0, \\ h_4(\boldsymbol{\delta}) \leq 0, \\ \boldsymbol{\delta} \in \mathbb{R}^4. \end{cases}$$

where \mathcal{SP}_0 correspond to the sub-problem created for $z_{ij} = 0$ and \mathcal{SP}_1 for $z_{ij} = 1$. Let \mathcal{R}_0 and \mathcal{R}_1 be denoted as the feasible regions of the sub-problems \mathcal{SP}_0 and \mathcal{SP}_1 , respectively, such as that:

$$\mathcal{R}_0 : \begin{cases} h_1(\boldsymbol{\delta}) \geq 0, \\ h_3(\boldsymbol{\delta}) \geq 0, \\ \boldsymbol{\delta} \in \mathbb{R}^4. \end{cases} \quad \mathcal{R}_1 : \begin{cases} h_2(\boldsymbol{\delta}) \leq 0, \\ h_4(\boldsymbol{\delta}) \leq 0, \\ \boldsymbol{\delta} \in \mathbb{R}^4. \end{cases}$$

4.8.2 Solution of Sub-Problems \mathcal{SP}_0 and \mathcal{SP}_1

Each sub-problem \mathcal{SP}_0 and \mathcal{SP}_1 can be solved individually by observing that the sub-problem is convex and deriving its first-order (KKT) optimality conditions. For the remainder of this section, only sub-problem \mathcal{SP}_1 is addressed. Let $\mathcal{L}(\boldsymbol{\delta})$ be the Lagrangian of \mathcal{SP}_1 :

$$\mathcal{L}(\boldsymbol{\delta}) = f(\boldsymbol{\delta}) + \mu_1 h_1(\boldsymbol{\delta}) + \mu_3 h_3(\boldsymbol{\delta}), \quad (4.34)$$

where $\mu_1 \geq 0$ and $\mu_3 \geq 0$ are the dual variables related to constraint (4.33a) and (4.33b) of the primal problem \mathcal{SP}_1 . Considering the function in Eq. (4.34), the Karush-Kuhn-Tucker (KKT) conditions can be applied. The gradient of the Lagrangian of \mathcal{SP}_1 :

$$\frac{\partial \mathcal{L}(\boldsymbol{\delta})}{\partial \delta_{i,x}} = -2(1 - \delta_{i,x}) + \mu_1 \frac{\partial h_1(\boldsymbol{\delta})}{\partial \delta_{i,x}} + \mu_3 \frac{\partial h_3(\boldsymbol{\delta})}{\partial \delta_{i,x}} = 0, \quad (4.35a)$$

$$\frac{\partial \mathcal{L}(\boldsymbol{\delta})}{\partial \delta_{i,y}} = 2\delta_{i,y} + \mu_1 \frac{\partial h_1(\boldsymbol{\delta})}{\partial \delta_{i,y}} + \mu_3 \frac{\partial h_3(\boldsymbol{\delta})}{\partial \delta_{i,y}} = 0, \quad (4.35b)$$

$$\frac{\partial \mathcal{L}(\boldsymbol{\delta})}{\partial \delta_{j,x}} = -2(1 - \delta_{j,x}) + \mu_1 \frac{\partial h_1(\boldsymbol{\delta})}{\partial \delta_{j,x}} + \mu_3 \frac{\partial h_3(\boldsymbol{\delta})}{\partial \delta_{j,x}} = 0, \quad (4.35c)$$

$$\frac{\partial \mathcal{L}(\boldsymbol{\delta})}{\partial \delta_{j,y}} = 2\delta_{j,y} + \mu_1 \frac{\partial h_1(\boldsymbol{\delta})}{\partial \delta_{j,y}} + \mu_3 \frac{\partial h_3(\boldsymbol{\delta})}{\partial \delta_{j,y}} = 0, \quad (4.35d)$$

where:

$$\begin{aligned} \frac{\partial h_1(\boldsymbol{\delta})}{\partial \delta_{i,x}} &= a_{i,x}^1, & \frac{\partial h_1(\boldsymbol{\delta})}{\partial \delta_{i,y}} &= a_{i,y}^1, \\ \frac{\partial h_1(\boldsymbol{\delta})}{\partial \delta_{j,x}} &= a_{j,x}^1, & \frac{\partial h_1(\boldsymbol{\delta})}{\partial \delta_{j,y}} &= a_{j,y}^1, \\ \frac{\partial h_3(\boldsymbol{\delta})}{\partial \delta_{i,x}} &= a_{i,x}^3, & \frac{\partial h_3(\boldsymbol{\delta})}{\partial \delta_{i,y}} &= a_{i,y}^3, \\ \frac{\partial h_3(\boldsymbol{\delta})}{\partial \delta_{j,x}} &= a_{j,x}^3, & \frac{\partial h_3(\boldsymbol{\delta})}{\partial \delta_{j,y}} &= a_{j,y}^3. \end{aligned}$$

In addition the primal feasibility constraints are carried over and complementary slackness conditions are required, such as that:

$$\mu_1 h_1(\boldsymbol{\delta}) = 0, \quad (4.37a)$$

$$\mu_3 h_3(\boldsymbol{\delta}) = 0. \quad (4.37b)$$

The conditions in Eq. (4.37) allows four different cases. Let $\boldsymbol{\delta}_k^*$ be the optimal solution for case k .

- Case I: If $h_1(\boldsymbol{\delta}) > 0$ and $h_3(\boldsymbol{\delta}) > 0$, then $\mu_1 = \mu_3 = 0$, which gives:

$$\boldsymbol{\delta}_1^1 = [1, 0, 1, 0] \quad (4.38)$$

- Case II: If $h_1(\boldsymbol{\delta}) > 0$ and $\mu_3 > 0$, then $\mu_1 = 0$ and $h_3(\boldsymbol{\delta}) = 0$. This results in:

$$\frac{\partial \mathcal{L}(\boldsymbol{\delta})}{\partial \delta_{i,x}} = -2(1 - \delta_{i,x}) + \mu_3 a_{i,x}^3 = 0, \quad (4.39a)$$

$$\frac{\partial \mathcal{L}(\boldsymbol{\delta})}{\partial \delta_{i,y}} = 2\delta_{i,y} + \mu_3 a_{i,y}^3 = 0, \quad (4.39b)$$

$$\frac{\partial \mathcal{L}(\boldsymbol{\delta})}{\partial \delta_{j,x}} = -2(1 - \delta_{j,x}) + \mu_3 a_{j,x}^3 = 0, \quad (4.39c)$$

$$\frac{\partial \mathcal{L}(\boldsymbol{\delta})}{\partial \delta_{j,y}} = 2\delta_{j,y} + \mu_3 a_{j,y}^3 = 0, \quad (4.39d)$$

this allows to express all the primal variables in terms of the dual variables:

$$\boldsymbol{\delta}_2^1 = \left[1 - \frac{\mu_3}{2} a_{i,x}^3, -\frac{\mu_3}{2} a_{i,y}^3, 1 - \frac{\mu_3}{2} a_{j,x}^3, -\frac{\mu_3}{2} a_{j,y}^3 \right] \quad (4.40)$$

Replacing those values into $h_3(\boldsymbol{\delta}) = 0$ results in a linear equation in function of μ_3 , that can be solved as:

$$\mu_3 = \frac{2(a_{i,x}^3 + a_{j,x}^3)}{(a_{i,x}^3)^2 + (a_{i,y}^3)^2 + (a_{j,x}^3)^2 + (a_{j,y}^3)^2}, \quad (4.41)$$

which is a constant based on the initial configuration of the pair of aircraft. Replacing such terms into Eq. (4.40), the second set of possible solutions is obtained.

- Case III: If $h_3(\boldsymbol{\delta}) > 0$ and $\mu_1 > 0$, then $\mu_3 = 0$ and $h_1(\boldsymbol{\delta}) = 0$. This results in:

$$\frac{\partial \mathcal{L}(\boldsymbol{\delta})}{\partial \delta_{i,x}} = -2(1 - \delta_{i,x}) + \mu_1 a_{i,x}^1 = 0, \quad (4.42a)$$

$$\frac{\partial \mathcal{L}(\boldsymbol{\delta})}{\partial \delta_{i,y}} = 2\delta_{i,y} + \mu_1 a_{i,y}^1 = 0, \quad (4.42b)$$

$$\frac{\partial \mathcal{L}(\boldsymbol{\delta})}{\partial \delta_{j,x}} = -2(1 - \delta_{j,x}) + \mu_1 a_{j,x}^1 = 0, \quad (4.42c)$$

$$\frac{\partial \mathcal{L}(\boldsymbol{\delta})}{\partial \delta_{j,y}} = 2\delta_{j,y} + \mu_1 a_{j,y}^1 = 0, \quad (4.42d)$$

this allows to express all the primal variables in terms of the dual variables:

$$\boldsymbol{\delta}_3^1 = \left[1 - \frac{\mu_1}{2} a_{i,x}^1, -\frac{\mu_1}{2} a_{i,y}^1, 1 - \frac{\mu_1}{2} a_{j,x}^1, -\frac{\mu_1}{2} a_{j,y}^1 \right] \quad (4.43)$$

Replacing those values into $h_1(\boldsymbol{\delta}) = 0$ results in a linear equation in function of μ_1 , that can be solved as:

$$\mu_1 = \frac{2(a_{i,x}^1 + a_{j,x}^1)}{(a_{i,x}^1)^2 + (a_{i,y}^1)^2 + (a_{i,x}^1)^2 + (a_{j,x}^1)^2}, \quad (4.44)$$

which is a constant based on the initial configuration of the pair of aircraft. Replacing such terms into Eq. (4.43), the third set of possible solutions is obtained.

- Case IV: If $\mu_3 > 0$ and $\mu_3 > 0$, then $h_3(\boldsymbol{\delta}) = 0$ and $h_3(\boldsymbol{\delta}) = 0$. This results in the same equations as in 4.35 which allows all the primal variables to be expressed in terms of both dual variables:

$$\boldsymbol{\delta}_4^1 = \left[1 - \frac{\mu_1}{2} a_{i,x}^1 - \frac{\mu_3}{2} a_{i,x}^3, -\frac{\mu_1}{2} a_{i,y}^1 - \frac{\mu_3}{2} a_{i,y}^3, 1 - \frac{\mu_1}{2} a_{j,x}^1 - \frac{\mu_3}{2} a_{j,x}^3, -\frac{\mu_1}{2} a_{j,y}^1 - \frac{\mu_3}{2} a_{j,y}^3 \right] \quad (4.45)$$

Replacing those expressions into the equations $h_1(\boldsymbol{\delta}) = 0$ and $h_2(\boldsymbol{\delta}) = 0$:

$$\begin{aligned} h_1(\boldsymbol{\delta}) = & a_{i,x}^1 \left(1 - \frac{\mu_1}{2} a_{i,x}^1 - \frac{\mu_3}{2} a_{i,x}^3 \right) + a_{i,y}^1 \left(-\frac{\mu_1}{2} a_{i,y}^1 - \frac{\mu_3}{2} a_{i,y}^3 \right) + \\ & a_{j,x}^1 \left(1 - \frac{\mu_1}{2} a_{j,x}^3 - \frac{\mu_3}{2} a_{j,x}^3 \right) + a_{j,y}^1 \left(-\frac{\mu_1}{2} a_{j,y}^3 - \frac{\mu_2}{2} a_{j,y}^3 \right) = 0, \end{aligned} \quad (4.46)$$

$$\begin{aligned} h_3(\boldsymbol{\delta}) = & a_{i,x}^3 \left(1 - \frac{\mu_1}{2} a_{i,x}^1 - \frac{\mu_3}{2} a_{i,x}^3 + a_{i,y}^3 \left(-\frac{\mu_1}{2} a_{i,y}^1 - \frac{\mu_3}{2} a_{i,y}^3 \right) \right) + \\ & a_{j,x}^3 \left(1 - \frac{\mu_1}{2} a_{j,x}^3 - \frac{\mu_3}{2} a_{j,x}^3 + a_{j,y}^3 \left(-\frac{\mu_1}{2} a_{j,y}^3 - \frac{\mu_2}{2} a_{j,y}^3 \right) \right) = 0. \end{aligned} \quad (4.47)$$

By solving Eq. (4.46) and (4.47) and replacing in Eq. (4.45), analytical expressions for μ_1 and μ_3 can be obtained.

With all those four set of solutions, an analytical solution for \mathcal{SP}_1 can be obtained. Let Σ_0 and Σ_1 be the set of of first-order optimality solutions associated with \mathcal{SP}_0 and \mathcal{SP}_1 , respectively:

$$\begin{aligned} \Sigma_0 &= \{\boldsymbol{\delta}_1^0, \boldsymbol{\delta}_2^0, \boldsymbol{\delta}_3^0, \boldsymbol{\delta}_4^0\}, \\ \Sigma_1 &= \{\boldsymbol{\delta}_1^1, \boldsymbol{\delta}_2^1, \boldsymbol{\delta}_3^1, \boldsymbol{\delta}_4^1\}, \end{aligned}$$

hence, the solution of the two-aircraft conflict resolution problem is:

$$\delta^* \in \operatorname{argmin}\{f(\delta) : \delta \in \{\Sigma_0 \cap \mathcal{R}_0\} \cup \{\Sigma_1 \cap \mathcal{R}_1\}\} \quad (4.49)$$

The set of four solutions can be visualized in the $(v_{ij,x}, v_{ij,y})$ -plane as a set of four points as highlighted in Figure 4.3. The point in orange corresponds to Case I and this solution corresponds to a no-deviation solution. Therefore, it can be concluded that for any two-aircraft conflict that can be solved with that Case I, it corresponds to a pair of aircraft in the set \mathcal{P}_F as described in Figure 3.1a. The points in green and in blue correspond to Case II and Case III, respectively. For Case III, it corresponds to the activation of $h_1(\delta)$ while $h_3(\delta) = 0$. Recalling that $h_3(\delta)$ corresponds to line R_2 as described in Section 3.3 and Figure 3.2, the point in red will always be in R_2 . Using the same reasoning, the point in blue will always be in Eq. N . The point coloured in black corresponds to Case IV, where both $h_1(\delta)$ and $h_3(\delta) = 0$. Therefore the intersection of Eq. N with R_2 . For Case II, III and IV, there is not correspondence of which each set (PF , PI and PS) that they can be without considering speed and heading angle bounds.

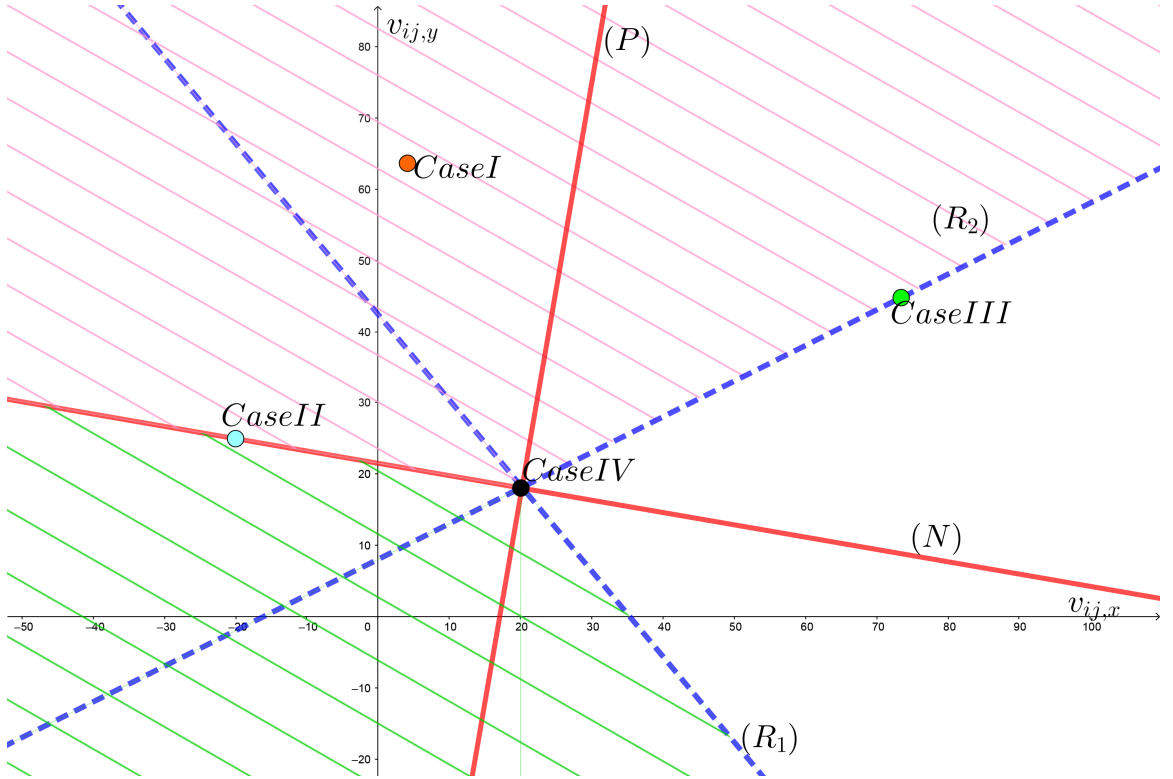


Figure 4.3: Four candidate solution obtained via the analytical solutions. The point in orange represents Case I, in blue Case II, in green Case III and in black Case IV.

4.8.3 Discussion

In order to test the validity of such approach, a set of 8 different configurations of two-aircraft conflict (see Figure 4.4) were solved using the approach described here and benchmarked against the Non-Convex Model present in Chapter 3.

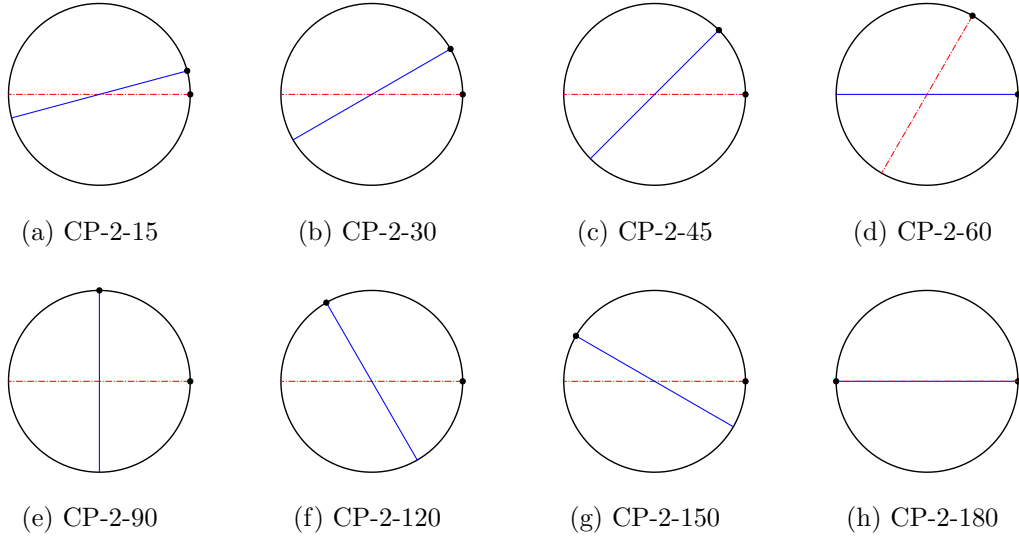


Figure 4.4: Extra instances representing different configuration of two-aircraft conflict

Those instances were used to benchmark the analytical formulation. The results reveal that both methods provide the same solution for all cases tested. This solidifies the efficiency of these analytical expressions and shows that those conflicts can be automatically solved without the assistance of any optimisation. At the same time, it shows that for some instances while it might takes a few seconds (even though very quick), those conflicts do not required any sophisticated software to solve it, because efficient solutions can be achieved only by analysing the initial configuration of the aircraft involved. Lastly, it shows that there is some potential in applying those analytical expressions to larger sets of aircraft.

The lack of control over the bounds of the decision variables is a considerable issue which hinder the utilisation of such expressions for denser instances with multiple aircraft. However, each pair of aircraft cannot be classified as "conflict-free", "infeasible" or "separable" without the bounds. In order to do that, the conflict region defined by \mathcal{B}_{ij} could be added to Model 4.49 to impose the speed bounds. Unfortunately, the region defined by \mathcal{B}_{ij} is based on the $v_{ij,x}, v_{ij,y}$ and do not prevent speed violations. However, the speed bound constraints in the disjunctive formulation are non-convex

quadratic terms and by utilising such terms, first-order optimality conditions are not sufficient anymore.

Even though the process of obtaining these expressions can be arduous, it is simply composed by operations using the initial conditions of the pair of aircraft observed. At the same time, this provides a closed-form solution of a two-aircraft conflict. It is important to notice that for such small conflicts, it is highly unlikely that the optimal solution violates bound constraints on speed or heading deviations. That is the reason why constraints related to such aspects can be removed without larger consequences. However, conflicts involving more aircraft might be initially solved via solutions which would require violations in speed and heading angle conditions. In addition, this expression represents a novel attempt in solving the two-aircraft conflict resolution problem without any form of optimisation, requiring simply pre-processing calculations. This can be a cornerstone into developing a formulation for the ACRP that does not require non-convex or non-linear constraints and intense optimisation.

4.9 Conclusion

The findings are summarised in Section 4.9.1 and discuss future research directions in Section 4.9.2.

4.9.1 Summary of Findings

A new mixed-integer formulations and exact solution methods for aircraft conflict resolution problems (ACRP) are proposed. First, it is considered the 2D ACRP with continuous speed and heading control manoeuvres and proposed compact disjunctive separation conditions. The proposed disjunctive separation conditions are linear with regards to aircraft relative velocity variables and only require a single binary variable per pair of aircraft. It has been formally shown that the proposed disjunctive linear separation conditions fully characterise the set of conflict-free aircraft trajectories. A simple pre-processing algorithm is introduced to identify aircraft pairs which are conflict-free or non-separable for any combination of controls, which may help in reducing the size of ACRPs by omitting conflict-free pairs. It is built on and extended the complex number formulation for the ACRP introduced by Rey and Hijazi (2017) by augmenting its objective function with a preference weight to balance the trade-off between speed and heading deviations. The resulting formulation is a non-convex mixed-integer program. This 2D formulation is extended to the context of altitude control by flight level (FL) change and a lexicographic optimisation is proposed to

solve the 2D+FL ACRP which aims to minimise the number of FL changes in priority and resolve outstanding conflicts by 2D trajectory control.

A novel exact solution algorithm is proposed to solve the non-convex 2D and 2D+FL ACRPs. The proposed algorithms refine the convex relaxations introduced by Rey and Hijazi (2017). For the 2D problem, the non-convex formulations are first relaxed to mixed-integer quadratic programs (MIQP) which solution may violate the speed control constraint. If such violations occur, convex quadratic constraints are added together with a constraint generation algorithm that iteratively refines an outer piecewise linear approximation of the speed control constraint by solving a sequence of mixed-integer quadratically constrained programs (MIQCP). The 2D+FL lexicographic optimisation problem is solved by decomposing the non-convex problem into a flight assignment problem and a series of FL-based 2D problems. The proposed flight assignment formulation is based on a reformulation of the FL separation constraint which requires an exponential number of constraints and is embedded into an iterative approach to generate altitude separation constraints as needed.

The performance of the proposed mixed-integer formulations and algorithms was tested on a total of 2072 benchmarking instances. These instances include four types of ACRPs with up to 60 aircraft per instance for 2D problems and 150 aircraft per instance for 2D+FL problems. The performance of the proposed solution algorithms highlights the scalability of the approach compared to existing methods in the literature. Further, it is concluded that the combination of the pre-processing algorithm with the MIQP convex relaxation is sufficient to solve FP and GP instances with up to 60 aircraft, and most RCP instances with up to 30 aircraft. It is also stated that the number of MIQCP iterations remains low on average when solving larger problems. For 2D+FL lexicographic optimisation problems, it is perceived that the pre-processing procedure generates enough altitude separation constraints to solve dense instances with an average of 50 aircraft per FL.

In the numerical experiments, the performance of the proposed method is also compared with two benchmarks based on state-of-the-art approaches for the ACRP. The proposed method is compared with the method proposed by Rey and Hijazi (2017) which is based on the same disjunctive linear separation conditions but differ in the solution algorithm (*Disjunctive-2017*). In addition, the proposed method is compared with an approach using the same algorithm but based the classical shadow separation conditions (*Shadow*). Our results reveal that the proposed method (*Disjunctive*) is able to solve 87.8% of the benchmarking instances compared to 70.4% using *Disjunctive-2017* and to 69.7% using *Shadow*. Upon examining all instances

that were solved by all three methods, it is observed that *Disjunctive* is systematically faster than *Disjunctive-2017* and *Shadow*, and an decreasing average in computing time of 81.5% is reported in comparison to *Disjunctive-2017* and 86.6% in comparison to *Shadow*.

4.9.2 Future Research and Perspectives

The proposed approaches for ACRPs rely on several assumptions which may be limiting in practice. One of the modelling assumptions at the core of the proposed mixed-integer formulations is the assumption of uniform motion laws, which translates into infinite acceleration and deceleration rates. While such an assumption may be plausible for constrained aircraft speed control, further research is needed to assess the practicality of this assumption when considering varying types of aircraft or different airspace environments, e.g. urban air mobility.

The usage of heading deviations for conflict resolution also raises concerns regarding aircraft trajectory recovery. It is well-acknowledged that resolving conflicts does not guarantee conflict-free recovery trajectories. Alonso-Ayuso et al. (2014) have proposed an efficient method to calculate the earliest time of recovery for aircraft but this approach does not ensure the existence of conflict-free recovery trajectories. Dias et al. (2020) presented a two-step algorithm for the aircraft conflict resolution with trajectory recovery which decomposes the collision avoidance procedure from the trajectory recovery component but the approach remains sub-optimal, and further research is needed to find global optimal solutions.

Future research may also explore asynchronous conflict resolution problems where aircraft do not require to be coordinated. Further, more efforts to incorporate trajectory prediction uncertainty in ACRPs, which may be caused by adverse weather or disrupted navigation systems, is needed to develop more robust conflict resolution formulations.

The coordination of aircraft conflict resolution manoeuvres also presents considerable operational challenges. As in the vast majority of exact methods for the ACRP, the proposed approach assumes that all manoeuvres start at the same time, which may not be always feasible in practice. Hence, there is a need to develop exact methods that are able to account for asynchronous conflict resolution manoeuvres. Future research is also needed to incorporate trajectory prediction uncertainty, which may be caused by adverse weather or disruption of navigation systems, within the proposed mixed-integer formulations in the aim to develop more robust conflict resolution formulations.

Chapter 5

Robust aircraft conflict resolution under trajectory prediction uncertainty

In this chapter, a robust optimisation approach is presented to solve the aircraft conflict resolution under uncertainty. Considering the weather and measurements errors as source of the randomness, the velocity component of each aircraft is adapted to incorporate the random effect caused by uncertainty. Starting off in Section 5.1, where the robust problem and the uncertainty model used are introduced, followed the robust counterpart formulation and the solution method. In Section 5.2, the experiment design used to test such algorithm and to benchmark against the deterministic counterpart is discussed and further, the analysis based on different size of uncertainty sets and different level of robustness is presented. At last, the findings are summarised in Section 5.3. This formulation presented in this chapter was submitted to the journal *Computer & Operations Research* (Dias and Rey, 2020).

5.1 Robust Aircraft Conflict Resolution Problem

Based on the formulation of the ACRP formulation presented in chapter 3, it is clear that those formulations do not account for interference caused by random components. Those elements are very relevant to ATC given that weather events as such as fog and rain as well as measurements can caused major alterations on flight patterns, delays and impairment to flight's safety. Therefore, it is imperative that such circumstances are handled carefully and taking into account in current formulations. To incorporate and properly solve the ACRP taking into account those problems, stochastic and robust optimisation are viable alternative. The first requires prior

knowledge of how those random events will impact the model and they are modelled as discrete probabilistic scenarios while for the latter, the range of unknown scenarios is model as a continuous set where little to nothing is known about the impact.

In this section, formulations for the robust aircraft conflict resolution problem are introduced. At first, the definition of the uncertainty model is presented followed by how it can be incorporated within the ACRP. Then, a tractable robust counterpart formulation for the robust ACRP is proposed.

5.1.1 Uncertainty Model

Assuming that each aircraft has a source of randomness and this affects its current velocity and position. Let $\epsilon_i = [\epsilon_{i,x}, \epsilon_{i,y}]^\top$ be a vector of random variables representing the uncertainty on the velocity components of aircraft $i \in \mathcal{A}$. Using this vector of random variables, aircraft-based uncertainty sets can be defined as:

Definition 4 (Uncertainty Set of Aircraft $i \in \mathcal{A}$). *The uncertainty set of aircraft $i \in \mathcal{A}$, is defined as:*

$$\mathcal{U}_i \equiv \{\epsilon_i \in \mathbb{R}^2 \mid -\bar{\epsilon}_{i,x} \leq \epsilon_{i,x} \leq \bar{\epsilon}_{i,x}, -\bar{\epsilon}_{i,y} \leq \epsilon_{i,y} \leq \bar{\epsilon}_{i,y}\}, \quad (5.1)$$

where $\bar{\epsilon}_{i,x} \geq 0$ and $\bar{\epsilon}_{i,y} \geq 0$ represent the maximum perturbation on the velocity components $v_{i,x}$ and $v_{i,y}$, respectively, of aircraft i .

Denoting $[\tilde{v}_{i,x}, \tilde{v}_{i,y}]^\top$ as the vector of random aircraft velocity components where the random variables $\tilde{v}_{i,x}$ and $\tilde{v}_{i,y}$ take values in $\tilde{v}_{i,x} \in [-v_{i,x}(1 + \bar{\epsilon}_{i,x}), v_{i,x}(1 + \bar{\epsilon}_{i,x})]$ and $\tilde{v}_{i,y} \in [-v_{i,y}(1 + \bar{\epsilon}_{i,y}), v_{i,y}(1 + \bar{\epsilon}_{i,y})]$, respectively. Accordingly, for each pair of aircraft $(i, j) \in \mathcal{P}$, the random relative velocity components $\tilde{v}_{ij,x}$ and $\tilde{v}_{ij,y}$ are:

$$\tilde{v}_{ij,x} = v_{i,x}(1 + \epsilon_{i,x}) - v_{j,x}(1 + \epsilon_{j,x}) = v_{ij,x} + v_{i,x}\epsilon_{i,x} - v_{j,x}\epsilon_{j,x}, \quad (5.2a)$$

$$\tilde{v}_{ij,y} = v_{i,y}(1 + \epsilon_{i,y}) - v_{j,y}(1 + \epsilon_{j,y}) = v_{ij,y} + v_{i,y}\epsilon_{i,y} - v_{j,y}\epsilon_{j,y}. \quad (5.2b)$$

Let $\underline{\tilde{v}}_{ij,x}, \bar{\tilde{v}}_{ij,x}$ and $\underline{\tilde{v}}_{ij,y}, \bar{\tilde{v}}_{ij,y}$ be the lower and upper bounds for $\tilde{v}_{ij,x}$ and $\tilde{v}_{ij,y}$, respectively. These bounds can be determined using Eq. (5.2) and the bounds on speed and heading control provided in Eqs. (3.8) and (3.9). The derived bounds on the random relative velocity components can be used to define the random relative velocity box which characterises all possible trajectories for the pair $(i, j) \in \mathcal{P}$ under uncertainty.

Definition 5 (Random relative velocity box). Consider a pair of aircraft $(i, j) \in \mathcal{P}$. Let \mathcal{U}_i and \mathcal{U}_j be the uncertainty sets of aircraft i and j , respectively. Let $\tilde{\mathcal{B}}_{ij}(\mathcal{U}_i, \mathcal{U}_j)$ be the parametric subset of \mathbb{R}^2 defined as

$$\tilde{\mathcal{B}}_{ij}(\mathcal{U}_i, \mathcal{U}_j) \equiv \{(\tilde{v}_{ij,x}, \tilde{v}_{ij,y}) \in \mathbb{R}^2 : \tilde{v}_{ij,x} \leq \tilde{v}_{ij,x} \leq \bar{v}_{ij,x}, \tilde{v}_{ij,y} \leq \tilde{v}_{ij,y} \leq \bar{v}_{ij,y}\}. \quad (5.3)$$

$\tilde{\mathcal{B}}_{ij}(\mathcal{U}_i, \mathcal{U}_j)$ is the random relative velocity box of $(i, j) \in \mathcal{P}$ under the uncertainty sets \mathcal{U}_i and \mathcal{U}_j .

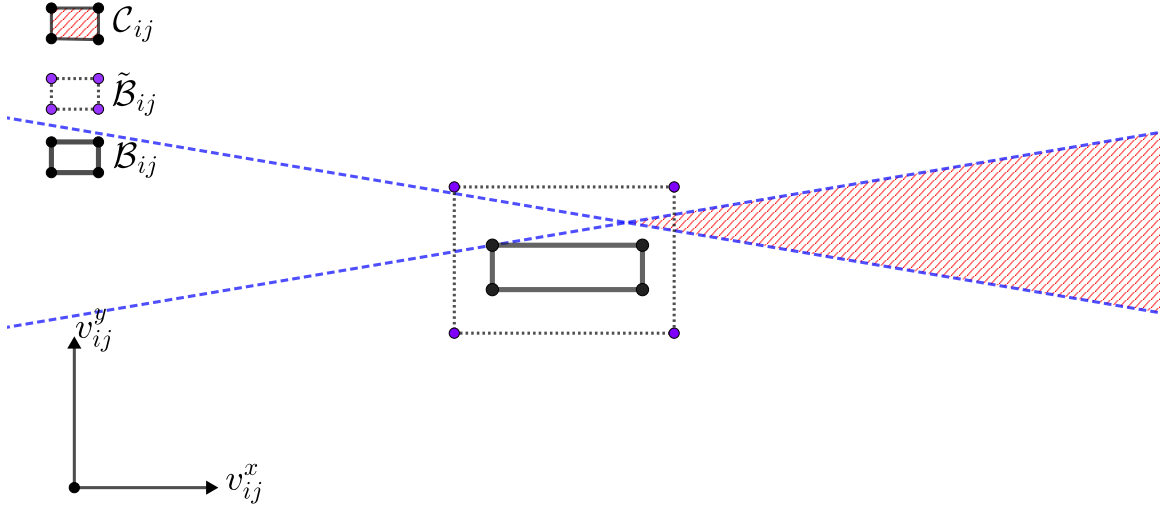


Figure 5.1: Illustration of a two-aircraft conflict in the plane $\{(v_{ij,x}, v_{ij,y}) \in \mathbb{R}^2\}$. The inner box with black lines corresponds to the velocity bounds \mathcal{B}_{ij} in the deterministic scenario while the box with purple dots $\tilde{\mathcal{B}}_{ij}(\mathcal{U}_i, \mathcal{U}_j)$ is the random relative velocity box. The region is hashed in red corresponds to the conflict region \mathcal{C}_{ij} . If the uncertainty sets \mathcal{U}_i and \mathcal{U}_j of aircraft i and j are empty, i.e. aircraft trajectories are deterministic, then aircraft i and j are conflict-free. In turn, if the uncertainty sets \mathcal{U}_i and \mathcal{U}_j are such that the random relative velocity $\tilde{\mathcal{B}}_{ij}$ intersects with the conflict region \mathcal{C}_{ij} , then there exists a risk of conflict.

The random relative velocity box is illustrated in Figure 5.1 for a two-aircraft conflict. To ensure that a pair of aircraft $(i, j) \in \mathcal{P}$ is separated for any realisation of the random variables $\epsilon_i \in \mathcal{U}_i$ and $\epsilon_j \in \mathcal{U}_j$, (3.20) and (3.21) can be redefined using the random velocity variables $\tilde{v}_{ij,x}$ and $\tilde{v}_{ij,y}$:

$$\tilde{v}_{ij,y}\hat{x}_{ij} - \tilde{v}_{ij,x}\hat{y}_{ij} \leq 0, \quad \text{if } z_{ij} = 1, \quad \forall (i, j) \in \mathcal{P}, \quad (N_1)$$

$$\tilde{v}_{ij,y}\hat{x}_{ij} - \tilde{v}_{ij,x}\hat{y}_{ij} \geq 0, \quad \text{if } z_{ij} = 0, \quad \forall (i, j) \in \mathcal{P}, \quad (N_0)$$

$$\tilde{v}_{ij,y}\gamma_{ij}^l - \tilde{v}_{ij,x}\phi_{ij}^l \leq 0, \quad \text{if } z_{ij} = 1, \quad \forall (i, j) \in \mathcal{P}, \quad (S_1)$$

$$\tilde{v}_{ij,y}\gamma_{ij}^u - \tilde{v}_{ij,x}\phi_{ij}^u \geq 0, \quad \text{if } z_{ij} = 0, \quad \forall (i, j) \in \mathcal{P}. \quad (S_0)$$

To find robust aircraft trajectories under uncertainty sets \mathcal{U}_i and \mathcal{U}_j , it is required that the pairwise separation constraints N_1 , N_0 , S_1 and S_0 hold for any $(\tilde{v}_{ij,x}, \tilde{v}_{ij,y}) \in \tilde{\mathcal{B}}_{ij}(\mathcal{U}_i, \mathcal{U}_j)$. Next, using state-of-the-art approaches in robust optimisation are used to integrate these constraints into a robust counterpart formulation.

5.1.2 Robust Counterpart Formulation

The state-of-art approaches to handle models with uncertainty sets and robustness are highlighted by Gorissen et al. (2015) where the authors describe different uncertainty sets and how to apply them directly into this formulation. This strategy provides a general framework based on the definition of the dual problem and the consequent equivalence between dual and primal. On the other hand, Bertsimas and Sim (2004), which is also based on primal-dual equivalence, proposed an alternative approach that allows controlling the robustness level via a single parameter.

The constraints N_1 , N_0 , S_1 and S_0 are function of the random variables $\tilde{v}_{ij,x}$ and $\tilde{v}_{ij,y}$. Using the approach of Bertsimas and Sim (2004) these robust separation constraints can be reformulated as integer-linear constraints with regards to deterministic relative velocity variables $v_{ij,x}$ and $v_{ij,y}$. The constraints N_1 , N_0 , S_1 and S_0 are of the form $a\tilde{v}_{ij,x} + b\tilde{v}_{ij,y} \leq 0$ (omitting the disjunction), and can be rearranged by separating deterministic and random elements as follows:

$$a(v_{i,x} - v_{j,x}) - b(v_{i,y} - v_{j,y}) + av_{i,x}\epsilon_{i,x} - av_{j,x}\epsilon_{j,x} - bv_{i,y}\epsilon_{i,y} + bv_{j,y}\epsilon_{j,y} \leq 0. \quad (5.5)$$

Introducing $\nu_{i,x} \geq 0$ and $\nu_{i,y} \geq 0$ as new variables for each $i \in \mathcal{A}$ through constraints (5.6), artificial bounds on aircraft velocity components $v_{i,x}$ and $v_{i,y}$ can be imposed as:

$$-\nu_{i,x} \leq v_{i,x} \leq \nu_{i,x}, \quad \forall i \in \mathcal{A}, \quad (5.6a)$$

$$-\nu_{i,y} \leq v_{i,y} \leq \nu_{i,y}, \quad \forall i \in \mathcal{A}. \quad (5.6b)$$

Let $\mathcal{RS} \equiv \{N_1, N_0, S_1, S_0\}$ be the set of robust separation constraints. Further, let $\alpha_k = 1$ for if $k = N_1$ or $k = S_1$, and let $\alpha_k = 0$ for if $k = N_0$ or $k = S_0$. Let Γ be a real parameter that takes values in the range $[0,4]$, where the upper bound is given by the number of decision variables in constraint (5.5). The parameter Γ determines the level of robustness for each robust separation constraint. To link the level of robustness Γ with each robust separation constraint $k \in \mathcal{RS}$ and each aircraft pair $(i, j) \in \mathcal{P}$, real decision variables $\psi_{ij}^k \geq 0$ are introduced. Further, each constraint

of the form (5.5) involves four decision variables, hence for each constraint $k \in \mathcal{RS}$ and $(i, j) \in \mathcal{P}$, associated variables $\rho_{ij,x}^{l,k} \geq 0$ and $\rho_{ij,y}^{l,k} \geq 0$ for $l \in \{i, j\}$ are also introduced. These artificial variables reflect how the level of robustness affects each velocity variable in 5.5 individually. The following constraints link variables ψ_{ij}^k , $\rho_{ij,x}^{l,k}$ and $\rho_{ij,y}^{l,k}$ with ν_i^x and ν_j^x :

$$\psi_{ij}^k + \rho_{ij,x}^{l,k} \geq \nu_{i,x} \bar{\epsilon}_{i,x}, \quad \text{if } z_{ij} = \alpha_k, \quad \forall (i, j) \in \mathcal{P}, \forall l \in \{i, j\}, \forall k \in \mathcal{RS}, \quad (5.7a)$$

$$\psi_{ij}^k + \rho_{ij,y}^{l,k} \geq \nu_{i,y} \bar{\epsilon}_{i,y}, \quad \text{if } z_{ij} = \alpha_k, \quad \forall (i, j) \in \mathcal{P}, \forall l \in \{i, j\}, \forall k \in \mathcal{RS}. \quad (5.7b)$$

Constraints of the form (5.5) can then be rewritten as:

$$a(v_{i,x} - v_{j,x}) - b(v_{i,y} - v_{j,y}) + \psi_{ij}^k \Gamma + \sum_{l \in \{i, j\}} (\rho_{ij,x}^{l,k} + \rho_{ij,y}^{l,k}) \leq 0, \quad \text{if } z_{ij} = \alpha_k, \forall (i, j) \in \mathcal{P}, \forall k \in \mathcal{RS}. \quad (5.8)$$

Combining the above constraints and artificial variables, the following integer-linear robust counterpart formulation is obtained.

Proposition 5. *The set of robust separation constraints $\mathcal{RS} = \{N_1, N_0, S_1, S_0\}$ can be represented by the following set of integer-linear constraints and real variables:*

$$\begin{aligned} & a(v_{i,x} - v_{j,x}) - b(v_{i,y} - v_{j,y}) \\ & + \psi_{ij}^k \Gamma + \sum_{l \in \{i, j\}} (\rho_{ij,x}^{l,k} + \rho_{ij,y}^{l,k}) \leq 0, \quad \text{if } z_{ij} = \alpha_k, \quad \forall (i, j) \in \mathcal{P}, \forall k \in \mathcal{RS}, \\ & \psi_{ij}^k + \rho_{ij,x}^{l,k} \geq \nu_{i,x} \bar{\epsilon}_{i,x}, \quad \text{if } z_{ij} = \alpha_k, \quad \forall (i, j) \in \mathcal{P}, \forall l \in \{i, j\}, \forall k \in \mathcal{RS}, \\ & \psi_{ij}^k + \rho_{ij,y}^{l,k} \geq \nu_{i,y} \bar{\epsilon}_{i,y}, \quad \text{if } z_{ij} = \alpha_k, \quad \forall (i, j) \in \mathcal{P}, \forall l \in \{i, j\}, \forall k \in \mathcal{RS}, \\ & \rho_{ij,x}^{l,k}, \rho_{ij,y}^{l,k} \geq 0, \quad \text{if } z_{ij} = \alpha_k, \quad \forall (i, j) \in \mathcal{P}, \forall l \in \{i, j\}, \forall k \in \mathcal{RS}, \\ & \psi_{ij}^k \geq 0, \quad \text{if } z_{ij} = \alpha_k, \quad \forall (i, j) \in \mathcal{P}, \forall k \in \mathcal{RS}, \\ & -\nu_{i,x} \leq v_{i,x} \leq \nu_{i,x}, \quad \forall i \in \mathcal{A}, \\ & -\nu_{i,y} \leq v_{i,y} \leq \nu_{i,y}, \quad \forall i \in \mathcal{A}, \\ & \nu_{i,x}, \nu_{i,y} \geq 0, \quad \forall i \in \mathcal{A}. \end{aligned}$$

The proof of Proposition 5 follows from Theorem 1 of Bertsimas and Sim (2004). The robust counterpart formulation of the ACRP is summarised below.

Model 9. *Robust Counterpart Formulation of the ACRP*

$$\text{Minimise} \quad \sum_{i \in \mathcal{A}} (1 - w)(1 - q_i)^2 + w\theta_i^2,$$

Subject to:

$$\begin{aligned}
v_{ij,x} &= q_i \widehat{v}_i \cos(\widehat{\theta}_i + \theta_i) - q_j \widehat{v}_j \cos(\widehat{\theta}_j + \theta_j) & \forall (i, j) \in \mathcal{P}, \\
v_{ij,y} &= q_i \widehat{v}_i \sin(\widehat{\theta}_i + \theta_i) - q_j \widehat{v}_j \sin(\widehat{\theta}_j + \theta_j) & \forall (i, j) \in \mathcal{P}, \\
a(v_{i,x} - v_{j,x}) - b(v_{i,y} - v_{j,y}) \\
&+ \psi_{ij}^k \Gamma + \sum_{l \in \{i,j\}} (\rho_{ij,x}^{l,k} + \rho_{ij,y}^{l,k}) \leq 0, & \text{if } z_{ij} = \alpha_k, \quad \forall (i, j) \in \mathcal{P}, \forall k \in \mathcal{RS}, \\
\psi_{ij}^k + \rho_{ij,x}^{l,k} &\geq \nu_{i,x} \bar{\epsilon}_{i,x}, & \text{if } z_{ij} = \alpha_k, \quad \forall (i, j) \in \mathcal{P}, \forall l \in \{i, j\}, \forall k \in \mathcal{RS}, \\
\psi_{ij}^k + \rho_{ij,y}^{l,k} &\geq \nu_{i,y} \bar{\epsilon}_{i,y}, & \text{if } z_{ij} = \alpha_k, \quad \forall (i, j) \in \mathcal{P}, \forall l \in \{i, j\}, \forall k \in \mathcal{RS}, \\
\rho_{ij,x}^{l,k}, \rho_{ij,y}^{l,k} &\geq 0, & \text{if } z_{ij} = \alpha_k, \quad \forall (i, j) \in \mathcal{P}, \forall l \in \{i, j\}, \forall k \in \mathcal{RS}, \\
\psi_{ij}^k &\geq 0, & \text{if } z_{ij} = \alpha_k, \quad \forall (i, j) \in \mathcal{P}, \forall k \in \mathcal{RS}, \\
- \nu_{i,x} &\leq v_{i,x} \leq \nu_{i,x}, & \forall i \in \mathcal{A}, \\
- \nu_{i,y} &\leq v_{i,y} \leq \nu_{i,y}, & \forall i \in \mathcal{A}, \\
\nu_{i,x}, \nu_{i,y} &\geq 0, & \forall i \in \mathcal{A}, \\
\underline{q}_i &\leq q_i \leq \bar{q}_i, & \forall i \in \mathcal{A}, \\
\underline{\theta}_i &\leq \theta_i \leq \bar{\theta}_i, & \forall i \in \mathcal{A}, \\
v_{ij,x}, v_{ij,y} &\in \mathcal{B}_{ij}, & \forall (i, j) \in \mathcal{P}, \\
z_{ij} &\in \{0, 1\}, & \forall (i, j) \in \mathcal{P}, \\
\underline{q}_i &\leq q_i \leq \bar{q}_i, & \forall i \in \mathcal{A}, \\
\underline{\theta}_i &\leq \theta_i \leq \bar{\theta}_i, & \forall i \in \mathcal{A}.
\end{aligned}$$

5.1.3 Solution Method for the Robust ACRP

The formulation presented in Model 9 is non-convex due to trigonometric functions and non-linear components. To solve the robust optimisation problem represented by Model 9, the approach proposed by Dias et al. (2021) can be adopted. This approach solves the deterministic ACRP by using the so-called complex number formulation of the ACRP (Rey and Hijazi, 2017) and embedding it within a cut generation algorithm. Recalling the main elements of the complex number formulation for the ACRP, it is outlined how this formulation is adapted for the robust ACRP.

The complex number reformulation of the robust is then constructed by substituting the original motion equations (3.2) with the reformulated aircraft velocities constraints to incorporate uncertainty; replacing the speed and heading control constraints and variables bounds with (3.8), (3.9) and (4.4), respectively; and substituting the original objective function (3.13) with (4.7). Observe that the robust separation

constraints (5.9) remain unchanged since aircraft velocity variables $v_{i,x}$ and $v_{i,y}$ are linked to variables $\delta_{i,x}$ and $\delta_{i,y}$ via constraints (4.3). The resulting formulation is referred as the robust complex number formulation and use Algorithm 2 from Dias et al. (2021) to solve this problem. This solution method initially relaxes the non-convex quadratic constraint in (4.5) and uses a cut generation procedure to iteratively solve the relaxed problems until global optimality is reached.

5.2 Numerical Experiments

The experimental framework used to test the proposed mixed-integer formulation for the robust problem is introduced in Section 5.2.2. Then a detailed analysis of four instances of the ACRP is presented in Section 5.2.1. The computational performance of the proposed approach and conduct sensitivity analyses on the level of robustness and the size of aircraft uncertainty sets is thoroughly explored in Section 5.2.3 and Section 5.2.4, respectively. The behaviour of the robust ACRP is further analysed by examining specific sets of instances in Section 5.2.5.

5.2.1 Experiments Design

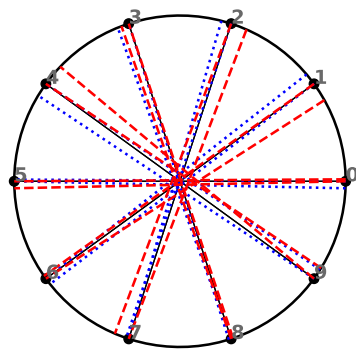
The performance of the proposed approach is tested using two benchmarking problems from the literature: the Circle Problem (CP) and the Random Circle Problem (RCP). Numerical results for problems with a subliminal speed control range of $[-6\%, +3\%]$ (Bonini et al., 2009). As commonly used in the literature (Cafieri and Omhni, 2017; Rey and Hijazi, 2017), a heading control range of $[-30^\circ, +30^\circ]$ is used. In addition, it is assumed that the maximum uncertainty on aircraft velocity components is uniform across directions and aircraft, and define $\bar{\epsilon} = \bar{\epsilon}_i^x = \bar{\epsilon}_i^y$ for all aircraft $i \in \mathcal{A}$. In those experiments, it is also considered the following maximum levels of uncertainty: $\bar{\epsilon} = 2.5\%$, 5% , 7.5% and 10% , and varying levels of robustness $\Gamma = 0, 1, 2, 3$ and 4 . The proposed robust formulations are compared against its deterministic counterpart, which corresponds to $\Gamma = 0$ and/or $\bar{\epsilon} = 0$.

All problems are solved with a relative optimality gap of 1% and a time limit of 10 minutes. All models are implemented using PYTHON on a personal computer with 16 GB of RAM and an Intel i7 processor at 2.9GHz, solved with CPLEX v12.10 (Cplex, 2009) API for PYTHON using default options.

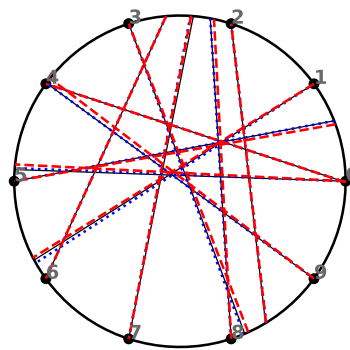
5.2.2 Analysis of the robust ACRP

To analyse and illustrate the behaviour of the proposed formulation for the robust ACRP, the focus is on four instances: CP-1, RCP-10-1, RCP-20-1 and RCP-30-1. The maximum uncertainty is set to $\bar{\epsilon} = 5\%$ and in Figure 5.2, there are plots of the optimal solutions obtained using the robust complex number formulation as described in Section 5.1.3: black lines represent aircraft nominal trajectories, blue lines represent aircraft optimal trajectories using $\Gamma = 0$ (which corresponds to the deterministic case), and green lines represent optimal trajectories using $\Gamma = 4$ (which corresponds to the maximum level of robustness).

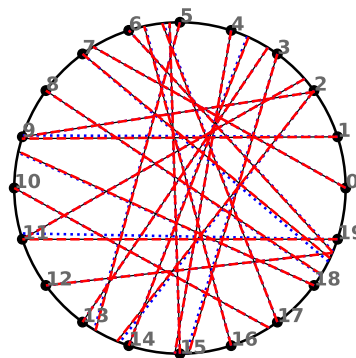
Figure 5.2 shows that there are significant differences between deterministic and robust aircraft trajectories, especially for instances with a high number of conflicts, such as CP-10 (Figure 5.2a) and RCP-30-1 (Figure 5.2d). For RCP instances, this difference increases with the number of aircraft. To further analyse the behaviour of the robust ACRP, the distribution of post-optimisation aircraft minimal separation distances, which is the distance $d_{ij}(t_{ij}^{\min})$ between each pair of aircraft $(i, j) \in \mathcal{P}$ after optimisation, is examined against the level of robustness (Γ) and size of the uncertainty set ($\bar{\epsilon}$), in Figures 5.3 and 5.4, respectively. For CP-10 (see Figure 5.3a), it is noted that the average post-optimisation minimal separation distance increases with Γ . Because this instance is symmetrical and all pairs are in conflict, the minimal separation to avoid conflict tends to grow rapidly with Γ . For RCP-10-1, RCP-20-1 and RCP-30-1 (see Figures 5.3b, 5.3c, 5.3d, which have a higher density of pairs of aircraft and less conflicts, it is observed that increasing the level of robustness does not significantly affect the distribution of aircraft minimal separation which remains near the minimal 5 NM mark. However, RCP-30-1 is found to be infeasible for $\Gamma = 3$ and $\Gamma = 4$, which suggests that even though trajectories may not be substantially affected overall, such highly robust configurations fail to admit feasible solutions. Examining the same instances for a varying maximum uncertainty reveals an overall similar pattern although with more significant changes. Figure 5.4 shows that the average minimum separation distance increases in all instances, particularly for CP-10. This puts in evidence that increasing the value of $\bar{\epsilon}$ has a higher impact on the behaviour of the solution obtained. For RCP-10-1, RCP-20-1 and RCP-30-1 (see Figures 5.4b, 5.4c and 5.4d), it is noticed that the distribution of aircraft pairwise minimal distances tends to increase for $\bar{\epsilon} \geq 5\%$. Further, it is observed that RCP-30-1 is infeasible for $\bar{\epsilon} = 7.5\%$ and 10% .



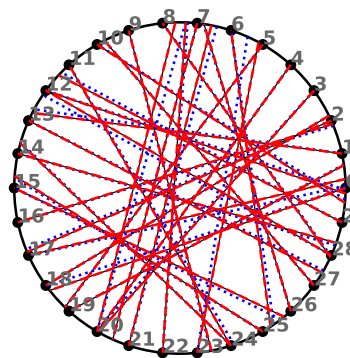
(a) CP-10



(b) RCP-10-1



(c) RCP-20-1



(d) RCP-30-1

Figure 5.2: Illustration of aircraft optimal trajectories using the robust complex number formulation with a maximum uncertainty of $\bar{\epsilon} = 5\%$. Black lines represent aircraft initial trajectories. Blue lines represent optimal trajectories obtained using $\Gamma = 0$. Red lines represent avoidance trajectories obtained using $\Gamma = 4$.

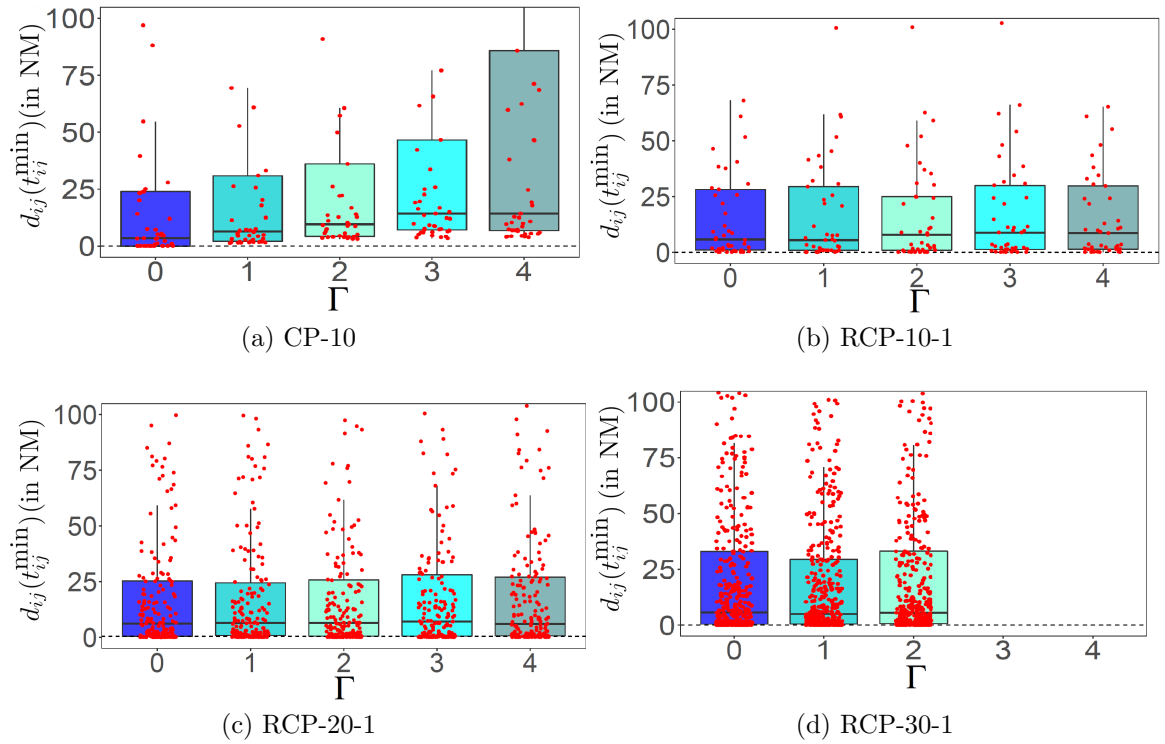


Figure 5.3: Distribution of aircraft pairwise minimal separation distances after optimisation for varying level of robustness Γ . The maximum uncertainty is set to $\bar{\epsilon} = 5\%$. The red dots correspond to individual values for each pair $(i, j) \in \mathcal{P}$. The black dashed line correspond to the minimal separation requirement of 5 NM.

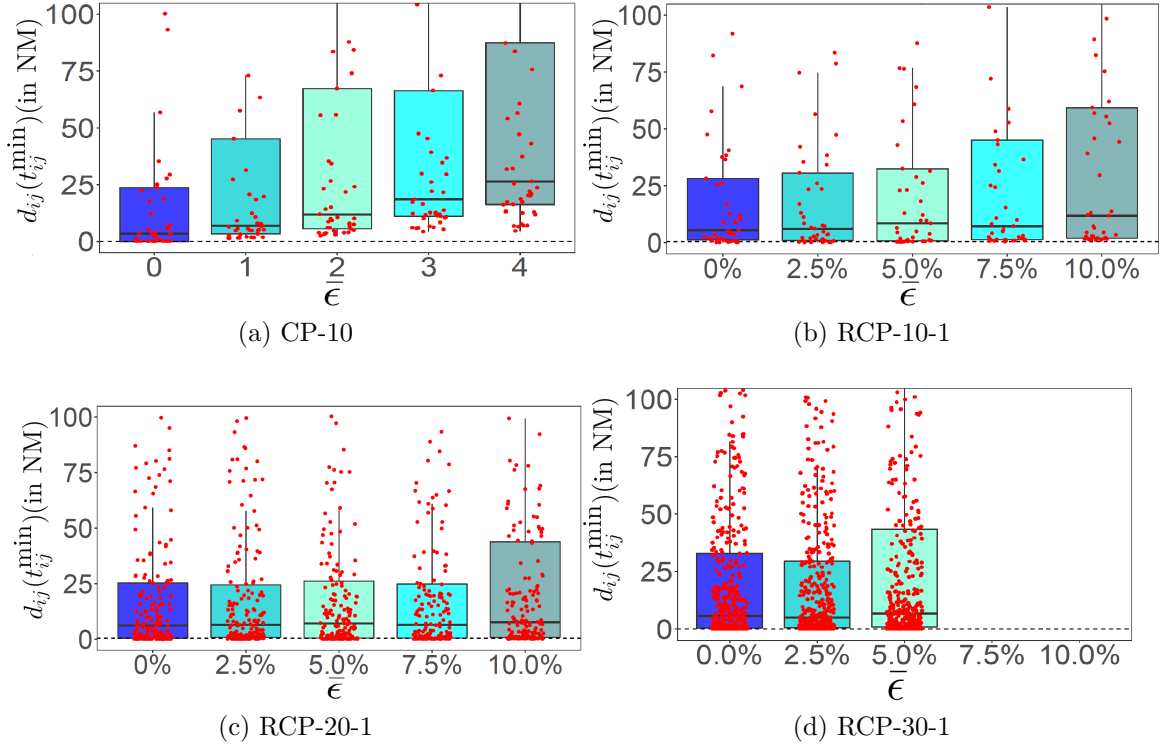


Figure 5.4: Distribution of aircraft pairwise minimal separation distances after optimisation for varying maximum uncertainty $\bar{\epsilon}$. The level of robustness is set to $\Gamma = 4$. The red dots correspond to individual values for each pair $(i, j) \in \mathcal{P}$. The black dashed line correspond to the minimal separation requirement of 5 NM.

For RCP instances, further examination of the minimum separation distance between aircraft before optimisation is available in Figure 5.5. Figures 5.5a, 5.5b and 5.5c correspond to instances RCP-10-1, RCP-20-1 and RCP-30-1, respectively. To be more specific, around 55%, 50% and 45% of the pair of aircraft are less than 5 NM of minimum separation (represented by the red dashed line on the plots) for RCP-10, RCP-20 and RCP-30, respectively. Most of the remaining pairs are within close distance to the minimum separation distance. This suggests that introducing robustness can make such instances harder to solved. For RCP-10-1, RCP-20-1 and RCP-30-1, it can be extrapolated that the distribution of aircraft initial minimal separation distance follows a chi-square distribution with small mean value. This confirms that in most instances, the mean value is close to 5 NM and a substantial number of aircraft pairs are in conflict or are only separated by a marginal amount in addition to the minimum separation distance.

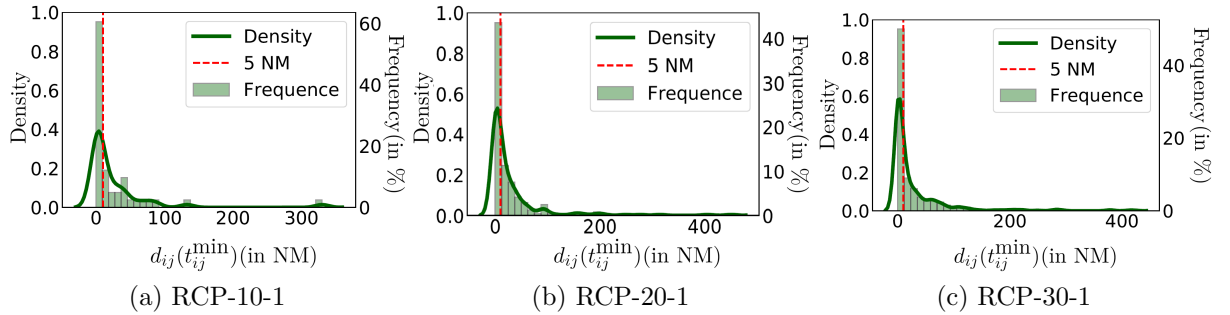


Figure 5.5: Histogram and density plot for instances RCP-10-1, RCP-20-1 and RCP-30-1. The red dashed line represents the minimum separation distance of 5 NM.

Next, a comprehensive computational benchmarking of the proposed solution method for the robust ACRP is conducted.

5.2.3 Sensitivity analysis on the level of robustness

In this section, the performance of the robust complex number formulation is analysed for a varying level of robustness (Γ) for a fixed maximum uncertainty of $\bar{\epsilon} = 5\%$. The results for 7 CP instances ranging from 4 to 10 aircraft are presented in Table 5.1. Results for RCP instances are reported in Table 5.2 for 3 instance sizes with 10, 20 and 30 aircraft per group. For each instance group, 100 RCP instances are randomly generated and the average performance reported along with the standard deviation in parenthesis. For all instances, the performance of the proposed formulations is compared for varying level of robustness where $\Gamma = 0$ corresponds to the deterministic case and $\Gamma = 4$ corresponds to the most robust configuration.

Each row in the results tables represents an instance (CP) or a group of instances (RCP). The header of the results tables is presented from left to right: Γ is the level of robustness; UB is the objective function value; Gap is the optimality gap in percent; Time is the total runtime in seconds, n_i is the number of MIQP iterations where $n_i = 0$ means that an optimal solution was found or the time limit was reached during the initial MIQP solve, n_t represents the proportion of instances that could not be solved within the time limit (10 minutes), i.e. the number of time-outs and n_\emptyset indicates the number/proportion of infeasible instances.

Table 5.1: Summary of results for CP instances with a speed control range of $[-6\%, +3\%]$ and a heading control range of $[-30^\circ, +30^\circ]$ using a maximal uncertainty of $\bar{\epsilon} = 5\%$.

Γ	Instance	UB	Gap (%)	Time (s)	n_i	n_t	n_\emptyset
0	CP-4	$6.25e^{-4}$	0.00	0.02	0	0	0
	CP-5	$1.14e^{-3}$	0.00	0.05	0	0	0
	CP-6	$1.81e^{-3}$	0.00	0.05	0	0	0
	CP-7	$2.37e^{-3}$	0.04	0.17	0	0	0
	CP-8	$3.46e^{-3}$	0.03	1.05	0	0	0
	CP-9	$4.31e^{-3}$	0.02	32.1	0	0	0
	CP-10	$5.55e^{-3}$	0.02	354	0	0	0
1	CP-4	$1.07e^{-3}$	0.03	0.16	0	0	0
	CP-5	$1.33e^{-3}$	0.00	0.05	0	0	0
	CP-6	$2.63e^{-3}$	0.00	0.13	0	0	0
	CP-7	$3.37e^{-3}$	0.00	0.45	0	0	0
	CP-8	$5.44e^{-3}$	0.01	3.73	1	0	0
	CP-9	$6.93e^{-3}$	0.01	68.9	4	0	0
	CP-10	$8.81e^{-3}$	0.01	51.9	1	0	0
2	CP-4	$1.21e^{-3}$	0.00	0.03	0	0	0
	CP-5	$1.49e^{-3}$	0.00	0.14	0	0	0
	CP-6	$3.13e^{-3}$	0.01	0.75	2	0	0
	CP-7	$4.18e^{-3}$	0.00	0.38	1	0	0
	CP-8	$6.93e^{-3}$	0.01	7.72	4	0	0
	CP-9	$8.92e^{-3}$	0.00	54.6	6	0	0
	CP-10	$1.39e^{-2}$	0.03	103	6	0	0
3	CP-4	$1.22e^{-3}$	0.00	0.02	0	0	0
	CP-5	$1.59e^{-3}$	0.00	0.05	0	0	0
	CP-6	$3.38e^{-3}$	0.07	0.92	2	0	0
	CP-7	$4.64e^{-3}$	0.01	0.67	1	0	0
	CP-8	$8.98e^{-3}$	0.03	32.2	10	0	0
	CP-9	$1.09e^{-2}$	0.01	54.1	6	0	0
	CP-10	$2.08e^{-2}$	0.00	174	8	0	0
4	CP-4	$1.22e^{-3}$	0.00	0.03	0	0	0
	CP-5	$1.63e^{-3}$	0.00	0.05	0	0	0
	CP-6	$3.49e^{-3}$	0.04	0.80	0	0	0
	CP-7	$4.77e^{-3}$	0.01	3.87	3	0	0
	CP-8	$9.20e^{-3}$	0.00	26.7	9	0	0
	CP-9	$1.24e^{-2}$	0.00	142	10	0	0
	CP-10	$2.38e^{-2}$	0.02	215	9	0	0

The experiments on the CP instances (Table 5.1) show that, as expected, the upper bound (UB) increases with the number of aircraft. Further, it is observed that UB increases with the level of robustness. It increases over 90% for CP-4 instances from $\Gamma = 0$ to $\Gamma = 4$ and over 300% for CP-10 in the same scenario. In average, it is

a growth of 143.62% which can be easily justified by the higher level of robustness. While the runtime increases exponentially with the number of aircraft, increasing Γ does not significantly impact runtime, even when compared to the deterministic case of $\Gamma = 0$. It is observed that increasing Γ tends to increase the number of iterations of the solution algorithm, which suggests that the higher levels of robustness require more deconfliction resources, i.e. speed or heading change.

The implementation of the proposed approach on CP instances reveals that while all instances up to CP-8 can be solved via the MIQP iteration when the value for $\Gamma = 0$ or $\Gamma = 1$, for any higher values may require additional MIQCP iterations. It is observed that for increasing Γ , the time limit is enough to solve all instances, but with a higher level of randomness, more speed deviation is observed and therefore, more MIQCP iterations are necessary to obtain a conflict-free and violation-free optimal solution. This shows an expected behaviour such as that with higher randomness effect granted by increasing Γ leads to a more complex problem and therefore a more difficult to solve. In addition to this, with a higher value of Γ which represents a higher level of robustness, it is expected that it would cause more violations in speed to compensate for a wider range of speed and angle manoeuvres. With more violations, the solution will consequently require more iteration to be solved to optimality. By the time limit imposed, some instances could not be solved for a higher Γ . However, as observed, the gamma formulation is enough to provide robust solutions given more runtime.

Γ	Instance	UB	Gap	Time	n_i	n_t	n_\emptyset
0	RCP-10	$2.2e^{-4}$ ($2e^{-4}$)	0.00 (0.0)	0.05 (0.01)	0.0 (0.0)	0	0
	RCP-20	$1.7e^{-3}$ ($9e^{-4}$)	0.00 (0.0)	0.26 (0.10)	0.0 (0.0)	0	0
	RCP-30	$7.1e^{-3}$ ($2e^{-3}$)	0.17 (0.7)	135 (239)	0.4 (0.6)	3	0
1	RCP-10	$1.0e^{-2}$ ($7e^{-6}$)	0.00 (0.0)	0.24 (0.06)	0.0 (0.0)	0	0
	RCP-20	$9.8e^{-2}$ ($4e^{-2}$)	0.00 (0.0)	10.2 (4.84)	0.0 (0.0)	0	0
	RCP-30	$7.5e^{-1}$ ($2e^{-1}$)	0.17 (0.7)	287 (116)	0.4 (0.0)	10	60
2	RCP-10	$2.7e^{-2}$ ($2e^{-2}$)	0.00 (0.0)	0.34 (0.13)	0.0 (0.0)	0	0
	RCP-20	$2.8e^{-2}$ ($9e^{-3}$)	0.00 (0.0)	25.1 (16.8)	0.0 (0.0)	8	34
	RCP-30	-	-	-	-	-	100
3	RCP-10	$4.2e^{-2}$ ($2e^{-2}$)	0.00 (0.0)	0.54 (0.18)	0.0 (0.0)	0	0
	RCP-20	$7.4e^{-1}$ ($2e^{-1}$)	0.00 (0.0)	134 (55.6)	0.0 (0.0)	10	46
	RCP-30	-	-	-	-	-	100
4	RCP-10	$5.3e^{-2}$ ($3e^{-2}$)	0.00 (0.0)	0.59 (0.19)	0.0 (0.0)	0	0
	RCP-20	$8.8e^{-1}$ ($2e^{-1}$)	0.00 (0.0)	201 (144)	0.0 (0.0)	15	67
	RCP-30	-	-	-	-	-	100

Table 5.2: Summary of results for RCP instances with a speed control range of $[-6\%, +3\%]$ and a heading control range of $[-30^\circ, +30^\circ]$ using a maximal uncertainty of $\bar{\epsilon} = 5\%$.

The results of the experiments on RCP instances are summarised in Table 5.2. Increasing the level of robustness in RCP instances also tends to increase the objective value (UB), and the effect is on average magnified on instances with larger number of aircraft. In percentage, the growth of the objective function is even larger when compared to previous results for CP instances, where it is up to 2000% for RCP-10 and 5000% for RCP-20. Those extremely larger values is due to the random nature of such instances and the substantial increase of deviation required to guarantee conflict free trajectories under higher level of robustness. It is noticed that RCP-10 instances can be solved within less than a second using for any level of robustness. RCP-20 instances require less than a minute for $\Gamma \leq 2$, on average, but using Γ equal to 3 and to 4, requires around 2 and 3 minutes, respectively. It also noted that 34%, 46% and 67% of RCP-20 instances cannot be solved when Γ is equal to 2, 3 and 4, respectively. The results for RCP-30 instances reveal that all problems with $\Gamma \geq 2$ are infeasible, while only 40% of these instances can be solved with $\Gamma = 1$ and all 100 RCP-30 instances are feasible in the deterministic case.

Overall, it is observed that reducing the robustness level tends to improve the performance of the proposed formulations while retaining comparable optimal solutions to its deterministic counterpart, as indicated by the similar UB values obtained. In term of total deviation, it is noticed that an increase of 500%, 239% and 3% in

objective function value when using $\Gamma = 4$ for CP-10 and RCP-10 and 20, respectively. The formulation is able to solve all instances with $\Gamma = 1$ whereas the results for higher values can result in timeouts or infeasibility for many instances, especially when Γ reaches its maximum value.

For example, for RCP-10 instances, all instances can be solved for any Γ value and no timeout case. For RCP-20, all instance can be solved to optimality using $\Gamma \leq 1$. With $\Gamma = 2$, there are 8 timeout instances and 34% as report beforehand. This percentage grows reaching 100% of infeasible solutions for $\Gamma = 4$. This trend is even stronger for RCP-30 where it can only be solved when $\Gamma \leq 1$, but with timeouts in 3% and 20% of the instances for $\Gamma = 0$ and $\Gamma = 1$, respectively.

Those outcomes show that the robust complex number formulation is capable of solving dense and complex scenarios, but with increasing randomness aspects, it can be observed that those scenarios are not solvable. As expected, in order to accommodate more error due to a larger level of robustness allowed, the model cannot solve instances where the density of pairs of aircraft is high. This summarises a valuable trade-off when approaching robustness in air traffic control: higher robustness level results in lower air capacity.

5.2.4 Sensitivity analysis on the size of the uncertainty set

For this experiment, the performance of the proposed formulation is compared for a maximum level of robustness, i.e. $\Gamma = 4$ under varying maximum uncertainty $\bar{\epsilon}$: 0% (for the deterministic counterpart), 2.5%, 5%, 7.5% and 10%. The performance is reported similarly as in the previous section. The results for 7 CP instances ranging from 4 to 10 aircraft are presented in Table 5.3 and results for RCP instances are reported in Table 5.4.

The experiments on the CP instances (Table 5.3) show that, as expected, UB increases with the maximum uncertainty. In this case, it is observed that for CP-4, a growth in 1000% while for CP-10, 7000% in the objective function value comparing $\bar{\epsilon}$ to 0% to 10%. This is considerably higher than the results found with different level of robustness, but this emphasises that changing the size of the uncertainty sets causes bigger impact in the model behaviour. It is observed that CP instances with up to 9 aircraft can be solved with up $\bar{\epsilon} = 10\%$, however CP-10 is infeasible for $\bar{\epsilon} = 7.5\%$ and $\bar{\epsilon} = 10\%$. All deterministic CP problems can be solved without any iteration ($n_i = 0$) of the algorithm. In turn, introducing uncertainty in the robust ACRP triggers several iterations of the solution algorithm which suggests that the relaxed mixed-integer convex programs are generating more violations due to the

$\bar{\epsilon}$ (%)	Instance	UB	Gap (%)	Time (s)	n_i	n_t	n_\emptyset
0.0	CP-4	$6.25e^{-4}$	0.00	0.20	0	0	0
	CP-5	$1.14e^{-3}$	0.00	0.40	0	0	0
	CP-6	$1.81e^{-3}$	0.00	0.64	0	0	0
	CP-7	$2.37e^{-3}$	0.00	0.39	0	0	0
	CP-8	$3.46e^{-3}$	0.02	3.04	0	0	0
	CP-9	$4.31e^{-3}$	0.02	7.97	0	0	0
	CP-10	$5.55e^{-3}$	0.02	72.3	0	0	0
2.5	CP-4	$1.22e^{-3}$	0.00	0.03	0	0	0
	CP-5	$1.63e^{-3}$	0.00	0.05	0	0	0
	CP-6	$3.49e^{-3}$	0.04	0.80	2	0	0
	CP-7	$4.77e^{-3}$	0.01	3.87	4	0	0
	CP-8	$9.20e^{-3}$	0.00	26.7	9	0	0
	CP-9	$1.24e^{-2}$	0.00	142	10	0	0
	CP-10	$2.38e^{-2}$	0.02	215	8	0	0
5.0	CP-4	$1.70e^{-3}$	0.00	0.03	0	0	0
	CP-5	$3.94e^{-3}$	0.02	0.65	2	0	0
	CP-6	$1.00e^{-2}$	0.00	4.12	6	0	0
	CP-7	$2.12e^{-2}$	0.00	16.2	9	0	0
	CP-8	$4.01e^{-2}$	0.53	12.9	5	0	0
	CP-9	$6.35e^{-2}$	2.13	31.9	5	0	0
	CP-10	$8.45e^{-2}$	3.23	20.4	2	0	0
7.5	CP-4	$3.80e^{-3}$	0.00	1.28	4	0	0
	CP-5	$1.14e^{-2}$	0.00	4.56	11	0	0
	CP-6	$3.02e^{-2}$	0.00	3.14	5	0	0
	CP-7	$6.12e^{-2}$	0.46	9.44	8	0	0
	CP-8	$9.53e^{-2}$	7.55	5.88	3	0	0
	CP-9	$1.52e^{-1}$	1.99	9.36	3	0	0
	CP-10	-	-	-	-	-	100
10.0	CP-4	$7.45e^{-3}$	0.00	4.15	12	0	0
	CP-5	$2.14e^{-2}$	0.00	2.81	8	0	0
	CP-6	$6.24e^{-2}$	0.00	3.92	6	0	0
	CP-7	$1.09e^{-1}$	0.25	4.68	5	0	0
	CP-8	$1.98e^{-1}$	3.52	4.14	3	0	0
	CP-9	$3.48e^{-1}$	18.8	5.57	3	0	0
	CP-10	-	-	-	-	-	100

Table 5.3: Summary of results for CP instances with a speed control range of $[-6\%, +3\%]$ and a heading control range of $[-30^\circ, +30^\circ]$ using a level of robustness of $\Gamma = 4$.

$\bar{\epsilon}$ (%)	Instance	UB	Gap (%)	Time (s)	n_i	n_t	n_0
0.0	RCP-10	$2.2e^{-4}$ ($2e^{-4}$)	0.00 (0.0)	0.05 (0.01)	0.0 (0.0)	0	0
	RCP-20	$1.7e^{-3}$ ($9e^{-4}$)	0.01 (0.0)	0.24 (0.1)	0.0 (0.0)	0	0
	RCP-30	$7.2e^{-3}$ ($2e^{-3}$)	0.01 (0.1)	66.3 (135)	1.4 (0.8)	3	0
2.5	RCP-10	$1.6e^{-2}$ ($1e^{-2}$)	0.00 (0.0)	0.47 (0.15)	0.0 (0.0)	0	1
	RCP-20	$8.9e^{-1}$ ($2e^{-1}$)	0.00 (0.0)	193 (138)	0.0 (0.0)	12	4
	RCP-30	-	-	-	-	-	100
5.0	RCP-10	$5.3e^{-2}$ ($3e^{-2}$)	0.00 (0.0)	0.60 (0.18)	0.0 (0.0)	0	1
	RCP-20	$8.8e^{-1}$ ($2e^{-1}$)	0.00 (0.0)	200 (144)	0.0 (0.0)	2	93
	RCP-30	-	-	-	-	-	100
7.5	RCP-10	$1.3e^{-1}$ ($6e^{-2}$)	0.00 (0.0)	0.76 (0.24)	0.0 (0.0)	0	9
	RCP-20	-	-	-	-	-	100
	RCP-30	-	-	-	-	-	100
10.0	RCP-10	$3.0e^{-1}$ ($1e^{-1}$)	0.00 (0.0)	0.89 (0.20)	0.0 (0.0)	0	26
	RCP-20	-	-	-	-	-	100
	RCP-30	-	-	-	-	-	100

Table 5.4: Summary of results for RCP instances with a speed control range of $[-6\%, +3\%]$ and a heading control range of $[-30^\circ, +30^\circ]$ using a level of robustness of $\Gamma = 4$.

required robustness. Using $\bar{\epsilon} = 2.5\%$, the instances can be solved within 0.03 s for CP-4 and up to 215 seconds for CP-10. Increasing $\bar{\epsilon}$ results in a reduced runtime for all instances compared to the deterministic case.

The results obtained using RCP instances (Table 5.4) reveal that while all problems are feasible under deterministic conditions, the proportion of infeasible problems increase with the maximum uncertainty and the number of aircraft. Notably, all RCP-30-1 instances are found to be infeasible for $\bar{\epsilon} \geq 2.5\%$ (recall that a maximal level of robustness is used). Comparing the objective value, it is stated that over 100000% and this exorbitant value is due to the larger uncertainty set and the fact those the deviation required to guarantee separation in such cases are quite massive when compared to the deterministic case. At the same time, such results highlight that increasing the dimension of uncertainty sets is the major bottleneck in the performance of this algorithm. In terms of runtime, RCP-10 instances, are solved within 1 s using any value of $\bar{\epsilon}$. RCP-20 instances, require on average 0.24 s in the deterministic case. Using $\bar{\epsilon} = 5\%$, 93 instances are infeasible, 2 timed-out and among the remaining 5 instances solved to optimality the average runtime is 200 s.

It is revealed that while all 10, 20 and 30 aircraft RCP instances can be solved via the MIQP iteration for lower and medium values of $\bar{\epsilon}$ (0% and 2.5%) but as

soon the values are closer to its upper capacity, it is required additional MIQCP iterations. For RCP-10 instances, it can be solved within 1s using any value of $\bar{\epsilon}$. For RCP-20 instances, it is required 0.24 s to 200 s, on average, using the values up to $\bar{\epsilon} = 5.0\%$, but, for $\bar{\epsilon} = 2.5\%$, there was 12% of timeout instances and 4% of infeasible instances and for $\bar{\epsilon} = 5.0\%$, it is also observed that 93% of the instances where infeasible. When solving RCP-30 even for relatively small values of $\bar{\epsilon}$ such as 2.5%, it is noticed infeasibility or solutions that could not be solved within the time limit are more common. For $\bar{\epsilon} \geq 2.5\%$, 100% of the instances are infeasible. The density of these instances plus the limited space to contain a larger deviation in speed can make such scenarios to be impossible to be solved.

Overall, it is observed that reducing the uncertainty sets to a more realistic range tends to improve the performance of the proposed formulations while it keeps in a comparable range from its deterministic counterpart, as indicated by the similar UB values obtained. In term of total deviation, it is noticed that an increase of 500%, 239% and 14% in objective function value when using $\bar{\epsilon} = 5.0\%$ for CP-10 and RCP-10 and 20, respectively. The formulation can solve all instances with $\bar{\epsilon} = 2.5\%$ whereas the results for higher values can result in timeout or infeasibility for many instances, especially when its values are closer to its maximum capacity.

The results of the sensitivity analyses conducted highlight that while the robust ACRP can be solved without significantly increasing the level of computational resources required, the impact of on system costs (total deviation) increase rapidly with the level of robustness and/or uncertainty, and the number of aircraft. Further, these analyses revealed that the likelihood of infeasibility increased rapidly along the same directions. In the next section, this behaviour of the robust ACRP is explained in details.

5.2.5 Feasibility analysis

In this section, the correlation between instance feasibility and infeasibility and the characteristics of the instance are tested and explored. The goal is to identify which features of conflict resolution instances can explain the existence of feasible solutions to the robust ACRP. Since CP instances are fully symmetric these instances are not examined. Further, since most RCP-30 instances are infeasible, the focus is on the analysis to RCP-10 and RCP-20 instances. For each group of 100 instances, two-dimensional scatter plots are generated where the x-axis dimension represents the number of conflicts (n_c) of this instance and the y-axis represents the total minimal pairwise distance $D^{\min} = \sum_{(i,j) \in \mathcal{P}} d_{ij}(t_{ij}^{\min})$ (in NM) of this instance. Each dot in

the plots represents in of the 100 instances of the corresponding group (RCP-10 or RCP-20) and the colour of the dot indicates whether this instance is feasible (blue) or infeasible (red). This is done to verify whether that instances with a low total minimal pairwise distance and a high number of conflicts are more likely to be infeasible when increasing the level of robustness or the maximum uncertainty in the system. The results of this experiment are reported in Figures 5.6, 5.7, 5.8 and 5.9: Figures 5.6 and 5.7 illustrate the outcome for varying level of robustness for RCP-10 and RCP-20 respectively; while Figures 5.8 and 5.9 illustrate the outcome for varying maximum uncertainty for RCP-10 and RCP-20, respectively.

As expected, for instances where the initial minimal separation per pair of aircraft is more than 5 NM, there is no expected initial conflict. On the other hand, if the pairwise distance is small or less than 5 NM as the minimal criteria, conflicts are expected. Based on the configuration of the instances used for testing, when the total minimal distance is small, meaning that all aircraft are close to each other and the density of conflict is higher, it is more likely that such instances cannot be solved for all level of robustness. In Figure 5.6 and 5.7, such behaviour is confirmed.

In Figure 5.6, it is observed that for all values of Γ , all RCP-10 instances but one (out of 100) with $n_c = 3$ conflicts and $D^{\min} \approx . 10$ NM can be solved. Figure 5.7 reveals that for RCP-20 instances and $\Gamma = 1$ only 3 infeasible instances. Increasing Γ , it is observed that the proportion of infeasible instances increase more rapidly the bottom-right quadrant of the plot, suggesting that on average instances with a high number of conflict and low total minimal pairwise distance are more likely to be infeasible.

Examining RCP-10 instances in Figure 5.8, it is observed that only a single instance is infeasible for $\bar{\epsilon} = 2.5\%$ and $\bar{\epsilon} = 5.0\%$. Increasing the maximum uncertainty to $\bar{\epsilon} = 7.5\%$ and 10% , more instances are infeasible and those instances exhibit a smaller total pairwise minimal distance and a higher number of conflicts. As shown in Figure 5.9, the proportion of infeasible RCP-20 instances increases rapidly with the maximum uncertainty. Using $\bar{\epsilon} = 2.5\%$, only 5 instances (out of 100) are infeasible and they mostly represent cases where the total minimal distance is smaller and the number of conflicts is above 15 which is relatively high. Using $\bar{\epsilon} = 5.0\%$ value, 94% of instances are infeasible and the feasible instances tend to have a large total minimal pairwise distance (above 70 NM) which suggests that aircraft have enough “room” to accommodate robust conflict-free trajectories. It is revealed that for $\bar{\epsilon} \geq 7.5\%$ all RCP-20 instances are infeasible.

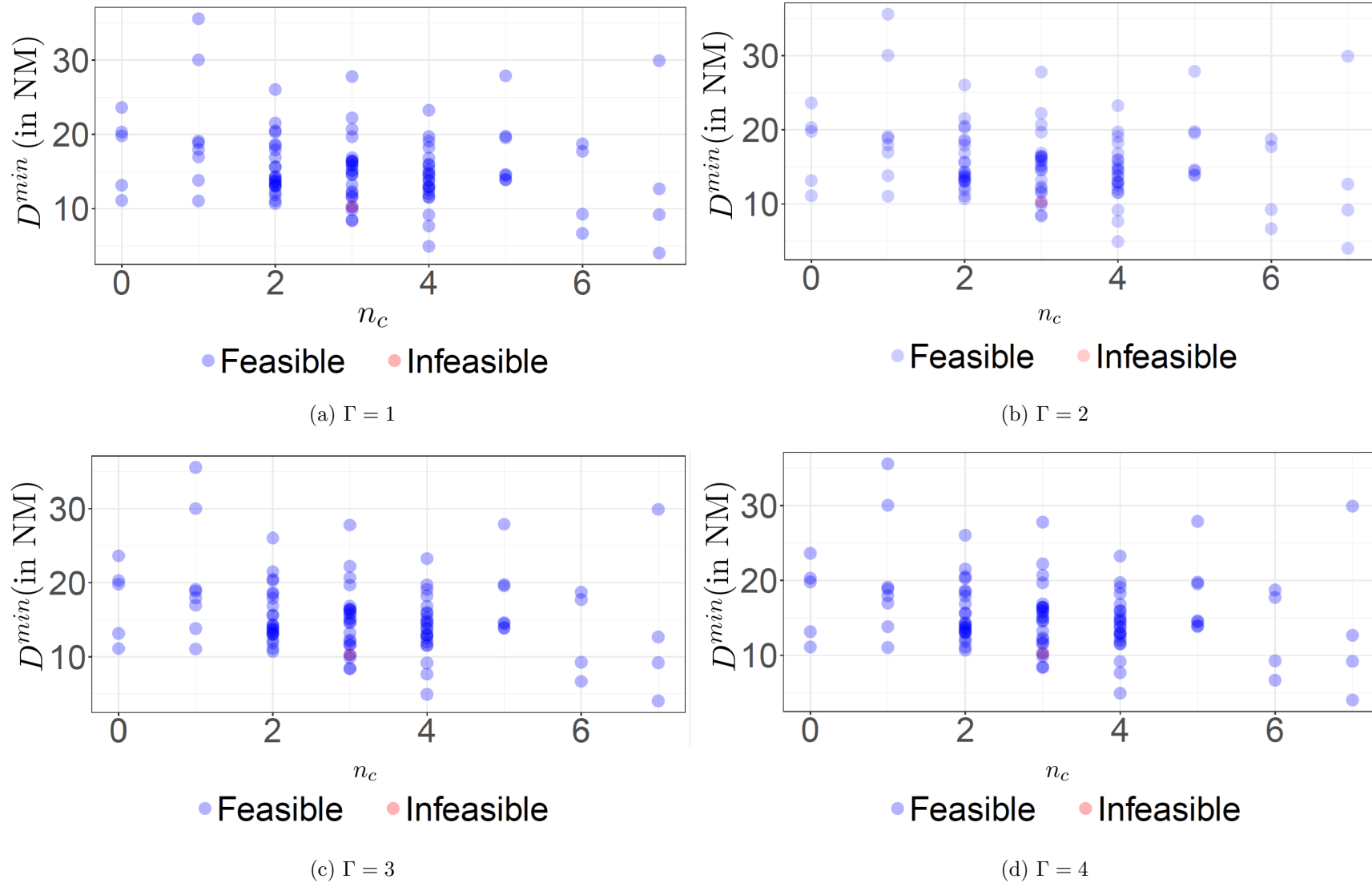


Figure 5.6: Feasibility of 100 RCP-10 instances based on the number of conflict n_c and the total pairwise minimal distance between all pairs of aircraft D^{\min} using $\bar{\epsilon} = 5\%$.

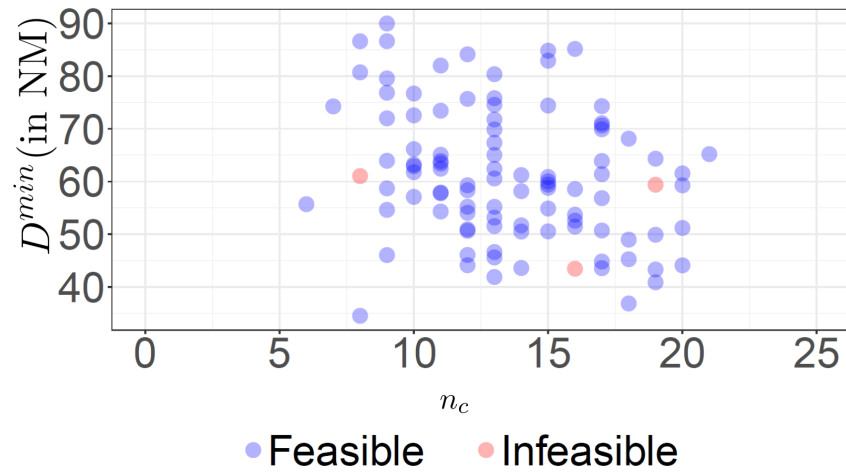
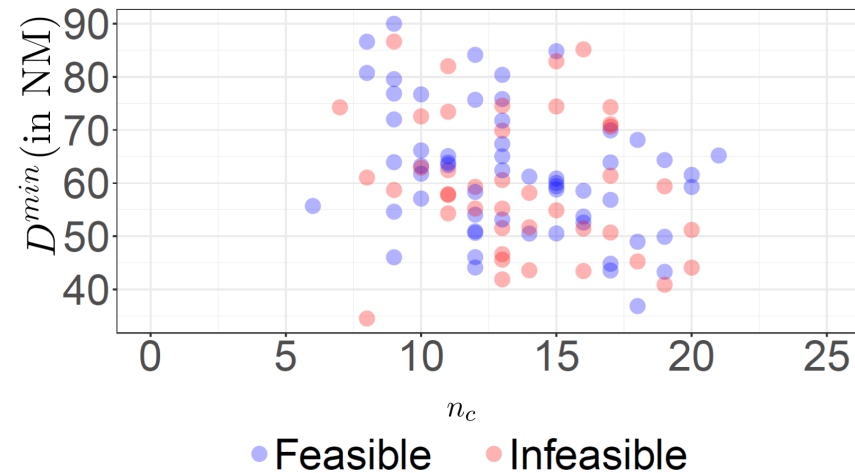
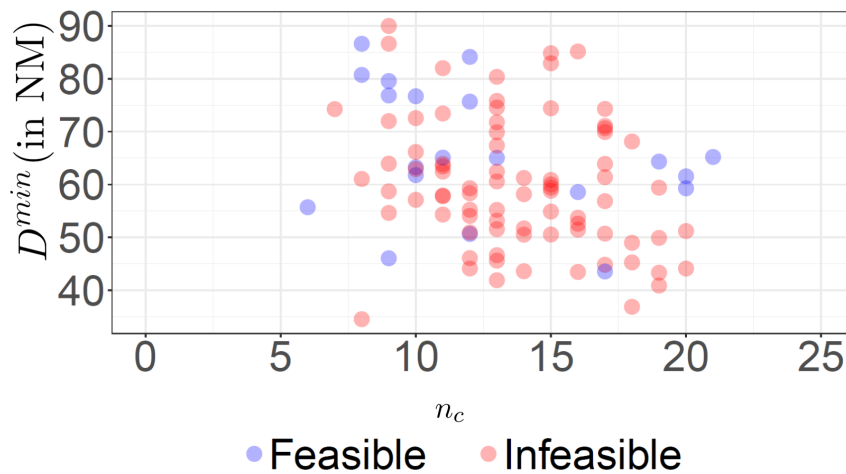
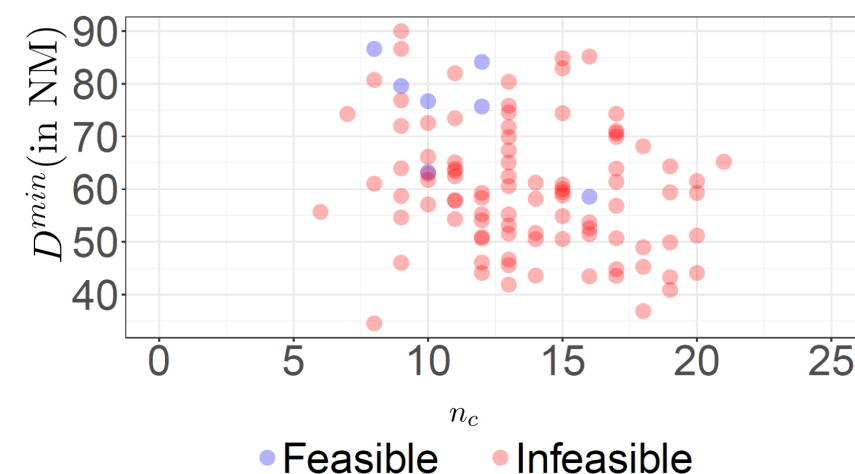
(a) $\Gamma = 1$ (b) $\Gamma = 2$ (c) $\Gamma = 3$ (d) $\Gamma = 4$

Figure 5.7: Feasibility of 100 RCP-20 instances based on the number of conflict n_c and the total pairwise minimal distance between all pairs of aircraft D^{\min} using $\bar{\epsilon} = 5\%$.

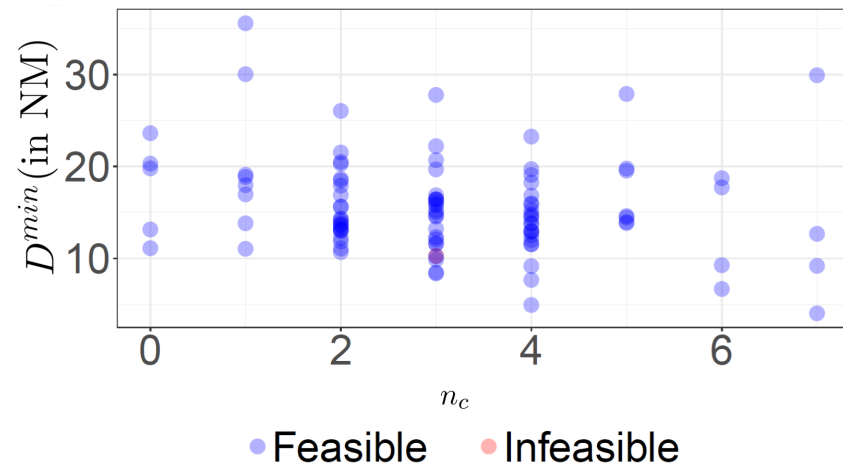
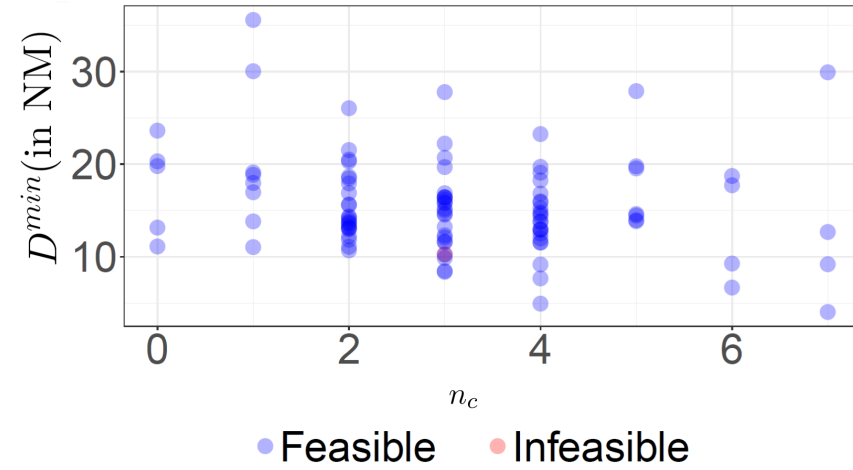
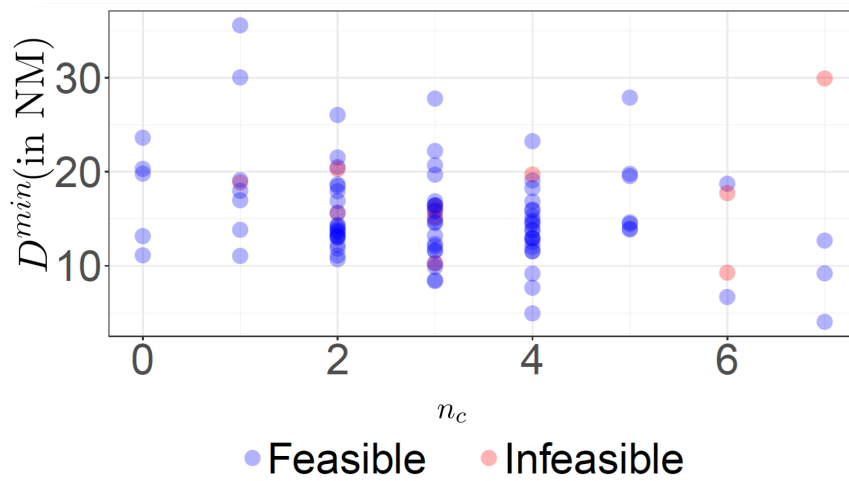
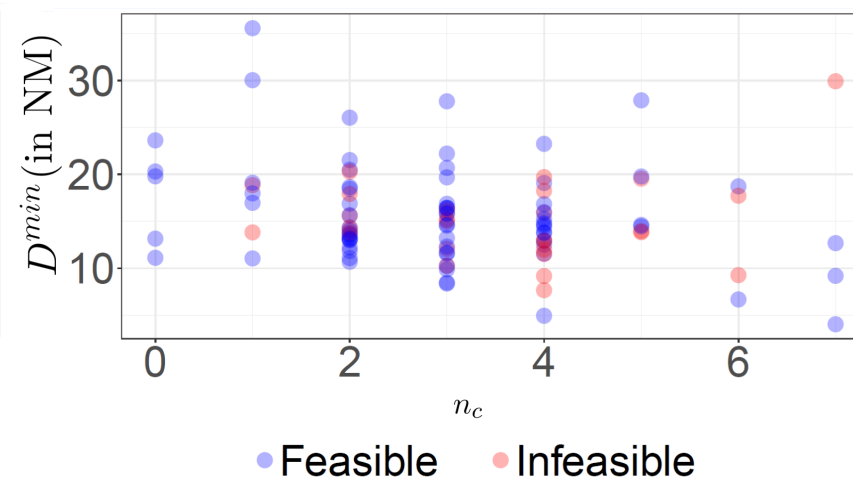
(a) $\bar{\epsilon} = 2.5\%$ (b) $\bar{\epsilon} = 5.0\%$ (c) $\bar{\epsilon} = 7.5\%$ (d) $\bar{\epsilon} = 10\%$

Figure 5.8: Feasibility of 100 RCP-10 instances based on the number of conflict n_c and the total pairwise minimal distance between all pairs of aircraft D^{\min} using $\Gamma = 4$.

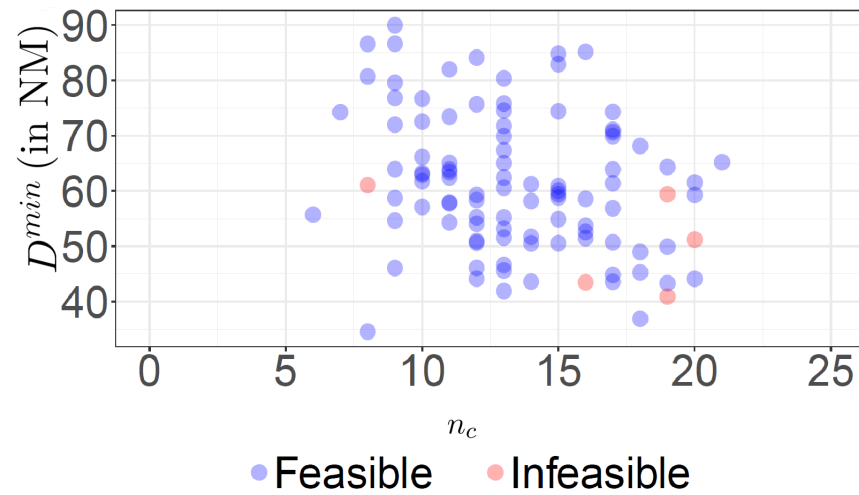
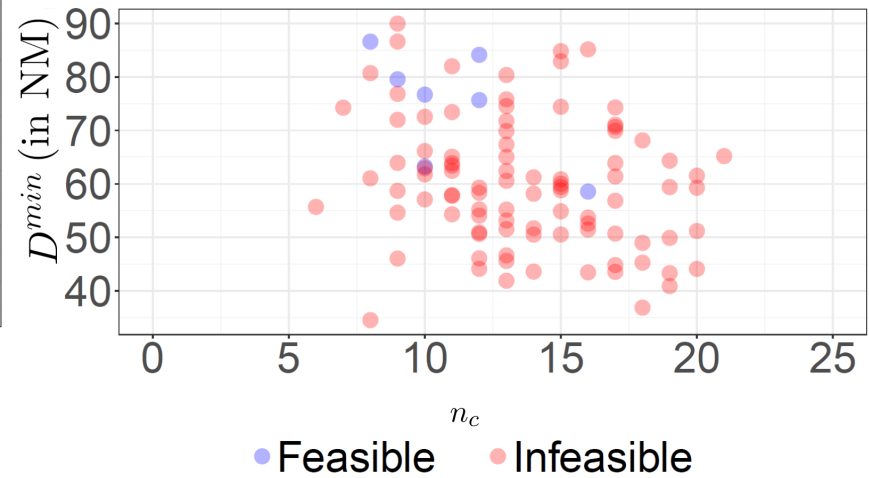
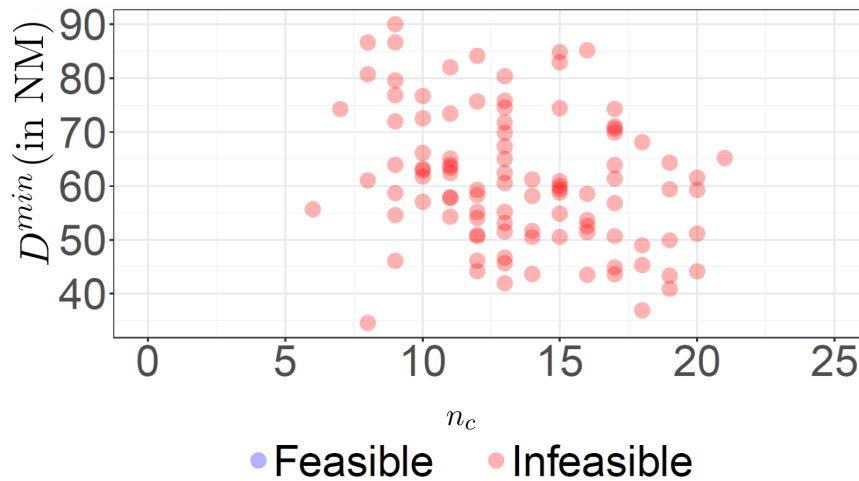
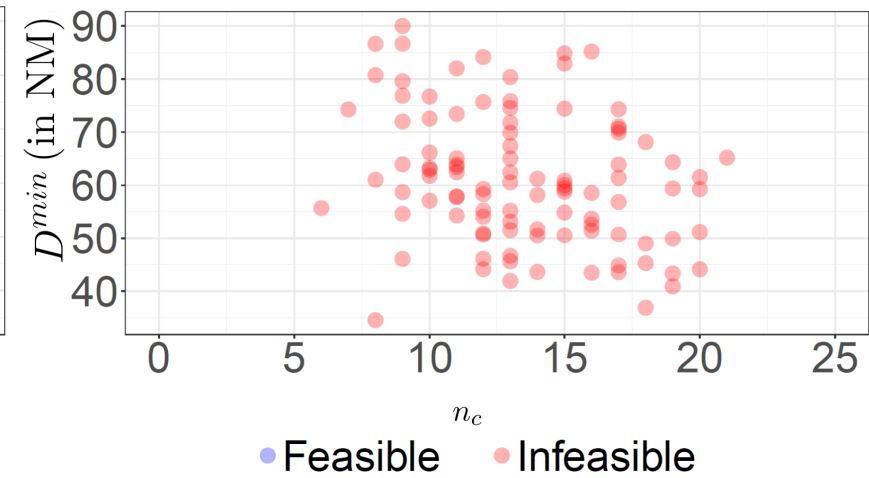
(a) $\bar{\epsilon} = 2.5\%$ (b) $\bar{\epsilon} = 5.0\%$ (c) $\bar{\epsilon} = 7.5\%$ (d) $\bar{\epsilon} = 10\%$

Figure 5.9: Feasibility of 100 RCP-20 instances based on the number of conflict n_c and the total pairwise minimal distance between all pairs of aircraft D^{\min} using $\Gamma = 4$.

5.3 Conclusion

5.3.1 Summary of Findings

In this study, a new formulation for the robust ACRP under trajectory prediction uncertainty is proposed. An aircraft trajectory prediction uncertainty model based on aircraft velocity components is introduced and showed that this approach can be incorporated into a robust optimisation formulation for the ACRP. In this, the ACRP with continuous speed and heading control manoeuvres is used and it showed that robust separation constraints can be reformulated as tractable integer-linear constraints using state-of-the-art approaches in robust optimisation. The complex number formulation for the ACRP is adapted and an exact algorithm is developed to solve the resulting robust complex number formulation model to optimality. A series of numerical experiments on benchmarking instances of the literature was conducted to explore the behaviour of the robust ACRP and test the computational performance of the proposed approach. The performance of the proposed approach was tested on a total of 1535 benchmarking instances. These instances include two types of ACRPs with up to 30 aircraft per instance for different levels of randomness reflected by the level of robustness and the size of the uncertainty set. The performance of the proposed solution algorithms highlights the scalability of the approach compared to existing deterministic methods in the literature. It is observed that the increasing the level of robustness and/or the maximum uncertainty in the model may lead to infeasible instances, when the number of aircraft and conflicts is significant. Further, pre- and post-optimisation analyses reveal that the number of conflicts and the total pairwise minimal distance between aircraft can explain the behaviour of the proposed robust ACRP in terms of instance feasibility. To the best of our knowledge, this is the first exact robust optimisation formulation for the ACRP.

In the numerical experiments, the proposed formulation is compared with the deterministic case ($\Gamma = 0$). The results reveal that by increasing Γ and the uncertainty set, the resulting model is still very competitive and it is observed that the runtime of the robust formulation does not increase significantly compared to the deterministic counterpart. Even though the gamma formulation requires more variables and constraints, it can solve most of the cases for lower values of Γ and uncertainty sets. However, using higher values for those parameters, it becomes more challenging to get feasible solutions within 10 minutes as the time limit and changes in Γ are more likely to be solved instead of changes in $\bar{\epsilon}$ as shown in previous section, which means

that controlling the level of robustness is easier than altering the dimension of such robustness.

Chapter 6

Aircraft Conflict Resolution Problem with Trajectory Recovery

In CDR problems, one of the biggest challenges is to find conflict-free aircraft trajectories that minimize the deviation to the original flight plan. This includes aircraft recovering their initial speed and/or heading after performing a conflict resolution manoeuvre. In mathematical programming approaches for CDR, this issue becomes even more difficult due to non-linearity and non-convexity components within aircraft velocity models. Therefore, it is a common strategy to divide the trajectory into two separated stages: avoidance and recovery. So far in this thesis, the avoidance stage has been addressed extensively through Chapters 3, 4 and 5. In those chapters, the output of those models are trajectories that are least-deviating and by definition, they may deviate the aircraft from their initial flight plan. Implicitly, it is expected that additional manoeuvres are required for aircraft to recover their initial trajectory. In this chapter, two-stage trajectory recovery algorithms are proposed to address the deterministic ACRP with trajectory recovery. For the avoidance stage, two different models are presented: a discretised heading control model and a continuous model using the same algorithm as presented in Chapter 4. For the trajectory recovery, a novel algorithm is proposed, where the recovery manoeuvres and the recovery time are calculated.

A first approach is presented in Section 6.1 where heading angles are discretised in the collision avoidance stage to simplify the formulation. The numerical results using this approach are presented in Section 6.2. This simplification is then relaxed in a second approach that builds on the first one and extends to continuous heading angles and attempts to further improve the quality of the trajectories constructed in Section 6.3. The numerical results emphasises the difference of both formulation even

further in Section 6.4. In the conclusion in Section 6.5, the summary of findings and future research are presented.

6.1 Conflict Resolution with Trajectory Recovery with Discretised Heading Change Angles

In this section, a two-stage approach for conflict resolution with trajectory recovery is presented, assuming that aircraft current and target positions are known and are conflict-free. This sets the context of the optimisation problem of interest: given a set of aircraft with known current and target positions, find least-deviating conflict-free trajectories for all aircraft, such that aircraft may safely reach their target destination. To address this problem, it is proposed to decompose the trajectory optimisation problem in two stages: 1) collision avoidance and 2) trajectory recovery. The first stage focuses on controlling aircraft heading and speed to avoid all conflicts while the second stage focuses on calculating the optimal time for aircraft to start safely recovering towards their target position. For brevity, the focus is on the two-dimensional conflict resolution problem and only considering horizontal aircraft manoeuvres. The extension to the vertical case can be addressed by incorporating flight level change manoeuvres in the collision avoidance stage (Dias et al., 2021) and ensuring safe recovery to aircraft target flight level and position. In the following sections, the continuous heading change angle case is addressed.

6.1.1 Collision Avoidance

In this first stage, the goal is to find conflict-free, least-deviating heading angles and speed changes.

6.1.1.1 Separation Conditions

Consider a set of aircraft \mathcal{A} sharing the same flight level. For each aircraft $i \in \mathcal{A}$, assuming uniform motion laws, its position is: $p_i(t) = [x_i(t) = \hat{x}_i + q_i v_i \cos(\hat{\theta}_i + \theta_i)t, y_i(t) = \hat{y}_i + q_i v_i \sin(\hat{\theta}_i + \theta_i)t]^\top$ in which v_i is the speed, \hat{x}_i and \hat{y}_i are the initial coordinates of i at the beginning of its trajectory, $\hat{\theta}_i$ is its initial heading angle, θ_i is its deviation angle and q_i is the speed deviation.

To avoid trigonometric functions, the set of heading change manoeuvres is discretised. Let \mathcal{H}_i be the set of deviation angles for each aircraft $i \in \mathcal{A}$, and let δ_{ik} be a

binary variable which is 1 if aircraft i selects deviation angle $\theta_k \in \mathcal{H}_i$. The relative velocity vector of i and j , denoted v_{ij} , can be expressed as $v_{ij} = [v_{ij,x}, v_{ij,y}]^\top$ where:

$$v_{ij,x} = \left(v_i \cos(\widehat{\theta}_i) \sum_{k \in \mathcal{H}_i} \phi_{ik} \cos(\widehat{\theta}_k) - v_i \sin(\widehat{\theta}_i) \sum_{k \in \mathcal{H}_i} \phi_{ik} \sin(\widehat{\theta}_k) \right) - \left(v_j \cos(\widehat{\theta}_j) \sum_{k \in \mathcal{H}_j} \phi_{jk} \cos(\widehat{\theta}_k) - v_j \sin(\widehat{\theta}_j) \sum_{k \in \mathcal{H}_j} \phi_{jk} \sin(\widehat{\theta}_k) \right), \quad (6.1a)$$

$$v_{ij,y} = \left(v_i \sin(\widehat{\theta}_i) \sum_{k \in \mathcal{H}_i} \phi_{ik} \cos(\widehat{\theta}_k) + v_i \cos(\widehat{\theta}_i) \sum_{k \in \mathcal{H}_i} \phi_{ik} \sin(\widehat{\theta}_k) \right) - v_j \sin(\widehat{\theta}_j) \sum_{k \in \mathcal{H}_j} \phi_{jk} \cos(\widehat{\theta}_k) + v_j \cos(\widehat{\theta}_j) \sum_{k \in \mathcal{H}_j} \phi_{jk} \sin(\widehat{\theta}_k), \quad (6.1b)$$

where the auxiliary variable ϕ_{ik} is used to linearise the bilinear terms of the form $q_i \delta_{ik}$, via the following constraints:

$$\underline{q}_i \delta_{ik} \leq \phi_{ik}, \quad \forall i \in \mathcal{A}, k \in \mathcal{H}_i, \quad (6.2a)$$

$$\phi_{ik} \leq \delta_{ik} \bar{q}_i, \quad \forall i \in \mathcal{A}, k \in \mathcal{H}_i, \quad (6.2b)$$

$$q_i - (1 - \delta_{ik}) \bar{q}_i \leq \phi_{ik}, \quad \forall i \in \mathcal{A}, k \in \mathcal{H}_i, \quad (6.2c)$$

$$\phi_{ik} \leq q_i - (1 - \delta_{ik}) \underline{q}_i, \quad \forall i \in \mathcal{A}, k \in \mathcal{H}_i. \quad (6.2d)$$

The relative position of aircraft i and j at time t can be represented as $p_{ij}(t) = p_i(t) - p_j(t)$. Let $d = 5NM$ be the horizontal separation norm, two aircraft $i, j \in \mathcal{A}$ are horizontally separated if and only if: $\|p_{ij}(t)\| \geq d, \quad \forall t \geq 0$.

6.1.1.2 Speed Control, Heading Changes and Objective Function

For each aircraft $i \in \mathcal{A}$, it is assumed that the speed rate variable is lower bounded by \underline{q}_i and upper bounded by \bar{q}_i , thus the speed control constraint is:

$$\underline{q}_i \leq q_i \leq \bar{q}_i, \quad \forall i \in \mathcal{A}. \quad (6.3)$$

To model heading angle changes, it is taking into account that each aircraft $i \in \mathcal{A}$ has access to a set of options for heading angles changes $k \in \mathcal{H}_i$. The selection is given by the binary variable δ_{ik} which is equal to 1 if aircraft i selects and angle θ_k . Heading angle selection is ensured via the constraint:

$$\sum_{k \in \mathcal{H}_i} \delta_{ik} = 1, \quad \forall i \in \mathcal{A}. \quad (6.4)$$

For the objective function, a quadratic penalty on speed and heading deviations is used and the parameter $w \geq 0$ is used to compromise between speed and angle change:

$$\text{minimise } \sum_{i \in \mathcal{A}} \left(w(1 - q_i)^2 + (1 - w) \left(\sum_{k \in \mathcal{H}_i} \delta_{ik} \theta_k \right)^2 \right) \quad (6.5)$$

6.1.1.3 Disjunctive formulation

The proposed approach for conflict resolution via speed and discrete heading control is summarised in Model 10.

Model 10. *Heading-Discretised Disjunctive Formulation*

$$\begin{aligned} & \text{minimise } \sum_{i \in \mathcal{A}} \left(w(1 - q_i)^2 + (1 - w) \left(\sum_{k \in \mathcal{H}_i} \delta_{ik} \theta_k \right)^2 \right), \\ & \text{subject to} \\ & v_{ij,x} = \left(v_i \cos(\hat{\theta}_i) \sum_{k \in \mathcal{H}_i} \phi_{ik} \cos(\hat{\theta}_k) - v_i \sin(\hat{\theta}_i) \sum_{k \in \mathcal{H}_i} \phi_{ik} \sin(\hat{\theta}_k) \right) - \\ & \quad \left(v_j \cos(\hat{\theta}_j) \sum_{k \in \mathcal{H}_j} \phi_{jk} \cos(\hat{\theta}_k) - v_j \sin(\hat{\theta}_j) \sum_{k \in \mathcal{H}_j} \phi_{jk} \sin(\hat{\theta}_k) \right), \quad \forall (i, j) \in \mathcal{P}, \\ & v_{ij,y} = \left(v_i \sin(\hat{\theta}_i) \sum_{k \in \mathcal{H}_i} \phi_{ik} \cos(\hat{\theta}_k) + v_i \cos(\hat{\theta}_i) \sum_{k \in \mathcal{H}_i} \phi_{ik} \sin(\hat{\theta}_k) \right) - \\ & \quad v_j \sin(\hat{\theta}_j) \sum_{k \in \mathcal{H}_j} \phi_{jk} \cos(\hat{\theta}_k) + v_j \cos(\hat{\theta}_j) \sum_{k \in \mathcal{H}_j} \phi_{jk} \sin(\hat{\theta}_k), \quad \forall (i, j) \in \mathcal{P}, \\ & v_{ij,y} \hat{x}_{ij} - v_{ij,x} \hat{y}_{ij} \leq 0, \quad \text{if } z_{ij} = 1, \quad \forall (i, j) \in \mathcal{P}, \\ & v_{ij,y} \hat{x}_{ij} - v_{ij,x} \hat{y}_{ij} \geq 0, \quad \text{if } z_{ij} = 0, \quad \forall (i, j) \in \mathcal{P}, \\ & v_{ij,y} \gamma_{ij}^l - v_{ij,x} \phi_{ij}^l \leq 0, \quad \text{if } z_{ij} = 1, \quad \forall (i, j) \in \mathcal{P}, \\ & v_{ij,y} \gamma_{ij}^u - v_{ij,x} \phi_{ij}^u \geq 0, \quad \text{if } z_{ij} = 0, \quad \forall (i, j) \in \mathcal{P}, \\ & \underline{q}_i \delta_{ik} \leq \phi_{ik}, \quad \forall i \in \mathcal{A}, k \in \mathcal{H}_i, \\ & \phi_{ik} \leq \delta_{ik} \bar{q}_i, \quad \forall i \in \mathcal{A}, k \in \mathcal{H}_i, \\ & q_i - (1 - \delta_{ik}) \bar{q}_i \leq \phi_{ik}, \quad \forall i \in \mathcal{A}, k \in \mathcal{H}_i, \\ & \phi_{ik} \leq q_i - (1 - \delta_{ik}) \underline{q}_i, \quad \forall i \in \mathcal{A}, k \in \mathcal{H}_i, \\ & \sum_{k \in \mathcal{H}_i} \delta_{ik} = 1, \quad \forall i \in \mathcal{A}, \\ & \underline{q}_i \leq q_i \leq \bar{q}_i, \quad \forall i \in \mathcal{A}, \\ & v_{ij,x}, v_{ij,y} \in \mathbb{R}, \quad \forall (i, j) \in \mathcal{P}, \\ & z_{ij} \in \{0, 1\}, \quad \forall (i, j) \in \mathcal{P}, \end{aligned}$$

$$\delta_{ik} \in \{0, 1\},$$

$$\forall i \in \mathcal{A}, k \in \mathcal{H}_i,$$

$$\phi_{ik} \in \mathbb{R},$$

$$\forall i \in \mathcal{A}, k \in \mathcal{H}_i.$$

This formulation is a mixed-integer quadratic program (MIQP) and it has $\mathcal{O}(|\mathcal{A}|^2 + |\mathcal{A}||\mathcal{H}|)$ constraints and $\mathcal{O}(|\mathcal{A}|^2 + |\mathcal{A}||\mathcal{H}|)$ binary variables. The model is built with indicator constraints which can be handled by commercial optimisation software.

The outputs of Model 10 are vectors of heading angle speed deviation, δ^* and q^* . Let θ_i^* be the optimal heading change for aircraft i , therefore: $\theta_i^* = \sum_{k \in \mathcal{H}_i} \delta_{ik}^* \theta_k$. The resulting conflict-free trajectories of Model 10 is used as an input for the recovery stage of the proposed conflict resolution algorithm.

6.1.2 Trajectory Recovery

The second stage aims to identify the optimal time for aircraft to recover towards its target position. To account for the cost of trajectory deviations at the first stage, a_i^* for $i \in \mathcal{A}$ represents the deviation corresponding to the optimal solution of Model 10:

$$a_i^* = (1 - w)(1 - q_i^*)^2 + w(\theta_i^*)^2 \quad (6.7)$$

Let t_i be the recovery time of aircraft $i \in \mathcal{A}$ and let \check{x}_i, \check{y}_i be the coordinates of the target position of i . For trajectory recovery, each aircraft need to perform opposing manoeuvres to cancel the deviation applied during avoidance. Similar to the avoidance model, the goal is to guarantee that all pair of aircraft are separated throughout the recovery stage. Since the separation condition Eq. (3.7) is based on linear motion, it is necessary to distinguish the trajectory stage of each aircraft $i \in \mathcal{A}$, i.e. before and

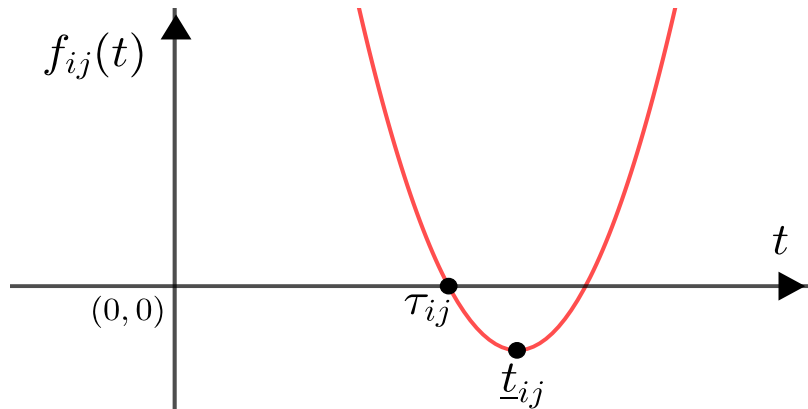


Figure 6.1: Illustration of $f_{ij}(t)$ for a configuration with $g_{ij} < 0$ and $t_{ij}^{\min} > 0$. τ_{ij} represents the start time of the conflict.

after its recovery time t_i . Let A_i be the avoidance trajectory of aircraft i and R_i its recovery trajectory. Given a pair (i, j) of aircraft, it is necessary to ensure that aircraft are separated during all pairwise trajectory stages, denoted A_iA_j , A_iR_j , R_iA_j and R_iR_j . Observe that separation for the stage A_iA_j is already ensured by the solution of Model 10. If aircraft i and j were to recover at the same time period, then aircraft will transition from A_iA_j to R_iR_j directly. Otherwise, if i (resp. j) recovers before j (resp. i), then A_iA_j will transition to R_iA_j (resp. A_iR_j) before transitioning to R_iR_j .

The distance flown during the collision avoidance stage is:

$$d_{A_i}(t_i) = \sqrt{(\hat{x}_i - x(t_i))^2 + (\hat{y}_i - y(t_i))^2}, \quad \forall i \in \mathcal{A}, \quad (6.8)$$

similarly, the distance flown during the trajectory recovery stage is:

$$d_{R_i}(t_i) = \sqrt{(x(t_i) - \check{x}_i)^2 + (y(t_i) - \check{y}_i)^2}, \quad \forall i \in \mathcal{A}. \quad (6.9)$$

If aircraft i has changed its speed only, then at t_i aircraft should recover its initial speed without any heading change. Otherwise, if i has made a turning movement, then aircraft should turn in the opposite direction at time t_i with the angle:

$$\theta_{R_i}(t_i) = \arcsin\left(\frac{d_{A_i}(t_i) \sin(\theta_{A_i})}{d_{R_i}(t_i)}\right), \quad (6.10)$$

To avoid trigonometric functions and obtain a tractable formulation, the time component is discretised, i.e. $t_i \in \{0, 1\epsilon, 2\epsilon, \dots, |\mathcal{T}|\epsilon\}$ where \mathcal{T} is the set of time periods available for recovery and ϵ is the length of time periods. Abusing notation, the separation condition is redesigned and expressed in Eq. (3.7) as: $g_{ij}(m, n) \geq 0$ and $t_{ij}^{\min}(m, n) \leq 0$, where the pair (m, n) indicates the time period indices of recovery times t_i and t_j , respectively.

Let $\Omega_{X_iX_j}$ be the set of conflict-free pairs of recovery times for aircraft $i, j \in \mathcal{A}$, where X_i represents the state of the trajectory of aircraft i , i.e. A_i or R_i ; and X_j represents the state of the trajectory of aircraft j , i.e. A_j or R_j . This set can be specified into three different sets corresponding to the three different states during the recovery stage. The set $\Omega_{R_iR_j}$ is defined as:

$$\Omega_{R_iR_j} = \{(m, n) \in \mathcal{T}^2 : g_{R_iR_j}(mn) \geq 0 \vee t_{R_iR_j}(m, n) \leq 0\} \quad (6.11)$$

For the states A_iR_j and R_iA_j an extra condition is required. Consider the state A_iR_j : if the lines of motion corresponding to trajectories A_i and R_j are in conflict but aircraft i turns into recovery prior to the start of this conflict, then no conflict

will occur. This illustrated in Figure 6.1 where $g_{A_i R_j} < 0$ and $t_{A_i R_j} > 0$. Let $\tau_{A_i R_j}(t_j)$ be the smallest root of $g_{A_i R_j} = 0$ if j recovers at time t_j . If aircraft i recovers prior to $\tau_{A_i R_j}(t_j)$, *i.e.* $t_i \leq \tau_{A_i R_j}(t_j)$, then the conflict will be avoided. Accordingly, those sets are defined as:

$$\Omega_{A_i R_j} = \{(m, n) \in \mathcal{T}^2 : g_{A_i R_j}(n) \geq 0 \\ \vee \underline{t}_{A_i R_j}(n) \leq 0 \quad \vee \quad m \leq \tau_{A_i R_j}(n)\}, \quad (6.12a)$$

$$\Omega_{R_i A_j} = \{(m, n) \in \mathcal{T}^2 : g_{R_i A_j}(m) \geq 0 \\ \vee \underline{t}_{R_i A_j}(m) \leq 0 \quad \vee \quad n \leq \tau_{R_i A_j}(m)\}. \quad (6.12b)$$

In the next section, an exact and a heuristic approach to optimise aircraft recovery times are proposed.

6.1.2.1 Exact-Recovery

Let ρ_{im} be a binary variable equal to 1 if aircraft $i \in \mathcal{A}$ recovers at time period $m \in \mathcal{T}$ and 0 otherwise. The goal is to minimise the total weighted recovery time, *i.e.* $\sum_{i \in \mathcal{A}} \sum_{m \in \mathcal{T}} a_i^* \rho_{im} t_m^2$. To track the states of aircraft pair (i, j) which are activated, two binary variables α_{ij} and β_{ij} are introduced. Those variables are used to identify whether $t_i < t_j$ ($\alpha_{ij} = 1$) which activates state $R_i A_j$, or if $t_i > t_j$ ($\beta_{ij} = 1$) which activates state $A_i R_j$. Variables α_{ij} and β_{ij} are defined via the constraints:

$$\alpha_{ij} \geq \frac{1}{|\mathcal{T}|} \left(\sum_{m \in \mathcal{T}} m \rho_{im} - \sum_{n \in \mathcal{T}} n \rho_{jn} \right) \quad \forall (i, j) \in \mathcal{P} \quad (6.13a)$$

$$\beta_{ij} \geq \frac{1}{|\mathcal{T}|} \left(\sum_{n \in \mathcal{T}} n \rho_{jn} - \sum_{m \in \mathcal{T}} m \rho_{im} \right) \quad \forall (i, j) \in \mathcal{P} \quad (6.13b)$$

$$\alpha_{ij} + \beta_{ij} \leq 1 \quad \forall (i, j) \in \mathcal{P} \quad (6.13c)$$

The following constraints is used to exclude conflicting trajectories from the solution. Observe that states $A_i R_j$ and $R_i A_j$ are conditional on the recovery times of t_i and t_j and thus the corresponding constraints are only active if i and j do not recover at the time period.

$$\rho_{im} + \rho_{jn} \leq 2 - \beta_{ij}, \quad \forall (i, j) \in \mathcal{P}, (m, n) \in \Omega_{A_i R_j}, \quad (6.14a)$$

$$\rho_{im} + \rho_{jn} \leq 2 - \alpha_{ij}, \quad \forall (i, j) \in \mathcal{P}, (m, n) \in \Omega_{R_i A_j}, \quad (6.14b)$$

$$\rho_{im} + \rho_{jn} \leq 1, \quad \forall (i, j) \in \mathcal{P}, (m, n) \in \Omega_{R_i R_j}. \quad (6.14c)$$

Aircraft are assigned a recovery time via the constraint:

$$\sum_{m \in \mathcal{T}} \rho_{im} = 1, \quad \forall i \in \mathcal{A}. \quad (6.15)$$

The exact trajectory recovery formulation is summarised in Model 11 which is a MILP and it has $\mathcal{O}(|\mathcal{A}|^2 + |\mathcal{T}|^2)$ constraints and $\mathcal{O}(|\mathcal{A}||\mathcal{T}| + |\mathcal{A}|^2)$ binary variables.

Model 11. *Exact-Recovery*

$$\begin{aligned} & \text{minimise} && \sum_{i \in \mathcal{A}} \sum_{m \in \mathcal{T}} a_i^* \rho_{im} t_m^2 \\ & \text{subject to} && \\ & \alpha_{ij} \geq \frac{1}{|\mathcal{T}|} \left(\sum_{m \in \mathcal{T}} m \rho_{im} - \sum_{n \in \mathcal{T}} n \rho_{jn} \right), && \forall (i, j) \in \mathcal{P}, \\ & \beta_{ij} \geq \frac{1}{|\mathcal{T}|} \left(\sum_{n \in \mathcal{T}} n \rho_{jn} - \sum_{m \in \mathcal{T}} m \rho_{im} \right), && \forall (i, j) \in \mathcal{P}, \\ & \alpha_{ij} + \beta_{ij} \leq 1, && \forall (i, j) \in \mathcal{P}, \\ & \rho_{im} + \rho_{jn} \leq 2 - \beta_{ij}, && \forall (i, j) \in \mathcal{P}, (m, n) \in \Omega_{A_i R_j}, \\ & \rho_{im} + \rho_{jn} \leq 2 - \alpha_{ij}, && \forall (i, j) \in \mathcal{P}, (m, n) \in \Omega_{R_i A_j}, \\ & \rho_{im} + \rho_{jn} \leq 1, && \forall (i, j) \in \mathcal{P}, (m, n) \in \Omega_{R_i R_j}, \\ & \sum_{m \in \mathcal{T}} \rho_{im} = 1, && \forall i \in \mathcal{A}, \\ & \rho_{im} \in \{0, 1\}, && \forall i \in \mathcal{A}, m \in \mathcal{T}, \\ & \alpha_{ij}, \beta_{ij} \in \{0, 1\}, && \forall (i, j) \in \mathcal{P}. \end{aligned}$$

6.1.2.2 Greedy-Recovery

This heuristic iterates over all time steps and uses a priority list to decide which aircraft can be recovered at each time step. The priority list used is based on a_i^* values (6.7). The algorithm first sorts aircraft accordingly and iterates over time periods. At each time period the algorithm iterates over the sorted list of aircraft and check if each aircraft can be recovered at the current time. The process is repeated until no aircraft can recover at the current time. The proposed algorithm has a worst-case time complexity of $\mathcal{O}(|T||A|^3)$. The pseudo-code of the proposed greedy algorithm for aircraft trajectory recovery is summarised in 4.

Now the proposed the two-stage algorithm is formally introduced: stage 1 solves initial conflicts using Model 10 by adjusting aircraft headings and speeds. The optimal

Algorithm 4 Greedy-Recovery Algorithm

Input: $\mathcal{A}, \mathbf{a}^*$ **Output:** t $\mathcal{R} \leftarrow \{i \in \mathcal{A} : a_i = 0\}$ $\mathcal{D} \leftarrow \mathcal{R} - \mathcal{A}$ $\mathcal{D} \leftarrow$ Sort based on decreasing a_i values**for** $t \in \mathcal{T}$ **do** update \leftarrow true **while** update = true **do** update \leftarrow false **for** $i \in \mathcal{D}$ **do** sep \leftarrow 0 **for** $j \in \mathcal{A}$ **do** **if** $i < j$ **then** **if** $j \in \mathcal{R}$ **then** **if** $(t, t_j) \in \Omega_{R_i R_j}$ **then**
 sep \leftarrow sep + 1 **else** **if** $(t, t_j) \in \Omega_{R_i A_j}$ **then**
 sep \leftarrow sep + 1 **if** $i > j$ **then** **if** $j \in \mathcal{R}$ **then** **if** $(t_j, t) \in \Omega_{R_j R_i}$ **then**
 sep \leftarrow sep + 1 **else** **if** $(t_j, t) \in \Omega_{A_j R_i}$ **then**
 sep \leftarrow sep + 1 **if** sep = $|\mathcal{A}| - 1$ **then** $t_i \leftarrow t$ $\mathcal{R} \leftarrow \mathcal{R} \cup \{i\}$ $\mathcal{D} \leftarrow \mathcal{R} \setminus \{i\}$ update \leftarrow true

solution of stage 1 is used as input for stage 2 which finds optimal aircraft recovery times. Stage 2 is solved either exactly via Model 11 or using the heuristic algorithm 4. In the next section, the numerical results for those methods are proposed.

6.2 Numerical Experiments

The experimental framework used to test the proposed mixed-integer formulation for the trajectory recovery is introduced in Section 6.2.1. Then a detailed analysis of four group of instances is presented in Section 6.2.2. The computational performance of the proposed approaches are thoroughly explored in Section 5.2.3 and Section 6.2.3, respectively.

6.2.1 Experimental Framework

For all tests, a speed regulation range of $\pm 10\%$ is used and it allows heading changes in the range $\pm \frac{\pi}{6}$ in steps of 10° , hence a total of 7 headings are available per aircraft (including the initial trajectory heading). For the preference weight, it is used as $w = 0.2$ in the objective of Model 10. This value was selected such that both heading and speed control terms were of comparable order of magnitude with an emphasis on penalising heading control. For stage 2, a total of $|\mathcal{T}| = 15$ time periods are used, with a step of $\epsilon = 2$ minutes. Models 10 and 11 are solved with CPLEX's Python API and a time limit of 5 minutes.

6.2.2 Illustration

To illustrate the proposed two-stage algorithm, the optimal solution obtained using Model 10 and Model 11 (ER) are plotted for CP instances with 5, 10 and 15 aircraft (CP-5, CP-10 and CP-15). For RCP instances, three instances of each instance size tested are shown, i.e. with 10, 20 and 30 aircraft. In the figures, dashed grey lines represent aircraft initial trajectories, red lines represent the avoidance trajectory of stage 1, and blue lines represent recovery trajectories of stage 2. For CP-5, all conflicts are solved using speed control only. Instead, for CP-10 and CP-15, some aircraft make a turn before recovering to their destination. The solutions of RCP instances highlight that increasing the number of aircraft tends to increase the duration of the collision avoidance trajectory (red line).

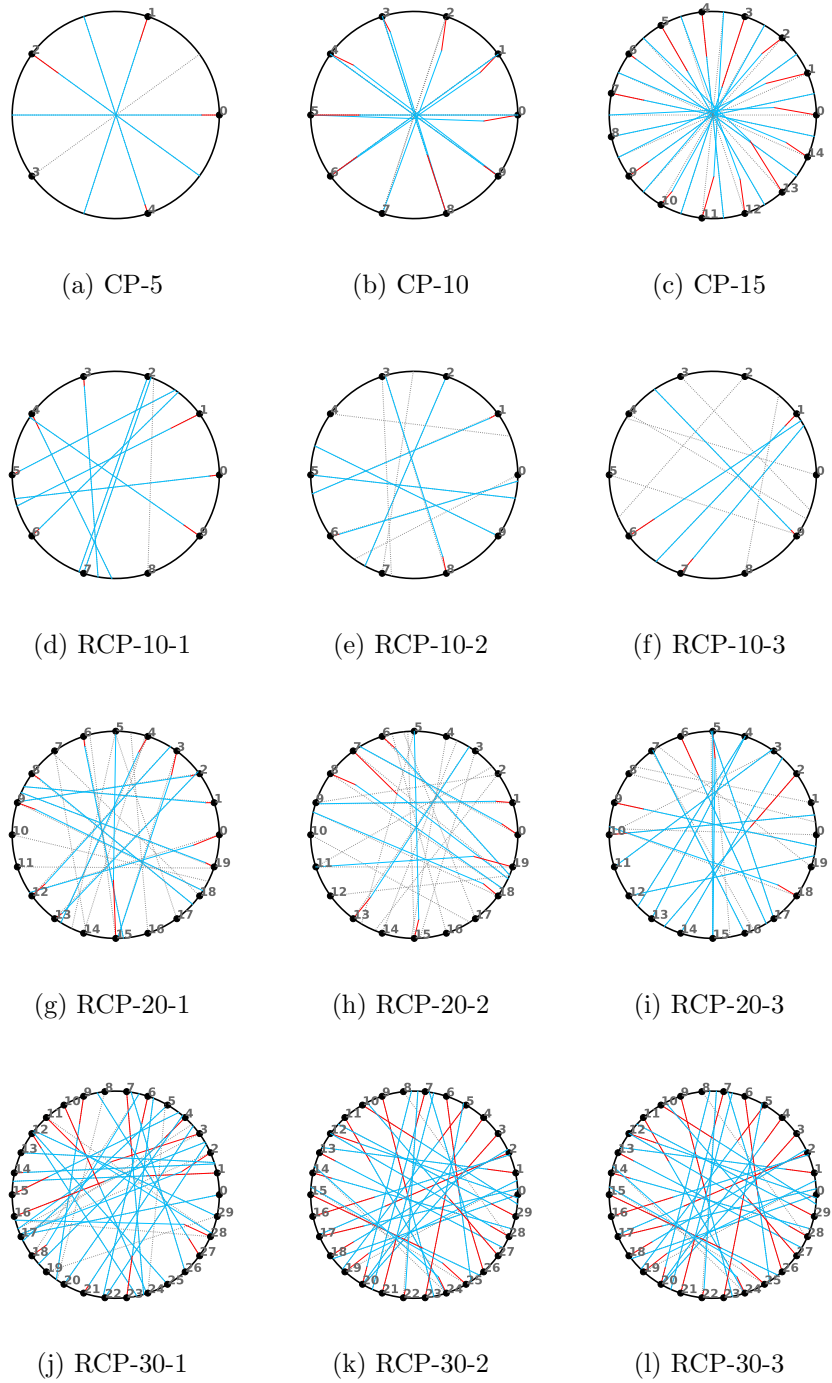


Figure 6.2: Illustration of the two-stage algorithm with Exact-Recovery. Dashed grey lines represent aircraft initial trajectories. Red lines represent aircraft collision avoidance trajectories obtained via Model 10. Blue lines represent recovery trajectories obtained via Model 11.

6.2.3 Performance of the Two-stage Algorithm

The performance of the two variants of the two-stage algorithm are examined, one where the trajectory recovery stage is solved using Model 11 (Exact Recovery – ER), and the other using Algorithm 4 (Greedy Recovery – GR). Table 6.1 summarises the results for CP instances. In the header $|\mathcal{A}|$ is the number of aircraft, n_c as the number of conflicts, $Obj.$ is the objective function and $Time(s)$ is the runtime in seconds. It is also reported the minimum recovery time among all aircraft $\min_{i \in \mathcal{A}} t_i$, the average recovery time $\frac{1}{|\mathcal{A}|} \sum_{i \in \mathcal{A}} t_i$, and the maximum recovery time $\max_{i \in \mathcal{A}} t_i$. $Gap\%$ is the relative gap difference between the objective values of ER and GR.

In terms of performance, it is observed that the runtime of Models 10 and 11 increase exponentially with the number of aircraft, highlighted the challenging nature of the problems. Comparing trajectory recovery approaches, GR scales very efficiently in terms of runtime compared to ER is able to find some optimal solutions. Overall the average recovery time of GR is comparable to that of ER. In some cases, ER is able to override the decision at the first stage by recovering aircraft initially deviated at $t = 0$, which means that such aircraft do not need to perform any avoidance manoeuvre.

A	n_c	Avoidance		Exact-Recovery					Greedy-Recovery					Gap(%)
		Obj.	Time (s)	Obj.	Time (s)	$\min_{i \in \mathcal{A}} t_i$	$\frac{1}{ A } \sum_{i \in \mathcal{A}} t_i$	$\max_{i \in \mathcal{A}} t_i$	Obj.	Time (s)	$\min_{i \in \mathcal{A}} t_i$	$\frac{1}{ A } \sum_{i \in \mathcal{A}} t_i$	$\max_{i \in \mathcal{A}} t_i$	
4	6	4.89E-02	0.02	3.25E-03	0.24	0.00	1.25	2.00	3.25E-03	0.06	0.00	1.00	2.00	0.06
5	10	3.08E-03	0.03	9.76E-05	0.35	0.00	2.00	4.00	3.19E-04	0.08	0.00	2.40	5.00	69.41
6	15	7.34E-02	0.06	4.89E-03	0.47	0.00	2.17	4.00	8.14E-03	0.10	0.00	2.17	5.00	39.9
7	21	2.86E-02	0.52	2.01E-03	0.87	0.00	2.71	7.00	3.84E-03	0.12	1.00	3.86	7.00	47.5
8	28	9.82E-02	0.11	8.23E-03	0.97	2.00	3.50	6.00	8.23E-03	0.14	0.00	2.38	5.00	0.02
9	36	7.72E-02	26.9	7.81E-03	1.52	1.00	3.33	6.00	7.81E-03	0.22	0.00	1.78	5.00	0.04
10	45	1.23E-01	5.48	1.32E-02	2.03	0.00	3.50	7.00	1.88E-02	0.25	0.00	3.30	10	29.8
11	55	1.05E-01	50.4	1.44E-02	17.1	2.00	4.73	8.00	2.17E-02	0.29	0.00	5.00	11.0	33.2
12	66	1.49E-01	39.6	1.91E-02	9.74	0.00	4.25	9.00	2.62E-02	0.26	0.00	3.67	10.0	27.0
13	78	1.52E-01	6.93	2.53E-02	301	0.00	4.62	8.00	3.43E-02	0.38	0.00	5.31	9.00	26.2
14	91	1.74E-01	130	2.57E-02	40.0	0.00	4.36	8.00	2.56E-02	0.36	0.00	3.21	8.00	0.01
15	105	1.98E-01	200	2.81E-02	225	0.00	4.07	8.00	3.70E-02	0.49	0.00	4.27	7.00	23.8

Table 6.1: Results on the Circle Problem with 4 to 15 aircraft.

It is also observed the performance of the two-stage algorithms for RCP instances in Figures 6.3-6.6. For stage 1, it is revealed that the objective function and its variance increase super-linearly with the number of aircraft (see Figure 6.3). All first stage problems are solved within less than 3 minutes, with 10- and 20-aircraft instances requiring less than 10 seconds (see Figure 6.4).

For stage 2, the performance of ER and GR on RCP instances is found to be comparable in terms of objective function values (see Figure 6.5). For 10- and 20-aircraft problems, GR is marginally sub-optimal. For 30-aircraft problems, it is observed that when using a time limit of 5 minutes for ER most instances time out (see Figure 6.6), and the feasible solution returned by ER is often less competitive than the one provided by GR. This highlights the potential of the proposed greedy heuristic for real-time decision support.

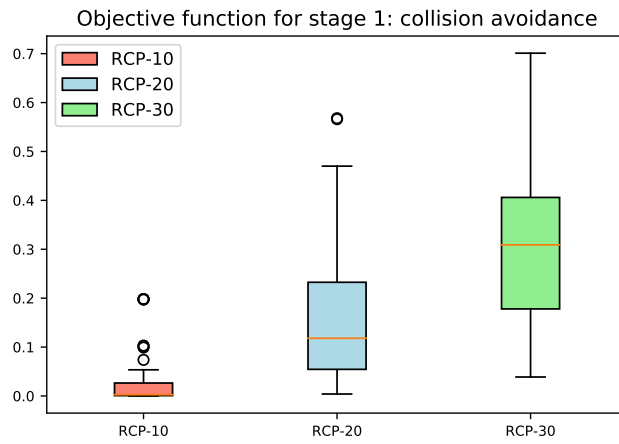


Figure 6.3: Stage 1: collision avoidance. Distribution of objective function values for Model 10. Each boxplot represent 100 instances of each instance size (10, 20 and 30 aircraft).

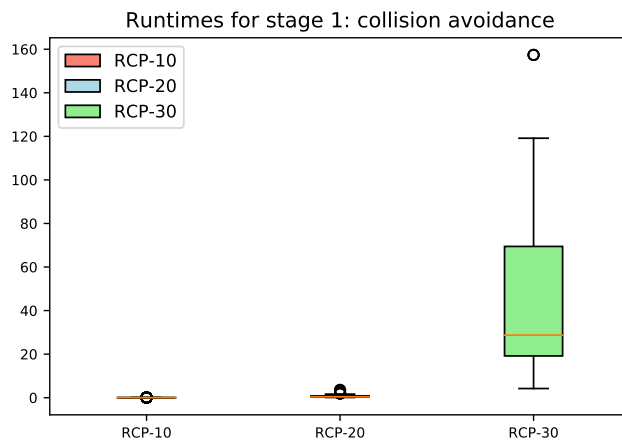


Figure 6.4: Stage 1: Collision avoidance. Distribution of runtimes for Model 10. Each boxplot represent 100 instances of each instance size (10, 20 and 30 aircraft).

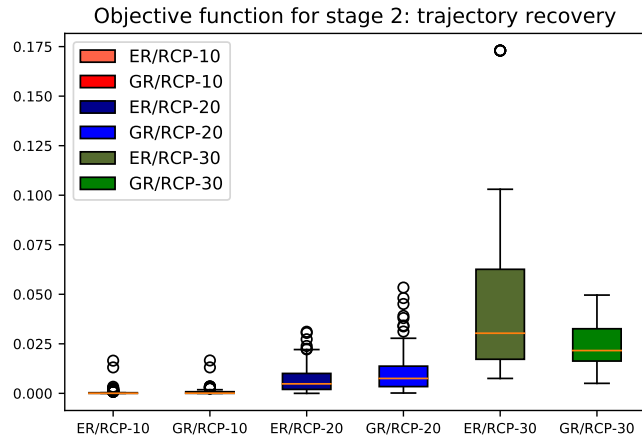


Figure 6.5: Stage 2: Trajectory recovery. Distribution of objective function values for ER (Model 11) and GR (Algorithm 4). Each boxplot represent 100 instances of each instance size (10, 20 and 30 aircraft).

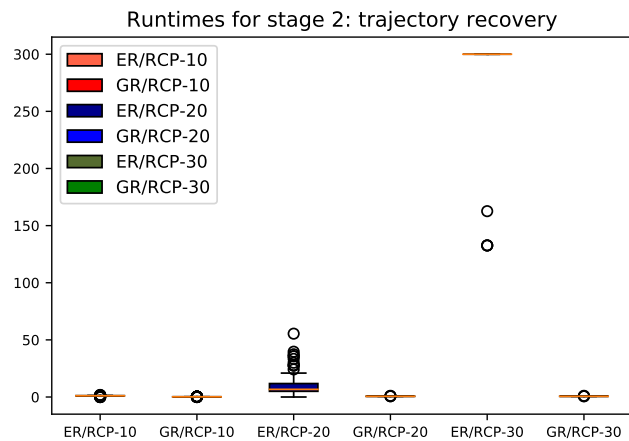


Figure 6.6: Stage 2: Trajectory recovery. Distribution of runtimes for ER (Model 11) and GR (Algorithm 4). Each boxplot represent 100 instances of each instance size (10, 20 and 30 aircraft).

6.3 Conflict Resolution with Trajectory Recovery with Continuous Heading Change Angle

One of the main drawbacks of using discretising angles in the avoidance stage is the limitations in terms of available manoeuvres. Although such formulation simplifies the avoidance problem, it lacks applicability and versatility. The quality and performance of such models are very much linked to how the heading angle discretisation is performed. More values guarantee more precision and diversity in the solutions, but at the same time requires higher computational power and longer runtime. Another drawback of the previous formulations is the lack of guarantee that any solution obtained is global. The previous method is composed of a two-stage sequential algorithm that only solves each stage only once. Because the avoidance and recovery are resolved separately, the solution for the entire problem is heavily dependent on the avoidance stage and therefore cannot be taken as a global solution. This section introduces a two-stage iterative algorithm to solve the aircraft conflict resolution problem with trajectory recovery under continuous heading angle control. In this attempt, it is expected that via multiple iterations, a trade-off between deviation and recovery time can be obtained to guarantee that the solution obtained is a well-balanced compromise between avoidance and trajectory recovery.

6.3.1 Collision Avoidance

For the collision avoidance stage, the **Disjunctive** method is used. As stated in Chapter 4, for conflict avoidance, the model used is based on the complex number formulation and the constraint-generation algorithm. In addition, there are infinity possibilities for the heading angle solution given that this variable is treated as continuous in such formulation. However, as it was observed in the discretised version, applying a two-stage approach, leads to smaller deviations on aircraft and at the same time, more aircraft altered. Deviations in speed are easy to be recovered, while deviation in heading angles is a larger inconvenience. Nevertheless, both types of manoeuvres alter aircraft nominal trajectory and require recovery. By imposing an iterative algorithm, it is expected that the cost to recover multiple aircraft with small deviations can exceed the cost of deviating less aircraft with larger deviations. Therefore, it is necessary to impose that fewer aircraft are affected in the avoidance stage but they are required to be affected, this has to be at least costly enough to be justified.

By examining the solution from the conflict avoidance stage, it is clear that most aircraft have deviated from nominal configurations. However, such deviations are

very small. As observed in the discretised model, even small deviations result in costly recovery manoeuvres. In order to generate trajectories where fewer aircraft are controlled and those that are controlled have a reduced total cost, an additional binary variable is introduced. This variable determines whether the aircraft is controlled or not. In this formulation, the avoidance stage has the objective of minimising the impact of the initial condition of the set of aircraft. Therefore, to guarantee such conditions, the combined deviation cost needs to be kept as minimal as possible. To achieve that, a new binary variable is introduced. Let $f_i \in \{0, 1\}$ for $i \in \mathcal{A}$ represent the control variable, where a “controlled” aircraft, assuming $f_i = 1$ if an aircraft has its speed or heading modified and $f_i = 0$, otherwise.

The initial usage of this binary variable is to guarantee that if a pair of aircraft is initially in conflict, at least one has to alter its original flight plan. By using the initial conditions, this can be pre-processed and those aircraft can be set up into a set. Let \mathcal{P}_0 be set the aircraft such as that $\mathcal{P}_0 \subset \mathcal{P}$ and that is initially in conflict. Recall that a pair (i, j) of aircraft is initially in conflict if and only if condition 3.7 is not satisfied. Therefore, for all pair of aircraft that are initially in the conflict in \mathcal{P}_0 , the following cuts are valid inequalities:

$$f_i + f_j \geq 1, \quad \forall (i, j) \in \mathcal{P}_0. \quad (6.16)$$

These cuts are added to strengthen the conflict resolution formulations by observing that for any pair of aircraft initially in conflict at least one of them must perform an avoidance manoeuvre.

Based on the binary variable f_i , if aircraft i is not controlled, its speed and heading control should remain unchanged. This can be expressed as:

$$\underline{q}_i f_i + (1 - f_i) \leq q_i \leq \bar{q}_i f_i + (1 - f_i), \quad \forall i \in \mathcal{A}, \quad (6.17a)$$

$$\underline{\theta}_i f_i \leq \theta_i \leq \bar{\theta}_i f_i, \quad \forall i \in \mathcal{A}, \quad (6.17b)$$

this is translated into the decision variables of the complex number formulation as:

$$\underline{q}_i \cos(\max\{|\bar{\theta}_i|, |\underline{\theta}_i|\}) f_i + (1 - f_i) \leq \delta_{i,x} \leq \bar{q}_i f_i + (1 - f_i), \quad \forall i \in \mathcal{A}, \quad (6.18a)$$

$$\bar{q}_i \sin(\underline{\theta}_i) f_i \leq \delta_{i,y} \leq \bar{q}_i \sin(\bar{\theta}_i) f_i, \quad \forall i \in \mathcal{A}, \quad (6.18b)$$

Therefore, for each aircraft, if they are not performing any manoeuvres, the value for its heading angle deviation should be equal to 0 and for speed change should be equal to 1.

The avoidance stage can be formulated exactly as presented in the Chapter 3 incorporating the manoeuvre control variable f_i as described in Eq. (6.18) and constraint (6.16).

Model 12. *MIQP 2D Formulation using Manoeuvre Control Variable*

$$\begin{aligned}
& \text{Minimise} && \sum_{i \in \mathcal{A}} w \delta_{i,y}^2 + (1-w)(1 - \delta_{i,x})^2 + \lambda_f f_i, \\
& \text{Subject to:} && \\
& v_{ij,x} = \delta_{i,x} \hat{v}_i \cos(\hat{\theta}_i) - \delta_{i,y} \hat{v}_i \sin(\hat{\theta}_i) - \delta_{j,x} \hat{v}_j \cos(\hat{\theta}_j) + \delta_{j,y} \hat{v}_j \sin(\hat{\theta}_j), && \forall (i, j) \in \mathcal{P}, \\
& v_{ij,y} = \delta_{i,y} \hat{v}_i \cos(\hat{\theta}_i) - \delta_{i,x} \hat{v}_i \sin(\hat{\theta}_i) - \delta_{j,y} \hat{v}_j \cos(\hat{\theta}_j) + \delta_{j,x} \hat{v}_j \sin(\hat{\theta}_j), && \forall (i, j) \in \mathcal{P}, \\
& v_{ij,y} \hat{x}_{ij} - v_{ij,x} \hat{y}_{ij} \leq 0, && \text{if } z_{ij} = 1, \quad \forall (i, j) \in \mathcal{P}, \\
& v_{ij,y} \hat{x}_{ij} - v_{ij,x} \hat{y}_{ij} \geq 0, && \text{if } z_{ij} = 0, \quad \forall (i, j) \in \mathcal{P}, \\
& v_{ij,y} \gamma_{ij}^l - v_{ij,x} \phi_{ij}^l \leq 0, && \text{if } z_{ij} = 1, \quad \forall (i, j) \in \mathcal{P}, \\
& v_{ij,y} \gamma_{ij}^u - v_{ij,x} \phi_{ij}^u \geq 0, && \text{if } z_{ij} = 0, \quad \forall (i, j) \in \mathcal{P}, \\
& f_i + f_j \geq 1, && \forall (i, j) \in \mathcal{P}_0, \\
& \underline{q}_i \cos(\max\{|\bar{\theta}_i|, |\underline{\theta}_i|\}) f_i + (1 - f_i) \leq \delta_{i,x} \leq \bar{q}_i f_i + (1 - f_i), && \forall i \in \mathcal{A}, \\
& \bar{q}_i \sin(\underline{\theta}_i) f_i \leq \delta_{i,y} \leq \bar{q}_i \sin(\bar{\theta}_i) f_i, && \forall i \in \mathcal{A}, \\
& v_{ij,x}, v_{ij,y} \in \mathcal{B}_{ij}, && \forall (i, j) \in \mathcal{P}, \\
& f_i \in \{0, 1\}, && \forall i \in \mathcal{A}, \\
& z_{ij} \in \{0, 1\}, && \forall (i, j) \in \mathcal{P}.
\end{aligned}$$

6.3.2 Trajectory Recovery

The second stage aims to identify the optimal time for aircraft to recover towards its target position as it was done for the discretised model. As used in Section 6.1.2, the avoidance cost function of aircraft i can be extended to incorporate the binary f_i . Let \bar{a}_i be defined as:

$$\bar{a}_i = (1-w)(1 - \delta_{i,x})^2 + w \delta_{i,y}^2 + \lambda_f f_i, \quad \forall i \in \mathcal{A}, \quad (6.20)$$

λ_f is the coefficient determining the importance of manoeuvre control. This cost function should be minimised in the avoidance stage. Considering that $f_i \gg (1 - \delta_{i,x})^2 + \delta_{i,y}^2$, it imposes that modifying the status of an aircraft is notoriously more costly and therefore it should be avoided. This can be justified by the fact that for

each aircraft, the cost of changing its trajectory is unitary while the deviation in angle and speed are very small in an optimized solution.

The cost function now needs to account for manoeuvres applied in the avoidance stage as well as the recovery time. Therefore, the recovery cost function \bar{a}_i^* is calculated based on avoidance cost function evaluated at the optimal solution of the avoidance stage such as that its value are based on $\delta_{i,x}^*$ and $\delta_{i,y}^*$. The objective function is then rewritten to:

$$\min \sum_{i \in \mathcal{A}} \bar{a}_i^* t_i^2 \quad (6.21)$$

where t_i is the recovery time of aircraft $i \in \mathcal{A}$. This expression comes from the approximated area created by the deviation during the avoidance stage and it is quadratic in t_i . This value is obtained in the same process described in Section 6.1.2: each aircraft need to perform its manoeuvres based on their deviation and at the same time, it is necessary to guarantee that all aircraft are separated throughout this stage too. Depending on the recovery time of each aircraft, three different pairwise trajectory stages can be created ($A_i A_j$, $A_i R_j$, $R_i A_j$ and $R_i R_j$). Because those stages depend on the initial conditions and the optimal deviation obtained after avoidance, all those possible stages can be calculated during pre-processing. Given that the heading angle is a continuous variable in this formulation, the alternative trajectory recovery is only known after the avoidance stage is optimised. The remaining details of this model are equivalent to the Exact Recovery Model described in Section 6.1.2.1.

6.3.2.1 Two-Stage Iterative Algorithm

The main idea behind the algorithm is to capture the cost of the recovery in the cost of the avoidance stage. Therefore, its goal is to influence the behaviour of the avoidance stage to anticipate the cost of trajectory recovery and attempt to construct an efficient trajectory across both stages. This can be achieved by altering the objective function in the avoidance stage to account for the recovery cost calculated in 6.21. The algorithm controls the variation between the overall costs of the solution in subsequent iterations. Let TC_i the total cost per aircraft defined as an approximation of the combined cost of avoidance (in Eq. (6.20)) and recovery cost (in the objective function stated in (6.21)).

$$TC_i = (1 - w)(1 - q_i)^2 + w\theta_i^2 + \lambda_f f_i^2 + \lambda_t t_i^2, \quad \forall i \in \mathcal{A}, \quad (6.22)$$

where TC_i is the overall cost of the trajectory, considering all the components in the avoidance stage and the recovery time and w is the preference weight over the two-dimensional and λ_t is the weight for the recovery time component. Let TC_i^n , the total cost for aircraft i at iteration n , therefore the cost variation ΔTC_i is defined as:

$$\Delta TC_i = \sum_{i \in \mathcal{A}} TC_i^n - TC_i^{n-1}. \quad (6.23)$$

If this variation is less a predefined threshold, the algorithm converges. The objective function in the avoidance stage is modified to account for the anticipated cost of trajectory recovery by adding the expression in Eq. (6.21) evaluated at the optimal solution obtained in the recovery stage. Hence, the avoidance stage objective function can be re-written as:

$$\min \sum_{i \in \mathcal{A}} \bar{a}_i^* (w \delta_{i,y}^2 + (1-w)(1 - \delta_{i,x})^2 + f_i \lambda_f) \quad (6.24)$$

At the first iteration, there is no value for \bar{a}_i^* , therefore it is initialized as uniform across for all aircraft $i \in \mathcal{A}$.

6.4 Numerical Results

The experimental framework used to test the proposed mixed-integer formulation for the trajectory recovery using continuous heading is introduced in Section 6.4.1. Then a detailed analysis of four groups of instances is presented in Section 6.4.2. The computational performance of the proposed approaches is thoroughly explored in Section 6.4.3, respectively.

6.4.1 Experimental Framework

For all tests, a speed regulation range based on the subliminal speed control $[-6\%, +3\%]$ is used and it allows heading changes in the range $\pm \frac{\pi}{6}$. For the preference weight, it is used as $w = 0.5$ in the objective of Eq. (6.20). This value was selected such that both heading and speed control terms were of a comparable order of magnitude with an emphasis on penalising heading control. For stage 2, a total of $|\mathcal{T}| = 15$ time periods are used, with a step of $\epsilon = 2$ minutes. To solve avoidance, `Disjunctive` was used and for recovery stage 11 and both are solved with `Cplex Python API` and a time limit of 5 minutes per solving and 15 minutes per instances. For the first iteration, ρ_i^* is assumed as 1 at the initial iteration and calculated after the recovery in the following

Algorithm 5 Solution algorithm for the 2D ACRP with Trajectory Recovery

Input: $\mathcal{A}, \hat{\theta}, \hat{v}, \underline{q}, \bar{q}, \underline{\theta}, \bar{\theta}, \epsilon$

Output: $q^*, \theta^*, t_i^*, f_i^*$, LB, UB

$\mathcal{P}, \mathcal{P}_I, \mathcal{P}_F, \mathcal{P}_S \leftarrow$ Algorithm 1

LB \leftarrow 0

UB \leftarrow $+\infty$

gap \leftarrow 0

$\bar{a}_i^* \leftarrow 1$ for all $i \in A$

$q, \theta, \delta_x, \delta_y, z, f$, LB \leftarrow Solve Stage 1 - Avoidance using Algorithm 2

if Infeasible **then**

└ Return INFEASIBLE

else

┌ CONVERGED \leftarrow False

┌ **while** CONVERGED = False **do**

┌ $q, \theta, \delta_x, \delta_y, z, f$, LB \leftarrow Solve Stage 1 - Avoidance using Algorithm 2

┌ **for** $(i, j) \in \mathcal{P}$ **do**

┌ Calculate sets $\Omega_{A_i R_j}, \Omega_{A_j R_i}$ and $\Omega_{R_i R_j}$ according to Eqs. (6.14)

┌ Calculate set \mathcal{P}_0

┌ Add cuts 6.16

┌ $t \leftarrow$ Solve Stage 2 - Recovery using Model 11

┌ **if** Infeasible **then**

┌└ Return INFEASIBLE

┌ **else**

┌ $t^* \leftarrow t$

┌ $q^* \leftarrow q$

┌ $\theta^* \leftarrow \theta$

┌ $t^* \leftarrow t$

┌ Update TC_i

┌ Update \bar{a}_i

┌ **if** $\Delta TC_i \leq \epsilon$ **then**

┌└ CONVERGED \leftarrow True

iterations. The preference weight w is considered as $w = 0.5$ as in Chapter 4 and λ is kept as 1.

The performance of the two-stage iterative algorithm is examined. The following tables represent the results for CP and RCP instances. In the header, there are four sections, the first is based on the instances containing $|\mathcal{A}|$ is the number of aircraft and n_c as the number of conflicts. The second group is based on the avoidance stage using the manoeuvre control variable: $Obj.$ is the objective function, ΔTC_i is the optimality gap, Time(s) is the runtime in seconds, followed by total deviation in terms of $|1 - q_i|$, $|\theta_i|$ and f_i , respectively. The third group contains the results from the recovery stage using Model 11. It is reported the average recovery time $\frac{1}{|\mathcal{A}|} \sum_{i \in \mathcal{A}} t_i$, the maximum recovery time $\max_{i \in \mathcal{A}} t_i$ and the minimum recovery time among all aircraft $\min_{i \in \mathcal{A}} t_i$. The fourth group is the overall performance of the algorithm corresponding to $Iter.$ with the number of iterations and overall runtime in seconds Time(s). The gap tolerance was 5%. Table 6.2 summarises the results for CP instances and Table 6.3 for the RCP instances with 10,20 and 30 aircraft.

6.4.2 Illustration

To illustrate the proposed two-stage iterative algorithm, the optimal solution obtained is plotted for CP instances with 5 aircraft and RCP instances with 10, 20 and 30 aircraft, comparing these results with the results obtained using discrete angle formulation. In the Figure 6.4.2, dashed grey lines represent aircraft initial trajectories, red lines represent the avoidance trajectory of stage 1, and blue lines represent recovery trajectories of stage 2 using Model 11 while green lines represent the avoidance trajectory of stage 1 and the orange line represents the trajectory of stage 2 using Algorithm 5.

Those results are very similar for the discretised and continuous angle models, but there are key differentiating factors. Starting with CP-5, it is clear that with a discrete angle (see Figure 6.7a), some aircraft have a small deviation in speed and in heading angle using Model 11. With Algorithm 5, the overall deviations are larger and the recovery time is later. This shows that in the continuous formulation (see Figure 6.7b), the algorithm tends to explore larger deviations in the avoidance stage, that would cause larger recovery time, but with an overall cost that justified such initial decision.

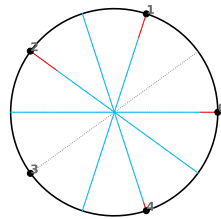
This behaviour is even more accentuated in RCP-10, RCP2-20 and RCP-30. In the first, using continuous angle, it is shown that only 3 aircraft are necessary to be

altered with relatively small deviations and that would be sufficient for guaranteeing separation conditions instead of deviating 9 out of 10 aircraft. The solutions obtained via the continuous angle causes the smallest disturbance in the network, which is a favourable trade for those formulations. For RCP-20 and RCP-30, the continuous angles (Figures 6.7f and 6.7h) cause more aircraft to be altered, but overall, they show the same behaviour: more aircraft with larger avoidance cost and reduced recovery costs but overall cost improved.

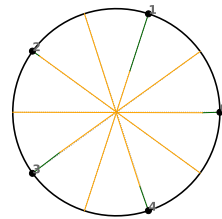
6.4.3 Performance of the Two-Stage Iterative Algorithm

The performance of Algorithm 5 is reported in Table 6.2 for CP instances with 4 to 15 aircraft. In the results, it is observed that the number of conflicts increases with the number of aircraft as expected from those instances where all the aircraft are moving towards to centre. In terms of the objective function value, because of the minimisation of the number of aircraft altered in speed and heading control, the objective function is largely composed of $\sum_{i \in \mathcal{A}} f_i$. For those instances, it is consistently observed that in each instance one aircraft can remain in its initial condition. This differs considerably from the results in Chapter 4 where the global solution would imply that all aircraft needs to perform some manoeuvres. For aircraft that changed speed, it is observed that in most instances, the aircraft does not change from its nominal configuration. In instances with 10 or more aircraft, there are only light deviations. Similarly, the variation in the heading angle is considered negligible for smaller instances. However, it does not increase proportionally with the number of conflicts, revealing that this manoeuvre is used sporadically. Compared with results in Chapter 4, the results obtained using the current model show that fewer aircraft are controlled, but the total deviation is larger. In terms of runtime, all instances with up to 12 aircraft can be solved within the time limit while the remaining instances time out. In the recovery stage, the average recovery time does not increase with the number of aircraft (around 0.32 hours on average), with the minimum recovery time around 5 minutes while the maximum peaks at almost 1 hour. However, all the values of instances with 12 aircraft or more results in time out solutions. For recovery time, most instances can be solved within the time limit, but for the larger instances, the solution obtained in the avoidance stage time-out, as well as the solution in the recovery stage. In terms of iterations, the algorithm only requires up to 3 iterations to obtain a solution within the convergence criterion used.

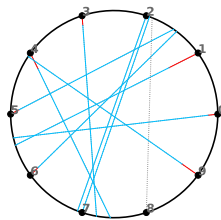
In Table 6.3, the results for RCP instances are presented. For the avoidance stage, the objective function reflects the amount of aircraft that are required to be separated as indicated by f_i , 2.16 for RCP-10, 6.66 for RCP-20 and 12.6 for RCP-30 which reflect the value obtained by $\sum_{i \in \mathcal{A}} f_i$. Comparing the two values, it is noticeable that a large component of the objective function is solely based on that variable. In terms of speed, most aircraft do not perform any relatively large deviation, the values are close to the nominal value, with only 0.02 for RCP-10, 0.10 for RCP-20 and 0.39 for RCP-30. For heading changes, the values are small which reflect the fact that most aircraft do not perform any deviation in heading either: 0.02 for RCP-10, 0.12 for RCP-20 and 0.40 for RCP-30. However, when compared to the heading deviation obtained in Chapter 4, it is clear that heading deviation obtained by Algorithm 2 are considerably smaller and that most of the total deviation is caused by speed changes. The opposite behaviour is observed here. The runtime for those instances is reasonably short and instances with up to 30 aircraft can be solved in less than 10 s. In comparison with the results in Chapter 4, the **Disjunctive** presented gives solutions are balanced with equal contribution from speed and heading control. In these current results, it is stated that speed and heading control are kept to their minimum while most of the control is set around whether certain aircraft need to be altered. Finally, the optimality gap is negligible in all instances. In the Recovery stage, the runtime increases considerably with the number of aircraft given that the number of alternative routes to solve increases drastically: up to 2.14 s for RCP-10, 259 s for RCP-20 and time out for 100% of the instances under 5 minutes of the time limit. In terms of iteration, RCP-10 instances and RCP-20 instances require up to 4 iterations to achieve convergence while solving RCP-30 instances, only up to two iterations are executed due to the time limit.



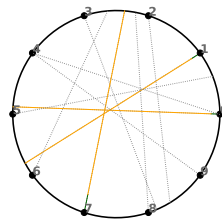
(a) CP-5



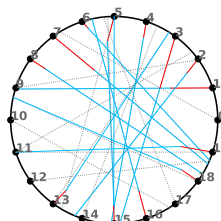
(b) CP-5



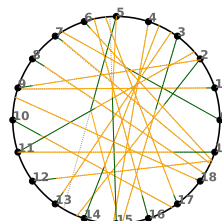
(c) RCP-10-1



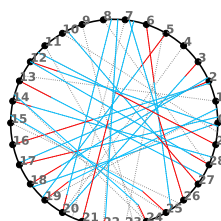
(d) RCP-10-1



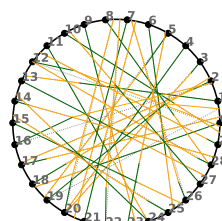
(e) RCP-20-1



(f) RCP-20-1



(g) RCP-30-1



(h) RCP-30-1

Figure 6.7: Comparison in the profile of solutions using discrete angle (first column) and using continuous angle (second column). In the first row, the avoidance stage is in red while the recovery stage is in blue. In the second row, the avoidance stage is in green while the recovery stage is in green.

A	n _c	Avoidance						Recovery					Algorithm 5			
		Obj.	Gap (%)	Time (s)	$\sum_{i \in \mathcal{A}} 1 - q_i $	$\sum_{i \in \mathcal{A}} \theta_i $	$\sum_{i \in \mathcal{A}} f_i$	Obj.	Time (s)	$\frac{1}{ A } \sum_{i \in \mathcal{A}} t_i$	$\max_{i \in \mathcal{A}} t_i$	$\min_{i \in \mathcal{A}} t_i$	TC_i^0	TC_i^n	Iter.	Time (s)
4	6	3.00	1.79E-05	0.02	0.001	7.00E-02	3	3.39E-04	0.23	0.36	0.43	0.30	4.72	4.01	2	0.25
5	10	4.00	9.93E-05	0.02	0.001	1.10E-01	4	1.19E-04	0.30	0.11	0.23	0.03	5.15	4.38	2	0.31
6	15	5.00	9.94E-05	0.03	0.002	8.00E-02	5	6.37E-04	0.66	0.35	0.63	0.03	8.78	7.46	3	0.69
7	21	6.00	9.88E-05	0.11	0.001	1.20E-01	6	3.45E-04	3.85	0.26	0.97	0.07	12.7	10.8	3	3.96
8	28	7.00	9.94E-05	0.23	0.009	1.60E-01	7	9.71E-04	1.86	0.32	0.57	0.07	11.5	9.83	3	2.09
9	36	8.00	1.00E-04	2.89	0.000	2.20E-01	8	6.38E-04	15.1	0.23	0.61	0.03	13.4	11.3	3	18.3
10	45	9.01	9.99E-05	15.4	0.058	2.20E-01	9	1.63E-03	10.6	0.31	0.47	0.07	13.7	11.6	3	26.1
11	55	10.01	1.00E-04	59.2	0.010	3.00E-01	10	1.56E-03	296	0.27	0.97	0.07	20.6	17.5	2	355
12	66	11.01	1.00E-04	230	0.000	3.60E-01	11	2.29E-03	34.2	0.27	0.43	0.12	16.1	13.7	2	264
13	78	12.01	3.59E-04	300	0.050	3.60E-01	12	2.05E-03	55.9	0.24	0.83	0.03	22.8	19.3	2	355
14	91	13.01	5.83E-04	300	0.010	4.00E-01	13	3.27E-03	52.3	0.27	0.43	0.07	19.0	16.1	2	352
15	105	14.02	6.80E-04	300	0.082	4.60E-01	14	3.22E-03	300	0.25	0.63	0.07	23.5	19.9	2	600

Table 6.2: Summary of results for 2D CP instances with a speed control range of $[-6\%, +3\%]$ and a heading control range of $[-30^\circ, +30^\circ]$. All runtimes (Time) are reported in seconds while $\frac{1}{|A|} \sum_{i \in \mathcal{A}} t_i$, $\max_{i \in \mathcal{A}} t_i$ and $\min_{i \in \mathcal{A}} t_i$ are in hours. The optimality gap (Gap) is reported in percentage.

		Avoidance							
$ A $	$ n_c $	Obj.	Gap (%)	Time (s)	$\sum_{i \in \mathcal{A}} 1 - q_i $	$\sum_{i \in \mathcal{A}} \theta_i $	$\sum_{i \in \mathcal{A}} f_i$		
RCP-10	3.10 (1.5)	2.16 (0.93)	3.4E-5 (3.5E-5)	0.01 (0.00)	0.02 (0.03)	0.02 (0.02)	2.16 (0.93)		
RCP-20	13.4 (3.4)	6.66 (1.19)	8.2E-5 (2.4E-5)	0.33 (0.31)	0.10 (0.08)	0.12 (0.06)	6.67 (1.19)		
RCP-30	33.7 (5.7)	12.6 (1.46)	9.1E-5 (1.6E-5)	6.46 (9.02)	0.39 (0.18)	0.40 (0.15)	12.6 (1.47)		

		Recovery				Algorithm 5				
$ A $		Obj.	Time (s)	$\frac{1}{ A } \sum_{i \in \mathcal{A}} t_i$	$\max_{i \in \mathcal{A}} t_i$	$\min_{i \in \mathcal{A}} t_i$	Iter.	ΔTC_i^0	ΔTC_i^n	Time (s)
RCP-10	5.28E-5 (1.7E-4)	2.14 (3.04)	0.24 (0.22)	0.61 (0.39)	0.00 (0.01)	2.6 (1.60)	4.58 (3.19)	3.89 (2.71)	2.16 (3.05)	
RCP-20	4.86E-4 (4.1E-4)	259 (68.8)	0.34 (0.09)	0.94 (0.08)	0.11 (0.01)	3.4 (0.50)	13.6 (3.16)	11.5 (2.69)	259 (61.1)	
RCP-30	8.32E-3 (1.0E-2)	300	0.65 (0.05)	0.95 (0.03)	0.02 (0.02)	1.1 (0.21)	32.2 (2.99)	27.3 (2.54)	600	

Table 6.3: Summary of results for 2D RCP instances with a speed control range of $[-6\%, +3\%]$ and a heading control range of $[-30^\circ, +30^\circ]$. All runtimes (Time) are reported in seconds while $\frac{1}{|A|} \sum_{i \in \mathcal{A}} t_i$, $\max_{i \in \mathcal{A}} t_i$ and $\min_{i \in \mathcal{A}} t_i$ are in hours. The optimality gap (Gap) is reported in percentage.

6.5 Conclusion

The findings are summarised in Section 6.5.1 and future research directions are discussed in Section 6.5.2.

6.5.1 Summary of Findings

A new mixed-integer formulation and two two-stage algorithms for ACRP with trajectory recovery are proposed. First, it is considered the 2D ACRP with discretised heading control and continuous speed manoeuvres and a compact model is proposed by adapting disjunctive separation conditions. The proposed formulation is linear with the decision variables and it can incorporate the bounds for speed and heading control directly without requiring any cut generation or additional constraint to impose speed-violation requirements. It is built on and extended the complex number formulation for the ACRP introduced by Rey and Hijazi (2017) by augmenting its equations of motion to incorporate the set of alternative heading angles. This formulation is assimilated into a two-stage sequential algorithm where the outputs of the avoidance stage are used in the trajectory recovery stage. This model selects the optimal route based on the avoidance angle and the set of timestamps and those routes can be pre-processed. The performance of the proposed formulation and algorithm was tested and the performance of the proposed solution algorithms highlights the scalability of the approach compared to existing methods in the literature. Further, it is concluded that the combination of the avoidance model and trajectory recovery model is capable to solve instances with up to 30 aircraft. Because the size of the pre-processed routes is vital to the performance of the algorithm, a greedy algorithm also was proposed and proved to be comparable to the exact formulation. However, discretising the heading angles is limiting. In terms of performance, for the discretised approach, the runtime of Models 10 and 11 increased exponentially with the number of aircraft, highlighted the challenging nature of the problems. Comparing trajectory recovery approaches, the greedy algorithm scales very efficiently in terms of runtime compared to the exact model is able to find some optimal solutions. Overall the average recovery time of the greedy algorithm is comparable to that of ER. In some cases, the exact algorithm is able to override the decision at the first stage by recovering aircraft initially deviated at $t = 0$, which means that such aircraft do not need to perform any avoidance manoeuvre.

The performance of the second approach revealed that by echoing the cost associated with trajectory recovery, the avoidance can be manipulated in order to pre-

emptively minimise the overall cost of ACRP. On average, in a couple of iterations, it showed that most instances can force the aircraft to have larger deviations in the avoidance stage, but with an earlier recovery time in the recovery stage. In this case, a trade-off between avoidance and recovery is observed. Another advantage of this addition is the concept of stability of the solutions throughout iterations. One of the main issues that happen by having an iterative algorithm, is the variation in the profile of the solution. In each iteration, the algorithm provides a different group of aircraft as a possible candidate to recover and each solution has a different deviation cost and this can be an improvement. As expected, with a higher deviation angle, the deviation cost is higher but the number of aircraft manoeuvring is small. In this situation, adding the f_i variable introduces an extra hurdle into modifying the status of an aircraft. With multiple iterations, it can be expected that less deviation in the whole set of aircraft will be observed, although a larger deviation in individual aircraft. This creates stability in the solution. In the point of view of air traffic controller, solutions where many aircraft are manoeuvring lead to higher workload and are not desirable or implementable solutions.

Alternatively, an adaption of the of Algorithm 2 is proposed to solve the avoidance stage considering speed, heading control and manoeuvre control as decision variables. This is incorporated into an iterative two-stage algorithm that incorporates the projected cost of recovering the aircraft into the avoidance stage. Throughout a relatively small number of iterations, it showed that it can increase the overall deviation in the avoidance pre-emptively to reduce the recovery cost and ultimately the total cost. In the numerical experiments, the performance of the proposed algorithms shows that the number of aircraft that are required to be altered is reduced and for those that are required to be changed, the deviation is larger in terms of heading angles but the recovery time is smaller compared to the discretised version. In comparison with the *Disjunctive* results, it also shows that while the former provides solutions that are more balanced in terms of manoeuvres, they are also more invasive because it affects the whole set of aircraft. The algorithm present in this chapter presents an alternative solution where fewer aircraft are controlled will higher deviations, suggesting that this behaviour improves the total cost.

6.5.2 Future Research and Perspectives

The biggest limitation in the iterative two-stage algorithm is the decomposition of conflict avoidance and trajectory recovery. Although this is a common practice in mathematical programming, there is not guarantee of the quality of the solution.

Ideally, a global solution should be created by jointly optimising both stages in a unified formulation. This is heavily challenged by the non-linearity and complexity that comes from such formulations. Therefore, further research into modelling this problem more simply and efficiently is needed. In addition, the cost of recovery is projected into the avoidance stage throughout the iterations. Alternatively, stochastic optimization methods can be used as an attempt to determine the expected cost of recovery manoeuvres already incorporate in the avoidance stage. Finally, the discretisation of any variable is a limitation and modelling recovery time as a continuous variable may help in reducing the total cost of trajectories.

Chapter 7

Conclusion

In this chapter, the contributions and the results discussed throughout this thesis are revisited. This thesis began with four main aims: i) to produce global optimisation methods based on mathematical programming that are scalable and efficient; ii) to introduce a formal analysis of the aircraft separation conditions as well as to characterise conflict-free trajectories for the deterministic version of the ACRP; iii) to incorporate uncertainty on trajectory prediction methods within mathematical programming based approaches for the ACRP and iv) to identify the limits of richer mathematical programming formulation that can be developed to accommodate realist ATC operations. These aims are pursued in the four core chapters of this thesis.

A summary of the thesis is presented in Section 7.1 where the main points of each chapter and the main contributions are summarised. Then, modelling assumptions and their limitations are discussed in Section 7.2, as well as the challenges and future research. Final remarks are discussed in Section 7.3.

7.1 Summary and Contributions

This thesis is dedicated to exploring the characteristics, analysis and implementation of novel mathematical programming formulations for the ACRP. After introducing the main components of air traffic control in Chapter 1 and reviewing the state-of-the-art in Chapter 2, basic mathematical programming formulations for the ACRP are presented in Chapter 3. The goal of the ACRP is to find optimal trajectories for a set of aircraft subject to separation constraints and available manoeuvres. The three state-of-the-art formulations were reviewed and numerical results illustrating their behaviour were reported. Three formulations for the two-dimensional problem with continuous speed and heading control are formally reviewed. It is also shown how a non-linear formulation can be linearised and that is the premise to obtain disjunctive

linear separation constraints. Further, the shadow formulation, it is showed that the disjunctive and the shadow formulation are equivalent. This solidifies the fact that all formulations are, at their core, equivalent. The difference between the disjunctive and shadow formulation are based on the number of binary variables: the shadow formulation requires at least four binaries while the disjunctive formulation requires only one. The difference between the non-linear formulation and the disjunctive is that the former has non-linear components, while the latter is composed by a set of linear conditions. Such conclusions revealed that even though those formulations are a solid cornerstone, they suffer from many issues such as non-linearity and trigonometric operators. Those factors can hinder the performance of such formulations in terms of complexity and scalability.

In Chapter 4, new mixed-integer formulations for the deterministic ACRP were proposed. The 2D ACRP is first considered with continuous speed and heading control manoeuvres based on the disjunctive separation conditions. Those conditions are linear with regards to aircraft relative velocity variables and only require a single binary variable per pair of aircraft. In addition, a simple pre-processing algorithm was introduced to identify aircraft pairs that are conflict-free or non-separable for any combination of controls. This can assist in reducing the size of instances by eliminating pairs that are in conflict-free trajectories. The complex number formulation is extended by augmenting its objective function with a preference weight to balance the trade-off between speed and heading deviations. This 2D formulation is extended to the context of altitude control by flight level (FL) change and a lexicographic optimisation is proposed to solve the 2D+FL ACRP which aims to minimise the number of FL changes in priority and resolve outstanding conflicts by 2D trajectory control. The following methodological contributions to the field can be stated about this chapter: i) the proposed disjunctive linear pairwise aircraft separation conditions introduced by Rey and Hijazi (2017) are shown to be equivalent to the classical non-linear separation conditions; ii) the set of 2D conflict-free trajectories based on aircraft velocity bounds is fully characterised and a simple pre-processing algorithm is proposed to identify aircraft pairs which are either always conflict-free, or which cannot be separated using speed and heading control only; iii) existing convex relaxations are used and a novel exact constraint generation algorithm for the 2D ACRP is presented; and, iv) altitude control is incorporated in the proposed formulations and lexicographic optimisation formulation is introduced, whose primary objective is to minimise the number of FL changes before resolving outstanding conflicts via 2D velocity control. Numerical experiments were conducted on four types of conflict

resolution benchmarking instances consisting of a total of 2072 instances to test the performance of the proposed mixed-integer formulations and algorithms. It is shown that the proposed mixed-integer formulations and exact solution methods improve on existing exact approaches in the literature in terms of scalability. Notably, the benefits of using the proposed method are quantified by benchmarking it against two methods based on state-of-the-art approaches. The first benchmark corresponds to the method proposed by Rey and Hijazi (2017) which uses the same disjunctive linear separation conditions as that of the proposed method, but in a less advanced algorithm that is not always able to find optimal or even feasible solutions. The second benchmark is based on the classical so-called shadow separation conditions and uses the same algorithmic structure as that of the proposed method. The experiments reveal that the proposed method significantly outperforms both benchmarks. In addition, an analytical approach was developed to solve two-aircraft conflict resolution problem based on the Lagrangian function and the applications of the Karush-Kuhn-Tucker conditions. Numerical tests using random variations of two-aircraft instances showed that the ACRP can be instantly solved and this has the potential to be used to develop global optimisation approaches for multi-aircraft problems.

In Chapter 5, the ACRP under trajectory prediction uncertainty is tackled. A robust optimisation approach is proposed and it aims to guarantee that aircraft are separated for any realisation of the random data and to identify minimum-deviation trajectories. The robust optimisation approach proposed by Bertsimas and Sim (2004) is proposed to control the level of robustness in the formulation and adapt state-of-the-art solution methods to the deterministic ACRP to solve the resulting robust ACRP. The sources of uncertainty are weather events and measurements errors and a new formulation for the robust ACRP under trajectory prediction uncertainty is proposed. For this, the ACRP with continuous speed and heading control manoeuvres is used and it is showed that robust separation constraints can be reformulated as tractable integer-linear constraints using state-of-the-art approaches in robust optimisation. The complex number formulation for the ACRP is adapted and an exact algorithm to solve the resulting robust complex number formulation model to optimality. The following methodological contributions to the field are made in this Chapter: i) a model of aircraft trajectory prediction uncertainty is created based on aircraft velocity components; ii) it is shown that the proposed uncertainty model can be incorporated in a robust optimisation formulation for the ACRP; iii) the complex number formulation of Rey and Hijazi (2017) is adapted and an exact algorithm of Dias et al. (2020) to solve the robust ACRP is proposed; iv) numerical experiments

conducted on benchmarking instances to test the proposed robust ACRP formulation. The tests reveal that increasing the level of robustness or the size of the uncertainty set rapidly increase the likelihood of infeasibility; and, v) re- and post-optimisation analyses reveal that the number of conflicts and the total minimal pairwise distance between aircraft trajectories can explain the behaviour of the model. A series of numerical experiments on benchmarking instances of the literature was conducted to explore the behaviour of the robust ACRP and test the computational performance of the proposed approach. Upon testing, the performance of the proposed solution algorithms highlights the scalability of the approach compared to existing deterministic methods in the literature. As far as the literature review in Chapter 2 goes, this is the first exact robust optimisation formulation for the ACRP.

In Chapter 6, new formulations for the deterministic ACRP are extended to incorporate aircraft trajectory recovery, which is absent in the vast majority of mathematical programming approaches for conflict resolution. Two new two-stage algorithms for aircraft conflict resolution with trajectory recovery are presented. In these approaches, the speed and heading of the aircraft are first optimised to avoid conflicts while minimising the deviation from their initial trajectories. Then, in a second stage, aircraft trajectories are modified to recover a target position on the aircraft's initial trajectories. The first approach considered the heading angle is discretised, therefore recovery analysis is done by selecting the optimal trajectories between a given finite set of alternative trajectories. In this case, the recovery can be simplified as a route selection problem. Based on the numerical results, this formulation represents an alternative solution to this problem. However, because it contains variable discretisation, this can be a limiting factor. The performance of this approach is tested via an exact recovery approach and a greedy recovery algorithm. A second approach was also implemented considering heading angle as a continuous variable.

In that approach, the avoidance stage is handled similarly as in Chapter 4 with the additional of discrete variable to indicate which aircraft is controlled. In this formulation, the proposed objective function minimises the total deviation in terms of speed and heading angle control as well as the amount of aircraft controlled. The performance of this approach was tested by an iterative two-stage algorithm. The following methodological contributions to the field are made in this Chapter: i) a model of aircraft trajectory recovery is created based on a two-stage algorithm; ii) it is shown that the proposed algorithm is capable to reduce the overall cost of conflict avoidance by increasing deviation in action and reducing recovery time in recovery; iii) the complex number formulation is adapted into a heading angle discretised model

and the exact algorithm of Dias et al. (2020) to solve ACRP is adapted; iv) numerical experiments conducted on benchmarking instances to test the proposed algorithms. The tests reveal that increasing the importance of avoidance and recovery can be controlled throughout different iterations to explore several behaviours; and, v) post-optimisation analyses reveal that the number of iterations and the different level of variable discretisation can explain the behaviour of the algorithms. The discrete formulation showed that solving recovery in an exact formulation or a greedy algorithm are comparable and it can provide solution with lower overall cost. In the continuous approach, the recovery cost can be incorporate into avoidance to obtain solutions with lower costs. In this case, a trade-off between avoidance and recovery is observed. The iterative approach is capable of building non-trivial solutions that do not compromise the recovery cost (keeping it at minimum value) while manipulates the trajectory of only a few aircraft.

7.2 Limitations and Future Research

The proposed approaches for the ACRP rely on several assumptions which may be limiting in practice. One of the modelling assumptions at the core of the proposed mixed-integer formulations is the assumption of uniform motion laws, which translates into infinite acceleration and deceleration rates. While such an assumption may be plausible for constrained aircraft speed control, further research is needed to assess the practicality of this assumption when considering varying types of aircraft or different airspace environments, e.g. urban air mobility. At the same time, empirical observations show that most scenarios have aircraft using different motion laws, which are not easily tractable via uniform linear formulations.

All formulations presented in this thesis assumed that it has a central control system that is in charge of determining all the variables for each aircraft. This concept is currently the most used format of ATC, but as the air capacity start to reach its limits and due to the air traffic controller high workload, the concept of free-flight can be incorporate, even though it might not be the most appealing technique in the future. This technique can be applied in areas with low flight density such as the Pacific Ocean, but it also leaves the aircraft vulnerable due to the lack of centralised assistance in case of emergency. Another issue is the necessity of continuous communication between aircraft will also cause security issues related data availability and substantiation. An additional assumption is that all aircraft start moving in that specific airspace at the same time, which is commonly used for simplifications

aspects, but it does not correspond to reality. The usage of altitude changes can also be challenged. In Chapter 4, a lexicographic approach is used, where the flight assignment is done before the 2D ACRP is solved in each flight level individually. Although the reasoning behind is in the accordance with the airspace structure, some solutions could also be obtained by optimising flight level, speed and heading control simultaneously. Such results could show a better performance than those presented.

For the robust components in Chapter 5, a simple model was used where a disturbance was incorporated in the velocity component. This formulation is standard, commonly used in the literature and very effective, but it is rather basic. It can be argued that a more sophisticated formulation could be used which can ultimately make the model more difficult, but can also represent a more dynamic version. In terms of computational experiments, the analysis used in the formulation has focused on a uniform uncertainty model across the aircraft. More realistic air traffic scenarios, possibly generated from weather data, should be explored to gain more practical insights into the impact of robustness in aircraft conflict resolution. Unfortunately, such data is not publicly available and future research efforts may be needed to augment existing data repositories for conflict resolution problems. The coordination of aircraft conflict resolution manoeuvres also presents considerable operational challenges. Although robust components were addressed, it is only taken into consideration in the avoidance stages (according to the conditions already reinforced in the thesis), there is also some level of uncertainty to be analysis in trajectory recovery.

The usage of heading deviations for conflict resolution also raises concerns regarding aircraft trajectory recovery. It is well-acknowledged that resolving conflicts does not guarantee conflict-free recovery trajectories. Once the aircraft have their trajectories altered in order to avoid conflict, to guarantee that they will eventually return towards their original destination will not be always free from conflict and further analysis is required. As stated before, the concept of "recovery" is also questionable. Some models such as heuristics and genetic programming handle the trajectory of the aircraft as a single profile component, which ultimately does not have to concern about recovery. However, using mathematical programming, as it was applied in this thesis, it also raises the same concern and therefore requires another level of optimisation. In Chapter 6, two attempts of solving this problem using mathematical programming were made. In those, the proposed algorithm is a two-stage iterative process that does not guarantee global optimisation. Although they showed positive results, such results still are based on significant conditions such as time discretisation

and space discretisation. There is also still room to improve on such formulations in terms of computational performance and scalability.

The results and contributions presented in this thesis showed that there is a solid effort into improving current state-of-the-art formulations, but many aspects require further attention. Future research can look into alternatives where different aircraft have the independence of movements and are controlled without a central component. In this scenario, free-flight algorithms could be put into practice. In such models, aircraft only have access to those that are in a limited vicinity and therefore many pairing that will not be in conflict do not need to be incorporated into any formulation.

Although robust optimisation was used, there is another way to incorporate randomness elements into those formulations and stochastic optimisation can be an alternative. Even though robust optimisation allows variations as a continuous variable, stochastic allows analysing scenarios in a limited way. If those scenarios are created properly, it shows that this formulation can be used even on larger scales. In addition, the presence of randomness concerns not only the avoidance (action) stage and therefore, a full analysis of trajectory recovery under uncertainty should be carried out.

7.3 Final Remarks

The motivation for this thesis was to address some of the gaps in the literature related to exact solutions of the ACRP, the effect of random events onto trajectory prediction and trajectory recovery. It is clear that the contributions presented in this thesis assisted on addressing some of those gaps and some level of novelty is proposed throughout the models. However, there is still much more research required to be done. Also, most of those formulations have a considerable runtime, their performance is towards obtaining optimal solutions in any case. With the gradual advent of automation technologies and computational performance, these models might become more and more relevant. Hence, it has never been timely enough to explore such aspects of ATC and to ask more complicated questions relating to this field.

It is hoped that the formulations presented in this thesis will kindle further interest in this field in future researchers and possible implementation of some version of those models and that the developments formulated in this thesis can be used to improve the efficiency of ATC and conflict resolution problem.

Bibliography

- Abu-Rayash, A. and Dincer, I. (2020). Analysis of mobility trends during the covid-19 coronavirus pandemic: Exploring the impacts on global aviation and travel in selected cities. *Energy research & social science*, 68:101693. 1.1
- Adler, N., Hanany, E., and Proost, S. (2014). Managing european air traffic control provision. *Fourth SESAR Innovation Days, 25th–27th November*. 1.4
- Alonso-Ayuso, A., Escudero, L. F., and Martín-Campo, F. J. (2011). Collision avoidance in air traffic management: A mixed-integer linear optimization approach. *IEEE Transactions on Intelligent Transportation Systems*, 12(1):47–57. 2.4.2, 2.4.3, 3.3, 3.4, 4.3, 4.7.1
- Alonso-Ayuso, A., Escudero, L. F., and Martín-Campo, F. J. (2014). Exact and approximate solving of the aircraft collision resolution problem via turn changes. *Transportation Science*, 50(1):263–274. 2.4.2, 2.4.3, 3, 4.9.2
- Alonso-Ayuso, A., Escudero, L. F., and Martín-Campo, F. J. (2016). An exact multi-objective mixed integer nonlinear optimization approach for aircraft conflict resolution. *TOP*, 24(2):381–408. 2.4.2, 3.3, 3.4, 4.7.1
- Andreatta, G. and Romanin-Jacur, G. (1987). Aircraft flow management under congestion. *Transportation Science*, 21(4):249–253. 2.2
- Andrews, J. (1977). A relative motion analysis of horizontal collision avoidance. In *SAFE Association, Annual Symposium, 15 th, Las Vegas, Nev*, pages 58–61. 2.4.1
- Atamtürk, A. and Zhang, M. (2007). Two-stage robust network flow and design under demand uncertainty. *Operations Research*, 55(4):662–673. 2.4.3
- Bakker, G. and Blom, H. A. (1993). Air traffic collision risk modelling. In *Proceedings of 32nd IEEE Conference on Decision and Control*, pages 1464–1469. IEEE. 2.4.1

- Barnier, N. and Allignol, C. (2009). 4d-trajectory deconfliction through departure time adjustment. In *ATM 2009, 8th USA/Europe Air Traffic Management Research and Development Seminar*, pages pp–xxxx. 1.5
- Bertsimas, D. and Sim, M. (2004). The price of robustness. *Operations research*, 52(1):35–53. 5.1.2, 5.1.2, 7.1
- Bianco, L. and Bielli, M. (1992). Air traffic management: Optimization models and algorithms. *journal of advanced transportation*, 26(2):131–167. 2.2
- Bienstock, D., Chertkov, M., and Harnett, S. (2013). Robust modeling of probabilistic uncertainty in smart grids: Data ambiguous chance constrained optimum power flow. In *52nd IEEE Conference on Decision and Control*, pages 4335–4340. IEEE. 2.4.3
- Bienstock, D., Chertkov, M., and Harnett, S. (2014). Chance-constrained optimal power flow: Risk-aware network control under uncertainty. *Siam Review*, 56(3):461–495. 2.4.3
- Bilimoria, K. (2000). A geometric optimization approach to aircraft conflict resolution. In *18th Applied aerodynamics conference*, page 4265. 2.4.2, 3.4
- Bilimoria, K., Lee, H., Mao, Z.-H., and Feron, E. (2000). Comparison of centralized and decentralized conflict resolution strategies for multiple-aircraft problems. In *18th Applied Aerodynamics Conference*, page 4268. 2.4.1, 3
- Bilimoria, K., Sridhar, B., and Chatterji, G. (1996). Effects of conflict resolution maneuvers and traffic density on free flight. In *Guidance, Navigation, and Control Conference*, page 3767. 4.3
- Bonini, D., Dupré, C., and Granger, G. (2009). How erasmus can support an increase in capacity in 2020. In *Proceedings of the 7th International Conference on Computing, Communications and Control Technologies: CCCT*, page 6. Citeseer. 3.7, 4.7.1, 5.2.1
- Brudnicki, D. and McFarland, A. (1997). User request evaluation tool (uret) conflict probe performance and benefits assessment. In *Proc. USA/Europe ATM Seminar*. Eurocontrol. 2.4.1

- Brudnicki, D. J., Lindsay, K. S., and McFarland, A. L. (1997). Assessment of field trials, algorithmic performance, and benefits of the user request evaluation tool (uret) conflict probe. In *16th DASC. AIAA/IEEE Digital Avionics Systems Conference. Reflections to the Future. Proceedings*, volume 2, pages 9–3. IEEE. 2.4.1
- Burdun, I. Y. and Parfentyev, O. M. (1999). Ai knowledge model for self-organizing conflict prevention/resolution in close free-flight air space. In *1999 IEEE Aerospace Conference. Proceedings (Cat. No. 99TH8403)*, volume 2, pages 409–428. IEEE. 2.4.1
- Bureau, A. T. (2020). Effects of novel coronavirus (covid-19) on civil aviation: Economic impact analysis. *International Civil Aviation Organization (ICAO), Montréal, Canada*. (document), 1.1, 1.2
- Burgess, D. W., Altman, S., and Wood, M. L. (1994). Tcas: Maneuvering aircraft in the horizontal plane. 2.4.1
- Cafieri, S. and Durand, N. (2014). Aircraft deconfliction with speed regulation: new models from mixed-integer optimization. *Journal of Global Optimization*, 58(4):613–629. 3.1
- Cafieri, S. and Omheni, R. (2017). Mixed-integer nonlinear programming for aircraft conflict avoidance by sequentially applying velocity and heading angle changes. *European journal of operational research*, 260(1):283–290. 2.4.2, 3, 3.1, 3.6, 3.7, 4.7.1, 5.2.1
- Cafieri, S. and Rey, D. (2017). Maximizing the number of conflict-free aircraft using mixed-integer nonlinear programming. *Computers & Operations Research*, 80:147–158. 2.4.2, 2.4.3, 3.1, 3.2, 3.6
- Carpenter, B., Kuchar, J., Carpenter, B., and Kuchar, J. (1997). Probability-based collision alerting logic for closely-spaced parallel approach. In *35th Aerospace sciences meeting and exhibit*, page 222. 2.4.1
- Cerulli, M., d’Ambrosio, C., Liberti, L., and Pelegrín, M. (2020). Detecting and solving aircraft conflicts using bilevel programming. 2.4.2
- Chakravarthy, A. and Ghose, D. (1998). Obstacle avoidance in a dynamic environment: A collision cone approach. *IEEE Transactions on Systems, Man, and Cybernetics-Part A: Systems and Humans*, 28(5):562–574. 2.4.1

- Chiou, S.-W. (2016). Robust stochastic design of signal-controlled road network under uncertain travel demands. *IEEE Transactions on Automatic Control*, 62(7):3152–3164. 2.4.3
- Clarke, J.-P. B., Solak, S., Chang, Y., Ren, L., and Vela, A. (2009). Air traffic flow management in the presence of uncertainty. In *Proceedings of the 8th USA/Europe Air Traffic Seminar (ATM’09)*. 2.4.3
- Coffrin, C., Hijazi, H. L., and Van Hentenryck, P. (2015). The qc relaxation: A theoretical and computational study on optimal power flow. *IEEE Transactions on Power Systems*, 31(4):3008–3018. 4.2
- Conway, E. M. (2004). Echoes in the grand canyon: Public catastrophes and technologies of control in american aviation. *History and technology*, 20(2):115–134. 1.1
- Cplex, I. I. (2009). V12. 1: User’s manual for cplex. *International Business Machines Corporation*, 46(53):157. 4.7.1, 5.2.1
- Darr, S., Ricks, W., and Lemos, K. A. (2008). Safer systems: A nextgen aviation safety strategic goal. In *2008 IEEE/AIAA 27th Digital Avionics Systems Conference*, pages 2–A. IEEE. 2.3
- Dias, F. H., Hijazi, H., and Rey, D. (2021). Disjunctive linear separation conditions and mixed-integer formulations for aircraft conflict resolution. *European Journal of Operational Research*. 4, 5.1.3, 6.1
- Dias, F. H., Rahme, S., and Rey, D. (2020). A two-stage algorithm for aircraft conflict resolution with trajectory recovery. In *ICRAT 2020 Ninth International Conference on Research in Air Transportation*. ICRAT. 4.9.2, 7.1
- Dias, F. H. and Rey, D. (2020). Robust aircraft conflict resolution under trajectory prediction uncertainty. *arXiv preprint arXiv:2012.08230*. 5
- Ding, T., Bie, Z., Bai, L., and Li, F. (2016). Adjustable robust optimal power flow with the price of robustness for large-scale power systems. *IET Generation, Transmission & Distribution*, 10(1):164–174. 2.4.3
- Dougui, N., Delahaye, D., Puechmorel, S., and Mongeau, M. (2013). A light-propagation model for aircraft trajectory planning. *Journal of Global Optimization*, 56(3):873. 2.4.2, 2.4.3

- Dougui, N. E., Delahaye, D., Puechmorel, S., and Mongeau, M. (2011). Light propagation algorithm for aircraft trajectory planning. In *American Control Conference (ACC), 2011*, pages 2143–2147. IEEE. 2.4.2
- Duong, V. N. and Hoffman, E. G. (1997). Conflict resolution advisory service in autonomous aircraft operations. In *16th DASC. AIAA/IEEE Digital Avionics Systems Conference. Reflections to the Future. Proceedings*, volume 2, pages 9–3. IEEE. 2.4.1
- Durand, N. and Alliot, J.-M. (2009). Ant colony optimization for air traffic conflict resolution. 2.4.2, 2.4.3, 3.6
- Durand, N., Alliot, J.-M., and Chansou, O. (1997). Optimal resolution of en route conflicts. In *Proceedings of the 1st USA/Europe Seminar*. 1.5, 2.4.1, 2.4.2, 2.4.3
- Eby, M. S. (1994). A self-organizational approach for resolving air traffic conflicts. *Lincoln Laboratory Journal*. 2.4.1
- Eby, M. S. and Kelly, W. E. (1999). Free flight separation assurance using distributed algorithms. In *1999 IEEE Aerospace Conference. Proceedings (Cat. No. 99TH8403)*, volume 2, pages 429–441. IEEE. 2.4.1
- Erotokritou, C. (2012). The legal liability of air traffic controllers. *Inquiries Journal*, 4(02). 1.1
- Ford, R. (1987). The conflict resolution process for tcas ii and some simulation results. *The Journal of Navigation*, 40(3):283–303. 2.4.1
- Ford, R. and Powell, D. (1990). A new threat detection criterion for airborne collision avoidance systems. *The Journal of Navigation*, 43(3):391–403. 2.4.1
- Fourer, R., Gay, D. M., and Kernighan, B. W. (1987). *AMPL: A mathematical programming language*. AT & T Bell Laboratories Murray Hill, NJ. 3.7
- Franco, A., Rivas, D., and Valenzuela, A. (2017). Optimal aircraft path planning considering wind uncertainty. In *Proceedings of the 7th European Conference for Aeronautics and Space Sciences, Milan, Italy*, pages 3–6. 2.4.3
- Frazzoli, E., Mao, Z.-H., Oh, J.-H., and Feron, E. (2001). Resolution of conflicts involving many aircraft via semidefinite programming. *Journal of Guidance, Control, and Dynamics*, 24(1):79–86. 2.4.1, 2.4.2, 3, 3.3

- Gaertner, M. and Lutz, A. (2016). Visual flight rules approach to airports. US Patent 9,424,756. 2.3
- Gazit, R. Y. (1997). Aircraft surveillance and collision avoidance using gps. 2.4.1
- González Arribas, D., Soler Arnedo, M. F., and Sanjurjo Rivo, M. (2016). Wind-based robust trajectory optimization using meteorological ensemble probabilistic forecasts. 2.4.3
- Gorissen, B. L., Yamkoğlu, İ., and den Hertog, D. (2015). A practical guide to robust optimization. *Omega*, 53:124–137. 5.1.2
- Grabbe, S., Sridhar, B., and Mukherjee, A. (2009). Sequential traffic flow optimization with tactical flight control heuristics. *Journal of Guidance, Control, and Dynamics*, 32(3):810–820. 2.4.3
- Harper, K., Mulgund, S., Guarino, S., Mehta, A., and Zacharias, G. (1999). Air traffic controller agent model for free flight. In *Guidance, Navigation, and Control Conference and Exhibit*, page 3987. 2.4.1
- Harrison, M. (1998). The economics of world war ii: an overview. *The economics of World War II: Six great powers in international comparison*, pages 1–42. 1.1
- Havel, K. and Husarčík, J. (1989). A theory of the tactical conflict prediction of a pair of aircraft. *The Journal of Navigation*, 42(3):417–429. 2.4.1
- Hentzen, D., Kamgarpour, M., Soler, M., and González-Arribas, D. (2018). On maximizing safety in stochastic aircraft trajectory planning with uncertain thunderstorm development. *Aerospace Science and Technology*, 79:543–553. 2.4.3
- Heuvelink, G. B. and Blom, H. A. (1988). An alternative method to solve a variational inequality applied to an air traffic control example. In *Analysis and optimization of systems*, pages 617–628. Springer. 2.4.1
- Hijazi, H., Coffrin, C., and Van Hentenryck, P. (2017). Convex quadratic relaxations for mixed-integer nonlinear programs in power systems. *Mathematical Programming Computation*, 9(3):321–367. 4.2
- Hijazi, H. L., Bonami, P., and Ouorou, A. (2014). A Note on Linear On/Off Constraints. *NICTA Technical Report*. 4.2

- Hoekstra, J., Van Gent, R., and Ruigrok, R. (1998). Conceptual design of free flight with airborne separation assurance. In *Guidance, Navigation, and Control Conference and Exhibit*, page 4239. 2.4.1
- Horonjeff, R., McKelvey, F. X., Sproule, W. J., and Young, S. B. (2010). *Planning and design of airports*. McGraw-Hill Education. 2.1
- Hu, J., Prandini, M., and Sastry, S. (2002). Optimal coordinated maneuvers for three-dimensional aircraft conflict resolution. *Journal of Guidance, Control, and Dynamics*, 25(5):888–900. 4.3
- ICAO, A. (2010). to the convention on international civil aviation. *Montreal, Canada*, 1. 1.5
- Irvine, R. (1998). The gears conflict resolution algorithm. In *Guidance, Navigation, and Control Conference and Exhibit*, page 4236. 2.4.1
- Irvine, R. (2002). A geometrical approach to conflict probability estimation. *Air Traffic Control Quarterly*, 10(2):85–113. 2.4.3
- Isaacson, D. R. and Erzberger, H. (1997). Design of a conflict detection algorithm for the center/tracon automation system. In *16th DASC. AIAA/IEEE Digital Avionics Systems Conference. Reflections to the Future. Proceedings*, volume 2, pages 9–3. IEEE. 2.4.1
- Jacquemart, D. and Morio, J. (2016). Adaptive interacting particle system algorithm for aircraft conflict probability estimation. *Aerospace Science and Technology*, 55:431–438. 2.4.3
- Janic, M. (1994). Modelling extra aircraft fuel consumption in an en-route airspace environment. *Transportation Planning and Technology*, 18(3):163–186. 2.2
- Janić, M. (1997). A model of air traffic control sector capacity based on air traffic controller workload. *Transportation Planning and Technology*, 20(4):311–335. 2.2
- Janić, M. and Tošić, V. (1991). En route sector capacity model. *Transportation Science*, 25(4):299–307. 2.2
- Kelly, W. E. (1999). Conflict detection and alerting for separation assurance systems. In *Gateway to the New Millennium. 18th Digital Avionics Systems Conference. Proceedings (Cat. No. 99CH37033)*, volume 2, pages 6–D. IEEE. 2.4.1

- Kim, J., Tandale, M., and Menon, P. (2009). Air-traffic uncertainty models for queuing analysis. In *9th AIAA Aviation Technology, Integration, and Operations Conference (ATIO) and Aircraft Noise and Emissions Reduction Symposium (ANERS)*, page 7053. 2.4.3
- Kosecka, J., Tomlin, C., Pappas, G., and Sastry, S. (1997). Generation of conflict resolution maneuvers for air trac management. In *International Conference on Intelligent Robots and Systems (IROS)*, pages 1598–1603. 2.4.1
- Krozel, J. and Peters, M. (1997). Conflict detection and resolution for free flight. *Air Traffic Control Quarterly*, 5(3):181–212. 2.4.1
- Kuchar, J. K. and Yang, L. C. (2000). A review of conflict detection and resolution modeling methods. *IEEE Transactions on intelligent transportation systems*, 1(4):179–189. 2.4, 2.4.1
- Lachner, R. (1997). Collision avoidance as a differential game: Real-time approximation of optimal strategies using higher derivatives of the value function. In *1997 IEEE International Conference on Systems, Man, and Cybernetics. Computational Cybernetics and Simulation*, volume 3, pages 2308–2313. IEEE. 2.4.1
- Lee, C., Lee, K., and Park, S. (2013). Benders decomposition approach for the robust network design problem with flow bifurcations. *Networks*, 62(1):1–16. 2.4.3
- Lee, K.-S. (2006). A study on change of aviation law and system to aviation security for major countries after 9. 11 aviation terror. *The Korean Journal of Air & Space Law and Policy*, 21(2):123–155. 1.1
- Lehouillier, T., Omer, J., Soumis, F., and Desaulniers, G. (2017). Two decomposition algorithms for solving a minimum weight maximum clique model for the air conflict resolution problem. *European Journal of Operational Research*, 256(3):696–712. 2.4.2, 2.4.3, 3.6, 3.6
- LOVE, W. (1988). Tcas iii-bringing operational compatibility to airborne collision avoidance. In *Digital Avionics Systems Conference*, page 4004. 2.4.1
- Machol, R. E. (1995). Thirty years of modeling midair collisions. *Interfaces*, 25(5):151–172. 1.1
- Mattos, B. (2004). Santos dumont and the dawn of aviation. In *42nd AIAA Aerospace Sciences Meeting and Exhibit*, page 106. 1.1

- McCormick, G. P. (1976). Computability of global solutions to factorable nonconvex programs: Part i—convex underestimating problems. *Mathematical programming*, 10(1):147–175. 4.5
- McDowell, J. C. (2018). The edge of space: Revisiting the karman line. *Acta Astronautica*, 151:668–677. 1.2
- McNally, B., Bach, R., and Chan, W. (1998). Field test evaluation of the ctas conflict prediction and trial planning capability. In *Guidance, Navigation, and Control Conference and Exhibit*, page 4480. 2.4.1
- Menon, P. K., Sweriduk, G. D., and Sridhar, B. (1999). Optimal strategies for free-flight air traffic conflict resolution. *Journal of Guidance, Control, and Dynamics*, 22(2):202–211. 2.4.1
- Morgan, M. G., Henrion, M., and Small, M. (1990). *Uncertainty: a guide to dealing with uncertainty in quantitative risk and policy analysis*. Cambridge university press. 2.4.3
- Murça, M. C. R. (2017). A robust optimization approach for airport departure metering under uncertain taxi-out time predictions. *Aerospace Science and Technology*, 68:269–277. 2.4.3
- Navazio, L. and Romanin-Jacur, G. (1998). The multiple connections multi-airport ground holding problem: Models and algorithms. *Transportation Science*, 32(3):268–276. 2.2
- Niedringhaus, W. P. (1992). Maneuver option manager: Automated simplification of complex air traffic control problems. *IEEE transactions on systems, man, and cybernetics*, 22(5):1047–1057. 2.4.1
- Niedringhaus, W. P. (1995). Stream option manager (som): Automated integration of aircraft separation, merging, stream management, and other air traffic control functions. *IEEE Transactions on Systems, Man, and Cybernetics*, 25(9):1269–1280. 2.2, 2.4.1
- Nilim, A., El Ghaoui, L., Duong, V., and Hansen, M. (2001). Trajectory-based air traffic management (tb-atm) under weather uncertainty. In *Proc. of the Fourth International Air Traffic Management R&D Seminar ATM*. 2.4.3
- Nolan, M. (2010). *Fundamentals of air traffic control*. Cengage learning. 2.3

- Odoni, A. R. (1987). The flow management problem in air traffic control. In *Flow control of congested networks*, pages 269–288. Springer. 2.2
- Omer, J. (2015). A space-discretized mixed-integer linear model for air-conflict resolution with speed and heading maneuvers. *Computers & Operations Research*, 58:75–86. 2.4.2, 2.4.3
- Omer, J. and Farges, J.-L. (2013). Hybridization of nonlinear and mixed-integer linear programming for aircraft separation with trajectory recovery. *IEEE Transactions on Intelligent Transportation Systems*, 14(3):1218–1230. 2.4.2
- Ordóñez, F. and Zhao, J. (2007). Robust capacity expansion of network flows. *Networks: An International Journal*, 50(2):136–145. 2.4.3
- Ota, T., Nagati, M., and Lee, D.-C. (1998). Aircraft collision avoidance trajectory generation. In *Guidance, Navigation, and Control Conference and Exhibit*, page 4241. 2.4.1
- Paielli, R. A. and Erzberger, H. (1997). Conflict probability estimation for free flight. *Journal of Guidance, Control, and Dynamics*, 20(3):588–596. 2.4.1
- Pallottino, L., Feron, E. M., and Bicchi, A. (2002). Conflict resolution problems for air traffic management systems solved with mixed integer programming. *IEEE transactions on intelligent transportation systems*, 3(1):3–11. 2.4.2, 2.4.3, 3, 3.3, 3.4, 3.4, 4.2, 4.7.1
- Pelegri n, M. and d’Ambrosio, C. (2020). Airspace conflict resolution: A unifying mathematical framework and review. 2.4, 2.4.2, 3, 3.5, 3.8
- Pepper, J. W., Mills, K. R., and Wojcik, L. A. (2003). Predictability and uncertainty in air traffic flow management. In *5th USA/Europe Air Traffic Management R&D Seminar (ATM-2003), Metrics and Performance Management, Budapest, Hungary*. 2.4.3
- Peterson, M. D., Bertsimas, D. J., and Odoni, A. R. (1995). Models and algorithms for transient queueing congestion at airports. *Management Science*, 41(8):1279–1295. 2.2
- Peyronne, C., Conn, A. R., Mongeau, M., and Delahaye, D. (2015). Solving air traffic conflict problems via local continuous optimization. *European Journal of Operational Research*, 241(2):502–512. 2.4.2, 2.4.3

- Prandini, M., Lygeros, J., Nilim, A., and Sastry, S. (1999). A probabilistic framework for aircraft conflict detection. In *Guidance, Navigation, and Control Conference and Exhibit*, page 4144. 2.4.1
- Preston, N. (2005). Faa historical chronology, 1926–1996. *nd <http://www.faa.gov/about/media/bchron.pdf>*. 1.1, 2.3
- Radmanesh, M., Kumar, M., and Sarim, M. (2018). Grey wolf optimization based sense and avoid algorithm in a bayesian framework for multiple uav path planning in an uncertain environment. *Aerospace Science and Technology*, 77:168–179. 2.4.3
- Ratcliffe, S. (1995). Long time-horizons for air traffic flow planning in europe. *The Journal of Navigation*, 48(2):279–288. 2.2
- Regnier, E. (2008). Doing something about the weather. *Omega*, 36(1):22–32. 2.4.3
- Rey, D. and Hijazi, H. (2017). Complex number formulation and convex relaxations for aircraft conflict resolution. In *2017 IEEE 56th Annual Conference on Decision and Control (CDC)*, pages 88–93. IEEE. 2.4.2, 2.4.3, 3, 3.1, 3.3, 3.6, 3.7, 4, 4.2, 4.2, 4.3, 4.4, 4.5, 4.5, 4.7.1, 4.9.1, 5.1.3, 5.2.1, 6.5.1, 7.1
- Rey, D., Rapine, C., Dixit, V. V., and Waller, S. T. (2015). Equity-oriented aircraft collision avoidance model. *IEEE Transactions on Intelligent Transportation Systems*, 16(1):172–183. 3.6
- Rey, D., Rapine, C., Fondacci, R., and El Faouzi, N.-E. (2012). Minimization of potential air conflicts through speed regulation. *Transportation research record: journal of the transportation research board*, (2300):59–67. 2.4.2
- Rey, D., Rapine, C., Fondacci, R., and El Faouzi, N.-E. (2016). Subliminal speed control in air traffic management: Optimization and simulation. *Transportation Science*, 50(1):240–262. 1.5, 2.4.2, 2.4.3
- Richetta, O. (1995). Optimal algorithms and a remarkably efficient heuristic for the ground-holding problem in air traffic control. *Operations Research*, 43(5):758–770. 2.2
- Richetta, O. and Odoni, A. R. (1993). Solving optimally the static ground-holding policy problem in air traffic control. *Transportation science*, 27(3):228–238. 2.2

- Richetta, O. and Odoni, A. R. (1994). Dynamic solution to the ground-holding problem in air traffic control. *Transportation research part A: Policy and practice*, 28(3):167–185. 2.2
- Rivas, D., Franco, A., and Valenzuela, A. (2017). Analysis of aircraft trajectory uncertainty using ensemble weather forecasts. In *Proc. 7th European Conference for Aeronautics and Space Sciences (EUCASS)*, pages 1–12. 2.4.3
- Rome, H. J. and Kalafus, R. (1988). Impact of automatic dependent surveillance and navigation system accuracy on collision risk on intersecting tracks. In *Proceedings of the 1988 National Technical Meeting of The Institute of Navigation*, pages 213–222. 2.4.1
- Schäfer, K., Jahn, C., Sturm, P., Lechner, B., and Bacher, M. (2003). Aircraft emission measurements by remote sensing methodologies at airports. *Atmospheric Environment*, 37(37):5261–5271. 1.2, 1.5
- Shepard, T., Dean, T., Powley, W., and Akl, Y. (1991). A conflict prediction algorithm using intent information. In *Proc. 36th Annual Air Traffic Control Assoc. Conf.* 2.4.1
- Shewchun, J. M., Oh, J.-H., and Feron, E. (1997). Linear matrix inequalities for free flight conflict problems. In *Proceedings of the 36th IEEE Conference on Decision and Control*, volume 3, pages 2417–2422. IEEE. 2.4.1
- Shumsky, R. A. (1998). Optimal updating of forecasts for the timing of future events. *Management science*, 44(3):321–335. 2.2
- Snyder, L. V. (2006). Facility location under uncertainty: a review. *IIE transactions*, 38(7):547–564. 2.4.3
- Sridhar, B. and Chatterji, G. (1997). Computationally efficient conflict detection methods for air traffic management. In *Proceedings of the 1997 American Control Conference (Cat. No. 97CH36041)*, volume 2, pages 1126–1130. IEEE. 2.4.1
- Taylor, D. H. (1990). Uncertainty in collision avoidance manoeuvring. *The Journal of Navigation*, 43(2):238–245. 2.4.1
- Teodorović, D. and Babić, O. (1993). Fuzzy inference approach to the flow management problem in air traffic control. *Transportation planning and technology*, 17(2):165–178. 2.2

- Terrab, M. and Odoni, A. R. (1993). Strategic flow management for air traffic control. *Operations research*, 41(1):138–152. 2.2
- Tofukuji, N. (1996). An airspace design and evaluation of enroute sector by air traffic control simulation experiments. *Electronics and Communications in Japan (Part I: Communications)*, 79(8):103–113. 2.2
- Tofukuji, N. (1997). Air traffic flow management methods: Development and testing by real-time dynamic simulation experiments. *Electronics and Communications in Japan (Part I: Communications)*, 80(5):35–44. 2.2
- Tomlin, C., Pappas, G. J., and Sastry, S. (1998). Conflict resolution for air traffic management: A study in multiagent hybrid systems. *IEEE Transactions on automatic control*, 43(4):509–521. 2.4.1
- Tosic, V. and Babic, O. (1995). Air route flow management—problems and research efforts. *Transportation Planning and Technology*, 19(1):63–72. 2.2
- Valenzuela, A., Franco, A., and Rivas, D. (2017). Sector demand analysis under meteorological uncertainty. In *Proc. 7th European Conference for Aeronautics and Space Sciences (EUCASS), Milan, Italy*, pages 1–15. 2.4.3
- Vanaret, C., Gianazza, D., Durand, N., and Gotteland, J.-B. (2012). Benchmarking conflict resolution algorithms. 3.6
- Vela, A., Solak, S., Singhose, W., and Clarke, J.-P. (2009a). A mixed integer program for flight-level assignment and speed control for conflict resolution. In *Decision and Control, 2009 held jointly with the 2009 28th Chinese Control Conference. CDC/CCC 2009. Proceedings of the 48th IEEE Conference on*, pages 5219–5226. IEEE. 2.4.2
- Vela, A. E., Salaun, E., Solak, S., Feron, E., Singhose, W., and Clarke, J.-P. (2009b). A two-stage stochastic optimization model for air traffic conflict resolution under wind uncertainty. In *2009 IEEE/AIAA 28th Digital Avionics Systems Conference*, pages 2–E. IEEE. 1.5, 2.4.2, 2.4.3
- Vela, A. E., Solak, S., Clarke, J.-P. B., Singhose, W. E., Barnes, E. R., and Johnson, E. L. (2010). Near real-time fuel-optimal en route conflict resolution. *IEEE Transactions on Intelligent Transportation Systems*, 11(4):826–837. 2.4.3

- Vela, A. E., Solak, S., Feron, E., Feigh, K., Singhose, W., and Clarke, J.-P. (2009c). A fuel optimal and reduced controller workload optimization model for conflict resolution. In *Digital Avionics Systems Conference, 2009. DASC'09. IEEE/AIAA 28th*, pages 3–C. IEEE. 2.4.2
- Verderame, P. M., Elia, J. A., Li, J., and Floudas, C. A. (2010). Planning and scheduling under uncertainty: a review across multiple sectors. *Industrial & engineering chemistry research*, 49(9):3993–4017. 2.4.3
- Vink, A., Kauppinen, S., Beers, J., and de Jong, K. (1997). Medium term conflict detection in eatchip phase iii. In *16th DASC. AIAA/IEEE Digital Avionics Systems Conference. Reflections to the Future. Proceedings*, volume 2, pages 9–3. IEEE. 2.4.1
- von Viebahn, H. and Schiefele, J. (1997). Method for detecting and avoiding flight hazards. In *Enhanced and Synthetic Vision 1997*, volume 3088, pages 50–56. International Society for Optics and Photonics. 2.4.1
- Vranas, P. B., Bertsimas, D., and Odoni, A. R. (1994a). Dynamic ground-holding policies for a network of airports. *Transportation Science*, 28(4):275–291. 2.2
- Vranas, P. B., Bertsimas, D. J., and Odoni, A. R. (1994b). The multi-airport ground-holding problem in air traffic control. *Operations Research*, 42(2):249–261. 2.2
- Waller, M. C. and Scanlon, C. H. (1996). Proceedings of the nasa workshop on flight deck centered parallel runway approaches in instrument meteorological conditions. 2.4.1
- Wangemann, J. P. and Stengel, R. F. (1998). Principled negotiation between intelligent agents: a model for air traffic management. *Artificial Intelligence in Engineering*, 12(3):177–187. 2.4.1
- Wangemann, J. P. and Stengel, R. F. (1999). Optimization and coordination of multiagent systems using principled negotiation. *Journal of Guidance, Control, and Dynamics*, 22(1):43–50. 2.4.1
- Warren, A. (1997). Medium term conflict detection for free routing: Operational concepts and requirements analysis. In *16th DASC. AIAA/IEEE Digital Avionics Systems Conference. Reflections to the Future. Proceedings*, volume 2, pages 9–3. IEEE. 2.4.1

- Wiener, E. L. (1989). Human factors of advanced technology (glass cockpit) transport aircraft. 4.3
- Williams, P. R. (1992). Aircraft collision avoidance using statistical decision theory. In *Sensors and sensor systems for guidance and navigation II*, volume 1694, pages 29–34. International Society for Optics and Photonics. 2.4.1
- Williamson, T. and Spencer, N. A. (1989). Development and operation of the traffic alert and collision avoidance system (tcas). *Proceedings of the IEEE*, 77(11):1735–1744. 2.4.1
- Wu, C.-L. and Caves, R. E. (2002). Research review of air traffic management. *Transport Reviews*, 22(1):115–132. 2.1
- Yang, L. and Kuchar, J. (1998). Using intent information in probabilistic conflict analysis. In *Guidance, Navigation, and Control Conference and Exhibit*, page 4237. 2.4.1
- YangL, K. (1997). Prototype conflict alerting logic for free flight. *Proc35th AIAA Airspace science meeting & Exhibit. Reno, NV*. 2.4.1
- Zeghal, K. (1998). A review of different approaches based on force fields for airborne conflict resolution. In *Guidance, Navigation, and Control Conference and Exhibit*, page 4240. 2.4.1
- Zenios, S. A. (1991). Network based models for air-traffic control. *European Journal of Operational Research*, 50(2):166–178. 2.2
- Zhao, Y., Schultz, R., Zhao, Y., and Schultz, R. (1997). Deterministic resolution of two aircraft conflict in free flight. In *Guidance, Navigation, and Control Conference*, page 3547. 2.4.1
- Zheng, Q. and Zhao, Y. (2011). Modeling wind uncertainties for stochastic trajectory synthesis. In *11th AIAA Aviation Technology, Integration, and Operations (ATIO) Conference, including the AIAA Balloon Systems Conference and 19th AIAA Lighter-Than*, page 6858. 2.4.3